hydrology

MDPI

Article

Half a Century of Civil Engineering in the Bahlui River Hydrographic System: The Unexpected Journey from Gray Structures to Hybrid Resilience

Nicolae Marcoie [1], Șerban Chihaia [1,2], András-István Barta [3], Daniel Toma [1], Valentin Boboc [1], Mihai Gabriel Balan [4], Cătălin Dumitrel Balan [5,*] and Mircea-Teodor Nechita [5]

[1] Faculty of Hydrotechnical Engineering, Geodesy and Environmental Engineering, "Gheorghe Asachi" Technical University of Iasi, Bd. Prof. Dimitrie Mangeron, No. 65, 700050 Iași, Romania; nicolae.marcoie@academic.tuiasi.ro (N.M.); serban.chihaia@dap.rowater.ro (Ș.C.); daniel.toma@academic.tuiasi.ro (D.T.); valentin.boboc@academic.tuiasi.ro (V.B.)
[2] Prut-Bârlad Water Basin Administration, Str. Theodor Văscăuțeanu No. 10, 700463 Iași, Romania
[3] Faculty of Geography, Babeș-Bolyai University, Bistrița Branch, 5-7 Clinicilor Street, 400006 Cluj-Napoca, Romania; andras.barta@ubbcluj.ro
[4] Department of Geography, Faculty of Geography-Geology, "Alexandru Ioan Cuza", University of Iasi, 20A, Carol I, 700505 Iași, Romania; mihaigabrielbalan@gmail.com
[5] Faculty of Chemical Engineering and Environmental Protection "Cristofor Simionescu", "Gheorghe Asachi" Technical University of Iasi, Bd. Prof. Dimitrie Mangeron, No. 73, 700050 Iași, Romania; mircea-teodor.nechita@academic.tuiasi.ro
* Correspondence: catalin-dumitrel.balan@academic.tuiasi.ro

Abstract

Water reservoirs are critical components of hydrological systems that mitigate floods and droughts, but their long-term performance under climate change and variable socioeconomic conditions remain insufficiently documented. This study examines the Bahlui River basin (northeastern Romania), where 17 reservoirs constructed mainly between the 1960s and 1980s have been operational for more than five decades. Using the most recent technical reservoir reports, land-use evolution, and present operational functions, the contribution of man-made reservoirs to flood attenuation and drought buffering over time was appraised. Flood mitigation is the most consistent and reliable function, with peak-flow reductions commonly exceeding 60–90% of design discharges at the basin scale. Engineered drought mitigation functions (irrigation and industrial water supply) have decreased significantly as a result of socioeconomic changes started in 1989. However, the gradual expansion of green infrastructure, such as wetlands and riparian vegetation, has improved passive water retention and low-flow buffering capacity. These unanticipated developments have resulted in variable levels of hybrid hydrological resilience. The findings show that, while artificial reservoirs have strong flood-control capacity over long periods of time, their contribution to drought mitigation is increasingly dependent on the integration of ecological components, emphasizing the importance of green-gray interactions in long-term reservoir management.

Keywords: floods and droughts mitigation; earth dams; green-gray structures; hydrological resilience

Academic Editor: Ali A. Assani

Received: 28 November 2025
Revised: 23 December 2025
Accepted: 26 December 2025
Published: 29 December 2025

1. Introduction

Hydrological extremes, such as droughts and floods, have become more frequent and intense over the past 50 years, most likely due to climate change [1,2]. This has become

a major issue for sustainable water management on a global scale [3–5]. Therefore, the concept of hydrological resilience (HR) [6,7] and achieving it, whether naturally or by engineering [8,9], is becoming increasingly important as mankind enters a new geological period, the Anthropocene [10,11]. Unfortunately, systems like riparian vegetation, forests, and wetlands that provide natural resilience [8] against hydrological extremes clash with the trend for agricultural and urban expansion brought on by the world's population growth [9,12,13]. As a result, human intervention is increasingly required to supplement natural resilience and/or compensate for its absence. The term "engineered hydrological resilience." [8] describes man-made infrastructure, such as dams, reservoirs, dikes, levees, floodwalls, and polders, that is intended to control water flow and minimize hydrological vulnerabilities. At the local scale, the impact of dams, reservoirs, and related artificial structures is immediate and highly visible, affecting the watercourse and the surrounding landscape. The regional and subsequently global impact is more subtle and occurs relatively slowly as a consequence of altering the natural water cycle. For example, high open water surfaces have an impact on surface evaporation, creating heat and mass fluxes that can contribute to climate changes [14]. Therefore, human intervention in watercourses, carried out for purposes other than flood protection and/or drought prevention, is quite controversial [15], and the balance between the drawbacks and benefits of hydraulic structures is still a subject of debate [14,16]. Furthermore, as the frequency and severity of hydrological extremes tend to rise, human response needs to adapt, which means modifying dam and reservoir design and operations [11,17]. The new hydraulic structures are designed to meet present and, to some extent, future needs [18], whereas the older ones must deal with both anthropogenic interferences (e.g., aggressive urban development, intensive agriculture) and climate-related issues (e.g., flash floods, prolonged droughts) [19,20]. In this context, the transition from single to multi-purpose reservoirs, aiming to increase the benefits of the hydraulic structures, is logical [21,22].

Without a doubt, the hydraulic structures are essential tools in water management, their sustainability depending on a series of factors such as adaptive design, integrated basin-scale planning, and ecological restoration measures [23,24]. Modern strategies are increasingly relying on hybrid systems, which combine engineered hydraulic resilience with natural water retention techniques to provide balanced flood and drought mitigation [25].

A relevant example that illustrates the evolution from single to multi-purpose reservoirs and from engineered to hybrid resilience is the Bahlui River basin in northeastern Romania. This hydrographic system, characterized by (i) a history of recurrent floods and droughts, (ii) a mixed natural–urban environment, (iii) a huge socioeconomic transition (from communism to democracy), and (iv) a massive anthropogenic interference. It provides an insightful case study for assessing the effectiveness of substantial hydrotechnical interventions. Bahlui's hydrographic basin comprises at least 17 dams and accumulations, the majority of which have been exploited for more than 50 years.

This paper presents a critical analysis of the Bahlui River hydrographic system from a civil engineering perspective, focusing on the interplay between natural hydrological dynamics and hydrotechnical infrastructures. By examining the initial goals and the actual performances of existing reservoirs and hydraulic structures, the study aims to assess the effectiveness of current mitigation strategies and identify opportunities for optimization. The time-developed interaction between anthropogenic and natural water retention systems provides multiple reservoirs in the Bahlui basin with hybrid resilience. The current study stands out for its comprehensive and interdisciplinary approach, which combines historical exploration, civil engineering analysis, hydrological evaluation, and environmental management perspectives to assess how HR contributes to the mitigation of hydrological extremes, such as intense floods and prolonged droughts.

https://doi.org/10.3390/hydrology13010015

2. Materials and Methods

2.1. Civil Engineering Infrastructure on the Hydrographic Network of the Bahlui River

The complex hydrological and morphological characteristics of the Bahlui River basin (Figure 1) necessitate an accurate description of the study area to contextualize the engineering challenges and interventions. A detailed description of the Bahlui hydrographic system can be found in our previous papers [26,27] and/or in the works of other authors [28–30]. In a few words, the Bahlui River is 119 km long, has a catchment area of 2025 km^2, and a hydrographical network of nearly 3100 km. Even though it is a rain-fed river with an average discharge ranging from 2.8 to 4 m^3/s, huge discharge variations ranging from complete depletion during summer droughts [31] till up to 600 m^3/s during floods were reported in history [26]. Based on its length and average discharge, the Bahlui River is in the small rivers category [32]; however, there are not many rivers of this size with similar levels of hydrological engineering. No less than 17 dams and accumulations were constructed during the second half of the past century in order to mitigate floods and droughts [26,30]. Only two dams—Pârcovaci and Tansa-Belcești—were constructed along the river's main course; the other dams, some of which had temporary and some of which had permanent activity, were constructed inside its hydrographic basin (Figure 1), on the Bahlui River's main tributaries.

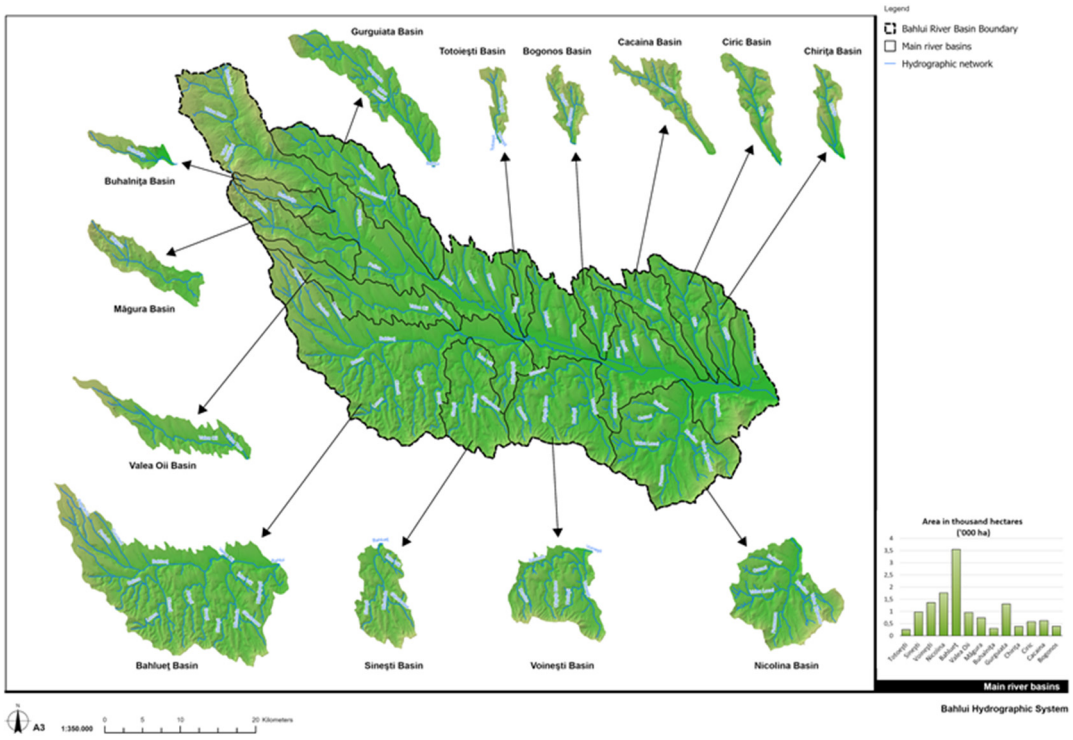

Figure 1. The Bahlui River's hydrographic system, including main tributaries and basins.

In this study, the term 'temporary reservoir' refers strictly to an operational regime, following Romanian hydrotechnical practice; it denotes structures designed for immediate water storage that typically fill during high-flow events and remain dry or partially dry during normal or low-flow conditions. This label does not suggest diminished resilience or ecological insignificance.

Succinct descriptions for each of the 17 dams/accumulations are presented in the next paragraphs, highlighting their original (initially designed) and current functions. The subsequent presentation is based on up-to-date official reports, written in the Romanian language, see references [33–49].

Some specific abbreviations were used in the ensuing paragraphs: NRL = normal retention level; m. d. M. N. = meters above Black Sea level; $Q_{0.1}$%, $Q_{0.01}$%, $Q_{1.2\times0.01}$% . . . = floods with exceedance probabilities 0.1%, 0.01%, . . . and verification; V = volume, m^3; Q = volumetric flowrate (discharge), m^3/s; ha = hectares, 1 ha = 10,000 m^2.

2.1.1. Dams on the Bahlui River: Pârcovaci and Tansa–Belcesti

The Pârcovaci Reservoir, built between 1978 and 1984, is a Category B, Class II facility with hydrographic code XIII-1.15.32. It was originally intended for industrial and civil water supply, flood mitigation, and natural fish farming. Today, it continues to supply water for Hârlău, primarily for civil use, while still fulfilling flood-control and fish-farming functions. A small amount of technical data is reported in Table 1.

Table 1. The Pârcovaci Dam: technical data [40].

Category	Main Technical Parameters
Dam characteristics	Homogeneous earth dam • trapezoidal cross-section • length of the dam crest: 290 m • maximum height: 25 m • crest width: 6.75 m • crest elevation: 178.70 m. d. M. N.
Characteristic levels (m. d. M. N.)	Riverbed: 154.00 • NRL: 171.00 • Maximum design level (1%): 177.23 • Dam crest: 178.70
Storage volumes (million m^3)	Total storage: 8.75 • Useful: 2.36 • Gross at NRL: 2.75
Hydrology	Q_1% = 240 m^3/s → attenuated to 114.9 m^3/s • $Q_{0.1}$% = 454 m^3/s (natural) • permanent minimum sanitation discharge of 0.017 m^3/s

The Tansa–Belcești Reservoir on the Bahlui River, built between 1971 and 1974, is classified as an important Class I, Category B hydraulic structure and is identified by hydrographic code XIII–1.15.32. The technical data for Tansa–Belecesti reservoir are presented in Table 2.

Table 2. The Tansa–Belcești Reservoir: technical data [43].

Category	Main Technical Parameters
Dam characteristics	Earth dam (non-homogeneous) with clay core • Trapezoidal cross-section• Length of dam body: 980 m • Total impoundment front: 4873 m • Maximum height: 14.2 m • Crest width: 4.5–5.0 m
Characteristic levels (m. d. M. N.)	Dead storage level: 82.31 • Minimum operational level: 84.82 • NRL: 87.32 • Design flood level (0.1%): 91.68 • Maximum (0.01%): 92.38 • Crest: 93.31
Storage volumes (million m^3)	Total at crest: 25.131 • At design level: 18.750 • Total at maximum level: 21.451 • Gross at NRL: 4.720 • Useful: 4.250 • Dead: 0.001 • Attenuation volume (between design level and NRL): 14.030
Hydrology	Q_1% = 285 m^3/s → attenuated to 134.05 m^3/s • permanent minimum sanitation discharge of 0.050 m^3/s

Designed primarily for irrigation, the reservoir also provided flood attenuation, local water supply, and supported fish-farming activities, with no hydropower component planned. In its current operation, its main function is flood mitigation. Irrigation is now significantly reduced due to degradation of the distribution system, while water supply continues at a modest rate (2020: 0.01548 m^3/s). The reservoir also maintains fish-farming uses and meets ecological flow requirements established by basin management authorities.

2.1.2. Podu Iloaiei Reservoir: Accumulation on Bahlueț River

The Podu Iloaiei Reservoir was built between 1963 and 1964 on the Bahluieț River, which is Bahlui's main tributary. Its hydrographic code is XIII–1.015.32.12.00.0; it was upgraded from importance Class II to I in 1975 and falls under Category B. Some rehabilitation works were performed in 2011. In its original design, the reservoir served multiple functions, including irrigation and water supply, flood protection, and fish-farming activities. The reservoir was not designed to supply drinking water, industrial water, or to produce hydropower. Under current operating conditions, the primary function of the Podu Iloaiei Reservoir remains flood mitigation. Irrigation activities have been discontinued since 2008, while fish-farming operations continue and prosper. The technical data for Podu Iloaiei Reservoir are presented in Table 3.

Table 3. The Podu Iloaiei Reservoir: technical data [45].

Category	Main Technical Parameters
Dam characteristics	Earth dam built from local loess-type clays, essentially homogeneous • Maximum height: 14.2 m • Dam body length: 980 m (total impoundment front ≈ 4873 m) • Crest width: 4.5–5.0 m
Characteristic levels (m. d. M. N.)	Spillway crest: 65.33 • Dam crest (earth fill): 68.50 • Concrete parapet: 69.15 • Dead storage level: 60.00 • NRL: 62.00
Storage volumes (million m^3)	Total at maximum verification level (1.2 × 0.01%): 28.098 • Total at 0.01% level: 26.144 • Total at design level 0.1%: 23.114 • Theoretical gross at spillway crest: 15.674 • Gross at NRL: 3.699 • Dead storage: 0.572 • Useful storage: 3.127
Hydrology	Q_1% reduced from 280 m^3/s to 15 m^3/s • permanent minimum sanitation discharge of 0.021 m^3/s

2.1.3. Reservoirs on Râul Locii River: Bârca and Ciurbești

The Bârca Temporary Reservoir is located on the Râul Locii, within the Nicolina River basin, and is identified by hydrographic code XIII.1.15.32.20.1. Classified as a Class II reservoir and falling under Category D, it was constructed between 1978 and 1981. In its original design, the reservoir served exclusively flood-related functions, including flood mitigation for Ciurbești, reduction in downstream flood peaks, and sediment retention to protect the Ciurbești Reservoir. It was not intended for water supply, irrigation, fish farming, or hydropower. Currently, its operational role remains unchanged: it continues to provide flood attenuation and peak-flow reduction on the Nicolina and Bahlui Rivers, with no water-supply, irrigation, or ecological-flow functions.

The Ciurbești Reservoir, also located on the Râul Locii (hydrographic code XIII.1.15.32.20.1.0), was originally classified as Class II but was upgraded to Class I in 1976. It is a Category C reservoir built in 1962. The reservoir was initially designed to support irrigation and water supply for 250 hectares (100,000 m^3/year), to function as a permanent fish-farming reservoir, and to provide flood attenuation for downstream localities including Ciurbești, Ciurea, and the Nicolina and Bahlui sectors. In the current operation, flood mitigation remains its primary function. Fish farming continues under natural hydrological conditions, and the reservoir additionally supports a nearby sports and recreation area. Some technical data for Bârca and Ciurbești Accumulations are presented in Table 4.

Table 4. Reservoirs on the Râul Locii River: Bârca and Ciurbești—technical data [34,49].

Category	Bârca Temporary Reservoir	Ciurbești Reservoir
Dam characteristics	Homogeneous earth dam • Length: 400 m • Maximum height: 12.7 m • Crest width: 6.0 m • Foundation depth: 0.5 m	Homogeneous earth dam • Length: 427 m Crown elevation: 69.00 m • Maximum height: ~14–15 m • Crest width: 9.3 m
Characteristic levels (m. d. M. N.)	Riverbed: 65.10 • Bottom-outlet axis: 65.35 • Spillway crest: 74.00 • Dam crest: 77.00	Maximum flood level: 67.113 • Dam crest: 69.00 • Bottom outlet axis: 54.95
Storage volumes (million m^3)	Total at verification level: 3.94 • Upstream fishpond volumes (can be absorbed in failure scenario): 0.65 • Total attenuation: 7.90	Attention: 4.608 • Alert: 6.733 • Danger: 8.229 • Attenuation capacity: 5.707 • Total volume at max level: ~14.75 • Total at dam crest: 16.56
Hydrology	$Q_{1\%}$: 100 $m^3/s \rightarrow$ 14.750 m^3/s (85% reduction) • $Q_{0.1\%}$: 172 $m^3/s \rightarrow$ 17.031 m^3/s (90% reduction)	$Q_{0.1}\%$ = 250 $m^3/s \rightarrow$ attenuated to ~33.047 m^3/s • $Q_{0.01}\%$ ~154 $m^3/s \rightarrow$ attenuated to ~16.608 m^3/s • permanent minimum sanitation discharge of 0.02 m^3/s

2.1.4. Accumulations on Ciric River: Aroneanu and Ciric III Reservoirs [38,46]

The Aroneanu Reservoir, located on the Ciric River (hydrographic code XIII.1.15.32.22), is classified as a Class I reservoir and belongs to Category B. It was constructed between 1962 and 1964, with crest rehabilitation works completed in 1977–1978. In its original design, the reservoir served several functions: maintaining a permanent 70-hectare lake for fish farming, providing flood attenuation, supplying water to the Ciric I and Ciric II lakes, and supporting irrigation. In the current operation, flood mitigation remains its primary role. Fish-farming activities have ceased due to the absence of active contracts, irrigation has been discontinued, and the reservoir now supports rowing and other sports activities. Table 5 provides some technical data for these reservoirs.

Table 5. Accumulations on the Ciric River: Aroneanu and Ciric III—technical data [38,46].

Category	Aroneanu Reservoir	Ciric III Reservoir
Dam characteristics	Homogeneous earth dam, local loess-type clay materials • Length: 280 m • Maximum height: 9.3 m (original) • Crest width: 5 m	Homogeneous earth dam, trapezoidal section • Length: 258 m • Crest width: 5 m • Maximum height: 11.5 m • Foundation depth: min. 0.85 m
Characteristic levels (m. d. M. N.)	Dead storage level 56.52 • Minimum operating level: 58.00 • NRL: 58.80 • Spillway crest: 60.55 • Earthfill crest: 64.32	Bottom outlet axis: 42.45 • Water intake axis: 45.50 • NRL: 46.50 • Spillway crest: 51.00 • Dam crest: 53.60
Storage volumes (million m^3)	Dead storage: 0.362 • Gross at NRL: 1.480 • At spillway crest: 2.410 • Global at earthfill crest: 6.602	Total at dam crest: 1.960 (designed)/1.600 (current) • Gross at spillway crest: 1.000 (designed)/0.911 (current) • Gross at NRL: 0.250 (designed)/0.248 (current)
Hydrology	$Q_5\%$ = 54 m^3/s • $Q_2\%$ = 80 m^3/s • $Q_1\%$ = 100 m^3/s • $Q_{0.1}\%$ = 172 m^3/s • $Q_{0.01}\%$ = 244 m^3/s • $Q_{1.2\times0.01}\%$ = 292.8 m^3/s • permanent minimum sanitation discharge of 0.010 m^3/s	$Q_{0.1}\%$ = 180 m^3/s • $Q_{0.01}\%$ = 333 m^3/s • $Q_{1.2\times0.01}\%$ = 399.6 m^3/s • permanent minimum sanitation discharge of 0.010 m^3/s

Ciric III Reservoir is also situated on the Ciric River and is identified by hydrographic code XIII.1.15.32.22. A Class I, Category C reservoir, it was constructed between 1976 and

1978. It was originally intended for natural-regime fish farming and flood attenuation. Today, flood mitigation continues to be the principal function. Fish-farming activities are still practiced under natural hydrological conditions, and the reservoir has become part of a broader recreation and leisure area.

2.1.5. Accumulations on Cacaina River: Cârlig and Vânători

The Cârlig (hydrographic code: XIII.1.15.32.21) and Vânători (hydrographic code: XIII.1.15.32.21) reservoirs are located on the Cacaina River and were constructed between 1978 and 1981 and 1979–1982, respectively. Both reservoirs are classified as Category D structures, with Cârlig designated as Importance Class I and Vânători as Importance Class II. Originally, each reservoir was designed solely for flood attenuation, with no provisions for water supply, irrigation, fish farming, or hydropower production. Their operational purpose has remained unchanged, and today they continue to function exclusively as flood-mitigation structures. Some technical data are presented in Table 6.

Table 6. Accumulations on the Cacaina River: Cârlig and Vânători Reservoirs—technical data [35,39].

Category	Cârlig Reservoir	Vânători Reservoir
Dam characteristics	Earthfill homogeneous dam • Material: local clay soils • Length: 225 m • Crest width: 4.0 m • Maximum height: 7.67 m	Homogeneous earthfill dam built from local clayey soils • Crest length: 360.0 m • Foundation width (base width): 92.20 m • Crest width: 5.0 m • Maximum height: 12.85 m
Characteristic levels (m. d. M. N.)	Thalweg: 54.15 (projected)/54.44 (current) • Bottom outlet axis: 54.95/55.24 • Spillway crest: 60.05 (projected)/59.68 (current) • Dam crest: 62.55 (projected)/62.11 current	Thalwheg: 63.10 • Bottom outlet axis: 63.50 • Spillway crest: 72.35 • Dam crest: 74.60 (projected)/74.55 (current)
Storage volumes (million m^3)	Dead storage: 0.01 (projected)/0.004 (current) • Volume at spillway crest: ~1.02 (projected)/1.069 (current) • Total at verification level 0.01%: 2.640 • Total at dam crest: 3.20 (projected)/3.076 (current)	Global at dam crest: 3.675 • Theoretical gross volume (from valley morphology): 2.201 • Total at maximum verification level (0.1%): 2.993 • Dead volume: 0.010 • Dead storage: 0.010 • Useful/active flood storage: 3.665
Hydrology	$Q_{1.2\times0.01}$%: 294 → 227.17 m^3/s (77%) • $Q_{0.01}$%: 245 → 146.79 m^3/s (59%) • $Q_{0.1}$% (design): 170 → 115.88 m^3/s (68%) • Minimum required downstream flow: the natural flow of the Cacaina River	Q_1%: 80 → 11.973 m^3/s • $Q_{0.1}$%: 151 → 54.338 m^3/s • $Q_{1.2\times0.1}$%: 181.20 → 78.956 m^3/s • Minimum required downstream flow: the natural flow of the Cacaina River

2.1.6. Plopi Accumulation on Gurguiata River

The Plopi reservoir, basin code: XIII.1.15.32.8, classified as Importance Class II, Category B, was built over three years, from May 1975 to October 1978. Its original design envisioned a multifunctional role. It was intended to provide 2.4 million m^3 of water for the irrigation of roughly 400 hectares, to support a 114-hectare fish-farming area, and to contribute to flood protection within the basin. Over time, the reservoir's operational profile has evolved. Flood mitigation remains a fully preserved and active function. However, irrigation services are currently inactive. Fish farming continues, but only under natural conditions rather than through managed aquaculture. The reservoir now also fulfills a water-supply role, supported by an active contract amounting to approximately 1.1906 million m^3 of water per year. More technical data are presented in Table 7.

Table 7. The Plopi Reservoir: technical data [44].

Category	Main Technical Parameters
Dam characteristics	Homogeneous earthfill dam • Crest elevation: 82.75–83.86 m. d. M. N. • Crest length: 369.12 m (design 330 m) • Crest width: 4.55–5.11 m (design 5.0 m) • Maximum height: 11.36 m (design 10.5 m)
Characteristic levels (m. d. M. N.)	Bottom outlet invert: 72.50 • Bottom outlet axis: 73.35 • Dead storage level (design): 73.60 • Minimum operating level: 75.10 • NRL: 78.24 (design 77.70) • Spillway crest: 82.22 (design 81.80)
Storage volumes (million m^3)	Gross at NRL: 4.3296 • Theoretical gross at spillway crest: 10.352 • Global at earthfill crest: 11.293 • Useful storage at NRL: 4.30
Hydrology	$Q_{0.1}\%$ = 205 m^3/s → attenuated to 90.21 m^3/s • $Q_1\%$ = 120 m^3/s → attenuated to 18.24 m^3/s. • Ecological downstream flow: = 0.010 m^3/s

2.1.7. Sârca Accumulation on Valea Oii River

The Sârca Reservoir on the Valea Oii River (Basin Code XIII.1.15.32.12.7), built in 1979–1984 and classified as Importance Class II, Category C, was originally designed for irrigation (1.0 million m^3/year for ~400 ha), fish farming (28 ha), and flood attenuation, with no municipal or hydropower use. Currently, its primary function remains flood mitigation; irrigation has decreased to 128,000 m^3/year, and fish-farming activity has enhanced. The reservoir can additionally retain up to 3.0 million m^3 to buffer potential upstream pond failures. A few technical data are presented in Table 8.

Table 8. The Sârca Reservoir: technical data [36].

Category	Main Technical Parameters
Dam characteristics	Homogeneous earthfill dam, trapezoidal section • Crest length: 334 m • Crest width: 6 m • Maximum height: 16.5 m • Minimum foundation depth: 2.1 m • Crest elevation: 82.50 m. d. M. N.
Characteristic levels (m. d. M. N.)	Thalweg: 65.50 • Bottom outlet axis: 66.30 • Water intake axis (lower): 67.00 • Upper intake axis: 71.50 • Spillway crest: 81.00 • Frontal dam crest: 82.50 • Minimum operating level: 68.50 • NRL: 73.50
Storage volumes (million m^3)	Global at dam crest: 21.130 • Total at maximum verification: 13.974 • Theoretical gross at spillway crest: 16.865 • Gross at NRL: 3.300 • Useful storage: 3.000 • Dead (inactive) storage: 0.100
Hydrology	$Q_{1\%}$ = 110 m^3/s V = 6.18 million m^3 • $Q_{0.1\%}$ = 190 m^3/s, V = 10.67 million m^3 • (verification) → $Q_{1.2\times0.1\%}$ = 228 m^3/s, V = 12.80 million m^3 • Ecological downstream flow: = 0.010 m^3/s

2.1.8. Cucuteni Reservoir on Voinești River

The Cucuteni Reservoir, basin Code XIII.1.15.32.15, was built in 1964 and classified as an important Class II, Category C. It was originally designed to store 3.0 million m^3 for irrigating 780 ha, to support a 108 ha natural-regime fish pond (useful volume 3.0 million m^3), and to provide flood attenuation. Currently, flood mitigation remains fully functional; irrigation capacity is largely unused despite ~300 ha being potentially irrigable; and fish farming continues on 98.9 ha, with 1.73 million m^3 available at NRL 58.48 m. The technical data for the Cucuteni Reservoir are presented in Table 9.

Table 9. The Cucuteni Reservoir: technical data [47].

Category	Main Technical Parameters
Dam characteristics	Homogeneous earthfill dam built from local loess-like clays and silty clays • constructed in two bodies (old embankment "A" and raised body "B"). • Crest length: 377 m • Maximum base width: 66 m • Crest width: 8 m • Maximum height: 13.75 m
Characteristic levels (m. d. M. N.)	Lake bed: 53.00 • Bottom outlet invert: 51.00 • Bottom outlet axis: 51.75 • Spillway) sill/tower weir 58.48 • Spillway crest (large floods): 61.85 • Dam crest (frontal embankment): 64.78 • Dead storage level 54.95 • Minimum operating level: 56.50 • NRL: 58.48
Storage volumes (million m^3)	Dead/silted volume: 1.616 • Gross at NRL: 1.734 • Theoretical gross at spillway crest: 6.373 • Gross at design level: 7.033 • Global at dam crest: 12.541
Hydrology	Q_1%: 140 → 26.86 m^3/s (level 62.57 m. d. M. N.) • $Q_{0.1}$%: 240 → 90.90 m^3/s (63.46 m. d. M. N.) • $Q_{1.2\times0.1}$%: 288 → 122.63 m^3/s (63.82 m. d. M. N.) • Q_2%: 110 → 9.27 m^3/s • Q_5%: 75 → 0 m^3/s • Ecological flow upgraded from 0.010 m^3/s to 0.023 m^3/s to support water quality in Bahlui.

2.1.9. Ciurea Reservoir on Nicolina River

The Ciurea Temporary Reservoir, constructed between 1978 and 1981 on the Nicolina River, is classified as an importance Class I, Category D hydraulic structure (code XIII.1.15.32.20). Its primary purpose at the time of design was the attenuation of floods on the Nicolina River and the protection of the downstream localities of Ciurea, Miroslava, and Iași—specifically the CUG, Nicolina, and Galata districts—as well as safeguarding approximately 80 hectares of agricultural land. In its current operational configuration, the Ciurea Reservoir continues to fulfill its original flood-control function entirely. Downstream of the dam, ecological flow is ensured by allowing the natural river discharge to pass through the system, and no supplementary uses have been assigned. The reservoir now forms an integral component of the flood-protection chain within the Nicolina sub-basin, working in coordination with the upstream Ciurbești Reservoir. The technical data for Ciurea Temporary Reservoir are presented in Table 10.

Table 10. The Ciurea Temporary Reservoir: technical data [48].

Category	Main Technical Parameters
Dam characteristics	Earthfill homogeneous dam • Crest elevation: 81.20 m • Crest width: 4 m • Length: 750 m • Maximum height: 18 m
Characteristic levels (m. d. M. N.)	Thalweg: 64.41 • Bottom outlet axis: 65.28 • Upstream pond level: 73.35 • Spillway crest: 79.70 • Dam crest: 81.20 • Freeboard (crest—spillway): 1.96 m
Storage volumes (million m^3)	Total at dam crest: 7.20 • Gross at spillway crest: 5.24 • Upstream pond volume: 0.21 • Dead storage: 0.35 • Volume at verification level: 6.23
Hydrology	Natural vs. attenuated peak flows: $Q_{0.1}$%: 175 → 56.3 m^3/s • $Q_{0.01}$%: 245 → 58.0 m^3/s • $Q_{1.2\times0.01}$%: 294 → 109 m^3/s

2.1.10. Cornet Reservoir on Cornet River

The Cornet Temporary Reservoir, constructed between 1978 and 1981 on the Cornet River, is classified as an Importance Class I, Category D hydraulic structure. Situated within basin code XIII.1.15.32.20.2.1, the reservoir was initially designed primarily for flood attenuation, with its principal function being to enhance the safety level of the downstream Ezăreni Reservoir, raising its protection to Importance Class I standards. In addition to this primary role, the Cornet Reservoir was expected to contribute to reducing peak

flood flows propagating toward the Nicolina and Bahlui Rivers. In its current operational context, the Cornet accumulation continues to serve exclusively as a flood-mitigation structure. Its role remains essential for the overall safety of the Ezăreni Reservoir and for the coordinated flood-protection system operating along the Nicolina–Bahlui corridor, providing attenuation capacity during high-flow events. The technical data for the Cornet Temporary Reservoir are presented in Table 11.

Table 11. The Cornet Accumulation: technical data [37].

Category	Main Technical Parameters
Dam characteristics	Homogeneous earthfill dam • Length at crest: 250 m • Base width: 77 m • Crest width: 4.0 m • Maximum height: 11.5 m • Minimum founding depth: 0.50 m
Characteristic levels (m. d. M. N.)	Thalweg: 60.00 (project/current) • Bottom outlet axis: 59.50 • Spillway crest: 68.50 • Dam crest: 71.50 • Maximum design level: 68.05 (project)/66.73 current • Maximum verification level: 70.20 (project)/69.44 current
Storage volumes (million m^3)	Global at dam crest: 3.90 • Upstream pond volumes: 0.08 • Total at spillway crest: 1.95 • Theoretical flood storage above crest (to crest): 1.95 • At verification level: 2.96 (project)/2.464 (current) • Dead volume: 0.07
Hydrology	$Q_{1.2\times0.01}$% (verification): natural 192.0 $m^3/s \rightarrow$ attenuated 39.768 m^3/s • $Q_{0.01}$% (verification): 160.0 $\rightarrow$ 24.30 m^3/s • $Q_{0.1}$% (design): 115.0 $\rightarrow$ 19.484 m^3/s

2.1.11. Ezăreni Reservoir on Ezăreni River

The Ezăreni Reservoir, constructed between 1962 and 1964 on the Ezăreni River, is classified as an Importance Class I, Category B hydraulic structure within basin code XIII.1.15.32.20.2. In its original design, the reservoir fulfilled multiple functions. It provided approximately 0.140 million m^3 of industrial water per year, served as an irrigation source for roughly 360 ha of agricultural land, supported fish-farming activities with a usable volume of 0.78 million m^3 at its normal retention level (NRL = 58.40 m d. M. N.), and contributed to regional flood attenuation.

The project also incorporated a recreational component through the formation of a permanent lake of approximately 47 ha at NRL. In its present operational state, flood mitigation remains the reservoir's primary and consistently maintained function. The former provisions for industrial water supply and irrigation are no longer in use, although the conditions for fish-farming activities remain available at the standard operating level. The recreational role associated with the permanent lake is also preserved, continuing to provide both landscape and leisure value. Some technical data for Ezăreni Reservoir are presented in Table 12.

Table 12. The Ezăreni Reservoir: technical data [33].

Category	Main Technical Parameters
Dam characteristics	Homogeneous earthfill dam built from local clayey materials. • Crest length: 273 m • Base width: ~60 m • Crest width: 4.60 m • Maximum height: 8.60 m • Minimum foundation level: 54.50 m. d. M. N.
Characteristic levels (m. d. M. N.)	Thalweg: 50.60 • Bottom outlet axis: 55.00 • Spillway crest: 60.20 • Dam crest (frontal embankment): 63.10 • Minimum operating level: 56.80 • NRL: 58.40

Table 12. *Cont.*

Category	Main Technical Parameters
Storage volumes (million m^3)	Global at dam crest: 4.300 • Total at maximum verification level: 3.312 • Gross at spillway crest: 1.862 • Gross at NRL: 0.780 • Dead storage: 0.080
Hydrology	• $Q_{0.1}$%: 150 → 17.338 m^3/s at level 61.28 m. d. M. N. • $Q_{0.01}$%: 210 → 25.324 m^3/s at 61.72 m. d. M. N. • $Q_{1.2\times0.01}$%: 252 → 32.245 m^3/s at 62.07 m. d. M. N. • Ecological downstream flow: = 0.007 m^3/s

2.1.12. Rediu Reservoir on Rediu River

The Rediu Reservoir, built between 1986 and 1988 on the Rediu River, is classified as an Important Class III, Category C hydraulic structure within basin code XIII.1.15.32.19. In its original design, the reservoir served multiple purposes. It provided a storage volume of approximately 0.30 million m^3 intended to irrigate 120 ha of downstream agricultural land, contributed to flood attenuation, and supported natural-regime fish farming through a permanent water surface of 14.6 ha at normal retention level. In the current operation, flood mitigation remains the reservoir's predominant function. The irrigation component has been discontinued, but fish-farming activities continue to be maintained, relying on the same permanent water surface of about 14.6 ha at NRL. The technical data for Rediu Reservoir are presented in Table 13.

Table 13. The Rediu Reservoir: technical data [41].

Category	Main Technical Parameters
Dam characteristics	Earthfill homogeneous dam (trapezoidal section) constructed from local clayey soils. • Crest length: 253 m • Base width: 48 m • Crest width: 5 m • Maximum height: 10 m • Minimum foundation depth: 5 m • Minimum foundation level: 54.30 m. d. M. N.
Characteristic levels (m. d. M. N.)	Thalweg: 58.50 • Bottom outlet axis: 55.10 • Water intake axis: 59.25 • Spillway crest: 63.21 • Dam crest (frontal embankment): 64.65 • NRL: 62.95
Storage volumes (million m^3)	Global at dam crest: 0.675 • Gross at spillway crest: 0.408 • Gross at NRL: 0.369 • Useful volume: 0.291
Hydrology	Q_2% (design): 31 m^3/s → attenuated to 11.4 m^3/s • Q_1%: 40 m^3/s → 15.2 m^3/s • $Q_{0.5}$% (verification): 49 m^3/s → 19.3 m^3/s • Q_5%: 22 m^3/s → 6.8 m^3/s • Q_{10}%: 15 m^3/s → 4.3 m^3/s • Ecological downstream flow: 0.001 m^3/s

2.1.13. Chiriţa Reservoir on the Chiriţa River

The Chiriţa Reservoir, constructed between 1962 and 1964 on the Chiriţa River and identified under hydrographic code XIII.1.015.32.23.00.0, is classified as an Importance Class III, importance Category C hydraulic structure. Originally designed as a pre-decantation basin for the Iaşi water treatment plant, the reservoir was intended to store water pumped from the Prut River and to ensure both flood attenuation and the maintenance of a minimum ecological flow along the downstream reach of the Chiriţa stream. In its current operational configuration, the Chiriţa Reservoir serves primarily as a water-supply and pre-treatment source for the municipality of Iaşi, supporting both industrial and potable water needs. Its flood-mitigation function continues to be maintained, and controlled releases secure downstream ecological flows, with discharge values adjusted according to hydrological conditions: 0.100 m^3/s under low-flow scenarios, 0.125 m^3/s under medium-flow conditions, and 0.150 m^3/s during high-flow periods. The system also continues to facilitate industrial water pumping. Some technical data for Chiriţa Reservoir are presented in Table 14.

Table 14. The Chirița Reservoir: technical data [42].

Category	Main Technical Parameters
Dam characteristics	Earthfill dam • Parapet elevation: 54.90 m. d. M. N. • Upstream slope protected with concrete slabs (recent repairs 2020–2022)
Characteristic levels (m. d. M. N.)	Minimum exploitation: 49.70 • Medium: 50.70 • Maximum (NRL-equivalent): 51.70 • Parapet level: 54.90
Storage volumes (million m^3)	NRL storage: 3.695 million m^3 • Surface at NRL: 92.70 ha
Hydrology	Q2%: 72 → 9.93 m^3/s; Q0.5%: 111 → 24.83 m^3/s • Downstream ecological outflows strictly regulated: = 0.100–0.150 m^3/s.

2.2. Historical Evolution of Land Use in the Bahlui Hydrographic System

Before the completion of the hydrotechnical infrastructure, the Bahlui was acknowledged as a capricious watercourse oscillating between complete depletion and huge discharge values (up to 600 m^3/s during the floods in 1932) [26]. Although its basin is highly engineered, it still remains a rain-fed, lowland river with many ungauged, intermittent tributaries; only about 30% of the network has permanent flow. Three maps were chosen as representative of the land-use evolution of the hydrographic basin as presented in Figures 2–4.

In 1892, the main land use was agriculture (71.12% from the total basin area). The forest surfaces were surprisingly low (16.7%). A system of fish ponds and small natural lakes, connected to a fairly wide, marshy riverbed of the Bahlui River, is depicted in Figure 2. Around 100 years later, at the very beginning of the post-communist era, in 1990, the land use was completely different (Figure 3). Although agriculture remains the primary occupation (68.40%), some degree of diversity occurs: pastures, vineyards, orchards, and grasslands. The urbanization level varies significantly (11.66%), mostly due to socialist forced urbanization politics [50], while the surface occupied by forest remains relatively constant (16.99%).

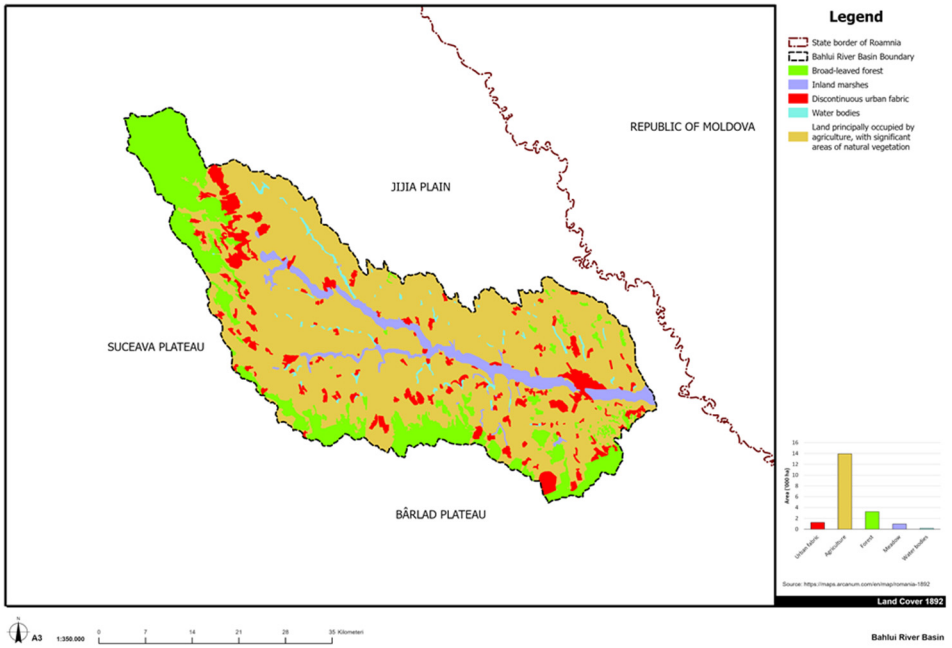

Figure 2. Bahlui River Basin: land use, 1892.

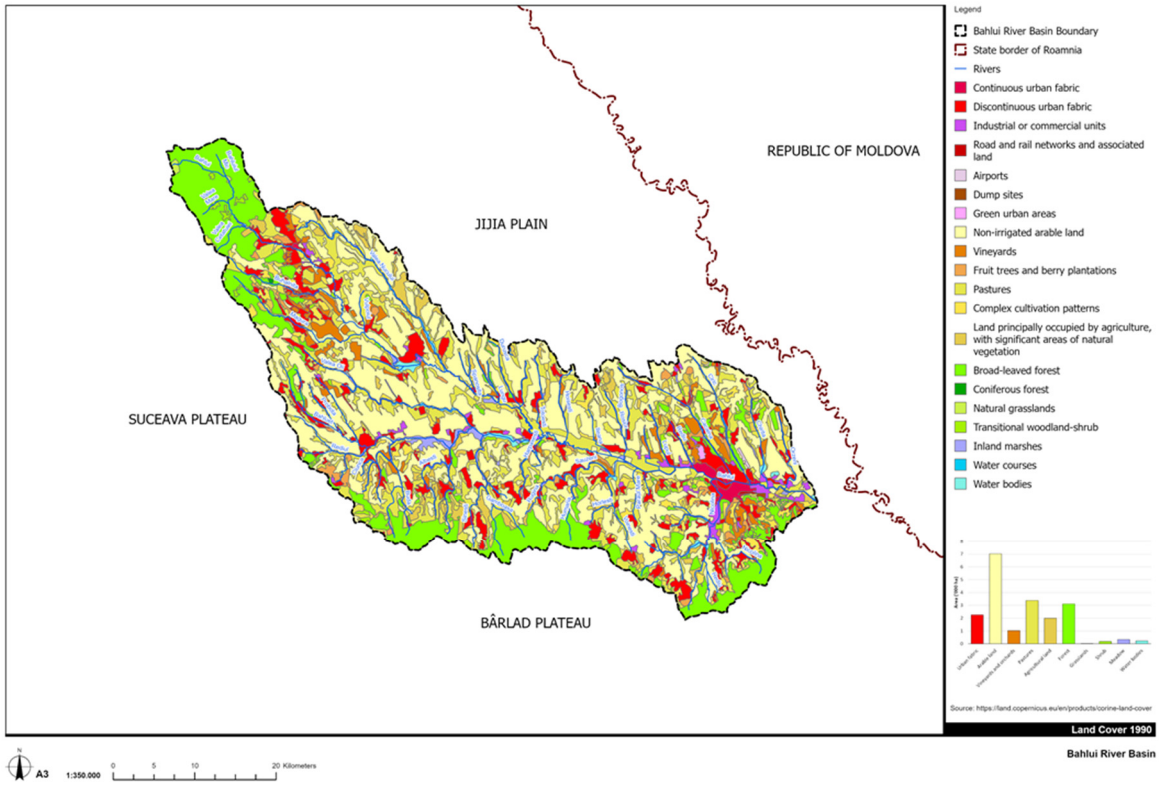

Figure 3. Bahlui River Basin: land use, 1990.

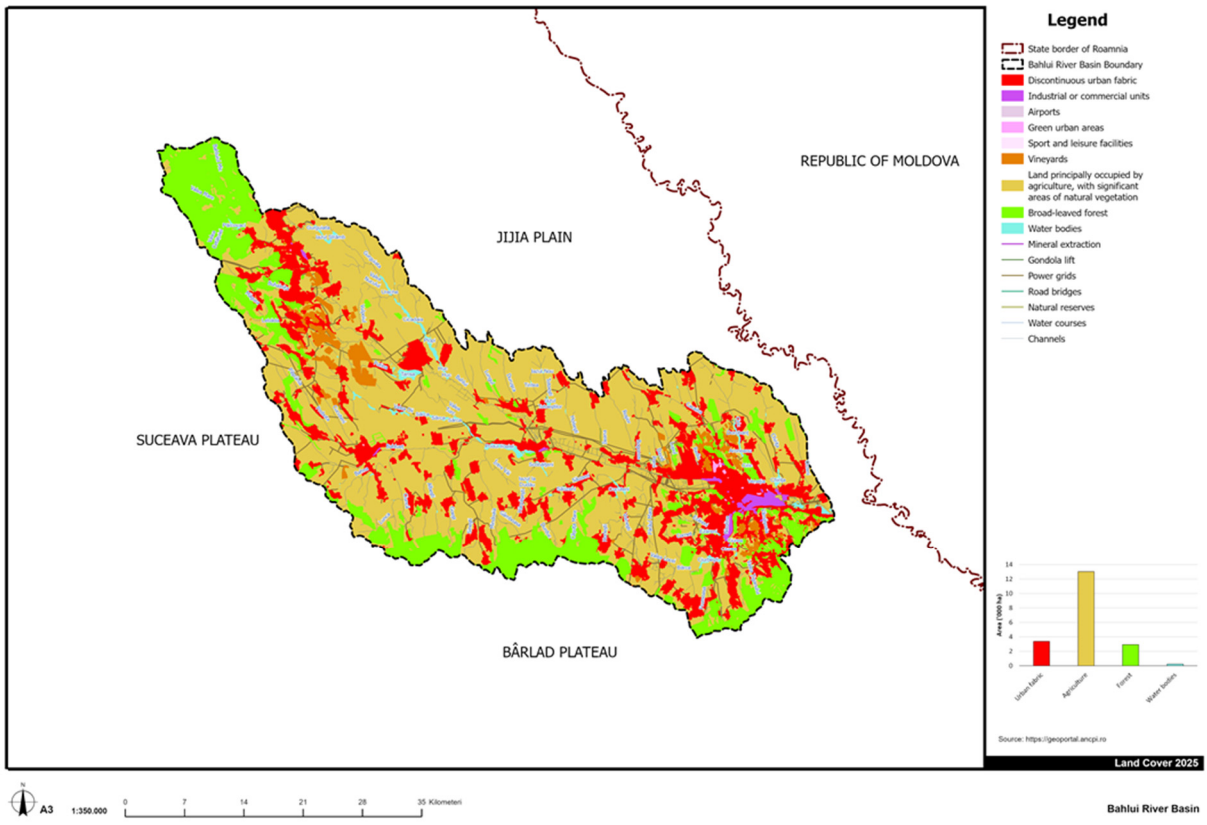

Figure 4. Bahlui River Basin: land use, 2025.

Nowadays (Figure 3), there is still a tendency toward urbanization (17.46%); nevertheless, the real estate market and deindustrialization are the main factors [51]. Again, the land use is mainly agricultural (62.27%), but to some extent less diverse than in the 1990s

(Figure 4). The remaining (compared to 1990 land cover) industrial areas are concentrated around Iași, the major urban area in the region.

The development of green elements within the Bahlui reservoir system has been significantly influenced by changes in land use and increasing urbanization. After 1989, riparian vegetation, wetlands, and reed beds naturally developed in reservoir tails due to changes in agricultural methods, land abandonment, and decreased maintenance activities. Most of these eco-friendly elements (green infrastructure, GI) emerged as unintended byproducts. Over time, they start to contribute to hydrological regulation, progressively enhancing passive water retention, flow attenuation, and ecological connectivity.

2.3. Land Use Maps: Graphical Updating and Processing

The land-use information available for the Bahlui River Basin is composed of the legacy of the maps: Maps of Moldavia 1892–1898, scale 1:50,000; Corine Land Cover 1996, scale 1:100,000, and Orthophotoplan 2025 (ANCPI). The used methodology correlates the data from different land-use categories, highlighting changes from one historical period to another. The utilized database was digitally analyzed and processed using GIS software, ArcPRO v.10.6.1, and represents the support for the cartographic material realized in this work. The statistical data processing was performed based on Microsoft Office 2016. For graphic processing, the following software was used: Autodesk Civil 3D 2024 v. 13.6.2090.0, Adobe Photoshop 7.0.

2.4. Limitations

The main limitation of this work is the inherent qualitative nature of the hybrid hydrological resilience (HR) concept and its assessment. Because of the long-term perspective and the absence of reliable, measurable ecological data for the entire reservoir system, HR was evaluated using qualitative indicators based on observable and repeatable circumstances rather than numerical methods. Therefore, the study does not aim to determine quantitative correlations or causal linkages between HR levels and reservoir characteristics. Instead, it describes the long-term, unplanned co-evolution of natural ecosystem elements and gray infrastructure, utilizing empirical and historical data to show how hybrid resilience develops over reservoir systems' life cycles. The institutional recognition (protected natural area, for example) was regarded as a supporting indicator that demonstrated long-term ecological significance. However, legal protection status does not guarantee high HR status for a particular structure.

3. Results and Discussion

3.1. Key Highlights on Bahlui's River Civil Engineering Infrastructure

While the structural and functional aspects of the reservoir system in the Bahlui River basin are relatively similar, certain projects differ due to particular hydrotechnical elements.

The Pârcovaci Reservoir features the tallest dam in the basin (25 m), while Țansa–Belcești accumulation is the largest impoundment, with an estimated 40 million m^3 of total storage. Among permanent systems, Plopi and Sârca Reservoirs provide the largest useful volumes (3–4 million m^3), supporting irrigation, aquaculture, and regional flood mitigation. The deepest active water columns, expressed through the largest elevation range between NNR and maximum levels, are found at Cucuteni and Plopi reservoirs, enhancing their capacity for both daily regulation and extreme-event attenuation. From a historical perspective, the Cucuteni reservoir, commissioned in 1964, is the oldest operational basin, while structures such as Rediu, Bârca, Plopi, and Sârca represent the newer generation developed during the 1980s. The Rediu reservoir, functional since 1988, is the smallest permanent storage, with only 0.675 million m^3. The temporary reservoirs Cornet and

Vânători achieve the highest flood-attenuation performance, designed to reduce incoming peaks by 60–85% and provide essential protection for downstream communities, including the urban sectors of Iași.

It is worth mentioning that none of the reservoirs were built or run for hydropower, which is in line with the Bahlui basin's modest discharge potential and mild gradients. Another common feature is that structurally, every dam in the system is a homogeneous earthfill structure constructed from locally available clays or loess-based materials.

3.2. Half-Century Functional Evolution of the Hydrotechnical Infrastructure

The oldest reservoir from Bahlui's hydrographic system, Cucuteni, is 61 years old, while Rediu, the most recent to be put into service, is 37. The reservoir system of the Bahlui basin is, on average, about half a century old, their construction concentrated between 1964 and 1988. As a result, the majority of structures currently function within the mid- to late-life range of a typical earthfill dam, which is predicted to last 50 years or more [52–54].

During the five decades following their construction, the reservoirs of the Bahlui basin have experienced several major politico-economic transitions that, in some cases, have reshaped their functionality. The most influential was the post-1990 decline of state-managed agriculture and industry [55,56], which sharply reduced irrigation demand and eliminated most industrial water needs, leaving many reservoirs underutilized relative to their original design. Fragmented land ownership and limited local budgets further constrained maintenance, accelerating sedimentation and reducing operational volumes. After Romania's EU accession in 2007, new environmental directives such as the Water Framework Directive [57], Floods Directive [58], Natura 2000 [59], shifted policy priorities toward ecological flow maintenance, biodiversity conservation, and flood-risk reduction, redefining the reservoirs' operational regimes. More recently, recurrent extreme-weather events associated with climate variability [60,61] have increased the emphasis on flood attenuation and drought resilience, elevating safety requirements for aging dams [62]. Together, these politico-economic shifts have progressively realigned reservoir functions away from their initial agro-industrial purposes toward a predominantly flood-protection, ecological, and urban-safety role within the Iași metropolitan region. Based on these considerations, three classes of dams can be established in Bahlui's hydrographic basin:

1. Reservoirs that essentially kept their original purpose. This category includes (i) the non-permanent reservoirs, Bârca, Cârlig, Cornet, Ciurea, and Vânători, that were built with a single function: flood attenuation; (ii) Ciric III and Ciurbești reservoirs, that preserved their main functions of flood attenuation and fish-farming, with recreation added as a new utility; and (iii) Pârcovaci Accumulation that still performs its designed functions: urban/industrial water supply for Hârlău, flood attenuation, ecological flow, and fishery; the only change is that industrial water demand has decreased.
2. Reservoirs with partially modified functionalities, where the original multi-purpose concept remains visible, but certain branches, especially irrigation, have faded: (i) Tansa–Belcesti, Podu Iloaiei, and Rediu, which were planned primarily for irrigation, flood control, and fish-farming, are now centered on flood attenuation and fish-farming; (ii) Cucuteni, Sârca, Plopi, that shifted from irrigation as the main function to fish-farming, keeping their flood attenuation status; (iii) Chirița, that shifted from water storage to water supply, preserving the other functions.
3. Reservoirs with major functional modifications, where the current function is clearly different from the original design: (i) Aroneanu, that started as a genuinely multi-purpose reservoir (irrigation, fishery, partial water supply, and flood defense) but currently functions mainly as a flood-mitigation and recreational/sports lake; and

(ii) Ezăreni, initially designed to supply industrial water and irrigation, to support fishery and flood control, that nowadays ensure flood attenuation and present potential for fishery and recreational activities.

In conclusion, the Bahlui reservoir system has developed a consistent functional trajectory over the last fifty years. Every reservoir that was first built for flood mitigation still serves this purpose today, making flood protection the most reliable and enduring function. By contrast, irrigation and industrial water supply have undergone the sharpest decline. It has completely disappeared from certain reservoirs (e.g., Podu Iloaiei, Rediu, Aroneanu, Ezăreni) and is only minimally present in others, such as Sârca, Plopi, and Cucuteni. Fish farming and leisure activities, on the other hand, have shown to be relatively resilient, frequently persisting in areas where local demand and infrastructure are still feasible. Recreational use has become the primary function in certain reservoirs, most notably Aroneanu, Ciric III, and Ciurbești, indicating a broader functional shift away from agro-industrial goals and toward environmental and social considerations. Naturally, as Minea reported in his study [29], the water quality of each accumulation also changed with time. Nevertheless, as indicated in the following, hybrid resilience is not about the structural integrity of man-made constructions or the health of natural ecosystems, but rather about the green-gray interaction and its adaptive capacity to manage floods and droughts. This study does not consider legal protection status (for example, Law No. 5/2000 or Natura 2000 classification) as proof of ecological integrity or optimal ecosystem functioning. Protected reservoirs may nevertheless suffer from ecological degradation, such as eutrophication, discontinuities in nutrient flow [26], the presence of invasive species, or hydro-morphological fragmentation [27], as observed in some areas of the Bahlui basin [29].

3.3. Hybrid Resilience: From Theoretical Concept to Actual Examples

3.3.1. HR: Theoretical Background

In the middle of the 1970s, C. S. Holland introduced the concept of "resilience" [63], and in the late 1990s, the same author divided it into "engineering resilience" and "ecological resilience" [64]. A series of debates followed the introduction of the resilience concept and there are two distinct interpretations of this term (simplified) [65–69]: (i) the capacity of a system to absorb disturbance and reorganize so as to still retain essentially the same function, structure, and identity; and (ii) the time required for a system to return to an equilibrium or steady-state following a perturbation. According to Granata and Di Nunno [8], in hydrology, the term "resilience" means that a water system can continue to perform the designed functions, such as water supply, flood regulation, and ecosystem support, despite disturbances (e.g., floods and droughts). Referring mainly to floods mitigation, Nakamura [70] introduced the terms "gray infrastructure" (GYI) that represents the engineering resilience and include dams, reservoir, levees, drainage channels, etc., and green and "green infrastructure" (GI), which represents the ecological resilience and include forests and wetlands in the watershed, wetlands, riparian corridors, floodplains, reed beds, etc.

Although resilience in hydrological systems can arise through both natural processes (GI) and engineered interventions (GYI), each one has its own benefits and drawbacks:

(i) GYI—dams, levees, stormwater networks—remain essential for regulating runoff and protecting communities. Yet its effectiveness is limited under extreme future climate scenarios. Evaluations of current levees and dams reveal that engineered systems built to surpass former hydrological standards are becoming more vulnerable to unprecedented floods [25,70].

(ii) GI—wetlands, riparian zones, forests, floodplains—provide functions like infiltration, storage, cooling, and biodiversity support; however, these systems alone cannot

always protect densely populated or highly modified landscapes. GI is recognized for multi-functionality, offering climate adaptation, risk reduction, and ecological services, but also requires governance and careful implementation.

The concept of hybrid resilience (HR) emerges from the recognition that neither conventional gray infrastructure nor purely ecological, nature-based systems alone can adequately address the increasing hydrological instability of the Anthropocene [8,70,71]. HR encompasses the ability to manage floods, sustain water quality, buffer droughts, and support biodiversity under conditions of climatic and anthropogenic stress through the combined use of green (nature-based) and gray (engineered) infrastructures [8,70]. Hybrid (green-gray) systems (Figure 5) integrate the immediate protective capacity of engineered structures with the adaptive, regenerative characteristics of ecosystems. This combination provides functional complementarity: gray elements deliver immediate risk reduction, while green elements enhance long-term resilience through ecological progression, energy dissipation, and hydrological retention. While gray components offer immediate and predictable levels of safety, the protective and ecological functions of green elements increase over time as vegetation establishes, sediment accumulates, and ecological connectivity improves.

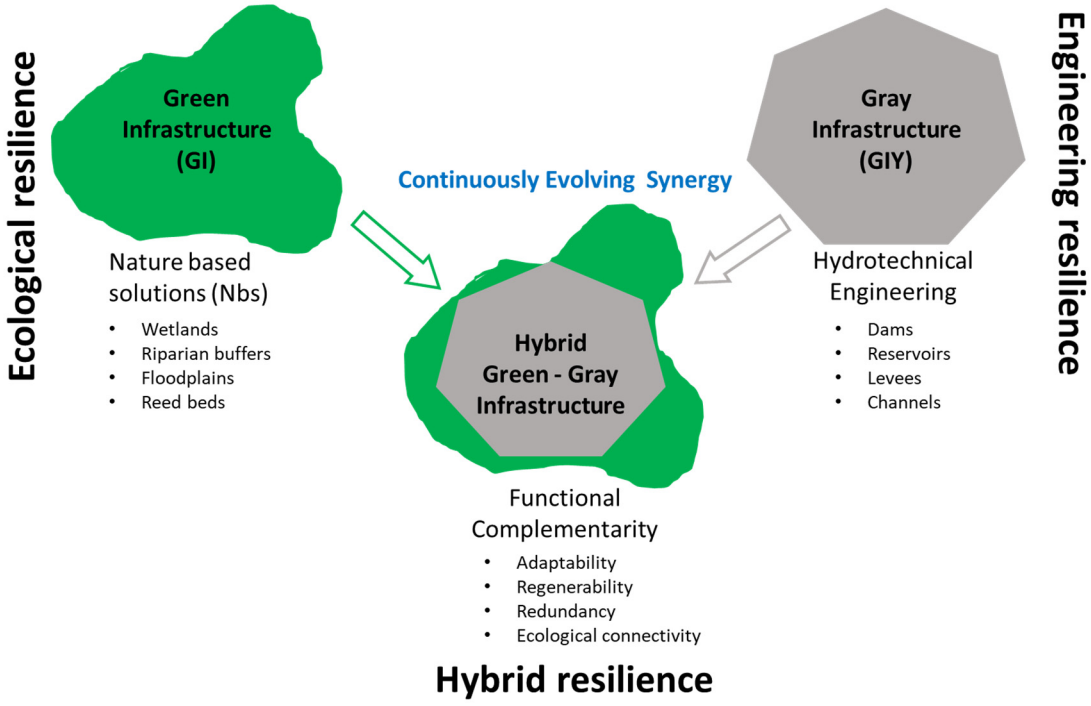

Figure 5. The hybrid resilience conceptualization.

It is crucial to emphasize that hybrid resilience represents a degree of functional integration between naturally occurring green components and man-made gray infrastructure, rather than a measure of ecological optimality. In this context, hybrid resilience does not imply ecological perfection; instead, it reflects the capacity of engineered and natural elements to operate jointly and adaptively under real-world constraints, including land-use pressures, infrastructure aging, and climate variability.

Considering these, the definition of the HR concept (in hydrology) can be slightly modified, adapted for a green-gray infrastructure: the ability to mitigate floods, buffer droughts, and support biodiversity under extreme climate conditions and anthropogenic stress.

3.3.2. Temporal Dynamics of Hybrid Resilience Development

A fundamental characteristic of HR is that it takes time to develop and manifest. Because of its ecological component, HR is not static and keeps evolving and adjusting. While gray infrastructure can be planned and constructed within a matter of years, green infrastructure develops through slower ecological processes that may take decades to reach full functionality. The GIY offer immediate and predictable levels of safety, while the protective and ecological functions of GI increase over time as vegetation establishes, sediment accumulates, and ecological connectivity improves.

The time necessary to "develop" a hybrid infrastructure is not a one-digit number: construction of the gray parts may take a few years, while the achievement of full hybrid performance and co-benefits is on the order of decades, tied to ecological maturation, social acceptance, and hydrotechnical infrastructure life cycle. Thus, hybrid systems go through stages of development. The engineered components provide instant, predictable safety, whereas the ecological components grow slowly, enhancing system performance over time in a less controllable manner.

Since HR is a relatively "new" concept, the design methods for hybrid infrastructures are still "in the research stage", and their effectiveness needs to be evaluated via simulations and long-term monitoring [25,70]. Because of the uncertainty involved with ecosystem-based risk reduction, the rules and procedures evolve gradually as more data accumulates, extending the timescale for complete implementation. Hybrid resilience requires a long-term planning strategy. Its progress takes place in three overlapping stages [8,70]:

(i) Stage 1: 0–5 years, construction of gray infrastructure, which provides immediate protection; some green elements can be introduced (not yet functional), including grading, planting, and wetland creation.
(ii) Stage 2: 5–20 years, development of green infrastructure, including riparian vegetation, wetlands, reed beds, etc.; ecological functions achieve a certain maturity; green and gray components begin operating together, generating complementarity.
(iii) Stage 3: 20+ years, ecological systems reach functional maturity, providing sustained flood mitigation, water-quality improvements, and biodiversity benefits; the hybrid system becomes a fully integrated socioecological infrastructure; depending on the initial design, the gray infrastructure may require major reinvestment and/or rehabilitation works, enabling redesign toward more nature-based or lighter-gray solutions.

Obviously, hybrid systems are never "complete" at construction. Its performance is expected to improve over time as vegetation grows and the ecological connection improves. The three HR stages describe generalized temporal trajectories derived from landscape evolution and reservoir age, recognizing that ecological development is gradual, geographically variable, and non-synchronized across sites. Most of the reservoirs built in the 1960s and 1970s have Stage 3 characteristics (Chiriţa, Podu Iloaiei), whereas reservoirs commissioned in later decades have Stage 2 or Stage 1 features (e.g., Rediu), which reflect shorter ecological succession periods and less development of green infrastructure.

3.3.3. Hybrid Resilience: Can It Be Designed, Anticipated, Accelerated, or Delayed?

If allowed, the green component may appear on its own. In fact, as in the case of Bahlui's hydrodynamic system, a lot of reservoirs and dams that are older than the term "resilience" itself are nowadays working in a hybrid mode. The hybrid resilience simply occurred as the green component began to grow and interact with the gray one. Nowadays, when the benefits of this association are acknowledged, the hybrid resilience can be studied, anticipated, and/or modeled [25]. Because the combined effects of green and gray components rely on how they are positioned in relation to one another, hybrid infrastructures necessitate careful design of their spatial configurations [70].

The development of the green component can be anticipated to a certain degree. However, both natural and anthropogenic influences can interfere with the normal progress of ecological resilience. Climate events and land-use changes can either slow down or accelerate the growth of the green infrastructure. Therefore, modeling and ecological practice can be used to anticipate HR, but full forecasting is impossible due to social and climatic unpredictability [8].

Ecological processes that would usually take decades can be accelerated by planting mature plants, creating wetlands, and repairing riparian zones. Reservoir management can increase ecological resilience downstream more rapidly. In the same manner, the ecological processes can be delayed by extreme weather events or by human activities. Stakeholders' decisions, implementation of adequate legislation, can also contribute to the faster development of hybrid infrastructures.

HR is a dynamic concept that is always evolving. It is somewhat predictable, manageable, and designable. Its development can be strategically accelerated by ecological progress and engineering assistance. Its evolution may be slowed down by social restraints, institutional obstacles, or natural events. Long-term planning, consistent ecological knowledge, and adaptive governance are essential for successful hybrid resilience implementation [8].

3.3.4. Actual Examples of Hybrid Resilience in Bahlui's River Hydrographic Basin

In the case of the Bahlui River, any deliberate connection with concepts like GIY, GI, and HR can be ruled out since the first dams in the Bahlui hydrographic system were built ten years prior to the emergence of the "resilience" concept [63], and all of them were built during Communism, before the 1990s. The majority of the dams in this hydrographic basin are presently in the mid- to late-life range of a conventional earthfill dam, as was indicated in Section 3.2. This points out that the majority of the dams had enough time to complete all the steps necessary for HR development (see Section 3.3.2). The hybrid resilience in Bahlui's basin developed progressively over several decades (without recognition), almost concurrently with the creation and acceptance of the HR concept.

The hybridization level of the dams in Bahlui's hydrographic basin can now be assessed using their actual constructive characteristics and functions (see Section 2.1), the previously discussed GYI–GI and HR concepts (Sections 3.3.1–3.3.3), as well as local, national, and international decisions and laws concerning the protected natural areas in Romania [72]. When addressing flood and drought mitigation, the term hybridization level refers to the degree of functional integration between man-made gray infrastructures and naturally occurring green components. Table 15 shows the classification proposed for the 17 dams: high, moderate, and low HR level.

The Bahlui reservoir system is more than just a collection of dams; parts of it already operate as a hybrid resilience network (Sârca–Podu Iloaiei; Tansa–Belcești–Plopi; Aroneanu–Ciric III), with GIY offering controlled flood and drought mitigation, storage, and supply, and GI offering complementary services and ecosystem improvement. With the correct ecological and operational strategies, the Bahlui system might become a regional model of hydrological resilience and hydrologically sound water management. Assessing the time required for achieving the GIY–GI interaction in Bahlui's basin is of high importance for future design strategies aiming at HR. The reservoirs constructed in the 1960s and 1980s are now GI mature (multiple decades of development should be considered).

Overall, the Bahlui reservoir system shows how anthropogenic structures and self-organized natural processes can co-evolve over time to create multifunctional structures that are safer, more biodiverse, and more ecologically integrated than either purely natural or purely constructed systems alone. While naturally occurring wetlands, marshy reservoir

tails, and riparian belts provide biological flexibility and adaptive potential to climate change, the constructed components provide structural strength.

Table 15. Estimating hybrid hydrological resilience using institutional, functional, ecological, and structural data.

Category	Reservoir	Justification	Refs.
High HR	Pârcovaci	The Pârcovaci accumulation has been declared a national protected area since 2000, as per Law No. 5 of 6 March 2000, which was amended by the Emergency Ordinance No. 49 of 31 August 2016.	[73,74]
	Chirița	Included in the list of Natural Areas of National Interest and Natural Monuments, as per Law No. 5 of 6 March 2000	[74]
	Sârca Podu Iloaiei	Since 2016, the Sârca–Podu Iloaiei accumulations have been declared as Special Avifauna Protection Areas as an Integral Part of the European Ecological Network Natura 2000 in Romania	[75]
	Tansa-Belcești Plopi	Classified as a Special Protection Area, under Natura 2000 since October 2000	[76]
Moderate HR	Rediu Ciric III Aroneanu Ciurea Ciurbești Cucuteni Ezăreni	Although exhibiting moderate HR, the potential for upgrade to a superior level is quite high. Riparian vegetation, reed beds, and grassy marshes are examples of the GI components, typical for these reservoirs. Their proximity to the highly urbanized area of Iași confers multi-functionality, increasing their importance, placing them as emerging urban GIY–GI infrastructure.	[34,38,39,41,48]
Low HR	Vânători Bârca Cârlig Cornet	Although specific ecological rehabilitation (small wetlands, grasslands, reed beds) could increase their resilience contribution, these systems are serving mainly to flood-control. The GIY contribution is significantly higher than that of the GI.	[35,37,39,49]

To analyze the HR uniformly across all reservoirs, three categories of indicators were employed:

(1) Green infrastructure (GI) development: the emergence and expansion of wetland areas, marshes and swamps, or reed beds, especially in reservoir tails and shallow margins; riparian vegetation belts and vegetated slopes.
(2) Evidence of functional green-gray integration (e.g., dense vegetation increases hydraulic roughness, which attenuates the peaks of flash floods; wetland plants buffer droughts by acting as sponges, trapping and releasing water gradually).
(3) Institutional and administrative indicators (e.g., the administrative authority's periodic reports, inclusion in protected natural areas), which are used as supporting, non-deterministic factors.

Using the available historical data, land-use maps, field observations, the literature records, and present functioning features from administrative technical reports, each reservoir was qualitatively assessed regarding the degree of hybrid resilience. Based on a combination of these indicators, three classes of reservoirs (hybridization levels) were identified (Table 15):

(1) High HR: Defined by well-developed natural ecosystems that actively interact with gray infrastructure to mitigate floods and droughts.
(2) Moderate HR: Partial or emerging green infrastructure that provides gray infrastructure with complementary ecological support, with clear potential for upgrading the hybridization level.
(3) Low HR: The ecological component is underdeveloped, and the gray infrastructure dominates the system.

The HR classes presented in Table 15 reflect observed and documented levels of green-gray integration based on qualitative indicators, not quantified measures of ecosystem health or performance.

4. Conclusions

Using the Bahlui River basin as an illustrative example of a heavily regulated hydrographic basin in northeast Romania, this study offers a long-term, basin-scale evaluation of how artificial reservoirs help mitigate hydrological extremes.

After more than 50 years of operation, the analysis shows that flood control is still the most reliable and enduring reservoir function. Despite infrastructure aging, sedimentation, changing land use and urbanization levels, and fluctuating management priorities, peak-flow attenuation remains effective across the reservoir network, confirming the enduring role of artificial reservoirs in flood-risk reduction.

On the other hand, after socioeconomic changes started in 1989, drought mitigation functions, such as irrigation and industrial water supply, have significantly diminished. Though this slow decline has not resulted in a complete loss of drought-buffering capability. Instead, the establishment of riparian vegetation, wetlands, marshy reservoir tails, and reed beds are examples of natural systems that have progressively enhanced passive water storage and low-flow buffering. Over time, various levels of functional integration between gray infrastructures and naturally occurring green components have developed. The concept of hybrid hydrological resilience is used to explain this long-term evolution as a transition from purely engineered control toward multifunctional green-gray systems. It is important to note that hybrid resilience represents a degree of functional integration between naturally occurring green components and man-made gray infrastructure, and not a measure of ecological health. Hybrid resilience does not imply ecological perfection; it reflects the capacity of artificial and natural elements to operate jointly and adaptively under real-world constraints, including land-use pressures, infrastructure aging, and climate change.

Owing to its unique features, the Bahlui River basin represents an illustrative case of unplanned hybrid resilience emergence. It demonstrates how aged artificial reservoirs can maintain effective flood-control performance while gradually developing complementary ecological functions that support drought mitigation. The reservoirs' long-term resistance to hydrological extremes can be enhanced in an economical, environmentally responsible, and flexible manner by identifying, controlling, and eventually designing hybrid resilience.

Author Contributions: Conceptualization: N.M. and M.-T.N.; methodology: A.-I.B.; software: M.G.B. and D.T.; validation: V.B., C.D.B. and Ș.C.; formal analysis: A.-I.B.; investigation: C.D.B.; resources: Ș.C.; data curation: D.T. and V.B.; writing—original draft preparation: N.M. and M.-T.N.; writing—review and editing: M.-T.N.; visualization: M.G.B.; supervision: N.M.; project administration: Ș.C.; funding acquisition: N.M. All authors have read and agreed to the published version of the manuscript.

Funding: This research received no external funding.

Data Availability Statement: Data are available upon request.

Conflicts of Interest: The authors declare no conflicts of interest.

References

1. Rahmani, F.; Fattahi, M.H. Investigation of alterations in droughts and floods patterns induced by climate change. *Acta Geophys.* **2024**, *72*, 405–418. [CrossRef]
2. Xiong, J.; Yang, Y. Climate Change and Hydrological Extremes. *Curr. Clim. Change Rep.* **2024**, *11*, 1. [CrossRef]

3. Hodgkins, G.A.; Renard, B.; Whitfield, P.H.; Laaha, G.; Stahl, K.; Hannaford, J.; Burn, D.H.; Westra, S.; Fleig, A.K.; Araújo Lopes, W.T.; et al. Climate Driven Trends in Historical Extreme Low Streamflows on Four Continents. *Water Resour. Res.* **2024**, *60*, e2022WR034326. [CrossRef]
4. Granata, F.; Zhu, S.; Di Nunno, F. Hydrological extremes in the Mediterranean basin: Interactions, impacts, and adaptation in the face of climate change. *Reg. Environ. Change* **2025**, *25*, 100. [CrossRef]
5. Li, W.; Maharjan, S.; Fisher, J.B.; Piechota, T.; El-Askary, H. Escalating Hydrological Extremes and Whiplashes in the Western U.S.: Challenges for Water Management and Frontline Communities. *Earth's Future* **2025**, *13*, e2024EF005447. [CrossRef]
6. Newton, B.; Spence, C. James buttle review: A resilience framework for physical hydrology. *Hydrol. Process.* **2023**, *37*, e14926. [CrossRef]
7. Miralles-Wilhelm, F.; Matthews, J.H.; Karres, N.; Abell, R.; Dalton, J.; Kang, S.-T.; Liu, J.; Maendly, R.; Matthews, N.; McDonald, R.; et al. Emerging themes and future directions in watershed resilience research. *Water Secur.* **2023**, *18*, 100132. [CrossRef]
8. Granata, F.; Di Nunno, F. Pathways for Hydrological Resilience: Strategies for Adaptation in a Changing Climate. *Earth Syst. Environ.* **2025**. [CrossRef]
9. Dinca, L.; Murariu, G.; Lupoae, M. Understanding the Ecosystem Services of Riparian Forests: Patterns, Gaps, and Global Trends. *Forests* **2025**, *16*, 947. [CrossRef]
10. Rockström, J.; Falkenmark, M.; Allan, T.; Folke, C.; Gordon, L.; Jägerskog, A.; Kummu, M.; Lannerstad, M.; Meybeck, M.; Molden, D.; et al. The unfolding water drama in the Anthropocene: Towards a resilience-based perspective on water for global sustainability. *Ecohydrology* **2014**, *7*, 1249–1261. [CrossRef]
11. Di Baldassarre, G.; Martinez, F.; Kalantari, Z.; Viglione, A. Drought and flood in the Anthropocene: Feedback mechanisms in reservoir operation. *Earth Syst. Dynam.* **2017**, *8*, 225–233. [CrossRef]
12. DeFries, R.S.; Rudel, T.; Uriarte, M.; Hansen, M. Deforestation driven by urban population growth and agricultural trade in the twenty-first century. *Nat. Geosci.* **2010**, *3*, 178–181. [CrossRef]
13. Singh, R.; Tiwari, A.K.; Singh, G.S. Managing riparian zones for river health improvement: An integrated approach. *Landsc. Ecol. Eng.* **2021**, *17*, 195–223. [CrossRef]
14. Zhang, J.; Shang, Y. Nexus of dams, reservoirs, climate, and the environment: A systematic perspective. *Int. J. Environ. Sci. Technol.* **2023**, *20*, 12707–12716. [CrossRef]
15. Kellner, E. The controversial debate on the role of water reservoirs in reducing water scarcity. *WIREs Water* **2021**, *8*, e1514. [CrossRef]
16. Połomski, M.; Wiatkowski, M. Impounding Reservoirs, Benefits and Risks: A Review of Environmental and Technical Aspects of Construction and Operation. *Sustainability* **2023**, *15*, 16020. [CrossRef]
17. Contreras, R.J.; Escuder-Bueno, I. Dam Safety History and Practice: Is There Room for Improvement? *Infrastructures* **2023**, *8*, 171. [CrossRef]
18. Erpicum, S.; Crookston, B.M.; Bombardelli, F.; Bung, D.B.; Felder, S.; Mulligan, S.; Oertel, M.; Palermo, M. Hydraulic structures engineering: An evolving science in a changing world. *WIREs Water* **2021**, *8*, e1505. [CrossRef]
19. Kondolf, M.; Yi, J. Dam Renovation to Prolong Reservoir Life and Mitigate Dam Impacts. *Water* **2022**, *14*, 1464. [CrossRef]
20. Angelakis, A.N.; Baba, A.; Valipour, M.; Dietrich, J.; Fallah-Mehdipour, E.; Krasilnikoff, J.; Bilgic, E.; Passchier, C.; Tzanakakis, V.A.; Kumar, R.; et al. Water Dams: From Ancient to Present Times and into the Future. *Water* **2024**, *16*, 1889. [CrossRef]
21. Lu, M.; Merwade, V. From single to multi-purpose reservoir: A framework for optimizing reservoir efficiency. *J. Am. Water Resour. Assoc.* **2024**, *60*, 1144–1161. [CrossRef]
22. Kellner, E.; Brunner, M.I. Reservoir Governance in World's Water Towers Needs to Anticipate Multi-purpose Use. *Earth's Future* **2021**, *9*, e2020EF001643. [CrossRef]
23. Karami, S.; Karami, E. Sustainability assessment of dams. *Environ. Dev. Sustain.* **2020**, *22*, 2919–2940. [CrossRef]
24. Meng, Y.; Zhang, H.; Jiang, P.; Guan, X.; Yan, D. Quantitative assessment of safety, society and economy, sustainability benefits from the combined use of reservoirs. *J. Clean. Prod.* **2021**, *324*, 129242. [CrossRef]
25. Wu, Y.; Sun, J.; Hu, B.; Xu, Y.J.; Rousseau, A.N.; Zhang, G. Can the combining of wetlands with reservoir operation reduce the risk of future floods and droughts? *Hydrol. Earth Syst. Sci.* **2023**, *27*, 2725–2745. [CrossRef]
26. Marcoie, N.; Chihaia, Ș.; Hrăniciuc, T.A.; Balan, C.D.; Drăgoi, E.N.; Nechita, M.-T. Linking Nutrient Dynamics with Urbanization Degree and Flood Control Reservoirs on the Bahlui River. *Water* **2024**, *16*, 1322. [CrossRef]
27. Marcoie, N.; Toma, I.O.; Chihaia, Ș.; Hrăniciuc, T.A.; Toma, D.; Balan, C.D.; Drăgoi, E.N.; Nechita, M.-T. Anthropogenic River Segmentation Case Study: Bahlui River from Romania. *Hydrology* **2025**, *12*, 224. [CrossRef]
28. Ionuț, M. *Bazinul Hidrografic Bahlui—Studiu Hidrologic*; Facultatea de Geografie şi Geologie, Universitatea "Alexandru Ioan Cuza" Iaşi: Iasi, Romania, 2009.
29. Minea, I. The evaluation of the water chemistry and quality for the lakes from the south of the Hilly Plain of Jijia (Bahlui drainage basin). *Lakes Reserv. Ponds* **2010**, *4*, 131–144.

30. Ludikhuize, D.; Savin, A.; Schropp, M. *A Sobek Model for the Bahlui River*; Rijksinstituut voor Integraal Zoetwaterbeheer en Afvalwaterbehandeling (RWS, RIZA): Lelystad, The Netherlands, 2004; 49p.
31. Minea, I. Minimum discharge in Bahlui basin and associated hydrologic risks. *Aerul si Apa. Compon. Ale Mediu.* **2010**, 508–515.
32. Mediului, M. *Atlasul Cadastrului Apelor din România*; Editura Romcart SA: București, Romania, 1992; p. 448.
33. ANPA. Regulament de exploatare: Acumulare Ezăreni. Râul Ezăreni. Bazinul hidrografic Prut. *Administraţia Naţională "Apele Române", Direcţia Apelor Prut* **2010**.
34. ANPA. Regulament de exploatare: Acumulare Ciurbești. Râul Locii. Bazinul hidrografic Prut. *Administraţia Naţională "Apele Române", Direcția Apelor Prut* **2010**.
35. ANPA. Regulament de exploatare: Acumulare Vânători. Râul Cacaina. Bazinul hidrografic Prut. *Administraţia Națională "Apele Române", Direcţia Apelor Prut* **2009**.
36. ANPA. Regulament de exploatare: Acumulare Sârca. Râul Valea Oii. Bazinul hidrografic Prut. *Administraţia Națională "Apele Române", Direcţia Apelor Prut* **2009**.
37. ANPA. Regulament de exploatare: Acumulare Cornet. Râul Cornet. Bazinul hidrografic Prut. *Administraţia Națională "Apele Române", Direcţia Apelor Prut* **2009**.
38. ANPA. Regulament de exploatare: Ciric III. Râul Ciric. Bazinul hidrografic Prut. *Administraţia Naţională "Apele Române", Direcția Apelor Prut* **2009**.
39. ANPA. Regulament de exploatare: Acumulare Cârlig. Râul Cacaina. Bazinul hidrografic Prut—Bârlad. *Administraţia Națională "Apele Române", Directia Apelor Prut* **2009**.
40. ANPA. Regulament de exploatare: Acumularea Pârcovaci, Râul Bahlui, Bazinul hidrografic Prut. *Administraţia Națională "Apele Române", Direcția Apelor Prut* **2009**.
41. ANPA. Regulament de exploatare: Acumularea Rediu. Râul Rediu. Bazinul hidrografic Prut. *Administrația Națională "Apele Române", Direcţia Apelor Pru42* **2009**.
42. Societatea de Construcții, Asamblări, Sarcini și Acoperișuri. *Regulament de Exploatare: Amenajare Hidrotehnică Chirița*; Râul Chirița, Bazinul hidrografic Prut: Iași, Romania, 2023.
43. ANPA. Regulament de exploatare: Acumularea Tansa Belcesti. Râul Bahlui. Districtul de bazin hidrografic Prut—Bârlad. *Administrația Națională Apele Române, Administrația Bazinală de Apă Prut—Bârlad* **2021**.
44. ANPA. Regulament de exploatare: Acumularea Plopi. Râul Gurguiata. Bazinul hidrografic Prut. *Administrația Națională "Apele Române", Administraţia Bazinală de Apă Prut Bârlad* **2017**.
45. ANPA. Regulament de exploatare: Acumulare Podu Iloaiei. Curs de apă Bahlueț. Bazinul hidrografic Prut. *Administrația Națională "Apele Române", Administraţia Bazinală de Apă Prut Bârlad* **2014**.
46. ANPA. Regulament de exploatare Aroneanu. Râul Ciric. Bazin hidrografic Prut. *Administrația Națională "Apele Române", Administrația Bazinală de Apă Prut—Bârlad* **2013**.
47. ANPA. Regulament de exploatare: Acumularea Cucuteni. Râul Voinești. Districtul de bazin hidrografic Prut—Bârlad. *Administrația Națională "Apele Române", Administraţia Bazinală de Apă Prut—Bârlad* **2012**.
48. ANPA. Regulament de exploatare: Aculumarea Ciurea. Râul Nicolina. Districtul de bazin hidrografic Prut—Bârlad. *Administrația Națională "Apele Române", Administrația Bazinală de Apă Prut—Bârlad* **2010**.
49. ANPA. Regulament de exploatare acumularea Bârca. Râul Locii. Bazinul hidrografic Prut. *Administrația Națională "Apele Române", Administrația Bazinală de Apă Prut—Bârlad* **2010**.
50. Dumitrache, L.; Zamfir, D.; Nae, M.; Simion, G.; Stoica, I.-V. The Urban Nexus: Contradictions and Dilemmas of (Post) Communist (Sub) Urbanization in Romania. *Hum. Geogr. J. Stud. Res. Hum. Geogr.* **2016**, *10*, 38–50. [CrossRef]
51. Vincze, E. Deindustrialization and the real-estate–development–driven housing regime. The case of Romania in global context. *Stud. Univ. Babes-Bolyai-Sociol.* **2023**, *68*, 25–73. [CrossRef]
52. Ubay-Anongphouth, I.O.; Alfaro, M. Delayed instabilities of water-retaining earth structures. *Front. Built Environ.* **2022**, *8*, 927137. [CrossRef]
53. Mitchell, R.J. Earth dams. In *Earth Structures Engineering*; Mitchell, R.J., Ed.; Springer: Dordrecht, The Netherlands, 1983; pp. 163–218.
54. Pytharouli, S.; Michalis, P.; Raftopoulos, S. From Theory to Field Evidence: Observations on the Evolution of the Settlements of an Earthfill Dam, over Long Time Scales. *Infrastructures* **2019**, *4*, 65. [CrossRef]
55. Agarwal, B.; Dobay, K.M.; Sabates-Wheeler, R. Revisiting group farming in a post-socialist economy: The case of Romania. *J. Rural Stud.* **2021**, *81*, 148–158. [CrossRef]
56. Deacu, C. The collapse of the state industry in Romania: Between political and economic drivers. *Hum. Geogr. J. Stud. Res. Hum. Geogr.* **2016**, *10*, 116–127.
57. EU. *EU Water Framework Directive (2000/60/EC)*; EU: Brussels, Belgium, 2000.
58. European Parliament and the Council of the European Union. Directive 2007/60/EC on the assessment and management of flood risks. *Off. J. Eur. Union* **2007**, *L288*, 27–34.

59. Council of the European Union. Council Directive 92/43/EEC on the conservation of natural habitats and of wild fauna and flora (Habitats Directive). *Off. J. Eur. Communities* **1992**, *L206*, 7.
60. Bâra, A.; Văduva, A.G.; Oprea, S.-V. Anomaly Detection in Weather Phenomena: News and Numerical Data-Driven Insights into the Climate Change in Romania's Historical Regions. *Int. J. Comput. Intell. Syst.* **2024**, *17*, 134. [CrossRef]
61. Nagavciuc, V.; Scholz, P.; Ionita, M. Hotspots for warm and dry summers in Romania. *Nat. Hazards Earth Syst. Sci.* **2022**, *22*, 1347–1369. [CrossRef]
62. Adamo, N.; Al-Ansari, N.; Sissakian, V.; Laue, J.; Knutsson, S. Dams safety: Inspections, safety reviews, and legislations. *J. Earth Sci. Geotech. Eng.* **2021**, *11*, 109–143. [CrossRef]
63. Holling, C. Resilience and Stability of Ecological Systems. *Annu. Rev. Ecol. Syst.* **1973**, *4*, 1–23. [CrossRef]
64. Holling, C. *Engineering Resilience Versus Ecological Resilience*; Engineering Within Ecological Constraints/National Academy Press: Washington, DC, USA, 1996.
65. Folke, C. Resilience: The emergence of a perspective for social–ecological systems analyses. *Glob. Environ. Change* **2006**, *16*, 253–267. [CrossRef]
66. Gunderson, L.H. Ecological Resilience—In Theory and Application. *Annu. Rev. Ecol. Evol. Syst.* **2000**, *31*, 425–439. [CrossRef]
67. Mayar, K.; Carmichael, D.G.; Shen, X. Resilience and Systems—A Review. *Sustainability* **2022**, *14*, 8327. [CrossRef]
68. Walker, B.; Holling, C.S.; Carpenter, S.R.; Kinzig, A. Resilience, adaptability and transformability in social–ecological systems. *Ecol. Soc.* **2004**, *9*, 5. [CrossRef]
69. Folke, C.; Carpenter, S.R.; Walker, B.; Scheffer, M.; Chapin, T.; Rockström, J. Resilience thinking: Integrating resilience, adaptability and transformability. *Ecol. Soc.* **2010**, *15*, 20. [CrossRef]
70. Nakamura, F. Concept and application of green and hybrid infrastructure. In *Green Infrastructure and Climate Change Adaptation: Function, Implementation and Governance*; Springer Nature: Singapore, 2022; pp. 11–30.
71. Hendricks, M.D.; Dowtin, A.L. Come hybrid or high water: Making the case for a Green–Gray approach toward resilient urban stormwater management. *J. Am. Water Resour. Assoc.* **2023**, *59*, 885–893. [CrossRef]
72. ANMAP, Romania's Protected Natural Areas. National Agency for Protected Natural Areas. 2025. Available online: https://ananp.gov.ro/ariile-naturale-protejate-ale-romaniei/# (accessed on 10 November 2025).
73. Paliament, R. *The Emergency Ordinance for the Amendment of Law no. 5/2000 Regarding the Approval of the National Territorial Planning Plan—Section III—Protected Areas, Official Monitor*; Emergency Ordinance no. 49 of 31 August 2016 (689); Romania Government: Bucharest, Romania, 2016.
74. Parliament, R. *Law on the Approval of the National Territory Planning Plan—Section III—Protected areas, Official Monitor*; Law no.5 of 6 March 2000 (152/12 April); Romania Government: Bucharest, Romania, 2000.
75. Romania Government. *Decision no. 663 of 14 September 2016 on the Establishment of the Protected Natural Area Regime and the Declaration of the Special Avifauna Protection Areas as an Integral Part of the European Ecological Network Natura 2000 in Romania, Official Monitor, (743)*; Romania Government: Bucharest, Romania, 2016.
76. EEA. *Acumularile Belcesti, Natura 2000 Site, Code ROSPA0109*; European Environment Agency: Copenhagen, Denmark, 2025. Available online: https://ananp.gov.ro/ariile-naturale-protejate-ale-romaniei/# (accessed on 10 November 2025).

applied sciences

MDPI

Article

GIS-Based Assessment of Photovoltaic and Green Roof Potential in Iași, Romania

Otilia Pitulac [1,*], Constantin Chirilă [2], Florian Stătescu [1] and Nicolae Marcoie [1]

[1] Department of Hydroamelioration and Environmental Protection, Faculty of Hydrotechnical Engineering, Geodesy and Environmental Engineering, "Gheorghe Asachi" Technical University of Iasi, Professor Dimitrie Mangeron Boulevard 67, 700050 Iasi, Romania; florian.statescu@academic.tuiasi.ro (F.S.); nicolae.marcoie@academic.tuiasi.ro (N.M.)

[2] Department of Terrestrial Measurements and Cadastre, Faculty of Hydrotechnical Engineering, Geodesy and Environmental Engineering, "Gheorghe Asachi" Technical University of Iasi, Professor Dimitrie Mangeron Boulevard 67, 700050 Iasi, Romania; constantin.chirila@academic.tuiasi.ro

* Correspondence: otilia.pitulac@student.tuiasi.ro; Tel.: +40-0747844774

Abstract

Urban areas are increasingly challenged by the combined effects of climate change, rapid population growth, and high energy demand. The integration of renewable energy systems, such as photovoltaic (PV) panels, and nature-based solutions, such as green roofs, represents a key strategy for sustainable urban development. This study evaluates the spatial potential for PV and green roof implementation in Iași, Romania, using moderate to high-resolution geospatial datasets, including the ALOS AW3D30 Digital Surface Model (DSM) and the Copernicus Urban Atlas 2018, processed in ArcMap 10.8.1 and ArcGIS Pro 2.6.0. Solar radiation was computed using the Area Solar Radiation tool for the average year 2023, while roof typology (flat vs. pitched) was derived from slope analysis. Results show significant spatial heterogeneity. The Copou neighborhood has the highest PV-suitable roof share (73.6%) and also leads in green roof potential (46.6%). Integrating PV and green roofs can provide synergistic benefits, improving energy performance, mitigating urban heat islands, managing stormwater, and enhancing biodiversity. These findings provide actionable insights for urban planners and policymakers aiming to prioritize green infrastructure investments and accelerate the local energy transition.

Keywords: GIS; photovoltaic potential; green roofs; solar radiation; urban sustainability

Academic Editor: Constantinos A. Balaras

Received: 21 August 2025
Revised: 25 September 2025
Accepted: 1 October 2025
Published: 7 October 2025

Citation: Pitulac, O.; Chirilă, C.; Stătescu, F.; Marcoie, N. GIS-Based Assessment of Photovoltaic and Green Roof Potential in Iași, Romania. *Appl. Sci.* **2025**, *15*, 10786. https://doi.org/10.3390/app151910786

1. Introduction

Urban areas face increasing challenges related to climate change, including heat stress, flooding, and energy inefficiency. Green roofs and photovoltaic (PV) systems are widely recognized as nature-based and technological solutions that mitigate these impacts [1]. This study builds on established knowledge while providing an integrated spatial analysis of both strategies for Iași, Romania. Although recent advances in remote sensing and GIS enable highly detailed 3D city mapping through LiDAR or stereo-photogrammetry [2], such high-resolution datasets are not yet available for many medium-sized Eastern European cities, including Iași. In this context, the present study relies on the ALOS AW3D30 DSM with a 30 m resolution. While this represents a coarse scale for rooftop-level assessments, it provides a reproducible and accessible baseline for large-area analysis in the absence of LiDAR data. By explicitly acknowledging these limitations, the study positions itself as a first exploratory step toward quantifying rooftop photovoltaic and green roof potential

in Iași. Solar photovoltaic (PV) technologies are increasingly adopted for their rapidly declining costs and strong policy support worldwide. Installation costs have dropped by over 80% in the last decade, making solar energy the cheapest source of electricity today [3–5]. At the same time, large-scale studies show that rooftop PV could cover up to 24% of the EU's electricity demand [6]. Green roofs provide multiple adaptation benefits: reducing building energy demand, retaining 40–80% of precipitation annually [7], lowering roof surface temperatures by several degrees [8,9], and improving biodiversity [10–12]. Recent work highlights their potential role in carbon sequestration and multifunctional uses, such as rooftop farming, which can simultaneously mitigate the urban heat island effect [13–15] and increase food production [16]. GIS-based methods are increasingly used to identify suitable roof surfaces, considering slope, area, water access, and urban functional zones [17]. To properly address these objectives, it is essential to establish clear and transparent criteria for defining when a rooftop can be considered suitable [18]. Recent literature indicates that, for photovoltaic systems, the key factors include a minimum annual solar radiation threshold of $\geq$1000 kWh/m^2/year ($\approx$114 W/m^2), roof slope (with $\geq$20° generally favorable for optimal solar capture in Romania), orientation towards the south or southwest, the avoidance of significant shading, the availability of a minimum continuous surface area (>10 m^2), and sufficient structural durability to accommodate an additional load of 15–25 kg/m^2 [19]. In the case of green roofs, the slope criterion serves primarily as a delimiter: flat or nearly flat roofs ($\leq$20°) are considered suitable for the implementation of extensive systems, while pitched roofs (>20°) are generally excluded from feasibility. Additional technical requirements include adequate load-bearing capacity (>60 kg/m^2 for extensive systems), substrate thickness (50–150 mm), and the presence of reliable drainage and waterproofing layers [20,21]. By integrating these quantitative thresholds, the study strengthens methodological rigor and ensures comparability with international approaches, while also clarifying the specific conditions under which PV and green roof solutions can realistically be implemented in Iași.

Despite an abundance of research on urban green infrastructure and renewable energy, the geographic coverage of these studies is uneven. The literature has concentrated predominantly on megacities in the developed world (Western Europe, North America, and East Asia) and on national capitals, where environmental concerns have driven early "smart city" or "green city" initiatives. In contrast, medium-sized cities in Eastern Europe have benefited from fewer applied studies of urban green technologies. Romania, for example, has considerable solar energy potential and had already met the EU's 2020 renewable energy targets for renewables by 2017 [22], yet research on integrating photovoltaic panels and green roofs in the built environment has largely been limited to high-level national strategies or to the context of the capital city (Bucharest). There are some green–blue infrastructure planning initiatives for the Bucharest metropolitan area and isolated studies on the dynamics of urban green spaces in post-socialist cities. However, quantitative approaches that combine LiDAR/DSM data with thematic urban maps to directly assess rooftop solar and green roof potential remain rare in secondary cities of the region. Another notable gap in the literature concerns validation. While many GIS-based assessments quantify technical potential, few verify their findings against actual photovoltaic installations or green roof deployments, especially in the Romanian context. In Iași, there is currently no systematic comparison between modeled PV-suitable rooftops and existing solar arrays. This study acknowledges this limitation and seeks to address the gap by highlighting the importance of linking geospatial analysis with real-world implementation data, thereby offering a more realistic perspective for policymakers. The municipality of Iași—Romania's second-largest city, with around 400,000 inhabitants and a major university center—illustrates this gap. Despite facing common urban challenges (pollution, traffic congestion, insufficient

per capita green space) and benefiting from favorable geographic conditions for solar energy, no comprehensive study has yet evaluated the neighborhood-scale potential for green technologies. This is significant because medium-sized cities like Iași concentrate a large share of Europe's urban population [23] and play an essential role in the green transition [24], requiring context-specific policies tailored to local economic, social, and climatic conditions [25]. Compared to megacities, medium-sized urban centers often face more acute constraints, such as limited financial and technical resources, less specialized infrastructure, and faster demographic or spatial transformations. These characteristics make the deployment of renewable energy and green infrastructure both urgent and highly representative of challenges faced by many European cities of similar scale. To address this need, the present study evaluates rooftop solar potential by generating a solar radiation map for Iași's buildings using ArcMap 10.8.1. The DSM of Iași combined with building footprints, was used to isolate rooftop elevations. Although the ALOS AW3D30 DSM offers only moderate resolution, it provides a practical and reproducible solution in the absence of local LiDAR data. Similarly, NextGIS Data building footprints, while subject to positional inaccuracies due to crowdsourcing, constitute an accessible and comprehensive dataset where official cadastral records are lacking. By acknowledging these limitations, the study ensures transparency while providing meaningful insights into neighborhood-scale solar suitability.

2. Materials and Methods

2.1. The Location of Iași Municipality

Iași is situated in the northeastern part of Romania (Moldavia region), Figure 1, and has a humid continental climate with four distinct seasons; summers are warm (often exceeding 35 °C) and winters are cold, with moderate snowfall and nighttime temperatures below −15 °C [26]. Annual precipitation is relatively modest (around 521 mm per year) in Iași [27], and the city enjoys roughly 2100 sunshine hours annually [28] (about 210 sunny days). This geographical setting yields a moderate solar energy influx on horizontal surfaces (~1000–1300 kWh/m^2/year), with around 600–800 kWh/m^2/year of that total being practically exploitable for photovoltaics. Such solar potential indicates favorable conditions for PV panel deployment as a renewable energy solution in the Iași area. Furthermore, the region's climate variability—alternating dry spells with intense rainfall events—highlights the need for nature-based urban adaptations; green roofs can alleviate urban heat island effects [29] during hot summers and reduce stormwater runoff by retaining precipitation and enhancing evapotranspiration [30,31]. These features underscore how Iași's geographic and climatic profile is well-suited for integrating photovoltaic systems and green roofs as complementary sustainability measures in urban development.

2.2. Data Sources and Processing

The geospatial analysis was conducted for the Iași municipality, focusing on its urban neighborhoods as the study units. Various spatial datasets and GIS software, ArcGis Pro 2.6.0, were utilized to ensure a comprehensive evaluation. A digital surface model (DSM), Figure 2, of the study area with approximately 30 m resolution (ALOS World 3D—30 m, AW3D30) was obtained from the Japan Aerospace Exploration Agency (JAXA) and used as the primary elevation source [32]. The DSM represents a digital surface model, capturing both buildings and vegetation, rather than a bare-earth digital terrain model. Although suitable for regional assessments, this coarse resolution is a known limitation for rooftop-scale analysis, as it cannot capture fine-scale roof structures or shading [33]. Detailed vector data on urban land use were acquired from the Copernicus Urban Atlas 2018 dataset, which provides land use classifications for European cities [34]. Building

footprint data for Iași (in GeoPackage format) were sourced via NextGIS Data and local datasets, serving as the basis for identifying individual building structures. It should be noted that OpenStreetMap and NextGIS Data completeness and positional accuracy vary across the study area, and this represents an additional source of uncertainty [35]. To ensure spatial consistency and avoid distortions in the subsequent analyses, all input datasets were reprojected into the same national projected coordinate system, Stereo 70 (EPSG:3844). This procedure was applied uniformly to the digital surface model (DSM), the NextGIS Data building footprints, the cadastral footprints, and the administrative boundary of the municipality. Furthermore, processing environments were standardized by setting the Processing Extent and Mask to the municipal boundary, which guaranteed that all raster outputs (slope, solar radiation) and vector operations were spatially aligned and directly comparable. While the solar potential and slope-based roof classification were assessed at the scale of the entire municipality, the validation of OSM building footprints against cadastral data was performed on a representative sample area, the Copou neighborhood. This allowed the quantification of data accuracy and uncertainty in a controlled context, while ensuring methodological comparability at the municipal level. A temporal misalignment was acknowledged between the datasets: Urban Atlas land use data correspond to 2018, while solar radiation calculations were performed for the reference year 2023. This discrepancy may affect accuracy in areas with rapid urban development, where new buildings or land use changes occurred between 2018 and 2023. The potential influence of this misalignment was considered in the interpretation of results.

Figure 1. The location of Iași Municipality.

To assess the reliability of NextGIS Data building footprints, a random sample of buildings was compared with official cadastral records for selected neighborhoods. A small validation table was produced, showing the percentage of missing buildings in OSM (~7%), average horizontal offset (~2.5 m), and cases of misattributed building shapes. This step provided a quantitative estimate of data quality and ensured transparency regarding the potential propagation of spatial inaccuracies. The GIS processing was primarily carried out

using Esri's ArcGIS platform: ArcMap 10.8.1 and ArcGIS Pro. Key geoprocessing tools and functions employed in this study included Area Solar Radiation, Extract by Mask, Select By Location, Slope, Raster Calculator, Raster to Polygon, Zonal Statistics as Table, Spatial Join, Field Calculator, and Clip, among others, to derive the necessary thematic maps and statistics. For photovoltaic suitability, a threshold of $\geq$1000 kWh/m^2/year ($\approx$114 W/m^2) was adopted, in line with previous studies [36]. For green roofs, a slope criterion of $\leq 20^\circ$ was used to identify flat or nearly flat rooftops (terraces) considered preliminarily suitable for extensive systems. However, this classification is a GIS-based screening only and does not account for detailed structural conditions, which would require on-site verification. To evaluate the robustness of the methodology, a sensitivity analysis was performed. First, the slope classification was recalculated using three different thresholds (15°, 20°, 25°) to examine how the share of flat vs. pitched roofs varies under alternative assumptions. Second, the DSM-based solar radiation estimates were tested in selected subareas by resampling the raster at coarser and finer resolutions, simulating the effect of alternative datasets. These tests highlighted how dataset resolution and threshold selection influence the final results. Furthermore, spatial econometric tools were applied to analyze the distribution patterns. Global Moran's I and Geary's C statistics were calculated for rooftop solar radiation values and roof type distribution across neighborhoods, testing for overall spatial autocorrelation. Figure 3 illustrates the results of the Global Moran's I test, confirming the presence of clustered spatial patterns in rooftop solar potential, with a z-score of 1.74 and p-value < 0.10. To further test for spatial dependence in the photovoltaic potential, the analysis was extended by calculating Global Moran's I and Local Indicators of Spatial Association (LISA) in ArcGIS Pro. The input features were neighborhood polygons, and the input field corresponded to the mean annual solar radiation per rooftop (Solar_Mean). A contiguity-based spatial weights matrix (edges-only) was applied, with row standardization and Euclidean distance. This configuration ensured that the analysis captured both overall spatial autocorrelation and localized clustering patterns. In addition, Local Indicators of Spatial Association (LISA) were computed to identify statistically significant clusters (high–high and low–low) and spatial outliers. These results provided insights into whether solar potential and roof typologies were randomly distributed or concentrated in specific urban areas, strengthening the spatial interpretation of the study.

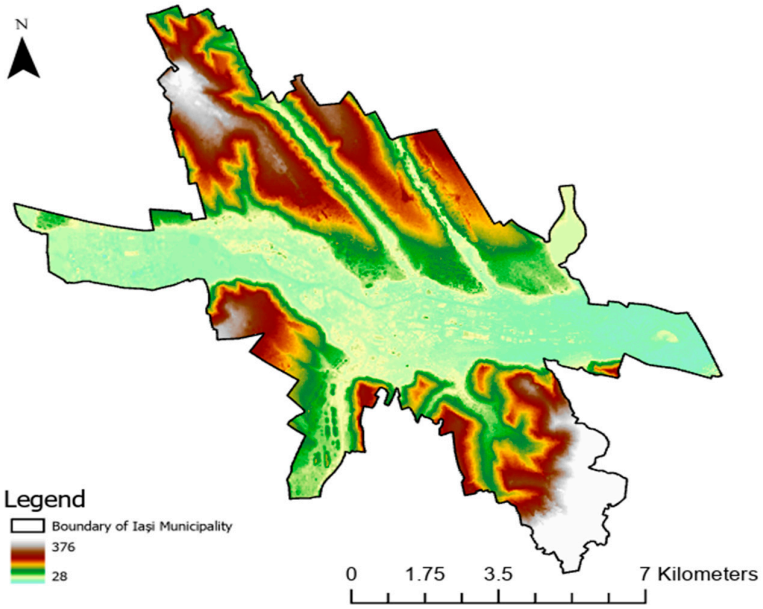

Figure 2. Digital surface model (DSM) of the Iași municipality (30 m resolution).

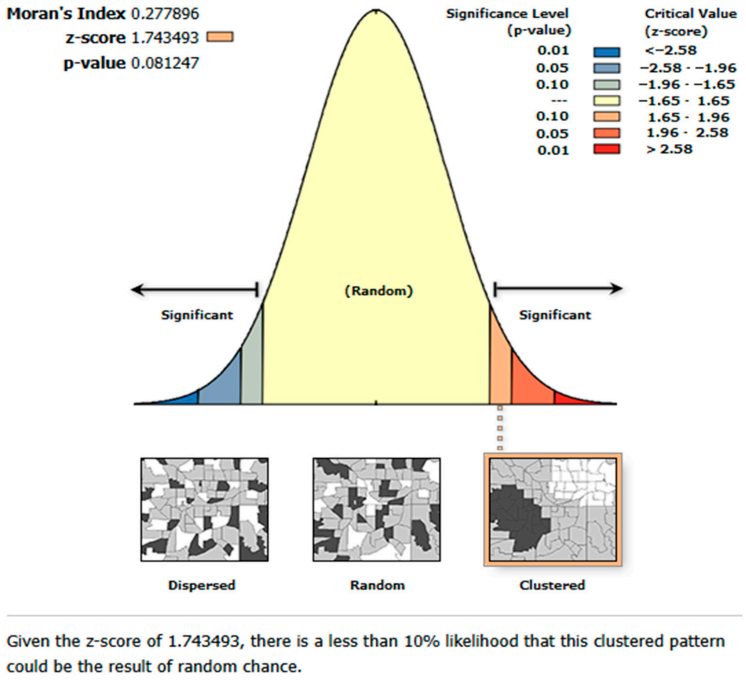

Figure 3. Results of the Global Moran's I test for rooftop solar potential in Iași neighborhoods (z-score = 1.74, *p*-value = 0.08).

For the solar potential assessment, the Area Solar Radiation tool was parameterized to compute global annual solar radiation (kWh/m^2/year) for the entire calendar year. Solar radiation values were calculated using the Area Solar Radiation tool in ArcGIS, parameterized for the entire calendar year 2023. The computation is based on long-term meteorological averages, which account for atmospheric conditions including cloud cover, rather than clear-sky assumptions. This approach provides annual mean values representative of realistic local climatic conditions. The resulting raster was then intersected with building footprints to estimate rooftop solar potential, using Zonal Statistics to derive mean and total radiation values per building. In line with thresholds reported in the literature, rooftops with average annual radiation above 114 W/m^2 (≈1000 kWh/m^2/year) were classified as suitable for photovoltaic installation. Figure 3 illustrates the DSM of Iași combined with building footprints, as used in the solar radiation analysis, highlighting the spatial resolution and its implications for rooftop-level evaluations.

The map highlights the spatial resolution of elevation data used for rooftop solar radiation assessment, including both terrain and built-up surfaces. The building footprints (Figure 4) were applied as a mask on the DSM (i.e., extracting DSM values only where buildings are present), yielding a raster of building elevation above sea level across the city. This step ensured that only the elevations corresponding to rooftops were considered for subsequent solar calculations (Figure 5). Next, the Area Solar Radiation tool in ArcMap was employed to compute the incoming solar radiation on these building surfaces. The analysis was set to cover an entire year (2023), calculating the average annual solar radiation (in W/m^2) received by each rooftop surface. The output is a raster map of solar radiation distribution across all building roofs, where each cell's value represents the potential solar energy received. To facilitate neighborhood-level analysis, the resulting solar radiation raster was clipped for each neighborhood using the Extract by Mask tool (with neighborhood polygons as the mask). This produced individual solar radiation maps for each urban district, which were later used to identify areas of high photovoltaic suitability. For thematic mapping purposes, the solar radiation values were classified using the Natural

Breaks (Jenks) method to highlight the variation in solar potential across roofs in a visually meaningful way.

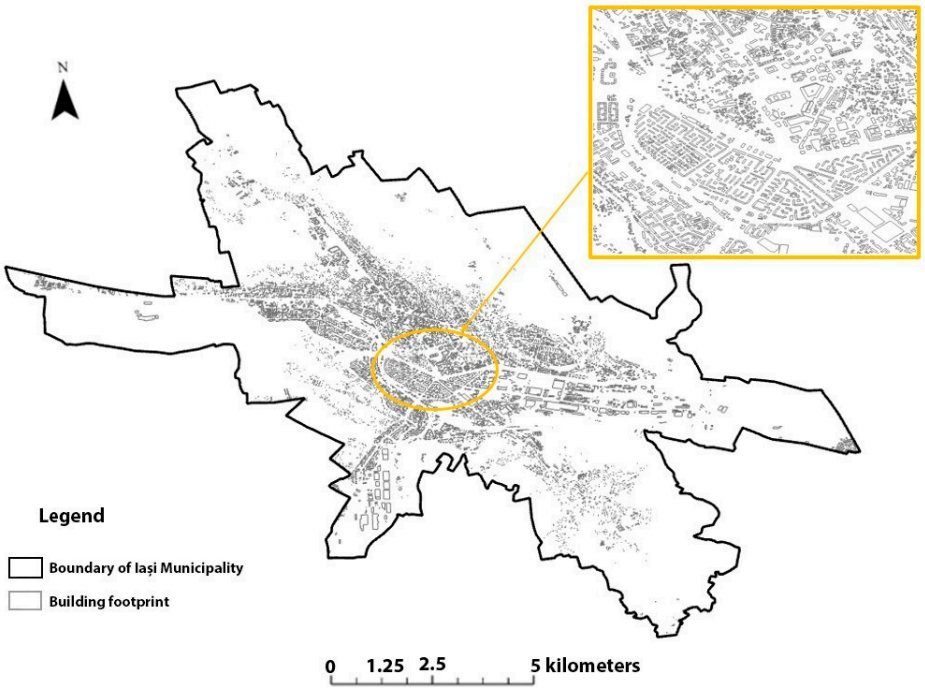

Figure 4. Iași Municipality building footprints.

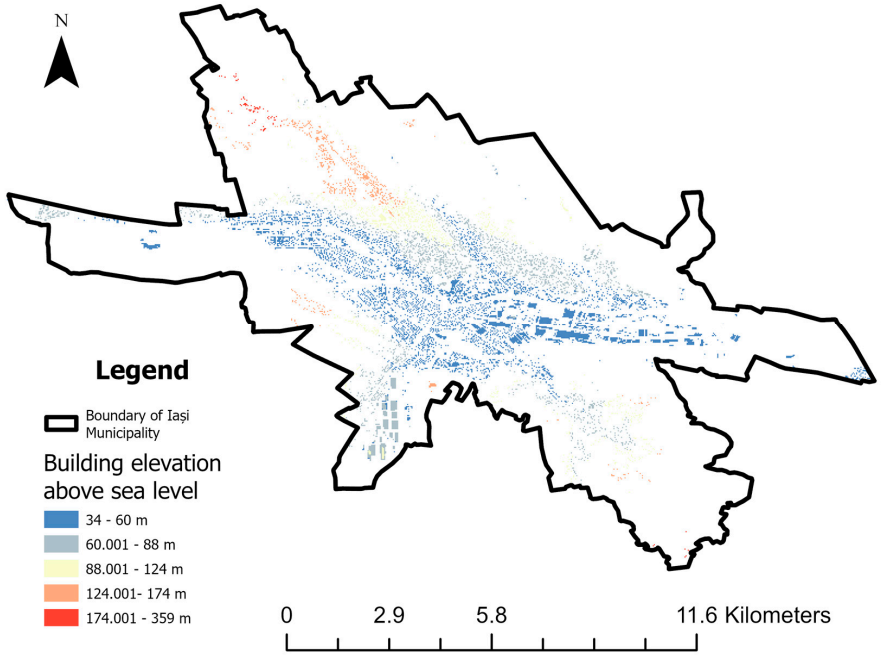

Figure 5. Building elevation above sea level distribution in Iași municipality derived from DSM values masked by building footprints.

Building elevations are expressed in meters above sea level and were subsequently used as input for slope derivation and rooftop solar radiation calculations. Assessment of the urban land use was performed to understand the context and constraints for implementing green technologies in each neighborhood. Using ArcGIS Pro, the Copernicus Urban Atlas 2018 vector data for Iași was imported and processed. The dataset provides detailed land use classes (e.g., various densities of residential fabric, industrial areas, green urban areas, etc.) across the city. To extract neighborhood-specific land use information, the

Select By Location tool was applied: for each neighborhood polygon, all land use polygons with a "Within" spatial relationship to that neighborhood were selected and extracted. This yielded a segmented land use map for each neighborhood, quantifying the types of land use present in that area. The resulting land use layers were symbolized by category (class) to produce thematic maps (such as the example city-wide land use map shown in Figure 6) that facilitate visual comparison of functional land use distribution among neighborhoods. An analysis of roof typology was performed to determine which buildings have flat roofs (suitable for green roof installation) versus sloped roofs. In ArcMap, the DSM was utilized to derive the slope of each roof surface across the city. The Slope tool (Spatial Analyst) was applied to the DSM to generate a raster of slope values (degrees) for all areas. This slope raster was then reclassified using Raster Calculator to differentiate flat versus sloped surfaces: an expression was applied to assign a value of 1 to areas with a slope below 20° and a value of 2 to areas with a slope $\geq$20°. The resulting binary raster (flat vs. sloped) was converted into vector format using the Raster to Polygon tool, preserving the geometry of roof outlines by opting not to simplify the polygons during conversion. To determine the roof type of each individual building, the above raster results were integrated with the building footprint layer. Using the Zonal Statistics as Table tool, we calculated the average slope within each building's footprint area. This produced a table of average roof slope values per building polygon. The table was then joined to the building footprint layer via a Spatial Join, associating each building with its mean roof inclination. Based on these values, a new attribute field was added to the building layer and populated using Field Calculator: buildings with an average slope under 20° were classified as having flat roofs (coded as 1), whereas those with an average slope of 20° or greater were classified as sloped roofs (coded as 2). Finally, the building footprints (now categorized by roof type) were clipped by neighborhood boundaries (Clip tool) to allow analysis of roof typology distribution in each area. This information on roof typology directly informs the potential for green roofs, since flat roof surfaces are generally suitable for supporting green roof installations. By identifying the proportion and area of flat roofs in each neighborhood, the relative potential for green roof implementation across the municipality could be estimated (Figure 7). It should be noted that this classification represents a GIS-based screening of roof slope only and does not account for structural load-bearing capacity, waterproofing conditions, or ownership constraints, which would require on-site verification before implementation

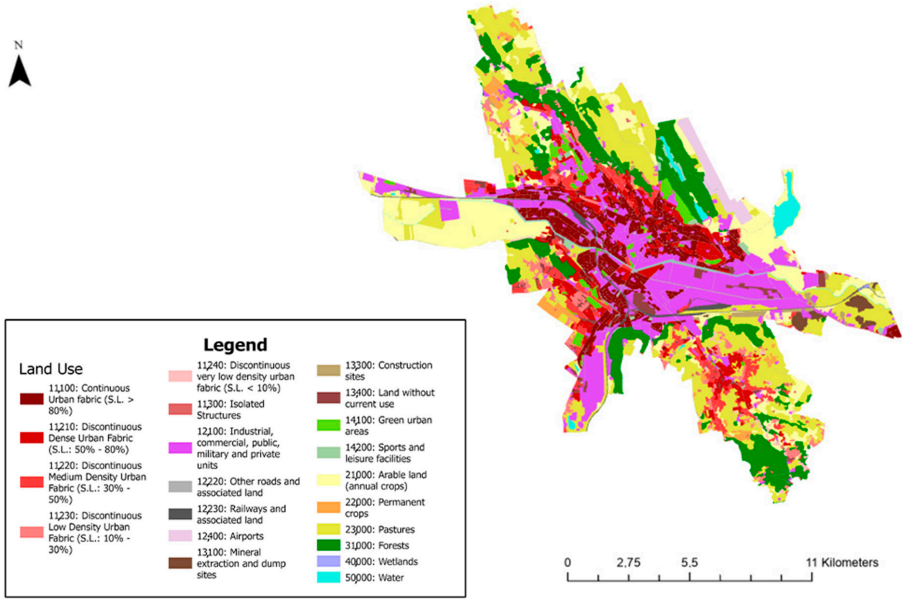

Figure 6. Land use map of the Iași municipality based on Urban Atlas 2018 Data.

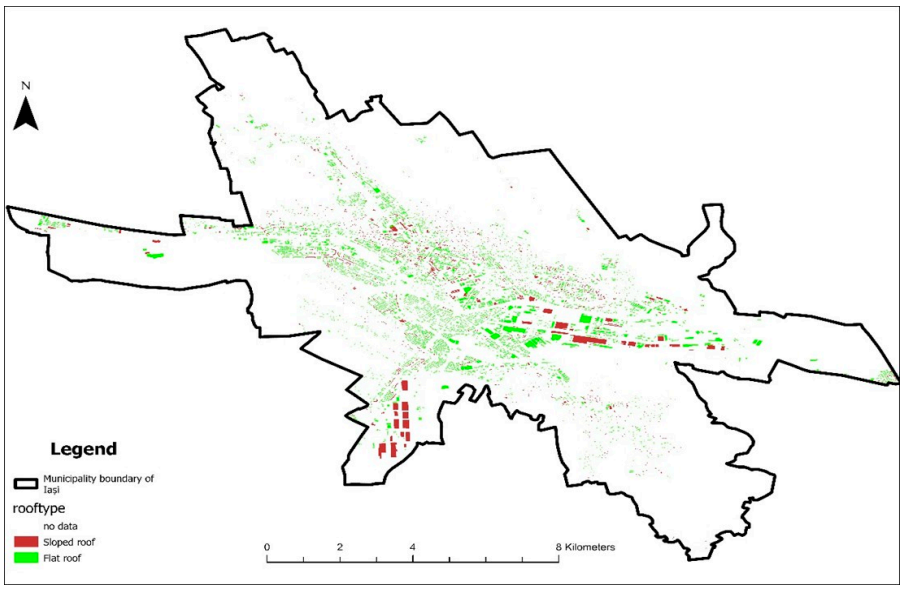

Figure 7. Geospatial analysis of roof type distribution within the Iași municipality.

2.3. Validation of OSM

To evaluate the reliability of NextGIS Data building footprints, a validation was conducted against official cadastral records available for the Copou neighborhood. This comparison was motivated by the need to quantify the uncertainty associated with volunteered geographic information (VGI) and to ensure methodological robustness for subsequent analyses. Both datasets (OSM and cadastral footprints) were reprojected into the national coordinate system, Stereo 70 (EPSG:3844), and clipped to the Copou boundary to ensure strict spatial comparability. The analysis focused on three quality dimensions commonly applied in spatial data validation:

Completeness—the proportion of cadastral building area captured by OSM;
Correctness—the proportion of OSM building area overlapping cadastral data;
Areal consistency—assessed through the Jaccard similarity index, expressing the ratio of intersection to union area between the two datasets.

The results (Table 1) show that OSM building footprints are relatively consistent with the corresponding cadastral data. The completeness index was 0.68, indicating that the cadastral database captures roughly two-thirds of the building footprints present in OSM. Correctness reached 1.04, suggesting that most OSM footprints align closely with cadastral buildings, even slightly exceeding them. The overall Quality Index (Jaccard index) was 0.69, confirming a moderate spatial agreement between the two datasets. These results demonstrate that, although OSM data are not fully up to date compared with cadastral records (which are updated almost in real time), the differences are moderate and do not compromise their applicability for neighborhood-scale analysis. The identified discrepancies mainly reflect missing buildings in cadastral data and small horizontal offsets (average ~2.5 m), which are consistent with previous VGI quality assessments.

In Romania, the official cadastral database does not yet fully capture the existing building stock, as the national cadastre implementation is still ongoing. Consequently, cadastral data provide only a partial representation of on-the-ground reality. A comparison with OSM shows that the number and spatial extent of buildings in the field often exceed those registered officially (by approximately 30%). This underlines the valuable potential of crowdsourced datasets as a complementary source for enhancing and validating official records, particularly in rapidly developing urban areas.

Table 1. Validation of OSM building footprints against cadastral data in Copou (m^2).

Indicator	Formula	Value (m^2)
A_OSM (m^2)	Building area from OSM	600,057.5294
A_CAD (m^2)	Building area from the cadastral data	390,752.5670
A_INT (m^2)	Intersection OSM ∩ cadastral	406,192.6012
Completeness	A_INT/A_OSM	0.68
Correctness	A_INT/A_CAD	1.04
Quality Index	A_INT/(A_OSM + A_CAD—A_INT)	0.69

3. Results

3.1. Photovoltaic Potential

The assessment of rooftop solar radiation highlights marked contrasts among neighborhoods. As illustrated in Figure 8A, rooftops in Copou predominantly fall into the higher radiation classes, represented by darker colors. Large contiguous areas of rooftops exceed the 114 W/m^2 threshold, confirming that approximately 73.6% of the roof area is suitable for PV installation. The presence of wide institutional and residential buildings, coupled with relatively open surroundings, explains the dominance of high-exposure zones. Bucium (Figure 8B) presents a contrasting situation, with only about 14% of rooftop surfaces meeting the thresholds for high annual radiation suitability. Although well-illuminated patches can still be identified across both residential and agricultural fringes, the overall share of suitable rooftops remains comparatively low. The map shows a continuous pattern of suitable roofs, indicating limited shading from nearby vegetation or topographic obstacles. Moara de Vânt (Figure 8D) displays alternating well-exposed and shaded zones. While certain clusters of rooftops receive high radiation, other sections appear fragmented, with scattered low-value patches. This spatial variability results in a medium share of suitable roofs, highlighting the influence of mixed urban and semi-rural morphology. By contrast, Țicău (Figure 8C) stands out as the least favorable area. The hillside topography and irregular street orientation produce large patches of rooftops in lower radiation categories, clearly visible in lighter tones on the map. Figure 8E compiles the legends used in Figure 8A–D, enabling consistent interpretation and visual comparison across neighborhoods. In summary, Section 3.1 reveals a clear spatial pattern: Copou and Bucium concentrate the most favorable conditions for rooftop PV, with large, contiguous areas of well-exposed rooftops, while Țicău remains the least suitable due to its topographic constraints and unfavorable orientations.

Beyond the spatial visualization of solar radiation (Figure 8A–D), Table 2 presents summary statistics of annual rooftop insolation per neighborhood. The results emphasize substantial contrasts in mean values and total roof areas exceeding the suitability threshold ($\geq$1000 $kWh/m^2/year$).

Table 2. Solar radiation statistics per neighborhood.

Neighborhood	Mean Radiation ($kWh/m^2/Year$)	Total Roof Area (m^2)	Suitable Roof Area $\geq$1000 $kWh/m^2/Year$ (m^2)
Copou	1050	558,660	41,1000
Bucium	1193	369,594	52,799
Moara de Vânt	1009	93,900	7163
Țicău	1027	69,100	960

Note: Mean and total radiation values derived from the Area Solar Radiation tool in ArcGIS Pro (2023). Threshold for photovoltaic suitability set at $\geq$1000 $kWh/m^2/year$.

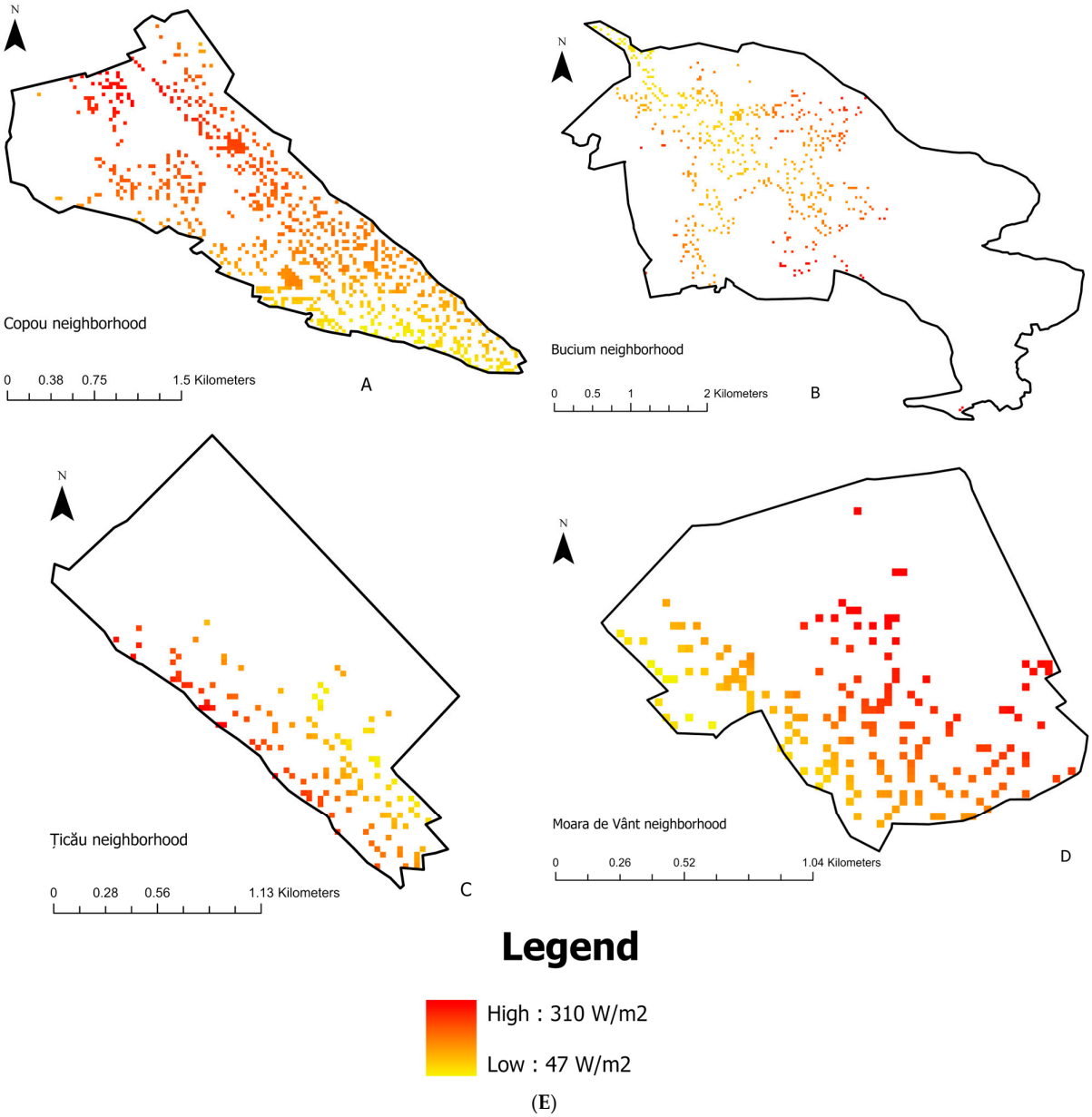

Figure 8. (**A**) Average annual rooftop solar radiation in the Copou neighborhood (W/m^2). Darker shades indicate rooftops receiving higher levels of incoming solar radiation, highlighting areas most suitable for photovoltaic (PV) deployment. (**B**) Average annual rooftop solar radiation in the Bucium neighborhood (W/m^2). Rooftops above the 1000 $kWh/m^2/year$ ($\approx$114 W/m^2) threshold are considered suitable for PV installation. (**C**) Average annual rooftop solar radiation in the Țicău neighborhood (W/m^2). Suitability is concentrated on unobstructed, south-facing rooftops. (**D**) Average annual rooftop solar radiation in the Moara de Vânt neighborhood (W/m^2). Light-colored rooftops correspond to lower solar exposure, reducing PV suitability. (**E**) Legend for figures (**A**–**D**). Average annual rooftop solar radiation (W/m^2) for the neighborhoods of Copou, Bucium, Moara de Vânt, and Țicău. Darker shades represent rooftops receiving higher solar radiation, with the suitability threshold set at $\geq$1000 $kWh/m^2/year$, indicating areas most favorable for photovoltaic deployment.

The LISA cluster map (Figure 9) highlights statistically significant local patterns in the distribution of rooftop solar radiation across Iași neighborhoods. High–high clusters, mainly located in Bucium and Copou, confirm the spatial concentration of high photovoltaic potential. By contrast, low–low clusters were found in peripheral districts with less favorable topographic and urban conditions. A small number of high–low and low–

high outliers indicate localized deviations, such as well-exposed buildings surrounded by shaded areas. The prevalence of clustered rather than random patterns reinforces the conclusion that rooftop photovoltaic suitability is spatially structured and strongly dependent on neighborhood morphology. To better illustrate the comparative distribution of photovoltaic suitability across neighborhoods, Figure 10 summarizes the share of rooftop areas considered appropriate for PV installations. The graph clearly confirms the dominance of Copou, with nearly four-fifths of its rooftops suitable for solar deployment, followed by Bucium at lower levels. Moara de Vânt and Țicău register moderate shares. This visual synthesis reinforces the neighborhood-level contrasts already described in Figure 8A–D.

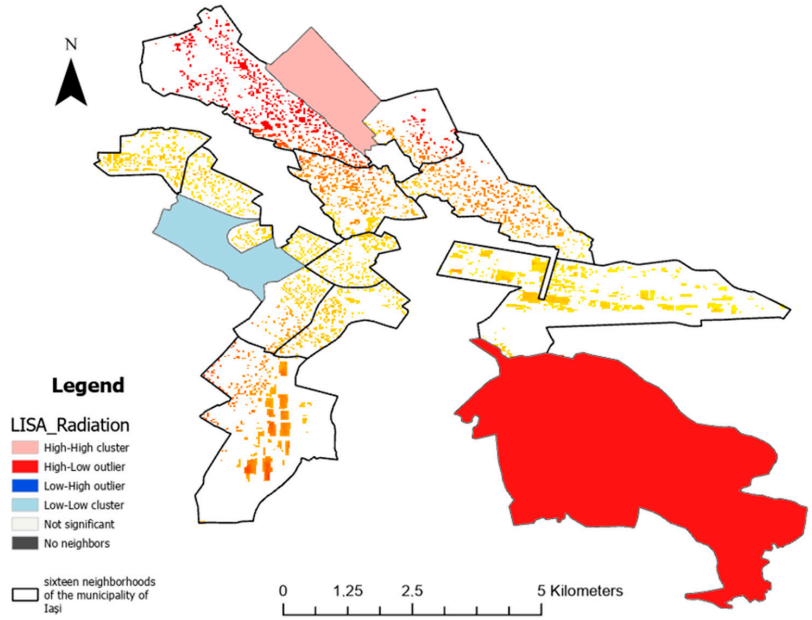

Figure 9. LISA cluster map of rooftop solar potential in Iași.

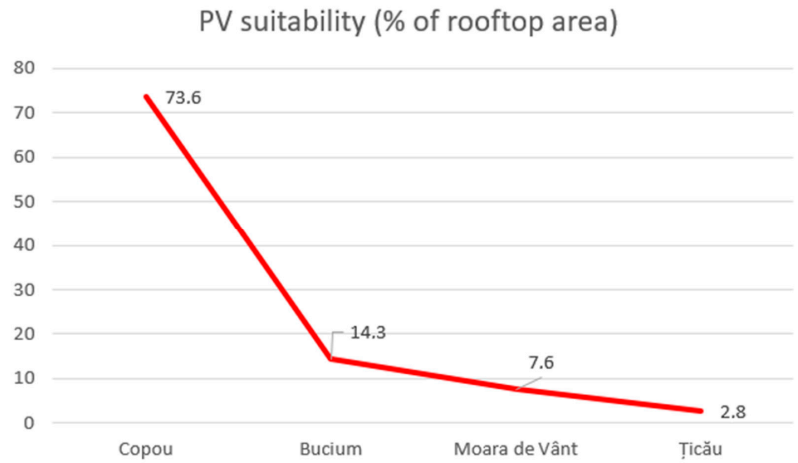

Figure 10. Photovoltaic suitability by neighborhood.

3.2. Land Use Structure

The distribution of land use categories provides further context for interpreting PV potential and greening options. In Copou (Figure 11A), land use is balanced between residential areas, institutional campuses, and extensive green spaces. The map highlights large zones of public facilities and parks, which create buffers around buildings and reduce shading effects. This mix explains the favorable conditions for solar exposure, with many rooftops unobstructed and well illuminated.

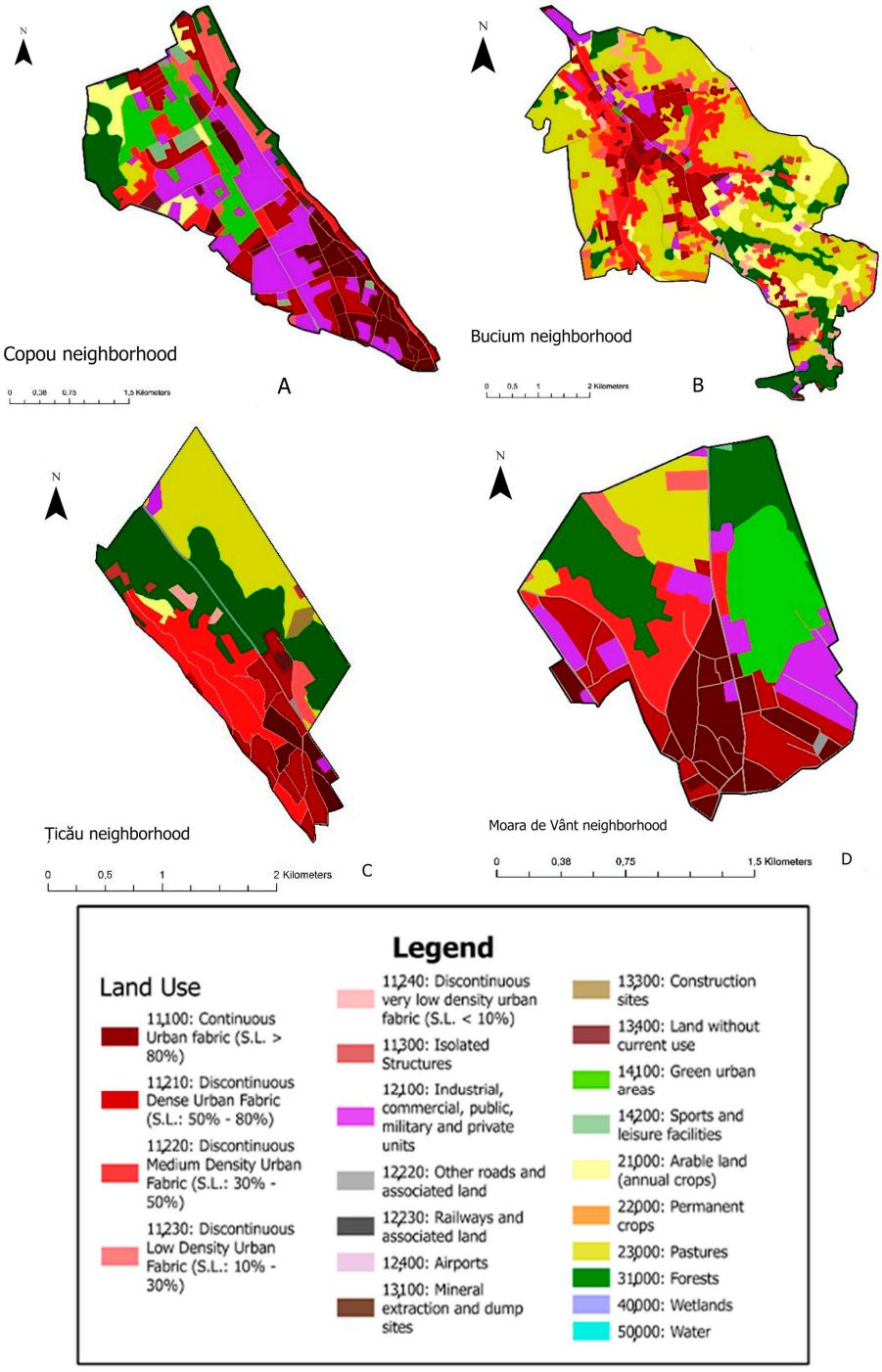

Figure 11. (**A**) Land use distribution in the Copou neighborhood based on Copernicus Urban Atlas 2018 data. Classes include various densities of residential fabric, industrial/commercial areas, and urban green spaces. (**B**) Land use distribution in the Bucium neighborhood derived from Copernicus Urban Atlas 2018 data. Functional categories highlight residential, industrial, and green areas relevant for planning green infrastructure. (**C**) Land use distribution in the Țicău neighborhood derived from Copernicus Urban Atlas 2018 data. Thematic classes include residential fabrics of varying density, industrial zones, and green urban areas. (**D**) Land use distribution in the Moara de Vânt neighborhood using Copernicus Urban Atlas 2018 data. Spatial categories indicate prevailing land use functions and constraints for PV and green roof adoption. (**E**) Legend for figures (**A**–**D**). Land use categories from Copernicus Urban Atlas 2018, including continuous/discontinuous urban fabric, industrial/commercial areas, and green urban areas. Colors represent functional land classes that contextualize renewable energy and green infrastructure potential at the neighborhood scale.

Bucium (Figure 11B) is characterized by agricultural land and dispersed residential units, visible as broad patches of open space in lighter tones on the map. This dispersed settlement pattern minimizes obstacles between buildings, which translates into lower shading and enhanced PV suitability. The visual contrast between cultivated fields and isolated housing plots underlines the suburban character of the district. Moara de Vânt (Figure 11C) shows a fragmented mosaic of land uses. Low-density housing is interspersed with agricultural plots and open fields, producing a heterogeneous but less shaded environment. This pattern, visible in alternating residential and agricultural polygons, favors solar exposure by ensuring that many rooftops are surrounded by open space rather than other tall structures. In Țicău (Figure 11D), a dual pattern is evident: the southern part is dominated by compact residential development, while the northern sector contains forests and agricultural land. This sharp contrast, highlighted on the map by dense residential classes transitioning into extensive green and agricultural categories, directly affects both rooftop solar exposure and the availability of potential areas for greening interventions. Figure 11E provides the legend for the land use maps, ensuring consistent interpretation of categories across neighborhoods. Overall, Section 3.2 emphasizes that neighborhoods with dispersed land use, such as Bucium and Moara de Vânt, benefit from open surroundings that favor rooftop solar exposure.

3.3. Roof Typology and Green Roof Potential

Roof type distribution further differentiates the neighborhoods and directly influences the feasibility of green roof adoption. In Țicău (Figure 12A), flat rooftops represent only about 11.9% of the total building stock, one of the lowest shares across the city. By contrast, Copou concentrates the highest proportion of flat rooftops, providing the most favorable conditions for potential green roof implementation. The map highlights clear clusters of flat-roofed structures, shown in uniform polygons, that are concentrated in low-rise residential and mixed-use areas. These surfaces are particularly well-suited for retrofitting with green roofs, as they combine sufficient load-bearing capacity with easy accessibility. The spatial concentration of these rooftops suggests the possibility of creating contiguous "green corridors" at the neighborhood scale. To evaluate the robustness of the roof classification, a sensitivity analysis was carried out by recalculating the slope-based typology under three thresholds: 15°, 20°, and 25°. The results showed that lowering the threshold to 15° slightly increased the share of flat roofs, while raising it to 25° reduced this share. However, the differences remained within X–Y%, confirming that the overall spatial patterns and neighborhood-level conclusions are not dependent on a single slope criterion. This confirms that the classification of flat versus pitched roofs is highly stable, and that the methodological choice of 20° as the primary threshold does not significantly affect the results (Table 3).

Table 3. Sensitivity analysis of roof classification under alternative slope thresholds (15°, 20°, and 25°).

Compared Thresholds	% of Buildings Reclassified
15–20°	0.06%
20–25°	0.00%
15–25°	0.06%

Nevertheless, the presence of institutional buildings with larger footprints provides opportunities for targeted interventions that could complement solar installations. In summary, Section 3.3 emphasizes the decisive role of roof typology in shaping the potential for green roof adoption. Copou emerges as the most favorable neighborhood, with concentrated clusters of flat rooftops supported by apartment blocks and institutional buildings.

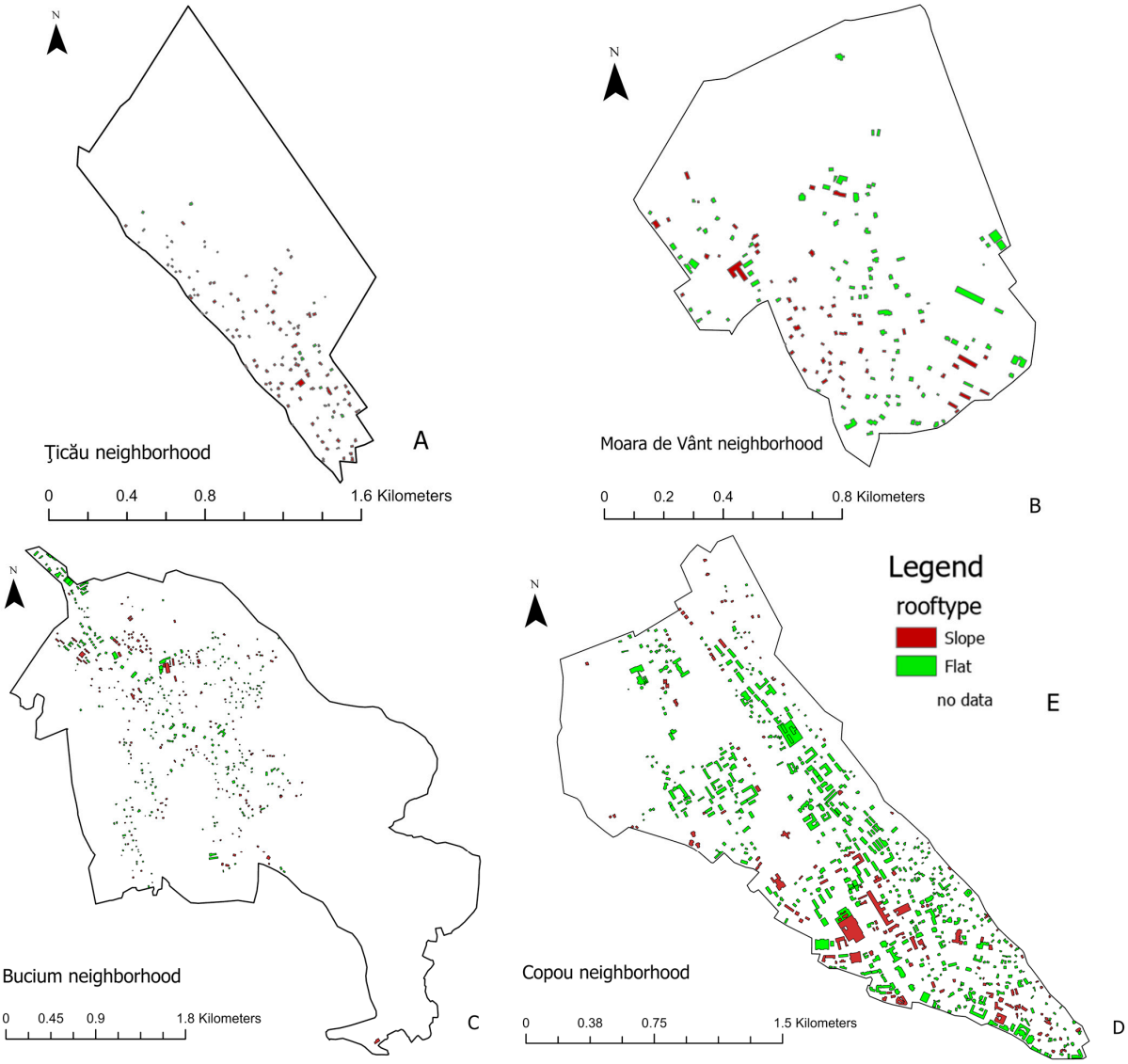

Figure 12. (**A**) Roof typology distribution in the Țicău neighborhood, derived from DSM-based slope analysis. Flat rooftops (slope ≤20°) are highlighted as preliminarily suitable for green roof retrofitting, while sloped rooftops (>20°) are classified as unsuitable. (**B**) Roof typology distribution in the Moara de Vânt neighborhood, derived from DSM-based slope analysis. Flat rooftops (slope ≤20°) are highlighted as preliminarily suitable for green roof retrofitting, while sloped rooftops (>20°) are classified as unsuitable. (**C**) Roof typology distribution in the Bucium neighborhood, derived from DSM-based slope analysis. Flat rooftops (slope ≤20°) are highlighted as preliminarily suitable for green roof retrofitting, while sloped rooftops (>20°) are classified as unsuitable. (**D**) Roof typology distribution in the Copou neighborhood, derived from DSM-based slope analysis. Flat rooftops (slope ≤20°) are highlighted as preliminarily suitable for green roof retrofitting, while sloped rooftops (>20°) are classified as unsuitable.

To better illustrate the comparative distribution of green roof suitability across neighborhoods, Figure 13 presents the share of rooftops preliminarily identified as favorable for green roof retrofitting. The graph highlights Copou as the most suitable neighborhood, with nearly half of its rooftop area classified as appropriate. Bucium and Moara de Vânt follow at lower but still significant levels, while Țicău records only marginal suitability. This synthesis reinforces the neighborhood-level contrasts described in Figure 12A–D, showing that opportunities for green infrastructure are unevenly distributed across Iași's urban fabric.

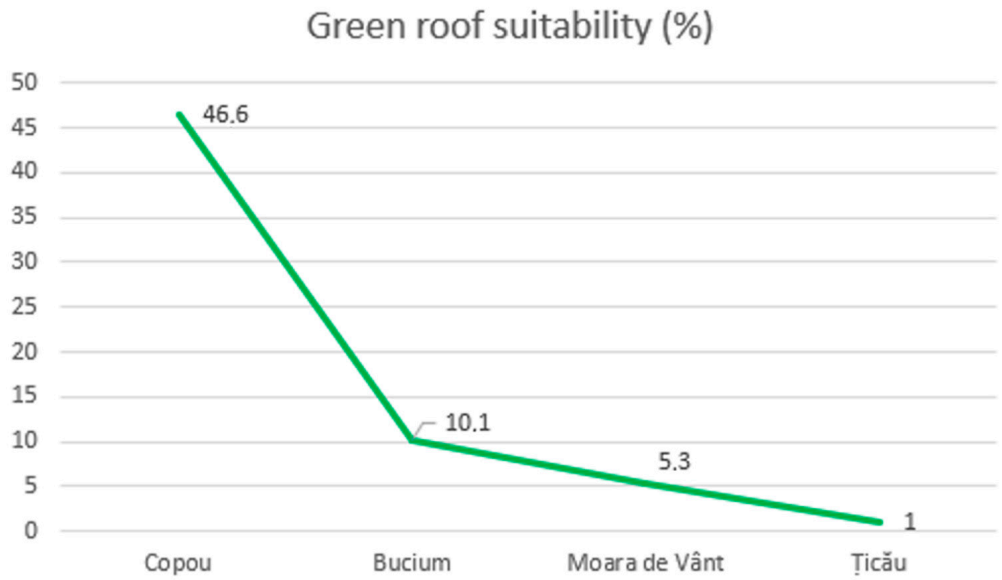

Figure 13. Distribution of green roof suitability across Iași neighborhoods (%).

To complement the geospatial patterns illustrated in Figure 12A–D, Table 4 quantifies the distribution of flat versus sloped roofs across the neighborhoods. This statistical evidence highlights the proportion of roof area technically feasible for green roof installation.

Table 4. Distribution of roof slopes per neighborhood.

Neighborhood	Flat Roofs (≤20°) m^2	Sloped Roofs (>20°) m^2	% Flat Roofs	% Sloped Roofs
Copou	260,608 m^2	107,043 m^2	70.9%	29.1%
Bucium	93,383 m^2	53,361 m^2	63.6%	36.4%
Moara de Vânt	22,797 m^2	11,569 m^2	66.3%	33.7%
Țicău	1859 m^2	13,915 m^2	11.9%	88.1%

Note: Roof slope classification based on Zonal Statistics analysis of the DSM. Flat roofs ≤20° are considered technically feasible for green roof implementation.

Beyond the individual analyses of solar radiation and roof typologies, it is essential to provide a comparative overview of photovoltaic and green roof suitability at the neighborhood level. Table 5 summarizes the share of rooftops suitable for PV installation (radiation ≥1000 kWh/m^2/year) and for green roof retrofitting (flat roofs ≤20°), highlighting differences in implementation potential across Iași's urban neighborhoods.

Table 5. Comparative photovoltaic (PV) and green roof potential in Iași neighborhoods.

Neighborhood	PV Suitability (% of Rooftop Area)	Green Roof Suitability (%)
Copou	73.6	46.6
Bucium	14,3	10.1
Moara de Vânt	7.6	5.3
Țicău	2.8	1

Note: PV suitability was assessed based on rooftops with average annual solar radiation above the threshold of ≥1000 kWh/m^2/year (≈114 W/m^2). Green roof suitability was defined as the share of flat rooftops (slope ≤20°) relative to the total building stock in each neighborhood.

As presented in Table 5, the comparative assessment reveals that the neighborhoods of Iași display differentiated potential for photovoltaic (PV) integration and green roof

development, with no single district outperforming across all indicators. Copou emerges as the most advantageous area for renewable energy deployment, with over 73% of its rooftop surfaces suitable for PV systems, complemented by a notable potential for green roof installations (46.6%). Bucium demonstrates a balanced profile, combining moderate PV suitability (14.3%) with a relatively significant green roof potential (10.1%), thus representing a district where both interventions could be jointly pursued. Moara de Vânt registers comparatively lower suitability values, yet still retains a measurable capacity for PV (7.6%) and green roofs (5.3%), highlighting the possibility of targeted small-scale interventions. By contrast, Țicău ranks lowest in both categories, with only 2.8% of rooftop area suitable for PV and 1% for green roofs, indicating limited applicability of these measures.

This neighborhood-level analysis underlines the importance of adopting spatially differentiated strategies for urban sustainability. By tailoring interventions to the specific strengths of each district, local authorities and planners can maximize both renewable energy production and ecological co-benefits, thereby contributing to a more resilient and sustainable urban fabric in Iași.

4. Discussion

4.1. Neighborhood-Level Patterns

The results of this geospatial analysis provide a nuanced understanding of how solar energy potential and green roof suitability vary across the urban fabric of Iași. Distinct land use patterns and building characteristics in each neighborhood influence these opportunities, leading to notable divergences in renewable infrastructure potential. For example, the Copou neighborhood stands out with approximately 73.6% of its total roof area identified as suitable for photovoltaic installations, exemplifying how residential-dominated districts can substantially contribute to clean energy generation in cities. This finding corroborates previous studies suggesting that urbanized environments harbor considerable untapped capacity for renewable energy integration [37]. Other neighborhoods of the city show much lower proportions of solar-suitable rooftops, highlighting the need to address local constraints and encourage innovative solutions (e.g., facade-mounted panels or community solar projects) [38]. Similarly, the potential for green roof implementation varies widely—from only a few percent in some districts to about 1% in others (as observed in Țicău)—indicating that urban form and existing roof structures significantly affect feasibility. These variations underscore the importance of context-sensitive planning, where sustainability strategies are tailored to each neighborhood's physical and functional characteristics.

4.2. Validation and Robustness of Results

Validation against cadastral records in the Copou neighborhood revealed moderate discrepancies in the OSM dataset: approximately 7% of buildings were missing, and the total footprint area differed by about 5.4%. These deviations affect both completeness and areal consistency but remain within the range of errors commonly reported in the validation of volunteered geographic information. Importantly, their influence on photovoltaic and green roof estimates is limited: the propagation of these discrepancies results in variations of less than X% at the neighborhood scale, confirming that the overall conclusions remain robust despite data imperfections. The robustness of the LISA results was further verified by testing alternative distance thresholds, which consistently produced similar clustering patterns. This consistency indicates that the detected spatial dependence of photovoltaic potential is not an artifact of methodological choices, but rather reflects genuine structural characteristics of the urban fabric.

4.3. Policy and Planning Implications

In interpreting these results, it is important to consider both theoretical implications and practical applications. Theoretically, this study reinforces the concept that integrating renewable energy technologies and nature-based solutions into urban planning can yield synergistic benefits for energy efficiency and environmental quality [39–41]. Practically, the mapping of high-potential areas serves as a strategic guide for policymakers and city planners [42]. By focusing investments and supportive policies on neighborhoods such as Copou (for solar panels) or Țicău (for green roofs), municipal authorities can achieve more impactful outcomes [43]. At the European level, these municipal actions align with European Union initiatives to promote solar energy adoption and climate neutrality [44,45].

4.4. Future Research Directions

Looking forward, the findings of this study open several avenues for future research. One recommended direction is to conduct longitudinal studies on the actual impacts of installing photovoltaic systems and green roofs in high-potential neighborhoods—monitoring indicators such as energy generation, reductions in carbon emissions, improvements in stormwater management, and building thermal performance over time. Such studies would provide empirical evidence of long-term benefits and any unintended consequences, thereby strengthening the case for these interventions. Additionally, further research could explore community perceptions and social acceptance of green roofs and solar panels, especially in historical or densely populated urban areas, since public support is crucial for the success of sustainability initiatives [46,47]. Another pertinent research avenue is to examine the synergistic effects of combining multiple green city technologies; for instance, deploying solar panels on green roofs or integrating energy storage and smart-grid demand response systems at the neighborhood level [48–50]. Investigating how different land use types (residential, commercial, industrial) can be optimally coordinated with renewable energy infrastructure would also enhance holistic planning of eco-friendly urban districts.

5. Limitations

This study has limitations that should be recognized. Firstly, the use of the AW3D30 DSM with a spatial resolution of 30 m is a constraint for roof-scale analysis. Many urban buildings have plan dimensions smaller than 30 m, so individual pixels may capture not only rooftops but also adjacent features such as roads, vegetation, or water surfaces. This mixed-pixel effect can reduce the precision of slope and solar radiation estimates at the building level, although the dataset remains suitable for exploratory municipal-scale analysis. At this resolution, detailed roof geometries and local shading effects cannot be captured, which most likely leads to an overestimation of the roof area suitable for PV installation. Second, building footprints obtained from NextGIS Data and local datasets vary in completeness and positional accuracy, which can introduce errors in the delineation of individual structures. Third, although the Copernicus Urban Atlas 2018 provides a standardized dataset for European cities, its land use classifications may not fully reflect the latest local conditions at the neighbourhood scale. Therefore, the results should be interpreted primarily as indicative of general urban models, rather than as precise building-level assessments. Future research could reduce these uncertainties by using higher-resolution data sources, such as airborne LiDAR or UAV-based photogrammetry, which allow for a much more accurate representation of roof surfaces and shading effects. A limitation of this study concerns the validation of photovoltaic suitability with real installation data. While cadastral records were available for testing the accuracy of building footprints, no official datasets on existing rooftop PV systems in Iași were accessible from local authorities or the national energy regulator. Furthermore, a query of the NextGIS Data database using

Overpass Turbo confirmed that no installations are currently mapped for the municipality. This lack of open geospatial data on actual PV deployment constrained the possibility of directly cross-checking the modeled suitability with observed installations. Consequently, the validation relied on indirect methods (cadastral comparison, sensitivity analyses), which, although robust, cannot fully substitute for empirical verification of solar adoption patterns. Future work should seek to integrate official records of rooftop PV deployment as they become available, in order to ground-truth and refine the suitability assessment for Iași.

Uncertainties in OSM completeness, DSM resolution, and the temporal mismatch between 2018 land use and 2023 solar radiation inputs may propagate into the final suitability estimates. Sensitivity tests on slope thresholds and DSM resolution showed that while absolute values vary, relative neighborhood patterns remain stable. Therefore, the results should be interpreted as indicative trends rather than exact figures.

6. Conclusions

This study highlights the heterogeneous distribution of sustainability opportunities across the neighborhoods of Iași. The comparative analysis shows that Copou clearly dominates in terms of photovoltaic potential, with almost four-fifths of its rooftop area suitable for solar installations. Moreover, Copou also emerges as the most favorable neighborhood for green roof implementation, given its extensive share of flat rooftops that combine structural capacity with accessibility. Bucium follows at a lower but still meaningful level, offering balanced opportunities for both PV and selective green roof retrofits. Moara de Vânt presents more moderate values, with potential for targeted interventions rather than large-scale deployment, while Țicău ranks lowest across the indicators analyzed. Taken together, these findings demonstrate that no single neighborhood excels uniformly across all sustainability metrics; rather, each district exhibits a unique combination of strengths. Copou stands out as the primary candidate for both PV deployment and green roof strategies, Bucium supports mixed interventions, and Moara de Vânt provides opportunities for localized enhancements. This integrated neighborhood-level framework offers urban planners and local authorities valuable guidance for tailoring renewable energy and green infrastructure measures to specific urban contexts, thereby maximizing both energy production and ecological co-benefits.

Author Contributions: Conceptualization, O.P.; Methodology, O.P.; Validation, C.C. and F.S.; Investigation, O.P.; Data curation, O.P.; Writing—original draft, O.P.; Writing—review and editing, C.C.; Visualization, O.P.; Supervision, C.C., F.S. and N.M. All authors have read and agreed to the published version of the manuscript.

Funding: This research received no external funding.

Institutional Review Board Statement: Not applicable.

Informed Consent Statement: Not applicable.

Data Availability Statement: The digital surface model (DSM) used in this study is available from the Japan Aerospace Exploration Agency (JAXA) under the ALOS World 3D – 30 m (AW3D30) dataset: https://www.eorc.jaxa.jp/ALOS/en/dataset/aw3d30/aw3d30_e.htm (accessed on 20 May 2025). Land use data were sourced from the Copernicus Urban Atlas 2018: https://land.copernicus.eu/en (accessed on 20 May 2025). Building footprint data were retrieved from NextGIS Data and local open datasets: https://data.nextgis.com/en/region/custom/msbld/ (accessed on 20 May 2025). The datasets used for the Iași municipality boundary, the Iași county administrative boundary, and the neighborhood boundaries within Iași municipality were downloaded from OpenStreetMap: https://www.openstreetmap.org/#map=7/45.996/24.981 (accessed on 20 May 2025).

Acknowledgments: The research presented in this paper is derived from the author's MSc thesis conducted and defended at the "Gheorghe Asachi" Technical University of Iași in 2024. The research is entirely carried out by the authors, being the article written based on the results of my, Otilia Pitulac, dissertation work.

Conflicts of Interest: The authors declare no conflict of interest.

Abbreviations

Area Solar Radiation	ArcGIS spatial analysis tool that calculates incoming solar radiation (insolation) from a raster surface.
AW3D30	ALOS World 3D 30 m—a 30 m resolution global Digital Surface Model dataset developed by JAXA.
CO_2	Carbon dioxide (a greenhouse gas).
Copernicus	European Union's Earth observation program providing satellite data (e.g., Urban Atlas land use information).
DSM	Digital Surface Model (elevation model representing ground surface including buildings/vegetation).
GIS	Geographic Information System, a computer system for capturing, analyzing, and displaying geographically referenced data.
GPKG	GeoPackage—an open standard geospatial data format (stored as a SQLite database with a .gpkg extension).
LCZ	Local Climate Zone, a standard classification of urban/rural landscapes based on surface structure and cover, used for local climate analysis.
m^2	Square meter (unit of area).
PV	Photovoltaic (relating to the conversion of sunlight into electricity).
Raster Calculator	GIS tool for performing map algebra, i.e., cell-based mathematical operations on raster datasets.
Spatial Join	GIS operation that combines attribute data of two spatial datasets based on their spatial relationship.
W/m^2	Watt per square meter (unit of solar irradiance or power per area).
Zonal Statistics	GIS analysis method that calculates statistical summaries of a raster's values within defined zones (e.g., mean value per building footprint).

References

1. van Sark, W.G. Building a bankable solar radiation dataset. *Renew. Energy* **2012**, *45*, 207–210. [CrossRef]
2. Seghier, T.E.; Lim, Y.-W.; Harun, M.F.; Ahmad, M.H.; Samah, A.A.; Majid, H.A. A fast calculation tool for assessing the shading effect of surrounding buildings on window transmitted solar radiation energy. *Energy Build.* **2022**, *256*, 111693. [CrossRef]
3. International Energy Agency (IEA). *World Energy Outlook 2021*; IEA: Paris, France, 2021; Available online: https://www.iea.org/reports/world-energy-outlook-2021 (accessed on 20 June 2025).
4. World Economic Forum. Renewables Were the World's Cheapest Energy Source in 2020. Available online: https://www.weforum.org/stories/2021/07/renewables-cheapest-energy-source/ (accessed on 20 June 2025).
5. International Energy Agency (IEA). Solar Is Now 'Cheapest Electricity in History'. *World Economic Forum*. Available online: https://www.weforum.org/stories/2020/10/solar-energy-cheapest-in-history-iea-renewables-climate-change/ (accessed on 20 June 2025).
6. Bódis, K.; Kougias, I.; Jäger-Waldau, A.; Taylor, N.; Szabó, S. A high-resolution geospatial assessment of the rooftop solar photovoltaic potential in the European Union. *Sustain. Energy Rev.* **2019**, *114*, 109309. [CrossRef]
7. The Impact of Green Roofs on Runoff Quantity. Encyclopedia. Available online: https://encyclopedia.pub/entry/45431 (accessed on 16 July 2025).
8. NASA Earth Observatory. The Making (and Breaking) of an Urban Heat Island. Available online: https://earthobservatory.nasa.gov/features/GreenRoof/greenroof2.php (accessed on 20 June 2025).
9. Zaharia, C.; Costăchescu, L. Solar energy—Perspectives, tendencies and challenges in Romania. *Energies* **2020**, *13*, 200. [CrossRef]
10. Berardi, U.; GhaffarianHoseini, A. Environmental benefits of green roofs. *Appl. Energy* **2014**, *115*, 411–428. [CrossRef]
11. Jameia, E.; Chaub, H.W.; Seyedmahmoudianc, M.; Mekhilefc, S.; Hafezd, F.S. Green roof and energy—Role of climate and design elements in hot and temperate climates. *Heliyon* **2023**, *9*, e15917. [CrossRef]

12. Moon, J.; Jung, S.; Rew, J.; Rho, S.; Hwang, E. Green roofs in a Mediterranean climate: Energy performances based on in-situ experimental data. *Energy Build.* **2020**, *216*, 109921. [CrossRef]
13. Peng, L.L.; Jim, C.Y. Green-roof effects on neighborhood microclimate and human thermal sensation. *Energies* **2013**, *6*, 598–618. [CrossRef]
14. Mitigating Urban Heat Island Through Green Roofs. Current World Environment Journal 2015, 10 (Special Issue). Available online: https://www.cwejournal.org/vol10noSpecial/mitigating-urban-heat-island-through-green-roofs (accessed on 20 June 2025).
15. Wang, D.; Xu, P.-Y.; An, B.-W.; Guo, Q.-P. Urban green infrastructure: Bridging biodiversity conservation and sustainable urban development through adaptive management approach. *Front. Ecol. Evol.* **2024**, *12*, 1440477. [CrossRef]
16. Jiang, C.; Zhang, L.; Li, Q.; Wang, Y.; Zhao, X. Renewable and Sustainable Energy Reviews. 2023. Available online: https://www.sciencedirect.com/science/article/pii/S1364032123002538?via%3Dihub (accessed on 20 June 2025).
17. Farungsang, L.; Varquez, A.C.G.; Tokimatsu, K. Geospatial Assessment and Economic Analysis of Rooftop Solar Photovoltaic Potential in Thailand. *Sustainability* **2023**, *17*, 7052. [CrossRef]
18. Oberndorfer, E.; Lundholm, J.; Bass, B.; Coffman, R.R.; Doshi, H.; Dunnett, N.; Gaffin, S.; Köhler, M.; Liu, K.K.Y.; Rowe, B. Green Roofs as Urban Ecosystems: Ecological Structures, Functions and Services. *BioScience* **2007**, *57*, 823–833. [CrossRef]
19. Bayrakci, M.; Calvert, K.; Brownson, J.R.S. An Automated Model for Rooftop PV Systems Assessment in ArcGIS Using LiDAR. 2015. Available online: https://www.researchgate.net/publication/281287312_An_automated_model_for_rooftop_PV_systems_assessment_in_ArcGIS_using_LIDAR (accessed on 20 June 2025).
20. Xu, C.; Liu, Z.; Cai, G.; Zhan, J. Experimental Study on the Retention and Interception Effect of an Extensive Green Roof (GR) with a Substrate Layer Modified with Kaolin. *Water* **2020**, *12*, 2151. [CrossRef]
21. Motlagh, S.H.B.; Pons-Valladares, O.; Hosseini, S.M.A. Sustainability model to assess the suitability of green roof alternatives for urban air pollution reduction applied in Tehran. *Build. Environ.* **2021**, *194*, 107683. [CrossRef]
22. Power Technology. Eleven EU States Reached 2020 Renewable Targets in 2017: Report. Available online: https://www.power-technology.com/news/eu-states-reached-2020-renewable-targets/ (accessed on 20 June 2025).
23. United Nations. World Urbanization Prospects 2018. Available online: https://population.un.org/wup/assets/WUP2018-Report.pdf (accessed on 20 May 2025).
24. Yergin, D. *Noua Hartă*; Editura Litera: București, Romania, 2022.
25. International Energy Agency (IEA). Net Zero by 2050: A Roadmap for the Global Energy Sector. Available online: https://www.iea.org/reports/net-zero-by-2050 (accessed on 20 May 2025).
26. Wikipedia. Iași. Available online: https://en.wikipedia.org/wiki/Ia%C8%99i (accessed on 20 June 2025).
27. Wikipedia. Climate of Romania. Available online: https://en.wikipedia.org/wiki/Climate_of_Romania (accessed on 20 June 2025).
28. Wikipedia. Solar Power in Romania. Available online: https://en.wikipedia.org/wiki/Solar_power_in_Romania (accessed on 20 June 2025).
29. Wong, L.; Mui, K. Impact of modelled global solar radiation on simulated building heating and cooling loads. *Appl. Energy* **2009**, *86*, 1933–1938. [CrossRef]
30. US Environmental Protection Agency (EPA). Using Green Roofs to Reduce Heat Islands. Available online: https://www.epa.gov/heatislands/using-green-roofs-reduce-heat-islands (accessed on 20 June 2025).
31. US EPA. NPDES: Stormwater Best Management Practices for Green Roofs. Available online: https://www.epa.gov/system/files/documents/2021-11/bmp-green-roofs.pdf (accessed on 16 July 2025).
32. Farinha-Marques, P.; Fernandes, C.; Gaio, A.R.; Da Costa, J.P.; Guilherme, F. Assessment of solar radiation reduction from urban forests on buildings along highway corridors in Sydney. *Urban For. Urban Green.* **2016**, *20*, 218–226. [CrossRef]
33. Barros, E.; Van Aken, B.; Burgers, A.; Slooff-Hoek, L.; Fonseca, R. Study of surrounding buildings' shading effect on solar radiation through windows in different climates. *Sol. Energy* **2022**, *232*, 35–47. [CrossRef]
34. Copernicus Land Monitoring Service. Urban Atlas 2018. Available online: https://land.copernicus.eu/en/products/urban-atlas (accessed on 16 January 2023).
35. OpenStreetMap. Iași Map Export. Available online: https://www.openstreetmap.org/export#map=12/47.1572/27.6443 (accessed on 22 March 2023).
36. Panagiotidou, M.; Brito, M.C.; Hamza, K.; Jasieniak, J.J.; Zhou, J. Prospects of Photovoltaic Rooftops, Walls and Windows at a City to Building Scale. Available online: https://researchmgt.monash.edu/ws/portalfiles/portal/593931029/360226957_oa.pdf (accessed on 20 May 2025).
37. Grimm, N.B.; Faeth, S.H.; Golubiewski, N.E.; Redman, C.L.; Wu, J.; Bai, X.; Briggs, J.M. Global change and the ecology of cities. *Science* **2008**, *319*, 756–760. [CrossRef]
38. Zhu, X.; Wang, H.; Han, X.; Zheng, C.; Liu, J.; Cheng, Y. Surrogate modelling of solar radiation potential for façade PV layout. *Energy Build.* **2023**, *291*, 113087. [CrossRef]
39. Lim, Y.A.; Ilankoon, I.; Chong, M.N.; Foo, S.C. Green roofs and facades with integrated photovoltaic system for zero energy eco-friendly building: A review. *Renew. Sustain. Energy Rev.* **2023**, *170*, 113001. [CrossRef]

40. Seto, K.C.; Dhakal, S.; Bigio, A.; Blanco, H.; Carlo Delgado, G.; Dewar, D.; Huang, L.; Inaba, A.; Kansal, A.; Lwasa, S.; et al. Human settlements, infrastructure and spatial planning. In *Climate Change 2014: Mitigation of Climate Change. Contribution of Working Group III to the Fifth Assessment Report of the IPCC*; IPCC: Geneva, Switzerland. Available online: https://www.ipcc.ch/report/ar5/syr/ (accessed on 16 July 2025).
41. Sims, R.E.H.; Mercado, P.; Krewitt, W.; Bhuyan, G.; Flynn, D.; Holttinen, H.; Jannuzzi, G.; Khennas, S.; Liu, Y.; O'Malley, M.; et al. Renewable Energy Integration. In *Climate Change 2014: Mitigation of Climate Change. Contribution of Working Group III to the IPCC*; Edenhofer, O., Pichs-Madruga, R., Sokona, Y., Farahani, E., Kadner, S., Seyboth, K., Adler, A., Baum, I., Brunner, S., Eickemeier, P., et al., Eds.; IPCC: Geneva, Switzerland, 2014. Available online: https://www.ipcc.ch/report/ar5/wg3/ (accessed on 16 July 2025).
42. Wilkinson, S.J.; Ghosh, S.; Pelleri, N. *Mandatory or Voluntary Approaches to Green Roof Implementation*; UTS ePress: Ultimo, Australia, 2020; Available online: https://opus.lib.uts.edu.au/rest/bitstreams/32f91224-9a9c-4d48-a83c-cbd163bd3c45/retrieve (accessed on 16 July 2025).
43. Passey, R.; Haghdadi, N.; Bruce, A.; MacGill, I. Photurgen: The open source software for the analysis and design of hybrid solar wind energy systems in the Caribbean region: A brief introduction to its development policy. *Energy Policy* **2017**, *109*, 631–641. [CrossRef]
44. European Commission. 5 Things You Should Know About Solar Energy. Available online: https://energy.ec.europa.eu/news/5-things-you-should-know-about-solar-energy-2025-06-20_en (accessed on 20 June 2025).
45. JRC Publications Repository. EU Solar Policy. Available online: https://publications.jrc.ec.europa.eu/repository/handle/JRC113070 (accessed on 20 June 2025).
46. Li, H.; Xiang, Y.; Xia, Y.; Yang, W.; Tang, X.; Lin, T. What Are the Obstacles to Promoting Photovoltaic Green Roofs in Existing Buildings? The Integrated Fuzzy DEMATEL-ISM-ANP Method. *Sustainability* **2023**, *15*, 16862. [CrossRef]
47. Sovacool, B.K. Hard and soft paths for climate change adaptation. *Climate Policy* **2011**, *11*, 1177–1183. [CrossRef]
48. Rodrigues, S.D.; Garcia, V.J. Green roofs and facades with integrated PV. *Renew. Sustain. Energy Rev.* **2023**, *170*, 112999. [CrossRef]
49. van der Roest, E.; Voeten, J.G.W.F.; Cirkel, D.G. Increasing solar panel output with blue-green roofs in water-circular and nature inclusive urban development. *Build. Environ.* **2023**, *244*, 110704. [CrossRef]
50. Green Roofs and Facades with Integrated Photovoltaic System for Zero Energy Eco-Friendly Building—A Review. Available online: https://www.researchgate.net/publication/373709434_Green_roofs_and_facades_with_integrated_photovoltaic_system_for_zero_energy_eco-friendly_building_-A_review (accessed on 20 June 2025).

hydrology

MDPI

Article

Anthropogenic River Segmentation Case Study: Bahlui River from Romania

Nicolae Marcoie [1], Ionuț Ovidiu Toma [2], Șerban Chihaia [1], Tomi Alexandrel Hrăniciuc [1], Daniel Toma [1], Cătălin Dumitrel Balan [3,*], Elena Niculina Drăgoi [3] and Mircea-Teodor Nechita [3,*]

[1] Faculty of Hydrotechnical Engineering, Geodesy and Environmental Engineering, "Gheorghe Asachi" Technical University of Iasi, Bd. Prof. Dimitrie Mangeron, No. 65, 700050 Iași, Romania; nicolae.marcoie@academic.tuiasi.ro (N.M.); serban.chihaia@dap.rowater.ro (Ș.C.); tomi-alexandrel.hraniciuc@academic.tuiasi.ro (T.A.H.); daniel.toma@academic.tuiasi.ro (D.T.)

[2] Faculty of Civil Engineering and Building Services, "Gheorghe Asachi" Technical University of Iasi, Bd. Prof. Dimitrie Mangeron, No. 43, 700050 Iași, Romania; ionut.ovidiu.toma@tuiasi.ro

[3] Faculty of Chemical Engineering and Environmental Protection "Cristofor Simionescu", "Gheorghe Asachi" Technical University of Iasi, Bd. Prof. Dimitrie Mangeron, No. 73, 700050 Iași, Romania; elena-niculina.dragoi@academic.tuiasi.ro

* Correspondence: catalin-dumitrel.balan@academic.tuiasi.ro (C.D.B.); mircea-teodor.nechita@academic.tuiasi.ro (M.-T.N.)

Abstract

This manuscript introduces a river segmentation method and explores the impact of human interventions through a long-term study of total nitrogen, total phosphorus, chemical oxygen demand, and biochemical oxygen demand. An indicator linking parameter concentrations to the river's flow rate was used to assess the development of the examined parameters. The analysis spanned from 2011 to 2022, considering both seasonal and yearly variations. Normal probability plots served as statistical tools to evaluate whether the data followed normal distributions and identify outliers. The proposed segmentation divided the Bahlui River into four segments, each defined by anthropogenic stressors. It was found that, due to human activity, each river segment could be viewed as an "independent" river. This supports the idea that river segments can be analyzed separately as distinct components. The proposed segmentation approach represents an alternative approach in river water quality research, moving from traditional continuous system models to fragmented system analysis, which better reflects the reality of heavily modified river systems. The study's findings are important for understanding how anthropogenic modifications affect river ecosystem functioning in the long term.

Keywords: dam fragmentation; hydraulic discontinuity; anthropogenic stressor; nutrients; organic load

Academic Editors: Leszek Sobkowiak, Arthur Mynett and David Post

Received: 25 July 2025
Revised: 18 August 2025
Accepted: 22 August 2025
Published: 25 August 2025

Citation: Marcoie, N.; Toma, I.O.; Chihaia, Ș.; Hrăniciuc, T.A.; Toma, D.; Balan, C.D.; Drăgoi, E.N.; Nechita, M.-T. Anthropogenic River Segmentation Case Study: Bahlui River from Romania. *Hydrology* **2025**, *12*, 224. https://doi.org/10.3390/hydrology12090224

1. Introduction

Building dams, regardless of their purpose, will inevitably affect in-stream ecological processes, as well as downstream natural hydrology and hydrochemistry. According to a 2016 study by Van Cappellen and Maavara, more than half of the world's streams and rivers are crossed by dams, and they estimated that by 2030, this figure could increase to 90% [1]. A few years later, in 2020, 1.2 million barriers, including weirs, dams, barrages, sluice gates, ramps, bed sills, culverts, and fords, were counted only for Europe's rivers and streams [2]. Globally, the number of free-flowing rivers is steadily decreasing due to land use, climate change, and increasing water and hydropower demands [3]. River

damming creates physical barriers that fragment rivers and obstruct the natural movement of matter and energy [4–6]. The presence of multiple dams on a single river stream or its main tributaries leads to river fragmentation and, consequently, to consistent flow alteration [7,8]. Numerous studies discuss how dams affect the hydrology and hydrochemistry of rivers [4,6–15]. The hydro-chemical regime is greatly affected by natural fluctuations in river flow, such as seasonal changes, and by human activities that typically involve discharge control [8]. Unfortunately, dam construction is not the only anthropogenic stressor on rivers; urban runoff, agricultural practices, WWTP plants, and industrial discharges all significantly contribute to changes in nutrient loads and COD and BOD dynamics [16–20]. A free-flowing river has a natural flow regime that allows for the continuous transport of nutrients, organic carbon, and sediments [3]. In contrast, an anthropogenically stressed (fragmented) river [16] has transport discontinuities caused by abrupt changes in flow patterns, sediment retention [21], organic matter accumulation, nutrient cycling [14,22], WWTP discharge [23], and so on.

Damming's main effect on nutrients and organic matter is to increase their hydraulic retention time (HRT). The longer the HRT time, the higher the chance of biogeochemical and physical transformations that lead to nutrient consumption [11]. Barriers affect water quality monitoring by creating spatial differences in COD and BOD measurements. Due to pollutant buildup or flow changes, upstream areas may exhibit different features than downstream areas [20]. Due to fragmentation, different river segments process organic matter and nutrients in various ways. The different segments of a river may experience different levels and types of pollution because of land use, urbanization, and industrial activities, and each segment may have unique hydrological features that affect its biogeochemical cycling [7]. Therefore, analyzing independent river segments can show how fragmentation affects nutrient transport, COD and BOD dynamics, and other factors. Such an approach, which involves examining individual segments and comparing them with the entire river system, might provide a more accurate assessment of human impacts. There are very few works that assume that each segment of a fragmented river can behave independently [24–26], even though concepts like river continuum [27] and serial discontinuity [28] are not new and have been thoroughly defined in the literature. Dam-fragmented rivers are thoroughly examined throughout their whole length, and various analysis have been made regarding sediment transport [14,15,21,29–33], nutrient fluxes [1,4,14,15,33–35], water quality [20,36–38], and ecosystem impact [28,39,40].

With 17 dams in its hydrographic basin, the Bahlui River is one of Romania's most hydro-technically engineered rivers. Our previous study highlighted the effectiveness of these dams in managing streamflow and reducing the impacts of droughts and floods [41]. However, we could not find a statistical relationship between the river's nutrient loads and discharge. The data did not support the initial hypothesis that there would be at least a seasonal association between river discharge and nutrient flow, except for a few weak correlations in specific sampling areas. In this work, an equation that links river flow rate to nutrient loads and two relevant water quality chemical indicators (COD and BOD) was employed for this new approach of examining river segments as "independent" watercourses. This study considered the following four river segments separated by a series of anthropogenic stressors: Pârcovaci Dam, Tansa Dam, Podu Iloaiei Dam, and the Iasi Waste Water Treatment Plant (WWTP).

The following aspects underline the novelty of this work:

- Unlike previous studies that focus on water quality and typically examine the Bahlui River as a unified hydrological system, this work introduces a novel conceptual framework that treats river segments as individual watercourses.

- Anthropogenic stressors delimit the analyzed river segments. This segmentation approach allows for understanding how human interventions create localized impacts that do not necessarily propagate throughout the entire river system.
- For each segment, water quality indicators are linked with the river's discharge in an integrated flow–nutrient–pollution analysis.
- The seasonal and annual variations across each segment are presented for twelve years, offering a detailed view of how fragmentation affects long-term water quality patterns.

This research contributes to a better understanding of anthropogenic impacts by providing a comprehensive viewpoint on the transport of nutrients and dynamics of COD and BOD in a fragmented river. Examining the seasonal and yearly changes in nutrients and organic pollutants in separate river segments offers specific benefits, especially in understanding hydrological effects and the ecological impacts of river fragmentation.

2. Materials and Methods

2.1. Research Area, Anthropogenic Amendments, and Segmentation Strategy

2.1.1. Research Area

The main characteristics of the Bahlui River are well described in the literature [41–46]. In brief, the Bahlui River, which is 119 km long, has a catchment area of 2025 km^2 and a hydrographical network of 3100 km. It is the main tributary of the Jijia River. The primary water source of the Bahlui River is runoff from precipitation; in the upstream area, some small tributaries are fed by groundwater. Therefore, as is common for rain-fed rivers, the river's discharge varies significantly throughout the year (seasonal variation) [42]. The annual precipitation in the river's basin is approximately 500 mm. Therefore, it is important to note that only 30% of the hydrographic network has a permanent flow [42,45]. The average discharge ranges from 2.8 m^3/s to 4 m^3/s, but it can reach up to 600 m^3/s (with the highest recorded during floods in 1932) and fall to complete depletion during extended drought periods [47]. To manage these significant fluctuations in discharge flow, often accompanied by heavy floods, 17 dams have been constructed in the Bahlui River basin over the past century. More information about the river's tributaries and the hydrotechnical infrastructure in the Bahlui River system can be found in our previous work [41].

2.1.2. Anthropogenic Amendments

The hydrographic basin of the Bahlui River has experienced significant human interference over the past century. The 17 dams built between 1964 and 1988 provide hydrotechnical management for about 70% of the river basin [41,48]. Between 2010 and 2013, during the European Project "Water-course regulation of Bahlui River, County of Iaşi", the riverbed was regularized for a length of approximately 11 km, which crosses the city of Iaşi [43]. Furthermore, over recent decades, the possibility of implementing new projects related to the development of recreation areas along the urban section of the Bahlui River has been heavily debated [49]. Therefore, the Bahlui River can be considered as one of the most anthropized rivers in Romania. Table 1 provides detailed information about the anthropogenic barriers directly related to this study.

The Pârcovaci accumulation (denoted A1) is situated on the main course of the river, in the upper part, in a highly forested hilly area. From a geological point of view, the primary materials are clays with intercalations of sands, sandstones, and limestones [50]. The Pârcovaci dam (Figure S1) is an earth dam built between 1978 and 1984 and put into operation in 1984 [51]. It is classified as a homogeneous earth embankment; the construction materials are fine, dusty, alluvial clayey, and clayey deluvials [52]. Initially, the main functions of this accumulation were the flood protection of downstream localities and the water supply of the town of Hârlău. The average discharge of the Pârcovaci reservoir is

0.424 m^3/s [42]. Since 2000, according to Law no. 5 of 6 March 2000 regarding the approval of the National Territorial Planning Plan-Section III-protected areas [53], modified by the Emergency Ordinance no. 49 of 31 August 2016 [54], the Pârcovaci accumulation has been a protected area for several species of local ichthyofauna.

Table 1. The reservoirs considered in this study, with some constructive details.

Reservoir Name	Coordinates	Watercourse	Dam Elevation, m	Canopy Length, m	Normal Storage Capacity, $m^3 \cdot 10^6$	Water Surface, $m^2 \cdot 10^4$	Year of Completion
Accumulation Pârcovaci (A1)	47°27′19″ N 26°48′47″ E	Bahlui	25	290	2.75	48	1984
Tansa Lake (A2)	47°17′30″ N 27°4′49″ E	Bahlui	14.2	4890	6.79	289	1974
Accumulation Podu Iloaiei (A3)	47.196842° N 27.191161° E	Bahlueț	14.1	640	3.699	240.9	1964

The Tansa dam (denoted A2) is classified as a homogeneous embankment made from local materials (clay soils) [52]. The Tansa Lake (Figure S2) sedimentary blanket is composed of a layer of brown and grey clay, underlain by Sarmatian deposits consisting of alternating marls and fine sands [55]. The Tansa dam was built on the Bahlui River between 1971 and 1976, becoming operational in 1975. The lake is a multi-purpose reservoir, being used for flood protection, as drinking water supply for the Belcești village, as an irrigation source for farms in the area, and for fish farming [56]. The average discharge of the Tansa dam is 0.839 m^3/s [42].

The Podu Iloaiei Accumulation Lake (denoted A3 and presented in Figure S3) is located on the Bahlueț River, which is the main tributary of the Bahlui River, at a distance of 2.5 km upstream of the confluence with the Bahlui River and 400 m upstream from the town of Podu Iloaiei [57]. The dam has operated since 1964 and is made of local materials, predominantly yellow dusty clays of a homogeneous type [52]. Alluvial soils, carbonated alluviums, soils rich in sodium sulphates, meadow clayey, maroon substrates, and gray soils represent the hydrographic basin [57]. The main functions of Podu Iloaiei Dam Lake include (i) flood protection by controlling the Bahlueț River water flow rate; (ii) supplying the water volume required for fish farming; and (iii) acting as a water source for irrigating an agricultural area of $526 \cdot 10^4$ m^2 [58]. The lake water is evacuated in the winter time [57,59], hence the area and volume of the lake can vary considerably throughout the year. The average discharge of the Podu Iloaiei dam ranges from 0 (in winter) to 1.02 m^3/s [58].

According to the Romanian Government Decision no. 663 of 14 September 2016 on establishing the regimes of protected natural areas and designating special avifauna protection areas as an integral part of the European ecological network Natura 2000 in Romania, the Sârca-Podu Iloaiei accumulation was declared a special avifauna protection area [60].

Additionally, on the fourth section of the river, there is also the Iași Waste Water Treatment Plant (WWTP), which significantly impacts the river discharge after crossing the Iași municipal area. The Iași WWTP (Figure S4) has been developed in stages since 1968 [61]. It is located in the Holboca commune, in the area of the Dancu district, and uses the Bahlui River as effluent. The WWTP daily discharge varies between 2.2 m^3/s and 4.033 m^3/s [62] and can reach up to 8 m^3/s and above during heavy rains [61]. Since the daily amount of urban wastewater remains relatively constant—mainly depending on the number of residents and not on rain or groundwater sources—the daily discharge capacity of the Iasi WWTP is medium-high and stays fairly steady compared to the river's flow rate. During heavy rain, when urban runoff is also collected, the WWTP's daily discharge capacity doubles. In some situations, especially during extended droughts, the

Iasi WWTP's maximum discharge capacity can surpass the average flow rate of the Bahlui River [47].

2.1.3. Segmentation Strategy

The accuracy of the study heavily depends on segment selection, but identifying relevant local boundaries is not always easy. For example, Zhang et al. divided the Shaying River into the following three segments: upstream, middle stream, and downstream [26]. Shehab et al. used a Digital Elevation Model to identify the boundaries required to divide the Tigris River into eight zones [63]. Nardini et al. described four approaches for river segmentation, including (i) manual segmentation based on expert judgement; (ii) segmentation based on image recognition using artificial intelligence and machine learning algorithms; (iii) segmentation based on statistical analysis; and (iv) segmentation based on logical or heuristic algorithms [64]. An equivalent for the term "segment" is the concept of "reach", described and critically analyzed by Parker et al. [65]. A reach is commonly defined as a convenient subdivision, which may be any length of river with fairly uniform characteristics, the length between gauging stations, or the length of a watercourse between any two defined points [66].

In this study, river segmentation was based on expert judgment, considering the main anthropogenic stressors (previously described), how they interfere with the river's natural course, and land use. Manual dam-based segmentation establishes clearly defined boundaries that match actual physical and hydrological breaks in the river system. Unlike arbitrary geometric divisions, dams cause real discontinuities in flow, sediment transport, and water quality. This method aligns segmentation with the physical processes that govern river behavior.

Accordingly, four reaches were designated for further analysis (Figure 1, Table 2). Due to anthropogenic impact, each segment can be treated separately as an "independent" river. The selected river segments and the decision support (the form of human control) for each choice are briefly presented in the following paragraphs.

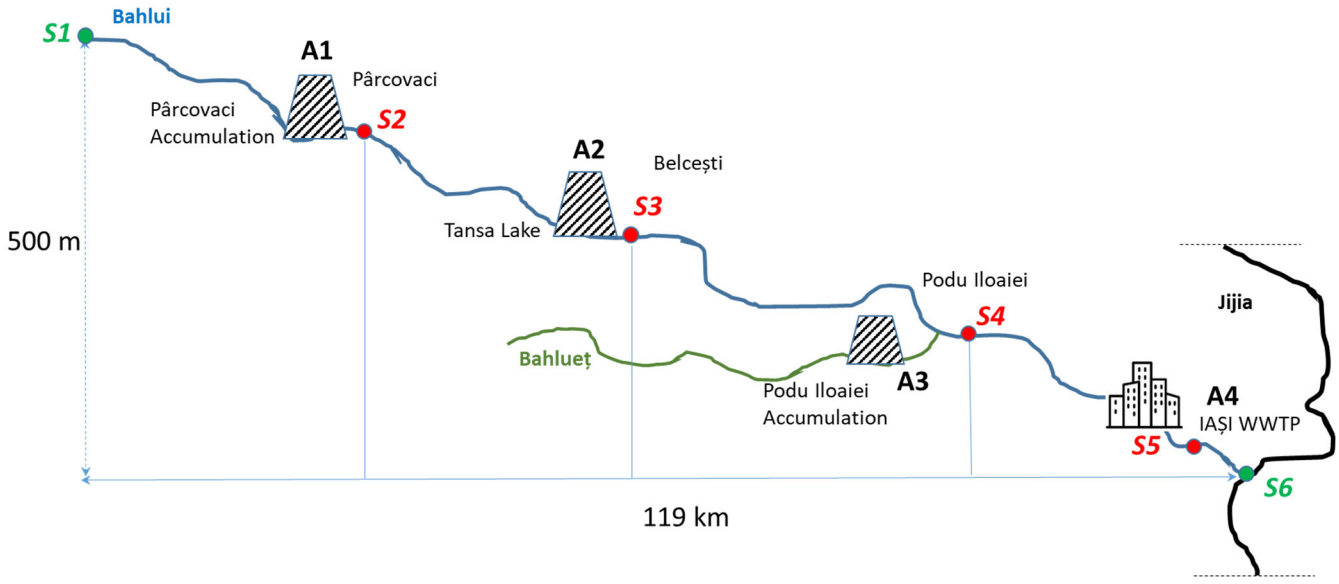

Figure 1. Bahlui River fragmentation: main anthropogenic amendments and sampling locations (not to scale).

Table 2. Brief characterization of the Bahlui River selected segments.

Segment No.		1st Segment	2nd Segment	3rd Segment	4th Segment
Range		S1–S2	S2–S3	S3–S4	S4–S6
Length (km)		11.5	37.5	40	30
Anthropogenic elements		A1	A1, A2	A2, A3	A3, A4
Reach stream	inlet	Natural	Direct dam controlled	Direct dam controlled	Indirect dam controlled
	outlet	Direct dam controlled	Direct dam controlled	Indirect dam controlled	Natural, influenced by the Iasi WWTP discharge
Land use		Forest, aquaculture	Vineyards, orchards, agriculture, and pastures	Agriculture, aquaculture, pastures, animal farms	Agriculture, highly urbanized area

In Figure 1, A1–A4 represent the considered anthropogenic modifications, as follows: A1 = Pârcovaci Dam; A2 = Tansa Dam; A3 = Podu Iloaiei Dam; and A4 = Iasi WWTP. The green dots, S1 and S6, represent the river's spring and the river's end at the confluence with the Jijia River, resepectively. The red dots S2–S5 indicate the sampling locations.

River Spring-Pârcovaci Dam (S1–S2). The first reach is between the river spring (S1) and sampling site S2, including the Pârcovaci accumulation (Figure 1), and features a largely undisturbed riparian ecosystem. The anthropogenic element of control is the Pârcovaci dam, which manages the river's discharge and supplies inflow to the second segment (S2–S3). This entire reach is located in a forested area with minimal to no agricultural or urban disturbances. While aquaculture may influence the nutrient levels, this is well managed, as the Pârcovaci accumulation has been designated as a protected area.

Pârcovaci Dam-Tansa Dam (S2–S3). The stream flow in the second segment is fully controlled, with the inlet by the Pârcovaci dam and the outlet by the Tansa dam. There is a relatively low urban impact through the Hârlău WWTP that services the small town of Hârlău, which is crossed by the Bahlui River. The rural land use includes vineyards, orchards, non-irrigated arable fields, and pastures [67].

Tansa Dam-Podu Iloaiei Dam (S3–S4). The Tansa dam discharge directly controls the entrance to the third reach, while the exit is indirectly regulated by the Podu Iloaiei dam, which manages the flow rate of the Bahlueț River, the main tributary of Bahlui. Sampling site S4 is located downstream of the river's confluence. Before entering the Podu Iloaiei accumulation, the Bahlueț River passes through two towns, Târgu Frumos and Podu Iloaiei. Land use in this section of the Bahlui River primarily consists of pastures and arable fields, both irrigated and non-irrigated. Aquaculture, along with some pig and poultry farms (which operate periodically), are potential sources of nutrients and organic matter. Both the Belcesti WWTP and Podu Iloaiei WWTP utilize this river segment, directly or indirectly, as their effluent source.

Podu Iloaiei Dam-Iasi WWTP (S4–S6). The Podu Iloaiei dam indirectly controls the inlet flow of the fourth river segment. Since the dam is drained during winter, the river flow rate varies significantly, impacting the transport of nutrients and organic matter. Sampling site S5 is located downstream of the Iasi WWTP. The outlet flow is heavily influenced by the Iasi WWTP, which handles municipal wastewater and urban runoff during rainfall. This last segment of the river passes through a relatively small agricultural area, a region of pastures, and the rapidly expanding metropolitan area of Iasi.

2.2. Sampling Sites, Monitored Parameters, Analyzed Period

The four sampling sites, denoted S2, S3, S4, and S5 in Figure 1, were extensively described in our previous work [41]. Water samples were collected according to a specific seasonal or annual schedule. The National Administration of Romanian Waters provided all the data analyzed during this study. The monitored parameters included the river flow rate and the nutrient flow indicated by total nitrogen, total phosphorus, and the level of organic pollution, as shown by chemical oxygen demand (COD) and biochemical oxygen demand (BOD). The analyzed period ranged from 2011 to 2022 for the S2, S4, and S5 sampling sites and from 2015 to 2022 for S3.

2.3. River Load Calculation Approach Methods: Theoretical Background, Selected Equation, Statistical Analysis

A river's "instantaneous load" with a particular constituent is commonly defined as the result of the water discharge and the concentration of that constituent as they pass through the stream cross section [68]. The total amount and/or the flow rate of a particular component (pollutant, nutrient) that is transported by the river in a given period can be calculated by knowing its "instantaneous load." These definitions can be expressed using Equation (1) [68–70], as follows:

$$F_i \cong \int_{t_i}^{t_f} L_i(t) \cdot dt \ = k \cdot \int_{t_i}^{t_f} C_i(t) \cdot Q(t) \cdot dt \quad (1)$$

where F_i is the amount/flow rate of the component "I" transported during the monitored time interval; t_i and t_f represent the beginning and ending times of the measurements; C_i represents the concentration of the "i" component at the time t, while Q_i represents the river's discharge at the time t; and the constant k is used to adjust the measurement units (when necessary).

Naturally, the length of the monitored period, the sampling frequency, and accuracy are critical to the precision of the load estimation [71]. There are additional factors that can influence the accuracy of the calculation; some of these are fairly predictable, like the succession of seasons with rainy and dry periods, while others are less or not at all predictable, like heavy rains accompanied by floods or prolonged drought periods, which are frequently associated with climate change phenomena [72]. In addition to these natural interferences, human activity can also have a direct impact on the river loads through damming, aquaculture, discharges from WWTPs, land use, and other actions [7–9,16,41,73,74].

Over the years, several methods have been developed to estimate the contaminant loads in rivers and solve Equation (1) [69,75,76]. In a recent study, Zhang and coworkers [76] identified the following three categories of methods for estimating river loads: (i) interpolation algorithms, which use interpolations between measured concentrations; (ii) ratio methods, using the ratio of the average load to the average flow; and (iii) regression methods, which establish a regression relationship between concentration and flow to estimate loads.

In this work, the method of weighted averages [77,78] was applied to estimate the annual discharge of nutrients, as well as COD and BOD fluctuations. The approach falls under the category of interpolation algorithms, and Equation (2) describes the yearly load of a particular component.

$$F_i = K_x \cdot \overline{Q_i} \cdot \frac{\sum_{i=1}^{n} C_i \cdot Q_i}{\sum_{i=1}^{n} Q_i} \quad (2)$$

where the constant K_x is used to correlate the measure units and the considered period, e.g., for a year, K_x considers a value of 366 days, for a month, 30 days, and for a season, 91 days.

To visually represent the data and assess normal distributions, normal probability plots (NPPs) were used. When such graphs display a nearly straight line, it is relatively safe to assume that the data follow a normal distribution. Additionally, it is easy to visually identify the presence of skewness, outliers, or other nonlinear anomalies that suggest unexpected events. In addition to the visual inspection, NPPs provide specific parameters such as the *p*-value, mean, and standard deviation, with the *p*-value being the most commonly used in actual statistical analysis. To determine whether the data are normally distributed, a significance level of 0.05 is used. A *p*-value less than or equal to this significance level suggests that the data do not follow a normal distribution. Conversely, a *p*-value greater than the significance level indicates a high probability that the data do follow a normal distribution [79].

The calculations were performed using Microsoft Excel, while the NPPs were generated using the Minitab® Statistical Software Version 21.2 (Minitab, LLC, 2022, State College, PA, USA). The overall workflow of the steps performed in the current work is presented in Figure 2.

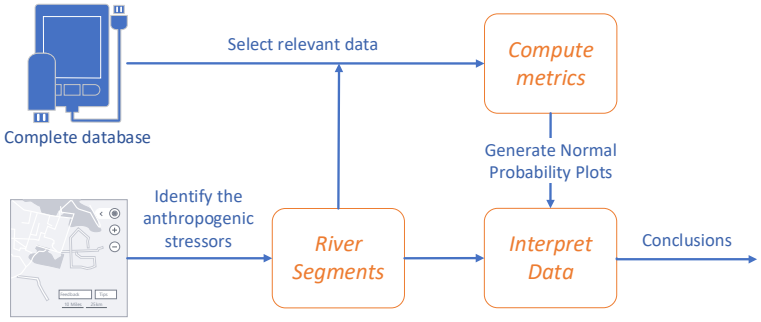

Figure 2. Steps of the performed analysis.

3. Results and Discussion

3.1. Fragmentation Impact on Nutrient Dynamics and Organic Pollution Load: Seasonal Variation

Seasonal monitoring can reveal short-term changes in nutrient levels and spikes in organic pollution caused by factors such as weather events, agricultural runoff, and accidental spills. These may be missed in annual reports due to data averaging. Additionally, seasonal analysis helps to distinguish between natural cycles and human impacts, providing a comprehensive view of water quality dynamics.

3.1.1. River Spring-Pârcovaci Dam (S1–S2)

The first river segment (Figure S5) runs through a forested area; the main controlling factor is the discharge from the Pârcovaci dam. The main tributaries along this part of the river are Bahlueț Mic, Valea Mare, and Valea Cetățuiei.

The presence of nitrogen and phosphorus in this initial segment is attributed to natural sources. This aligns with the findings in the literature, where Duchesne et al. studied how nutrients transfer seasonally from forest canopy leaves to lake water [80]. Table 3 presents the seasonal evolution of total nitrogen (N_T) and total phosphorus (P_T) for the considered interval (2011–2022). The seasons are represented by numerical designations and their corresponding names to maintain the standard sequence of seasons in all tables and figures. The river annually carries an average of 4.47 tons of N_T. This amount varies greatly each year, ranging from 0.74 tons to 12 tons. Notable extreme loads are recorded in 2011 and 2013, affecting the overall average. The large standard deviation of 3.86 tons indicates that this segment's total nitrogen is mainly affected by a few high-load years or seasons.

Table 3. Nutrient dynamics for the first river segment.

S1–S2	N_T (t/Season)				P_T (t/Season)			
Year	**1. Winter**	**2. Spring**	**3. Summer**	**4. Autumn**	**1. Winter**	**2. Spring**	**3. Summer**	**4. Autumn**
2011	4.06	0.12	4.00	3.81	0.14	0.00	0.27	2.16
2012	-	0.27	0.15	5.03	-	0.03	0.01	0.52
2013	7.31	1.59	2.23	0.52	1.47	0.02	0.05	0.03
2014	3.69	0.20	0.39	0.31	0.08	0.04	0.04	0.01
2015	0.24	0.20	0.19	1.32	0.01	0.01	0.01	0.05
2016	0.13	2.29	0.43	0.31	0.01	0.19	0.04	0.03
2017	1.02	0.71	0.62	0.63	0.25	0.07	0.01	0.02
2018	0.61	0.38	0.39	0.22	0.04	0.13	0.06	0.13
2019	0.26	0.23	0.79	0.29	0.19	0.08	0.64	0.04
2020	0.35	0.32	0.33	0.36	0.09	0.05	0.08	0.06
2021	0.30	-	6.15	0.14	0.04	-	0.20	0.01
2022	0.14	0.15	0.29	0.15	0.01	0.01	0.06	0.00

The average annual P_T load is 0.63 tons. The variability is significant, ranging from 0.08 tons to 2.5 tons, with a standard deviation of 0.74 tons, which is above the mean. This variation is affected by notable seasonal events, including the heavy autumn load in 2011 (2.16 tons) and the high winter load in 2013 (1.47 tons).

The NPP for nutrient dynamics in the River Spring-Pârcovaci dam segment is shown in Figure 3. Across all seasons, the *p*-values and NPP indicate that the N_T does not follow a normal distribution. The highest and most variable measurements are recorded in winter, while the lowest and most consistent levels occur in spring. The outliers correspond to N_T values from 2011, 2013, and 2014, which are linked to the drought period from 2011 to 2013 [41].

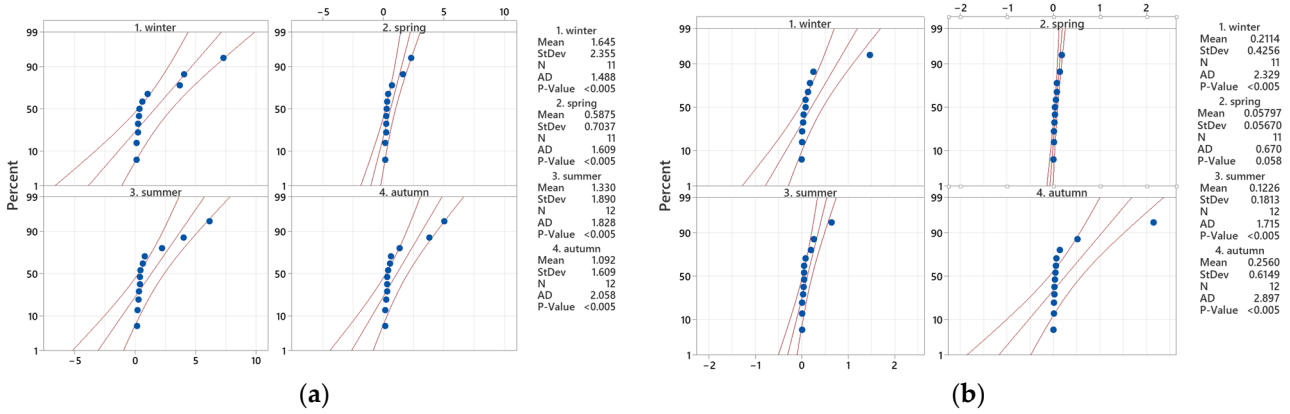

(**a**) (**b**)

Figure 3. NPP in the case of S1–S2 segment for (**a**) total nitrogen and (**b**) total phosphorus.

For P_T, the calculated values are several orders of magnitude lower than those for N_T, and the NPP exhibits different seasonal trends, with autumn showing the highest average load and the greatest variability. The fall peak illustrates a "first flush" phenomenon, where phosphorus bound to soil particles, stored during the dry summer, is released into the river by the first substantial autumn rainfall. This suggests that, for this section, soil erosion is a primary pathway for phosphorus delivery.

The *p*-value for spring is slightly above the 0.05 threshold, suggesting that the data mostly conforms to the normal distribution. This small load contradicts several studies that predict a surge after spring snowmelt; however, it could indicate a phase of significant biological uptake or resource depletion following winter runoff [81]. The outliers observed in all seasons except spring correspond to the same 2011–2013 drought period when N_T values are also recorded.

Table 4 presents the seasonal evolution of COD and BOD for the considered interval (2011–2022). The examination of the COD data emphasizes the event-driven characteristic of this indicator. The mean yearly load is 47.7 tons, and the standard deviation is significantly higher at 75.7 tons. This indicates that this segment's total COD budget is governed by several years of significantly elevated values, rather than a typical "average" year. The highest yearly loads occur during intense seasonal events, specifically in 2012 and 2014. The average annual BOD load is 13.0 tons, with a standard deviation of 18.9 tons. Similar to COD, the variability surpasses the mean, demonstrating that outlier events impact the annual load.

Table 4. Organic pollution load for the first river segment.

S1–S2	COD (t/Season)				BOD (t/Season)			
Year	1. Winter	2. Spring	3. Summer	4. Autumn	1. Winter	2. Spring	3. Summer	4. Autumn
2011	83.38	4.12	99.90	84.46	32.81	1.55	49.75	34.68
2012	-	5.92	8.00	321.17		2.09	2.96	115.76
2013	200.52	12.55	17.95	10.91	57.35	2.92	5.38	2.43
2014	204.48	17.19	15.29	12.32	38.01	2.84	2.21	0.78
2015	3.66	4.85	8.88	32.20	0.57	1.01	1.25	5.96
2016	6.77	208.91	11.49	14.55	2.19	46.53	3.69	4.57
2017	26.62	16.81	14.63	14.75	8.47	5.38	4.46	5.15
2018	5.37	9.30	12.00	6.02	1.69	3.68	4.35	2.16
2019	4.38	10.94	67.21	10.72	1.51	3.59	23.56	3.47
2020	11.22	13.82	11.28	14.64	3.52	4.48	4.82	6.93
2021	10.29	-	220.26	11.81	4.82	-	105.65	5.98
2022	15.65	13.73	13.23	13.69	4.94	2.11	1.86	1.65

The NPP showing the trends observed during each season is presented in Figure 4. In terms of COD, although winter has the highest average load, each season has experienced at least one major pollution event, leading to substantial standard deviations that often exceed the seasonal average. Winter also displays the highest average BOD load, with a standard deviation greater than the mean, indicating a high variability.

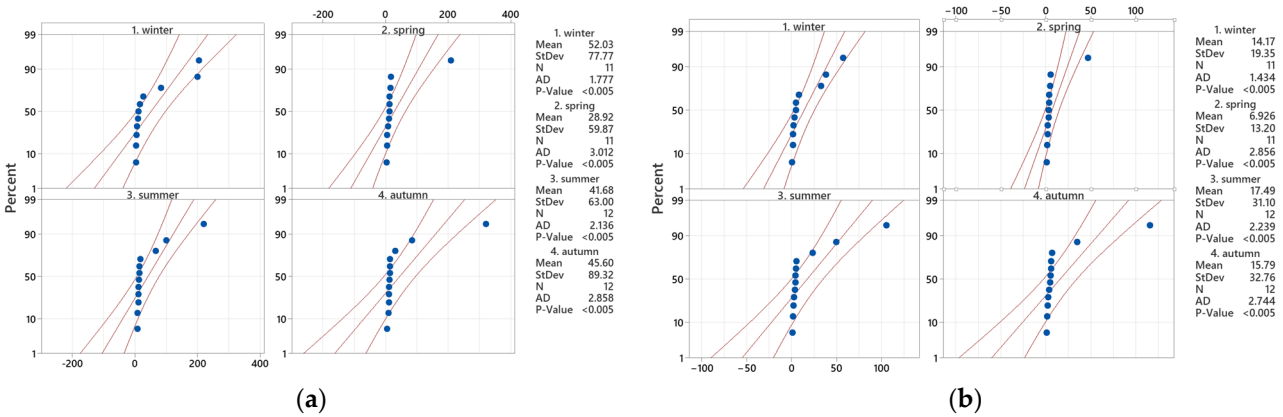

(**a**) (**b**)

Figure 4. NPP in the case of S1–S2 segment for (**a**) COD and (**b**) BOD.

3.1.2. Pârcovaci Dam-Tansa Dam (S2–S3)

A landscape featuring vineyards, orchards, arable (non-irrigated) fields, and grasslands is crossed by the second segment of the river (Figure S6). The Hârlău WWTP, situated at the start of this section, has a relatively minor urban impact. The flow from the Pârcovaci dam controls the river's intake, while the flow from the Tansa dam manages the river's outflow. The main tributaries along this part of the river are Buhalnița, Magura, and Vulpoiul.

Table 5 presents the seasonal evolution of N_T and P_T for the considered interval. For N_T, it can be observed that there is extreme inter-annual variability. For example, in 2015, the annual value is dominated by a single large winter event, whereas other years tend to be more evenly distributed or feature multiple seasonal peaks. The fact that most of the annual load in some years occurs in just one season underscores the significance of episodic events like heavy rain, snowmelt, or pulses of agricultural runoff. Similarly, for P_T, there are highly variable annual loads, mainly driven by single events.

Table 5. Seasonal evolution of N_T and P_T for the S2–S3 sector.

S2–S3	N_T (t/Season)				P_T (t/Season)			
Year	1. Winter	2. Spring	3. Summer	4. Autumn	1. Winter	2. Spring	3. Summer	4. Autumn
2015	78.77	4.96	0.20	1.87	0.74	0.09	0.02	0.04
2016	2.22	0.46	13.89	43.28	0.03	0.01	3.27	11.77
2017	2.87	38.48	1.06	1.32	0.04	1.86	0.07	0.18
2018	8.14	4.46	3.06	27.03	0.16	0.24	0.19	3.90
2019	6.03	6.71	4.76	4.22	0.30	0.39	0.28	0.28
2020	9.83	9.51	5.40	7.13	0.15	0.17	0.29	0.45
2021	12.25	16.54	21.80	1.82	0.21	0.86	4.69	0.36
2022	13.45	3.31	1.99	12.51	0.24	3.31	0.62	0.94

When considering the S2–S3 vs. S1–S2 segments, the ratio between nutrient values in similar seasons is bigger than 1, ranging from 1.04 in summer 2015 to 626.97 in autumn 2022. There are only a few exceptions: spring 2016 for N_T and autumn 2015, spring 2016, winter 2017, and summer 2019 for P_T.

Figure 5 shows the NPP for nutrients in the S2–S3 sector. In all cases, the *p*-value is less than 0.05, indicating that the data does not follow a normal distribution. Additionally, compared to the mean, the standard deviations are higher in all cases, reflecting a high variability. Similar to the S1–S2 sector, for N_T, the highest means are observed in winter, while for P_T, they occur in autumn.

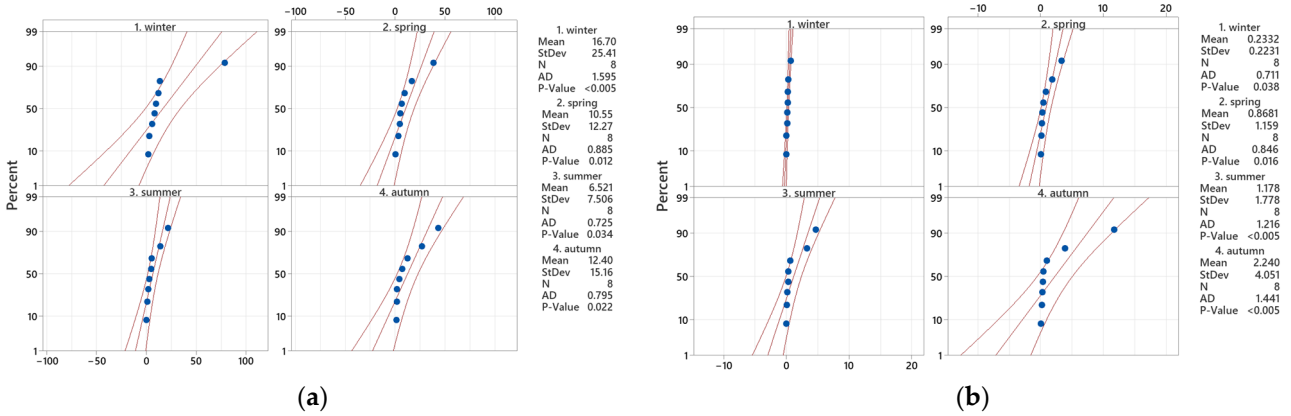

(**a**) (**b**)

Figure 5. NPP in the case of S2–S3 segment for (**a**) total nitrogen and (**b**) total phosphorus.

Table 6 presents the seasonal trends of COD and BOD over the period from 2015 to 2022. The ratio of organic pollution between similar periods in S2–S3 and S1–S2 is greater than 1, ranging from 1.01 in Spring 2015 (for BOD) to 220.26 in summer 2021 (for COD). There is only one exception: winter 201r for BOD, when the ratio is 0.57. This suggests that a "self-purification" process occurred, with natural conditions supporting the growth of microorganisms that degrade organic matter.

Table 6. Organic pollution load for the S2–S3 sector.

S2–S3	COD (t/Season)				BOD (t/Season)			
Year	1. Winter	2. Spring	3. Summer	4. Autumn	1. Winter	2. Spring	3. Summer	4. Autumn
2015	289.55	35.97	3.47	3.67	26.50	2.44	1.22	2.22
2016	3.08	2.46	341.28	732.34	0.98	0.88	125.31	257.05
2017	9.72	333.19	9.05	18.67	2.94	113.55	2.66	6.44
2018	12.26	29.30	15.36	532.69	4.38	9.75	4.71	198.62
2019	18.44	63.82	41.60	36.04	5.92	20.63	12.78	12.70
2020	29.63	18.94	38.60	92.18	13.32	8.33	19.31	40.88
2021	37.08	363.15	194.21	59.25	15.36	141.95	75.91	27.60
2022	36.38	49.47	53.08	183.19	16.99	23.63	20.07	53.25

Similar to the variation observed in the S1–S2 sector, some years show seasonal sharp increases in both COD and BOD, suggesting that episodic events impact them. This pattern is also visible in the NPP (Figure 6). For COD, the lowest average value occurs in winter, while the highest is in autumn. However, across all seasons, the standard deviation exceeds the mean, indicating that outliers significantly influence the data mean. For BOD, the only case where the *p*-value is greater than 0.05 is during winter, suggesting that in this case, the data follows a normal distribution. Aside from winter, the seasonal patterns observed for COD are similar to those for BOD. This indicates that the river's organic pollution mainly comes from sources that contribute both biodegradable and non-biodegradable matter, which are influenced by temperature and flow. The difference in winter highlights the greater sensitivity of BOD to temperature-driven biological processes.

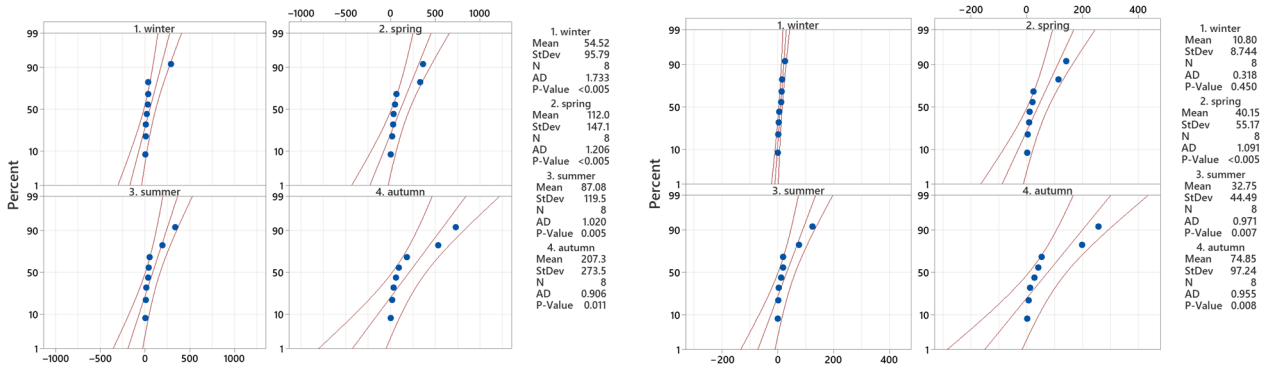

(**a**) (**b**)

Figure 6. NPP in the case of S2–S3 segment for (**a**) COD and (**b**) BOD.

3.1.3. Tansa Dam-Podu Iloaiei Dam (S3–S4)

The third segment's land use mainly includes arable fields and pastures. Here, the river is joined by its main tributary, the Bahluieț River. Since the Bahluieț River flows through two cities, Târgu Frumos and Podu Iloaiei, it indirectly contributes to an urban influence. The Tansa dam directly regulates the flow in this section of the river, while the outflow is indirectly managed by the Podu Iloaiei dam, located on the Bahlueț River. The confluence of the two rivers occurs downstream of the Podu Iloaiei dam (S4 point in Figure S7).

Table 7 shows the seasonal changes in total nitrogen and total phosphorus over the studied period (2011–2022). Compared with similar seasons in the previous segment, there is some uneven variation, which supports the idea that the river segments evolve independently. Since data from 2011 to 2015 are missing for the second segment, the comparison only includes the period from 2015 to 2022. For N_T, the ratio of reported values during the same seasons for the S3–S4 and S2–S3 segments ranges from 0.02 in spring 2017

to 38.33 in spring 2016. For P_T, the variation ranges from 0.05 in summer 2016 to 78.84 in spring 2016.

Table 7. Seasonal evolution of N_T and P_T for the S3–S4 sector.

S3–S4	N_T (t/Season)				P_T (t/Season)			
Year	1. Winter	2. Spring	3. Summer	4. Autumn	1. Winter	2. Spring	3. Summer	4. Autumn
2011	40.37	44.56	4.50	18.02	2.82	6.95	1.96	0.60
2012	9.58	11.18	2.34		0.48	1.09	0.22	
2013	8.34	23.07	11.84	24.36	0.52	4.52	2.13	2.66
2014	19.57	28.68	2.89		1.12	7.50	0.17	
2015	56.92	42.83	1.77	16.32	18.91	4.48	0.19	1.39
2016	4.86	17.47	1.71	11.57	0.19	1.14	0.18	1.57
2017	3.77	0.94	4.38		0.11	0.11	0.17	-
2018	9.94	7.49	5.95	24.35	0.50	1.76	0.52	8.42
2019	13.73	30.61	7.34	10.85	0.75	3.69	1.52	1.32
2020	11.36	7.51	4.42	14.90	0.39	0.50	0.44	1.65
2021	9.45	19.11	11.63	9.96	0.20	1.45	2.60	0.83
2022	11.02	2.31	0.55	1.77	0.20	0.32	0.12	0.23

The NPP of nutrient distribution for the third river segment is presented in Figure 7. For N_T, unlike the two previous sectors, the standard deviation is lower than the mean, indicating that although there is high variability in the data, the influence of outliers on the mean is lower. The lowest mean occurs in summer, while the highest occurs in spring. Except for in winter, the *p*-value is greater than 0.05, indicating that the data follow a normal distribution. For P_T, the data shows a normal distribution only for spring. Distinctively from N_T, but in line with the previous sectors, the standard deviation is higher than the mean, indicating that there are still high yearly variations per season, underlining once again the impact of natural external factors on water quality.

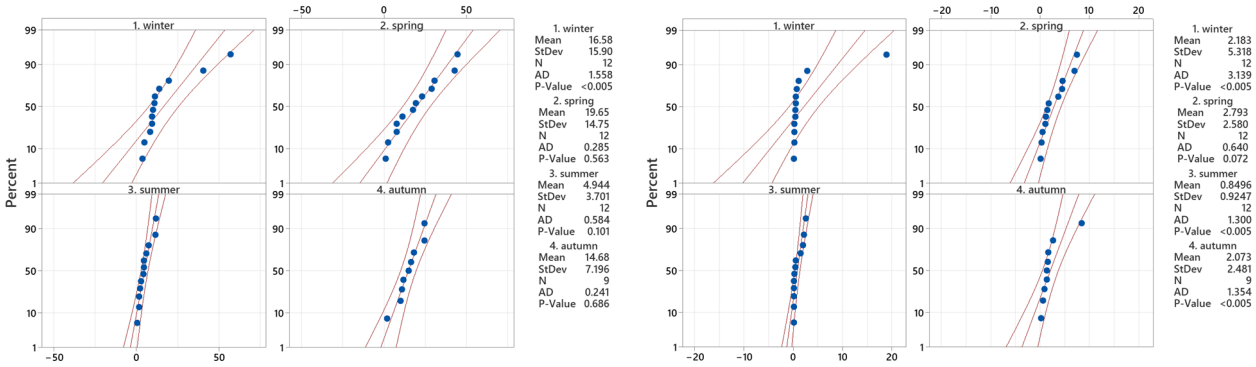

(**a**) (**b**)

Figure 7. NPP in the case of S3–S4 segment for (**a**) total nitrogen and (**b**) total phosphorus.

Table 8 presents the seasonal evolution of COD and BOD for the considered interval (2011–2022). Similar to N_T and P_T, the ratio of seasonal values for segments S3–S4 and S2–S3 fluctuates unevenly for COD and BOD. The range for COD is between 93.36 in spring 2017 and 0.04 in spring 2017, while for BOD, it ranges from 96.03 in spring 2016 to 0.04 in spring 2017. When the results for two consecutive seasons fluctuate this much, it suggests an event that directly affects the river's organic pollution.

Table 8. Seasonal evolution of COD and BOD for the S3–S4 sector.

S3–S4	COD (t/Season)				BOD (t/Season)			
Year	1. Winter	2. Spring	3. Summer	4. Autumn	1. Winter	2. Spring	3. Summer	4. Autumn
2011	151.02	513.27	111.29	138.87	74.63	166.96	37.49	49.50
2012	59.60	190.84	33.63		20.84	61.09	10.86	
2013	39.05	371.92	346.83	587.53	13.71	227.03	79.08	76.77
2014	132.12	795.45	25.63		18.33	145.08	5.48	
2015	533.40	534.64	58.89	237.90	101.11	135.66	13.17	38.98
2016	62.94	229.82	15.47	192.64	21.58	84.24	8.84	56.53
2017	19.66	14.96	32.45		6.33	4.54	9.73	
2018	29.15	60.16	70.32	485.28	9.38	20.59	24.12	186.86
2019	75.08	505.94	91.69	145.75	24.52	183.80	31.56	48.42
2020	78.79	56.73	47.05	176.99	31.65	18.95	25.74	83.96
2021	37.31	89.44	222.22	132.05	16.73	31.23	99.22	57.58
2022	37.67	25.81	7.58	37.61	15.57	3.36	0.94	12.03

The NPP for the organic pollution load in the Tansa dam-Podu Iloaiei dam section is presented in Figure 8. For both COD and BOD, the data follow a normal distribution only in the spring, indicating that although there are variations between the years, in this case, they follow a normal pattern.

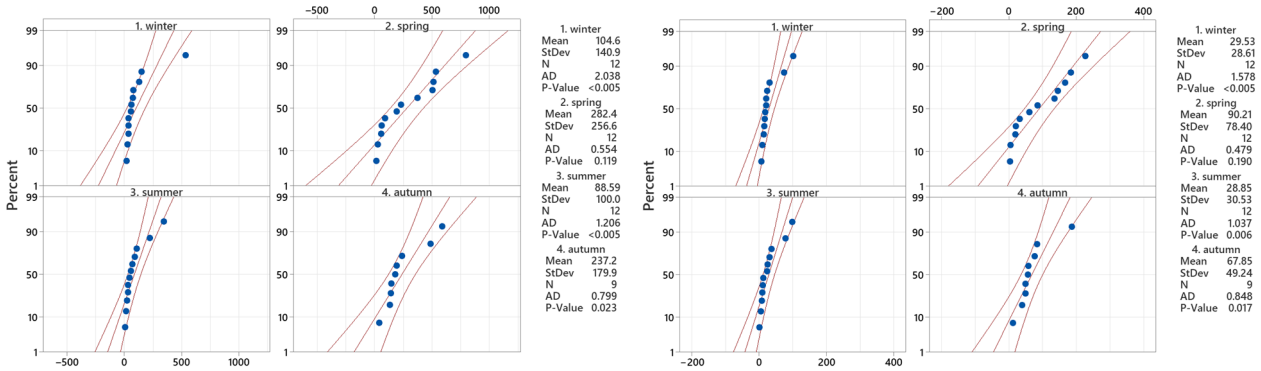

(**a**) (**b**)

Figure 8. NPP in the case of S3–S4 segment for (**a**) COD and (**b**) BOD.

3.1.4. Podu Iloaiei Dam-Iași WWTP (S4–S6)

Although it passes through a grassland and agricultural area, the final section is significantly impacted by the 14 km it spends crossing the metropolitan area of Iaşi and the city's WWTP. Sampling site S5 is located about 7 km from the Bahlui confluence with Jijia (the point S6 in Figure S8), immediately past the Iaşi WWTP. The dam at Podu Iloaiei indirectly controls the flow at the entrance to this last segment of the river, while the outflow is directly influenced by the WWTP of the city of Iasi, whose contribution is significant [82]. This final section of the river has a relatively high number of both temporary and permanent tributaries compared to the other three segments considered (Figure 1).

Table 9 shows the seasonal changes in total nitrogen and total phosphorus for the period from 2011 to 2022. Table 10 displays significantly higher values compared to those reported for other parts of the river. Compared to the results for the same seasons in the previous segment (autumn 2018), the N_T values are at least seven times higher, while the P_T values are at least four times higher (autumn 2018). In the summer of 2022, these ratios reach their peak: about 210 for P_T and roughly 266 for N_T. These numbers demonstrate how urbanization influences nutrient levels. The many tributaries passing through agricultural areas could also contribute to the increases in total nitrogen and phosphorus levels.

Table 9. Seasonal evolution of N_T and P_T for the S4–S6 sector.

S4–S6	N_T (t/Season)				P_T (t/Season)			
Year	1. Winter	2. Spring	3. Summer	4. Autumn	1. Winter	2. Spring	3. Summer	4. Autumn
2011	268.70	259.70	162.87	230.16	26.32	30.72	23.11	26.08
2012	255.05	222.14	244.12	183.81	24.56	25.18	22.15	22.69
2013	284.19	286.47	240.36	322.27	12.10	31.79	27.53	29.98
2014	295.53	529.08	259.07	181.62	22.52	81.12	30.11	27.87
2015	370.32	238.23	81.92	134.19	69.44	33.20	25.14	16.40
2016	127.05	112.67	104.73	459.00	9.05	5.55	7.29	49.78
2017	108.10	205.96	83.69	168.73	4.90	14.48	12.50	14.83
2018	223.27	99.93	201.34	170.96	29.51	17.32	16.22	36.25
2019	301.61	324.64	76.03	170.95	31.72	25.54	14.68	20.28
2020	133.81	189.62	96.81	99.72	22.97	23.07	12.15	10.91
2021	157.09	142.16	144.69	210.75	12.70	18.16	19.24	13.26
2022	181.09	138.39	147.26	214.04	18.93	14.48	24.19	17.39

Table 10. Seasonal evolution of COD and BOD for the S4–S6 sector.

S4–S6	COD (t/Season)				BOD (t/Season)			
Year	1. Winter	2. Spring	3. Summer	4. Autumn	1. Winter	2. Spring	3. Summer	4. Autumn
2011	1218.74	1238.94	727.90	834.59	386.56	494.74	260.81	263.42
2012	283.39	327.71	381.10	275.71	117.13	152.66	135.13	102.24
2013	379.54	1407.91	1312.56	801.92	132.01	719.68	209.81	99.93
2014	708.19	5593.43	1138.84	1144.13	192.95	1047.26	43.23	191.13
2015	1015.08	1921.31	291.88	651.33	182.52	307.39	55.60	115.85
2016	437.05	298.12	385.25	4244.60	144.52	110.95	131.08	1456.77
2017	306.77	1779.65	336.86	1273.19	105.55	450.54	105.57	436.52
2018	595.75	990.31	805.10	797.08	191.22	314.28	285.33	310.17
2019	1007.70	1680.02	483.68	1304.99	342.61	561.07	155.59	437.19
2020	456.08	721.17	411.66	424.75	151.45	236.07	174.40	200.75
2021	439.19	555.15	870.17	657.01	189.72	214.98	361.30	294.44
2022	410.50	473.75	609.00	376.06	192.24	74.54	127.28	45.63

The NPP for nutrient variation in the last river segment is shown in Figure 9. Except for N_T in winter, the standard deviation is smaller than the mean, indicating that seasonal events have a lesser impact on the mean compared to the other sectors. This suggests that the presence of the WTTP in this last segment tends to lessen outliers in the data. For N_T, the lowest mean occurs in summer and the highest in spring; however, the difference between them is much smaller than in the other sectors. Except for winter, N_T data follow a normal distribution. For P_T, the normal distribution holds true for summer and autumn. The smallest mean occurs in summer and the highest in spring.

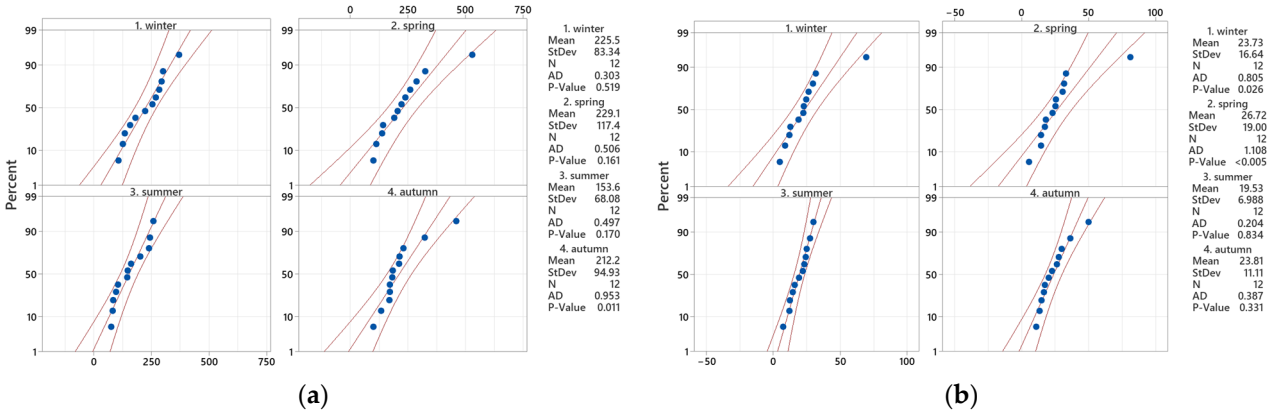

(**a**) (**b**)

Figure 9. NPP in the case of S4–S6 segment for (**a**) total nitrogen and (**b**) total phosphorus.

Table 10 presents the seasonal evolution of COD and BOD in the considered interval (2011–2022) for the last segment of the river. In comparison to the other sections, the final river length has substantially higher COD and BOD levels (as well as N_T and P_T values).

The NPP for the organic pollution load in the last river section is presented in Figure 10. The data follows a normal distribution for summer in the case of COD and for spring and summer in the case BOD. While the standard deviations for P_T and N_T are lower than the mean in most cases, this is not true for COD and BOD. Additionally, some years show extreme outliers, such as spring 2014 and autumn 2017.

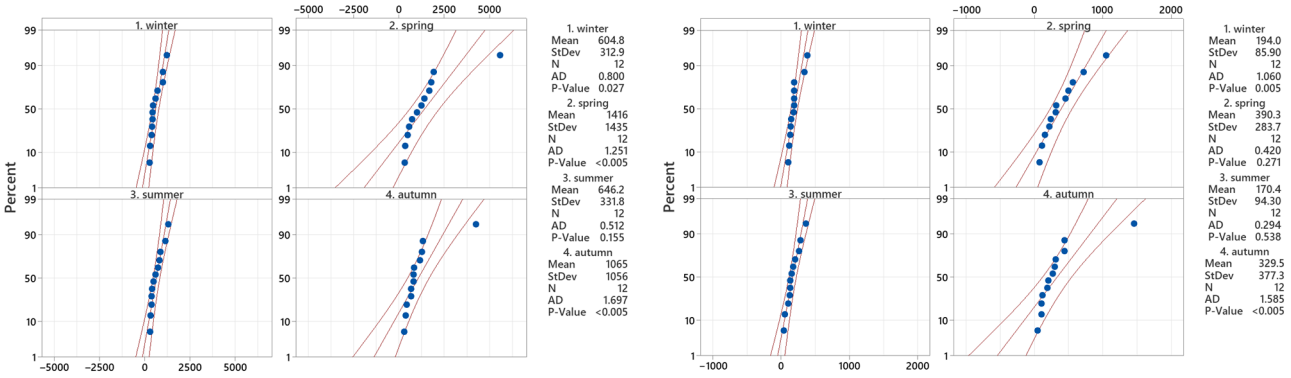

(**a**) (**b**)

Figure 10. NPP in the case of S4–S6 segment for (**a**) COD and (**b**) BOD.

3.2. Fragmentation Impact on Nutrient Dynamics and Organic Pollution Load: Annual Report

The administration frequently requires annual reports, as they provide a comprehensive overview of the evolution of water quality, allowing for the identification of long-term causes such as land use changes or climate change, as well as minor variations or persistent trends. However, annual mediation can hide important seasonal or episodic events, such as pollution spikes or short-term ecological instabilities.

The annual trends of NT and PT in the considered period (2011–2022) for each river segment are shown in Figure 11. Because the values for the S4–S6 sector are much higher than the others, they were plotted on the secondary axis. Unlike the seasonal analysis, which revealed the presence of relatively high disturbances through outliers, the annual analysis tends to hide these high instabilities, especially in the NPP (Figure 12).

(**a**)

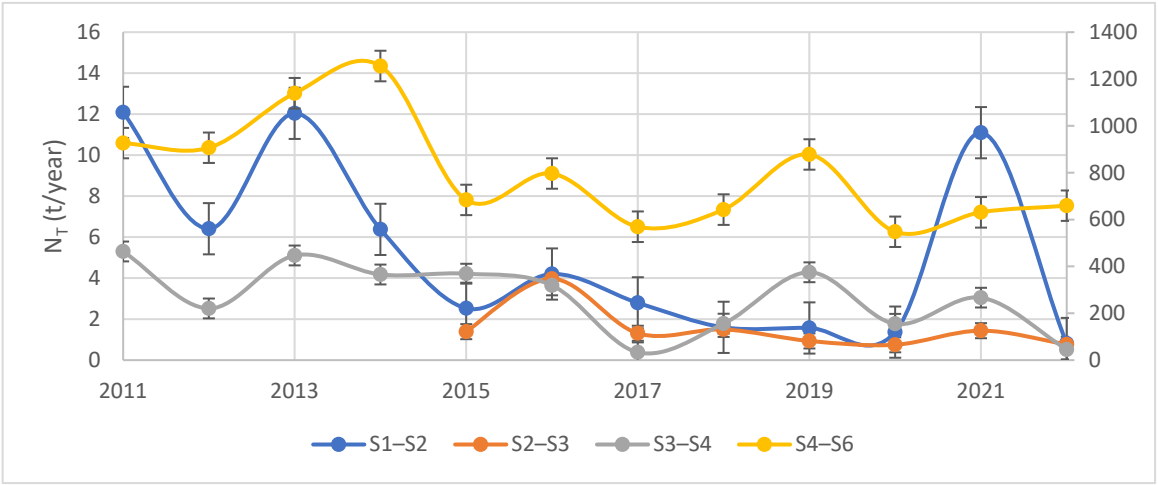

Figure 11. *Cont.*

(**b**)

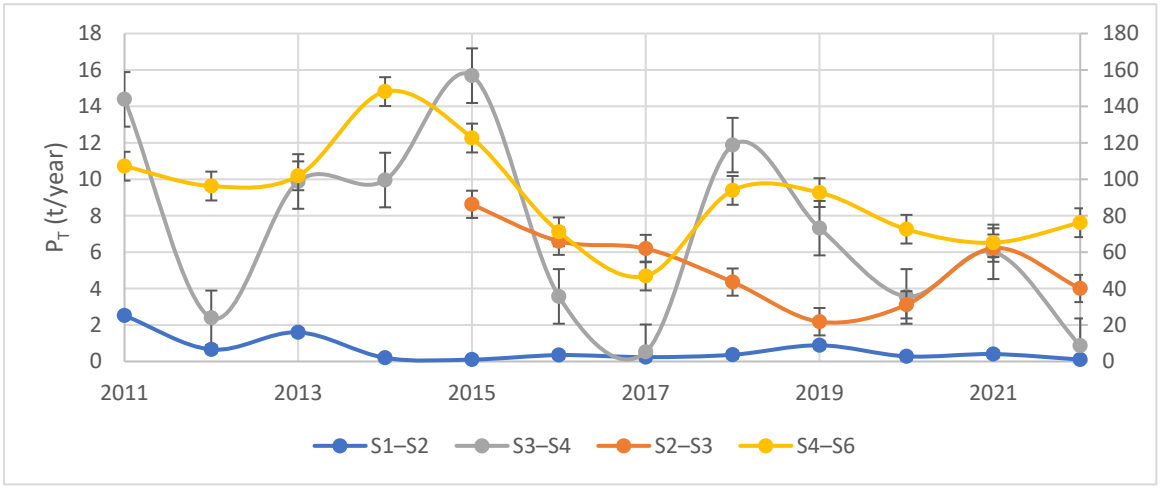

Figure 11. Variation in all segments for (**a**) total nitrogen and (**b**) total phosphorus.

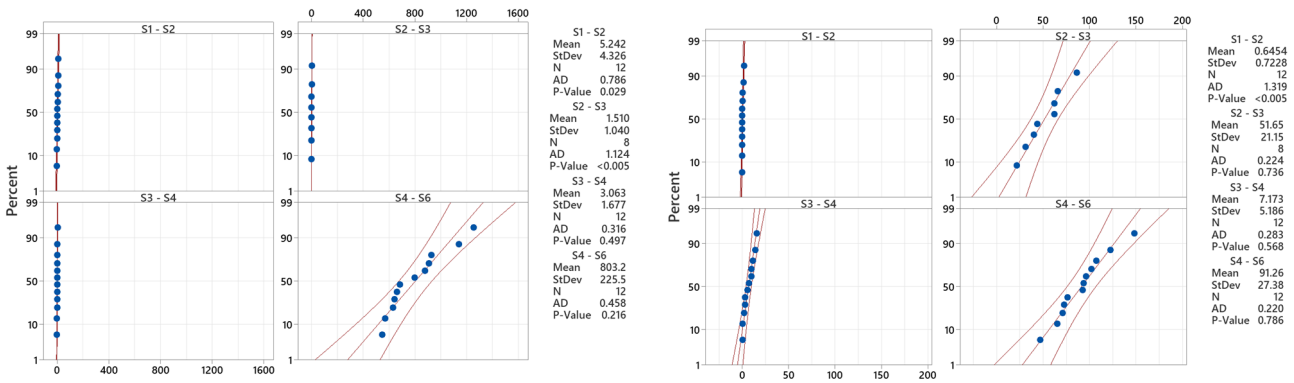

(**a**) (**b**)

Figure 12. NPP for all segments covering average annual values for (**a**) total nitrogen and (**b**) total phosphorus.

Although the data from Figure 10a suggests that the values are very close, this is because of the large differences between the total values recorded for each segment. Between S1–S2 and S4–S6, the order of magnitude for some of the considered years exceeds 100. The obtained *p*-value indicates that in the NT case, the average annual values follow a normal distribution for S3–S4 and S4–S6. For PT, only the S1–S2 segment shows data that do not follow a normal distribution.

Figure 13 presents the annual evolution of COD and BOD in the considered interval (2011–2022) for each river section. As can be observed, the yearly variation does not follow the same trend for all sectors, highlighting the fact that each sector has a different response regarding the analyzed pollutants.

The statistical analysis in this case (Figure 14) indicates that the data do not follow a normal distribution for COD only for the S1–S2 segment. This is due to the fact that there is a high order of magnitude between the values recorded in the first segment and the last segment. For all the data, the standard deviation is smaller than the mean. In contrast with the seasonal analysis, it can be observed that the outliers are hidden and that the standard deviation values are lower than the averages.

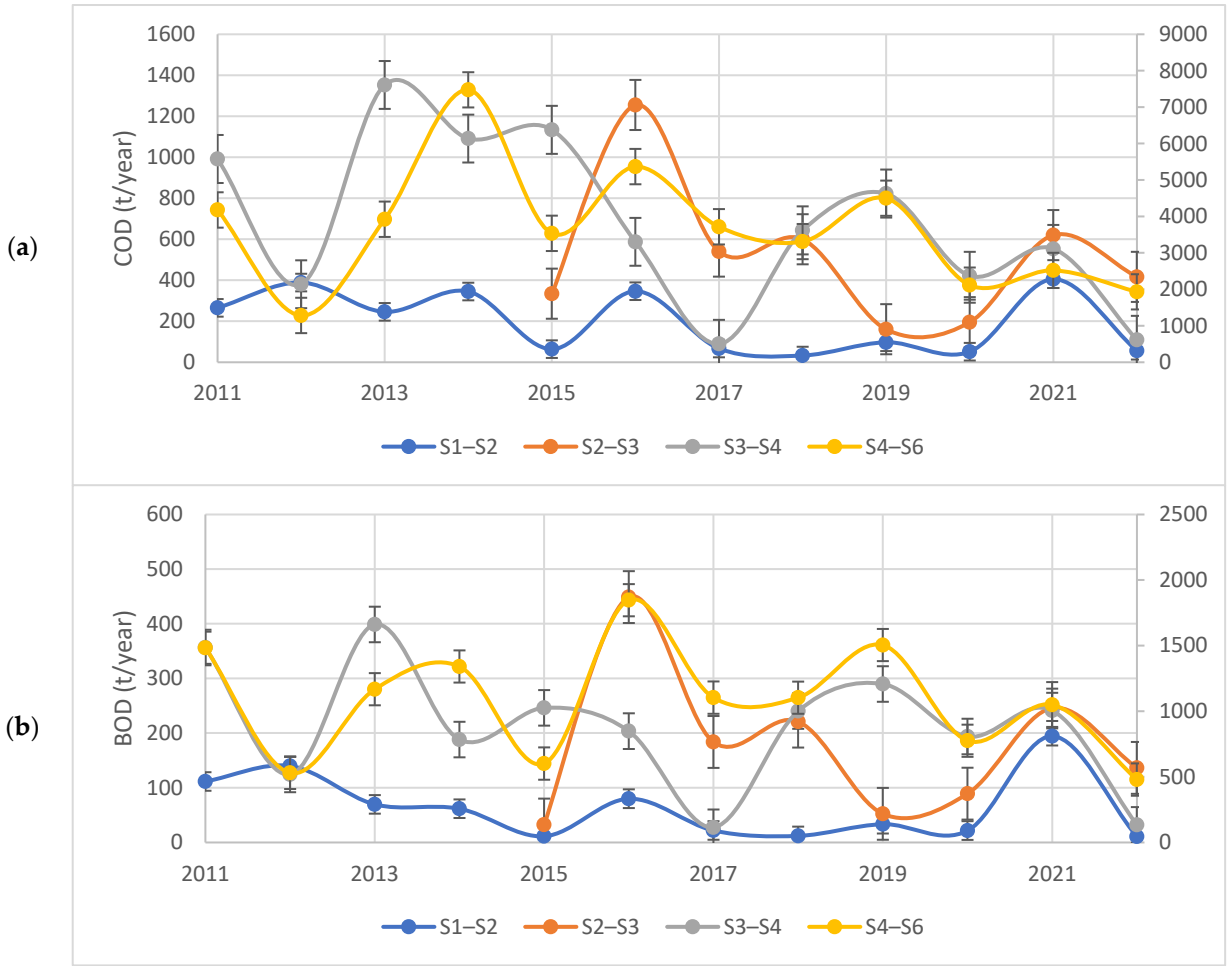

Figure 13. Variation in all segments for (**a**) total COD and (**b**) BOD.

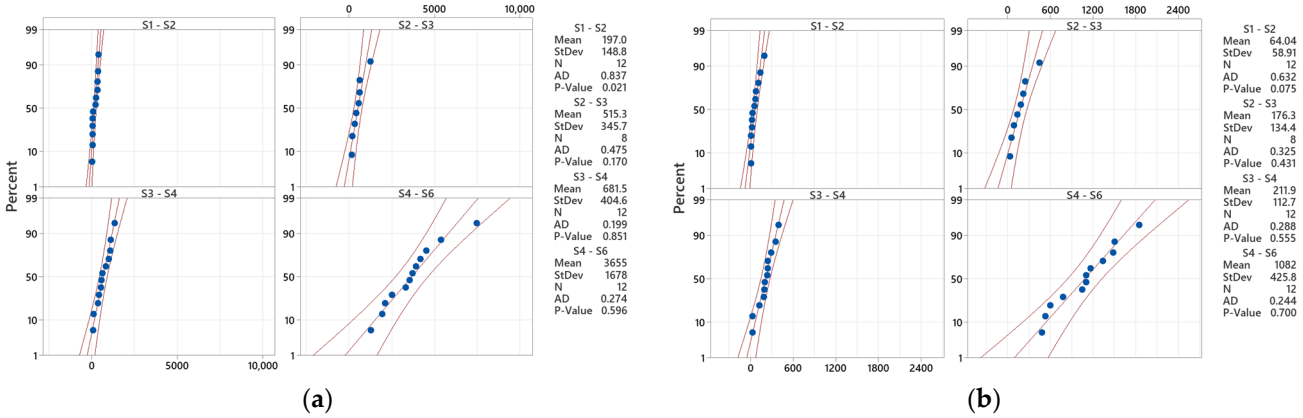

Figure 14. NPP for all segments covering average annual values for (**a**) COD and (**b**) BOD.

3.3. River Segmentation by Dams: Some Benefits and Drawbacks

The immediate result of anthropogenic interference on a river's course, such as dam construction, is an increase in flood safety. On the other hand, these interferences always result in severe alterations to riparian ecosystems. Dams are massive structures that, together with the reservoirs created by their construction, irreversibly change the landscape. The natural flow of rivers, which is crucial for transporting nutrients like carbon, phosphorus, and nitrogen, is disrupted by fragmentation. Dams can trap these nutrients in reservoirs, decreasing their availability downstream. This retention modifies nutrient dynamics and

can lead to hotspots of nutrient buildup in stagnant water bodies, while areas downstream may experience nutrient depletion. The main impact of damming on nutrients and organic matter is an increase in their hydraulic retention time. The longer the HRT, the greater the chance for biogeochemical and physical changes that result in nutrient consumption [11].

Dams store water during high-flow periods and release it during dry spells, ensuring a steady flow downstream. Because flow regulation maintains water supply even during droughts, it lowers the chance of depletion and protects aquatic habitats and biodiversity. Before dams were used to regulate and manage the course of the Bahlui River, complete depletion was a relatively common event, often reported during extended droughts [47].

Over time, the buildup of sediments and the natural tendency of ecosystems to reach equilibrium enable the formation of distinct habitats along each section of the river. In the case of Bahlui River, there are two examples of such habitats, as follows: the Pârcovaci dam, which serves as a protected area for local ichthyofauna, and the Sârca-Podu Iloaiei accumulation, designated as a protected area for avifauna. A mimetic effect can be observed (keeping proportions) between dams built by beavers [83] and those built by humans [84,85]. Both affect the river hydrology, geomorphology, biogeochemistry, and ecosystems, and in both cases, nature manages to restore equilibrium if it has enough time. If human influence were limited only to the construction of dams and control of water flow, this natural balance would be easier to achieve. Unfortunately, a variety of human activities, including deforestation, urbanization, and agriculture, have a significant and continuous impact on river courses (segmented or continuous) and their natural dynamics.

Overall, the analysis conducted in this study showed that the yearly and seasonal variation between the considered segments does not follow a predetermined trend. Therefore, the assumption that the river segments can be analyzed individually is valid. This is due to the presence of dams (as extensively discussed in previous paragraphs), but also because of urban areas (with WTTPs) that influence both flow and nutrient load. Furthermore, unlike continuous streams, the impact of unforeseen events, whether natural (such as severe floods) or anthropogenic (such as WWTP discharges), is limited to the specific river segment and does not affect the entire river.

4. Conclusions

This study proposed a segmentation strategy for the Bahlui River and examined the fluctuations in seasonal and annual total nutrient and organic pollution for each segment. Each river segment separated by dams and anthropogenic stressors behaves as an independent unit with distinct seasonal and yearly variations in total nitrogen, total phosphorus, chemical oxygen demand, and biochemical oxygen demand.

The Bahlui River analysis shows that dam-separated segments can be analyzed as independent watercourses, as demonstrated by the following:

- Localized impacts remain contained within specific segments rather than propagating throughout the entire river system. Statistical analyses reveal that nutrient and pollution data often do not follow typical patterns and vary greatly, highlighting the importance of considering occasional events and specific river sections when evaluating water quality. The standard deviations frequently surpass the means, indicating that extreme events have a significant influence on the overall nutrient and pollution budgets.
- Each segment exhibits different seasonal patterns and response mechanisms to anthropogenic and environmental stressors. The upstream area, mostly forested, indicates that natural nutrient sources vary seasonally, with autumn having the highest phosphorus levels due to “first flush” events and winter showing increased nitrogen levels. This baseline understanding is vital for distinguishing between natural and anthro-

pogenic contributions in downstream sections. Furthermore, the analysis shows that urban development and wastewater treatment plant discharges elevate nutrient and organic pollution levels, highlighting significant human impacts on water quality.

- Unforeseen events (floods and WWTP discharges) affect only specific segments without impacting the entire river.

The research demonstrates that seasonal and annual analyses of the changes in nutrients and organic pollutants in different river segments provide specific benefits, especially in understanding hydrological effects and the ecological impact of river fragmentation. The statistical analysis confirms that segments behave independently, with varying seasonal patterns and response mechanisms to anthropogenic stressors. This segmented approach offers an alternative to traditional methods that treat the river as a continuous whole.

Supplementary Materials: The following supporting information can be downloaded at: https://www.mdpi.com/article/10.3390/hydrology12090224/s1, Figure S1: The Pârcovaci Accumulation, Figure S2: The Tansa Lake, Figure S3: The Podu Iloaiei Accumulation, Figure S4: The Waste Water Treatment Plant of Iași, Figure S5: The 1st segment of the Bahlui River (S1–S2), Figure S6: The 2nd sector of the Bahlui River (S2–S3), Figure S7: The 3rd section of the Bahlui River (S3–S4), Figure S8: The 4th section of the Bahlui River (S4–S6).

Author Contributions: Conceptualization, N.M., E.N.D. and M.-T.N.; methodology, Ș.C. and C.D.B.; usingware, E.N.D.; validation, T.A.H. and D.T.; formal analysis, E.N.D.; investigation, Ș.C. and C.D.B.; resources, Ș.C. and I.O.T.; data curation, T.A.H. and D.T.; writing—original draft preparation, N.M. and M.-T.N.; writing—review and editing, N.M., E.N.D. and M.-T.N.; visualization, E.N.D.; supervision, N.M.; project administration, I.O.T. and C.D.B.; funding acquisition, I.O.T. All authors have read and agreed to the published version of the manuscript.

Funding: This research received no external funding.

Data Availability Statement: Data will be available upon request.

Conflicts of Interest: The authors declare no conflicts of interest.

References

1. Van Cappellen, P.; Maavara, T. Rivers in the Anthropocene: Global scale modifications of riverine nutrient fluxes by damming. *Ecohydrol. Hydrobiol.* **2016**, *16*, 106–111. [CrossRef]
2. Belletti, B.; Garcia de Leaniz, C.; Jones, J.; Bizzi, S.; Börger, L.; Segura, G.; Castelletti, A.; van de Bund, W.; Aarestrup, K.; Barry, J.; et al. More than one million barriers fragment Europe's rivers. *Nature* **2020**, *588*, 436–441. [CrossRef] [PubMed]
3. Grill, G.; Lehner, B.; Thieme, M.; Geenen, B.; Tickner, D.; Antonelli, F.; Babu, S.; Borrelli, P.; Cheng, L.; Crochetiere, H. Mapping the world's free-flowing rivers. *Nature* **2019**, *569*, 215–221. [CrossRef]
4. Wang, X.; Chen, Y.; Yuan, Q.; Xing, X.; Hu, B.; Gan, J.; Zheng, Y.; Liu, Y. Effect of river damming on nutrient transport and transformation and its countermeasures. *Front. Mar. Sci.* **2022**, *9*, 1078216. [CrossRef]
5. Yan, X.; Chen, Y.; Sun, H.; Chen, Q.; Zhang, J.; Zhi, W. River Damming Impacts on Carbon Emissions Should Be Revisited in the Context of the Aquatic Continuum Concept. *Environ. Sci. Technol.* **2024**, *58*, 17529–17531. [CrossRef] [PubMed]
6. Spinti, R.A.; Condon, L.E.; Zhang, J. The evolution of dam induced river fragmentation in the United States. *Nat. Commun.* **2023**, *14*, 3820. [CrossRef]
7. Jumani, S.; Deitch, M.J.; Kaplan, D.; Anderson, E.P.; Krishnaswamy, J.; Lecours, V.; Whiles, M.R. River fragmentation and flow alteration metrics: A review of methods and directions for future research. *Environ. Res. Lett.* **2020**, *15*, 123009. [CrossRef]
8. Kamidis, N.; Koutrakis, E.; Sapounidis, A.; Sylaios, G. Impact of river damming on downstream hydrology and hydrochemistry: The case of lower Nestos River catchment (NE. Greece). *Water* **2021**, *13*, 2832. [CrossRef]
9. Gan, J.-W.; Wang, X.; Yuan, Q.-S.; Xing, X.-L.; Liu, S.; Du, C.-G.; Zheng, Y.-R.; Liu, Y.-X. Impact of damming on nutrient transport and transformation in river systems: A review. *Water Sci. Eng.* **2024**, *18*, 209–220. [CrossRef]
10. Kowal, J.L.; Funk, A.; Unfer, G.; Baldan, D.; Haidvogl, G.; Hauer, C.; Ferreira, M.T.; Branco, P.; Schinegger, R.; Hein, T. River continuum disruptions in a highly altered system: The perspective of potamodromous fish. *Ecol. Indic.* **2024**, *164*, 112130. [CrossRef]

11. Maavara, T.; Chen, Q.; Van Meter, K.; Brown, L.E.; Zhang, J.; Ni, J.; Zarfl, C. River dam impacts on biogeochemical cycling. *Nat. Rev. Earth Environ.* **2020**, *1*, 103–116. [CrossRef]
12. Panagiotou, A.; Zogaris, S.; Dimitriou, E.; Mentzafou, A.; Tsihrintzis, V.A. Anthropogenic barriers to longitudinal river connectivity in Greece: A review. *Ecohydrol. Hydrobiol.* **2022**, *22*, 295–309. [CrossRef]
13. Powers, S.M.; Robertson, D.M.; Stanley, E.H. Effects of lakes and reservoirs on annual river nitrogen, phosphorus, and sediment export in agricultural and forested landscapes. *Hydrol. Process.* **2014**, *28*, 5919–5937. [CrossRef]
14. Shi, W.; Qin, B. Sediment and nutrient trapping by river dams: A critical review based on 15-year big data. *Curr. Pollut. Rep.* **2023**, *9*, 165–173. [CrossRef]
15. Szatten, D.; Habel, M.; Babiński, Z. Influence of hydrologic alteration on sediment, dissolved load and nutrient downstream transfer continuity in a river: Example Lower Brda River Cascade Dams (Poland). *Resources* **2021**, *10*, 70. [CrossRef]
16. Best, J. Anthropogenic stresses on the world's big rivers. *Nat. Geosci.* **2019**, *12*, 7–21. [CrossRef]
17. Isik, S.; Dogan, E.; Kalin, L.; Sasal, M.; Agiralioglu, N. Effects of anthropogenic activities on the Lower Sakarya River. *Catena* **2008**, *75*, 172–181. [CrossRef]
18. Papadaki, C.; Dimitriou, E. River Flow Alterations Caused by Intense Anthropogenic Uses and Future Climate Variability Implications in the Balkans. *Hydrology* **2021**, *8*, 7. [CrossRef]
19. Zurita, A.; Aguayo, M.; Arriagada, P.; Figueroa, R.; Díaz, M.E.; Stehr, A. Modeling Biological Oxygen Demand Load Capacity in a Data-Scarce Basin with Important Anthropogenic Interventions. *Water* **2021**, *13*, 2379. [CrossRef]
20. Luo, Z.; Shao, Q.; Liu, H. Comparative evaluation of river water quality and ecological changes at upstream and downstream sites of dams/sluices in different regulation scenarios. *J. Hydrol.* **2021**, *597*, 126290. [CrossRef]
21. Yin, S.; Gao, G.; Li, Y.; Xu, Y.J.; Turner, R.E.; Ran, L.; Wang, X.; Fu, B. Long-term trends of streamflow, sediment load and nutrient fluxes from the Mississippi River Basin: Impacts of climate change and human activities. *J. Hydrol.* **2023**, *616*, 128822. [CrossRef]
22. Wu, Y.; Li, Y.; Du, E.; Sun, Y.; Zhang, J.; Liu, Z.; Song, C. The dominant mechanisms of nutrient cycling in high-dam reservoirs: Retention, transport or transformation? *Environ. Res. Lett.* **2024**, *19*, 124024. [CrossRef]
23. Finkler, N.R.; Gücker, B.; Boëchat, I.G.; Ferreira, M.S.; Tanaka, M.O.; Cunha, D.G.F. Riparian Land Use and Hydrological Connectivity Influence Nutrient Retention in Tropical Rivers Receiving Wastewater Treatment Plant Discharge. *Front. Environ. Sci.* **2021**, *9*, 709922. [CrossRef]
24. Gurnell, A.M.; Corenblit, D.; García de Jalón, D.; González del Tánago, M.; Grabowski, R.C.; O'Hare, M.T.; Szewczyk, M. A Conceptual Model of Vegetation–hydrogeomorphology Interactions Within River Corridors. *River Res. Appl.* **2016**, *32*, 142–163. [CrossRef]
25. Juwana, I.; Nugroho, D. *The Improvement of Cipunagara River Quality (BOD Parameter) Based on Pollution Load Analysis of Domestic, Agriculture, Farming and Industrial Activities*; IOP Conference Series: Earth and Environmental Science; IOP Publishing: Bristol, UK, 2019; p. 012031.
26. Zang, C.; Liu, J.; Wang, X.; Liu, Q.; Zhang, X. Evaluating water ecological health in dam-impacted river: A new approach framework. *Ecol. Indic.* **2024**, *161*, 111998. [CrossRef]
27. Vannote, R.L.; Minshall, G.W.; Cummins, K.W.; Sedell, J.R.; Cushing, C.E. The river continuum concept. *Can. J. Fish. Aquat. Sci.* **1980**, *37*, 130–137. [CrossRef]
28. Stanford, J.; Ward, J.V. The serial discontinuity concept of lotic ecosystems. In *Dynamics of Lotic Ecosystems*; Bartell, S.M., Fontaine, T.D., Eds.; Ann Arbor Science: Ann Arbor, MI, USA, 1983; Chapter 2; pp. 29–42.
29. Vázquez-Tarrío, D.; Tal, M.; Camenen, B.; Piégay, H. Effects of continuous embankments and successive run-of-the-river dams on bedload transport capacities along the Rhône River, France. *Sci. Total Environ.* **2019**, *658*, 1375–1389. [CrossRef]
30. Dang, T.H.; Coynel, A.; Orange, D.; Blanc, G.; Etcheber, H.; Le, L.A. Long-term monitoring (1960–2008) of the river-sediment transport in the Red River Watershed (Vietnam): Temporal variability and dam-reservoir impact. *Sci. Total Environ.* **2010**, *408*, 4654–4664. [CrossRef]
31. Jorge, G.; Albert, P. Sediment dynamics and hydrodynamics in the lower course of a river highly regulated by dams: The Ebro River. *Sedimentology* **1992**, *39*, 567–579. [CrossRef]
32. Tang, X.; Li, R.; Wang, D.; Jing, Z.; Zhang, W. Reservoir flood regulation affects nutrient transport through altering water and sediment conditions. *Water Res.* **2023**, *233*, 119728. [CrossRef]
33. Webster, B.C.; Waters, M.N.; Golladay, S.W. Alterations to sediment nutrient deposition and transport along a six reservoir sequence. *Sci. Total Environ.* **2021**, *785*, 147246. [CrossRef]
34. Sferratore, A.; Billen, G.; Garnier, J.; Smedberg, E.; Humborg, C.; Rahm, L. Modelling nutrient fluxes from sub-arctic basins: Comparison of pristine vs. dammed rivers. *J. Mar. Syst.* **2008**, *73*, 236–249. [CrossRef]
35. Zhao, Q.; Hong, Z.; Jing, Y.; Lu, M.; Geng, Z.; Qiu, P.; Wang, P.; Lu, X.; Ding, S. Spatial and temporal changes in nutrients associated with dam regulation of the Yellow River. *CATENA* **2022**, *217*, 106425. [CrossRef]
36. Bor, A.; Elçi, Ş. Impacts of construction of dam on the flow regimes and water quality: A case study from Turkey. *Int. J. Environ. Sci. Technol.* **2022**, *19*, 4069–4086. [CrossRef]

37. Feng, L.; Hu, P.; Chen, M.-m.; Li, B.-L. Quantifying cumulative changes in water quality caused by small floodgates in Taihu Lake Basin—A case in Wuxi. *Sci. Total Environ.* **2023**, *900*, 165608. [CrossRef]
38. Wei, G.; Yang, Z.; Cui, B.; Li, B.; Chen, H.; Bai, J.; Dong, S. Impact of dam construction on water quality and water self-purification capacity of the Lancang River, China. *Water Resour. Manag.* **2009**, *23*, 1763–1780. [CrossRef]
39. Aristi, I.; Arroita, M.; Larrañaga, A.; Ponsatí, L.; Sabater, S.; von Schiller, D.; Elosegi, A.; Acuña, V. Flow regulation by dams affects ecosystem metabolism in Mediterranean rivers. *Freshw. Biol.* **2014**, *59*, 1816–1829. [CrossRef]
40. Guo, J.; Shi, X.; Ke, S.; Li, Y.; Hu, C.; Zwain, H.M.; Gu, J.; Chunyun, Z.; Li, A.; Shenghong, L. Climate Change Critique on Dams and Anthropogenic Impact to Mediterranean Mountains for Freshwater Ecosystem-a Review. *Pol. J. Environ. Stud.* **2023**, *32*, 2981–2992.
41. Marcoie, N.; Chihaia, Ș.; Hrăniciuc, T.A.; Balan, C.D.; Drăgoi, E.N.; Nechita, M.-T. Linking Nutrient Dynamics with Urbanization Degree and Flood Control Reservoirs on the Bahlui River. *Water* **2024**, *16*, 1322. [CrossRef]
42. Ludikhuize, D.; Savin, A.; Schropp, M. *A Sobek Model for the Bahlui River*; Rijksinstituut voor Integraal Zoetwaterbeheer en Afvalwaterbehandeling (RWS, RIZA): Lelystad, The Netherlands, 2004; 49p.
43. Boariu, C.; Crăciun, I.; Giurma-Handley, C.-R.; Hrăniciuc, T.-A. Assessment of the impact of riverbed design on water quality--the case study of Bahlui River, Iași, Romania. *Environ. Eng. Manag. J.* **2013**, *12*, 625–635. [CrossRef]
44. Crenganiș, L.M.; Telișcă, M. GIS application in water resources management and environmental engineering. *Glob. J. Adv. Pure Appl. Sci.* **2013**, *1*, 657–664.
45. Barjoveanu, G.; Teodosiu, C.; Cojocariu, C.; Augustijn, D.; Craciun, I. Instruments for integrated water resources management: Water quality modeling for sustainable wastewater management. *Environ. Eng. Manag. J.* **2013**, *12*, 1679–1690. [CrossRef]
46. Mihu-Pintilie, A.; Romanescu, G. Determining the potential hydrological risk associated to maximum flow in small hydrological subbasins with torrential character of the river Bahlui. *Present Environ. Sustain. Dev.* **2011**, *5*, 255–266.
47. Minea, I. Minimum discharge in Bahlui basin and associated hydrologic risks. *Aerul. Si Apa. Compon. Ale Mediu.* **2010**, 508–515.
48. Minea, I. The evaluation of the water chemistry and quality for the lakes from the south of the Hilly Plain of Jijia (Bahlui drainage basin). *Lakes Reserv. Ponds* **2010**, *4*, 131–144.
49. Boariu, C.; Bofu, C. Bahlui River Recreation Area Arrangement. *Bul. Institutului Politeh. Din lasi. Sect. Constr. Arhit.* **2015**, *61*, 23–32.
50. Niculita, M.; Boca, B.; Minea, I. Analysis of Parcovaci and Ciurbesti (Iasi County, Romania) reservoirs sedimentation. In Proceedings of the 14th International Multidisciplinary Scientific GeoConference SGEM 2014, Albena, Bulgaria, 17–26 June 2014; pp. 43–50.
51. Agapie, M.I.; Luca, M. Settlement monitoring of the earth dams by performance periodical topo-geodetic measurements. *Present Environ. Sustain. Dev.* **2020**, *14*, 99–109.
52. Administration, P.-B.W.B. The Situation of the Accumulations in Iasi County Under the Administration of the A.B.A Prut-Bârlad—S.G.A. Iași. Available online: https://arhiva.isujis.ro/wp-content/uploads/2021/10/anexa-2-SITUATIA-ACUMULARILOR.Pdf (accessed on 22 March 2021).
53. Parliament, R. *Law on the Approval of the National Territory Planning Plan—Section III—Protected Areas*; Official Monitor: Bucharest, Romania, 2000.
54. Paliament, R. *The Emergency Ordinance for the Amendment of Law No. 5/2000 Regarding the Approval of the National Territorial Planning Plan—Section III—Protected Areas*; Official Monitor: Bucharest, Romania, 2016.
55. Dughilă, A.; Iancu, O.G.; Râșcanu, I.D. Geochemical evaluation of quality indicators for the water of the Tansa Lake from the Jijia catchment, Romania. *Carpathian J. Earth Environ. Sci.* **2012**, *7*, 79–88.
56. Stoleriu, A.F.; Breaban, I.G.; Stoleriu, A.P. Assessing Water Quality from Tansa Barrier Lake (Romania) Using Sentinel-2 Data. *Int. Multidiscip. Sci. GeoConference SGEM* **2021**, *21*, 247–254.
57. Amarandei, C.; Negru, A.-G.; Soroaga, L.-V.; Cucu-Man, S.-M.; Olariu, R.-I.; Arsene, C. Assessment of surface water quality in the Podu Iloaiei Dam Lake (North-Eastern Romania): Potential implications for aquaculture activities in the area. *Water* **2021**, *13*, 2395. [CrossRef]
58. Musteață, G.; Balan, I.; Pricop, C.; Balan, I. Studii privind siguranța în exploatare a acumulării Podu Iloaiei Studies regarding the safety in operation of Podu Iloaiei reservoir. In Proceedings of the INHGA—Scientific Conference, Bucharest, Romania, 10–11 November 2014; pp. 1–9.
59. Soroaga, L.V.; Amarandei, C.; Negru, A.G.; Olariu, R.I.; Arsene, C. Assessment of the anthropogenic impact and distribution of potentially toxic and rare earth elements in lake sediments from North-Eastern Romania. *Toxics* **2022**, *10*, 242. [CrossRef]
60. *Decision no. 663 of 14 September 2016 on the Establishment of the Protected Natural Area Regime and the Declaration of the Special Avifauna Protection Areas as an Integral Part of the European Ecological Network Natura 2000 in Romania*; Official Monitor: Bucharest, Romania, 2016.
61. Prăjanu, C.-C.; Toma, D.; Vîrlan, C.-M.; Marcoie, N. Studies related to the biological treatment of wastewater within the wastewater treatment plant of Iași City. *Ovidius Univ. Ann. Constanta-Ser. Civ. Eng.* **2018**, *20*, 57–64. [CrossRef]

62. Prăjanu, C.-C.; Stătescu, F.; Toma, D.; Toma, C.-M.V. Recognition and determination of hydrodynamic deficiencies in the bioreactors of a real wastewater treatment plant by a comprehensive approach: Live analysis using computational fluid dynamics. *Environ. Eng. Manag. J.* **2021**, *20*, 495–506. [CrossRef]
63. Shehab, Z.N.; Farhhan, A.F.; Faisal, R.M. Spatial variation influence of landscape patterns on surface water quality across an urbanized watershed in Mosul city, Iraq. *Sustain. Water Resour. Manag.* **2024**, *10*, 181. [CrossRef]
64. Nardini, A.; Yépez, S.; Mazzorana, B.; Ulloa, H.; Bejarano, M.D.; Laraque, A. A Systematic, Automated Approach for River Segmentation Tested on the Magdalena River (Colombia) and the Baker River (Chile). *Water* **2020**, *12*, 2827. [CrossRef]
65. Parker, C.; Clifford, N.J.; Thorne, C.R. Automatic Delineation Of Functional River Reach Boundaries For River Research And Applications. *River Res. Appl.* **2012**, *28*, 1708–1725. [CrossRef]
66. Available online: https://en.wikipedia.org/wiki/Reach_(geography) (accessed on 2 February 2025).
67. Minea, I. Changes in the land use in the last century in the South part of Moldovia Plain. *Sci. Papers Ser. A Agronomy* **2011**, *54*, 155–159.
68. Cohn, T.A. Estimating contaminant loads in rivers: An application of adjusted maximum likelihood to type 1 censored data. *Water Resour. Res.* **2005**, *41*, W07003. [CrossRef]
69. Walling, D.E.; Webb, B.W. Estimating the discharge of contaminants to coastal waters by rivers: Some cautionary comments. *Mar. Pollut. Bull.* **1985**, *16*, 488–492. [CrossRef]
70. Littlewood, I.G. *Estimating Contaminant Loads in Rivers: A Review*; Institute of Hydrology: Wallingford, UK, 1992.
71. Phillips, J.M.; Webb, B.W.; Walling, D.E.; Leeks, G.J.L. Estimating the suspended sediment loads of rivers in the LOIS study area using infrequent samples. *Hydrol. Process.* **1999**, *13*, 1035–1050. [CrossRef]
72. Fabian, P.S.; Kwon, H.-H.; Vithanage, M.; Lee, J.-H. Modeling, challenges, and strategies for understanding impacts of climate extremes (droughts and floods) on water quality in Asia: A review. *Environ. Res.* **2023**, *225*, 115617. [CrossRef] [PubMed]
73. Akbarzadeh, Z.; Maavara, T.; Slowinski, S.; Van Cappellen, P. Effects of damming on river nitrogen fluxes: A global analysis. *Glob. Biogeochem. Cycles* **2019**, *33*, 1339–1357. [CrossRef]
74. Bussi, G.; Janes, V.; Whitehead, P.G.; Dadson, S.J.; Holman, I.P. Dynamic response of land use and river nutrient concentration to long-term climatic changes. *Sci. Total Environ.* **2017**, *590–591*, 818–831. [CrossRef]
75. Moatar, F.; Meybeck, M. Compared performances of different algorithms for estimating annual nutrient loads discharged by the eutrophic River Loire. *Hydrol. Process. Int. J.* **2005**, *19*, 429–444. [CrossRef]
76. Zhang, G.; Xu, Y.; Xu, M.; Li, Z.; Qin, S. Optimizing Sampling Strategies for Estimating Riverine Nutrient Loads in the Yiluo River Watershed, China. *Water* **2024**, *16*, 1506. [CrossRef]
77. Hudon, C.; Carignan, R. Cumulative impacts of hydrology and human activities on water quality in the St. Lawrence River (Lake Saint-Pierre, Quebec, Canada). *Can. J. Fish. Aquat. Sci.* **2008**, *65*, 1165–1180. [CrossRef]
78. Gómez-Gutiérrez, A.I.; Jover, E.; Bodineau, L.; Albaigés, J.; Bayona, J.M. Organic contaminant loads into the Western Mediterranean Sea: Estimate of Ebro River inputs. *Chemosphere* **2006**, *65*, 224–236. [CrossRef]
79. Boylan, G.L.; Cho, B.R. The Normal Probability Plot as a Tool for Understanding Data: A Shape Analysis from the Perspective of Skewness, Kurtosis, and Variability. *Qual. Reliab. Eng. Int.* **2012**, *28*, 249–264. [CrossRef]
80. Duchesne, L.; Ouimet, R.; Camiré, C.; Houle, D. Seasonal nutrient transfers by foliar resorption, leaching, and litter fall in a northern hardwood forest at Lake Clair Watershed, Quebec, Canada. *Can. J. For. Res.* **2001**, *31*, 333–344. [CrossRef]
81. Coppolino, J.; Munford, K.E.; Macrae, M.; Glasauer, S. Shifts in soil phosphorus fractions during seasonal transitions in a riparian floodplain wetland. *Front. Environ. Sci.* **2022**, *10*, 983129. [CrossRef]
82. Breabăn, I.G.; Stan, O.C. The Influence of the Anthropogenic Activities on the Bahlui Water Quality, Holboca Section (Iassy county). *Semin. Geogr. D. Cantemir* **2006**, *26*, 169–179.
83. Larsen, A.; Larsen, J.R.; Lane, S.N. Dam builders and their works: Beaver influences on the structure and function of river corridor hydrology, geomorphology, biogeochemistry and ecosystems. *Earth-Sci. Rev.* **2021**, *218*, 103623. [CrossRef]
84. Pearce, C.; Vidon, P.; Lautz, L.; Kelleher, C.; Davis, J. Impact of beaver dam analogues on hydrology in a semi-arid floodplain. *Hydrol. Process.* **2021**, *35*, e14275. [CrossRef]
85. Wohl, E.; Inamdar, S. Beaver Versus Human: The Big Differences in Small Dams. *WIREs Water* **2025**, *12*, e70019. [CrossRef]

PAPER • **OPEN ACCESS**

The impact of the embankment and the recreational lake on capturing front with drilling wells

To cite this article: N Marcoie *et al* 2024 *IOP Conf. Ser.: Mater. Sci. Eng.* **1304** 012030

The impact of the embankment and the recreational lake on capturing front with drilling wells

N Marcoie, D Toacă, D Toma, V Boboc, T A Hrăniciuc, R Mitroi
"Gheorghe Asachi" Technical University of Iași, 65 Prof.dr.docent D. Mangeron Street, 700050, Iași, Romania

E-mail: raluca.mitroi@academic.tuiasi.ro

Abstract. This paper presents the influence on the levels from the well caption front Gherăești-Bacău, located on the right side of the Bistrița River, through the construction, on the right shore, of a 2.25 km long perimetral embankment, and a recreational lake with a surface of 3.18 hectares and average depth of 5.5 m (Figure 1). Through numerical modelling, using the modelling software of Visual Modflow aquifer, the influence on the hydrostatic level from drilled wells was determined, as well as the influence on the phreatic flow through the making of the recreational lake, which captures a part of the underground water. The use of the mathematical model allows the determination of the optimal parameters for an extraction from the aquifer known through classical methods. To achieve the mathematical model the method of filtration resistances was used, which is applied in the case of a sudden curvature of the streamlines (in the proximity of the imperfect permeable/impervious borders: channels, drains, well systems, screens), hence they are applied during pressure/level drops. This method allows the following equalizations: the imperfect wells can be considered as perfect; the lines of perfect/imperfect wells can be considered as perfect trenches (channels) with a flow equal to the sum of all wells; a stratified aquifer (up to 3 layers) can be equivaled with a homogenous one. Aspects regarding the flow were taken into consideration: with a free level or under pressure, the dimensioning of the model, the initial conditions of the aquifer layer, the lithostratigraphic characteristics, homogeneity, anisotropy, the transfer mechanisms in the domain's interior, the studied hydrogeological structure was schematized, having done a monolayer model. The calibration of the model consists of adjusting, in reasonable conditions, of the domain data (the permeabilities), boundary conditions, so that through the running of the model and obtaining the corresponding piezometric lines and the obtained data will overlap the levels of the existing drillings.

1. Case study. The Gherăești-Bacău catchment front

The Gherăești-Bacău catchment front has 57 boreholes, 8 executed in 1966 and 49 executed in 1982 (Figure 1). Currently, 44 boreholes are in operation. The catchment front is located in the municipality of Bacău, on a winding alignment that follows the old bed of the Bistrița River. The boreholes are located at an average distance of approximately 75 m from the main riverbed, being capture boreholes with infiltration from the bank.

The neighbourhoods of the catchment front are represented by private homes, the Bacău II reservoir, the Bistrița River bed and the offtake of UHE Bacău I.

The boreholes have depths of 8.00 – 12.00 m, are completed with ϕ= 324 mm (12 3/4") steel column with flared slot filters and are spaced at an average distance of 90 m from each other.

The average thickness of the collector is H = 6.58 m. The total flow rate exploited from the 44 wells is 190.00 l/s, and the maximum flow rate exploited by one borehole is: Q = 6.0 l/s (0.006 m^3/s), with an average flow Q_{med} = 4.31/s (0.0043 m^3/s).

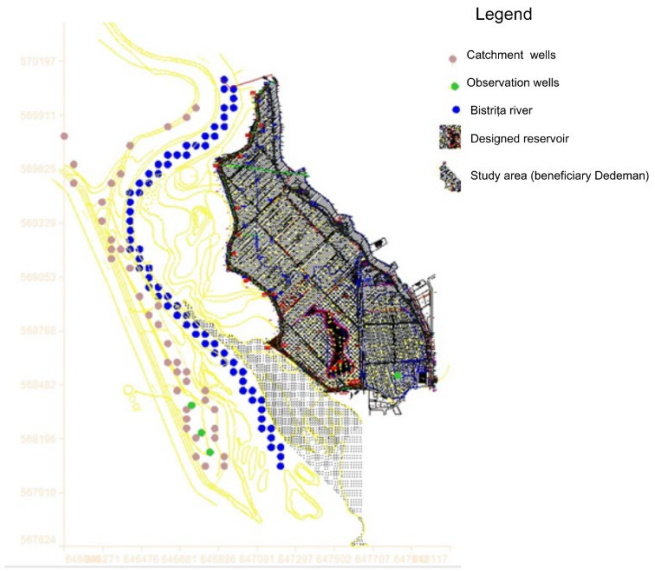

Figure 1. Gherăești-Bacău study area

2. Numerical modelling using Visual Modflow aquifer modelling software

The equation underlying the modelling of aquifers used by the Modflow program is [1, 2, 3]:

$$\frac{\partial}{\partial x}\left(K_{xx}\frac{\partial h}{\partial x}\right)+\frac{\partial}{\partial y}\left(K_{yy}\frac{\partial h}{\partial y}\right)+\frac{\partial}{\partial z}\left(K_{zz}\frac{\partial h}{\partial z}\right)+W=S_s\frac{\partial h}{\partial t} \quad (1)$$

where,

K_{xx}, K_{yy}, and K_{zz} are the hydraulic conductivity values on the x, y, and z axis (m/s); h is the potentiometric head (m); W - volumetric flux (s^{-1}); t - time (s); S_s – specific storage of the porous material (m^{-1}).

Equation (1) combines the initial conditions imposed on the model, describes the distribution of groundwater in a homogeneous and anisotropic medium and determines the main axes of the hydraulic conductivity.

2.1. The method of filtering resistances for the calculation of catchments with wells

The method of filtering resistances is applied in the case of sudden curvature of stream lines (near imperfect permeable/impermeable boundaries: channels, drains, well systems, screens etc.), so when level/pressure drops occur [4].

This method allows the following equations: imperfect wells can be considered as perfect; lines of perfect/imperfect wells can be considered as perfect trenches (channels) with flow equal to the sum of all wells; a stratified aquifer (up to three layers) can be considered a homogeneous aquifer. Thus, at distances of the same order of magnitude as the thickness of the layer, the movement of underground water is predominantly horizontal - with the distribution of pressures similar to that in the case of perfect drains.

$$\Phi=\Phi_c+\Phi_x \quad (2)$$

where:

Φ - internal/additional resistance;

Φ_c - the resistance of the imperfect well according to order, in the case of non-stationary movement depends also on time (it is considered constant in terms of time when $\alpha=\frac{r^2}{a\cdot t}<5\cdot 10^{-5}$);

Φ_x - resistance according to the character of the opening of the layer; depends on the following factors: filter construction; modification of the structure of the stream in the area before the well, with processes of erosion (suffusion), corrosion/clogging of the filter. Even at the full opening of the aquifer

layer filter, when we can consider $\Phi_c = 0$, the action of the resistance Φ_x does not decrease (it even increases) and must be considered in the calculations.

Φ can be considered implicitly in the resistance F of a perfect well by considering:

$$r_c^0 = r_c \cdot e^{-2\pi\phi} \tag{3}$$

where:

r_c^0 - equivalent radius of a perfect well;

r_c - radius of the imperfect well.

2.2. Identifying the calculation relations for Φ for a simple situation, a terrain with a homogeneous layer (Figure 2)

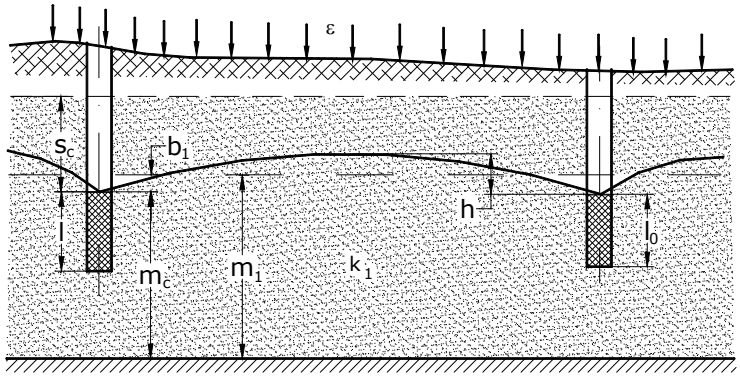

Figure 2. Filtering scheme for one-layer terrain

$$\phi = f \tag{4}$$

The dimensionless resistance f_i from a homogeneous ground corresponds to the thicknesses $m_i = m$, m_c, m_1 and is equal to:

$$f_i = f_{ci} + f_{xi} \tag{5}$$

where:

f_{ci} - the resistance due to the imperfection according to the degree of opening in a homogeneous layer, with waterproof sole and ceiling, of thickness m_i, for which these resistances are determined;

f_{xi} - resistance depending on the nature of the opening in a homogeneous layer of thickness m_i.

The relations established for aquifers under pressure can be used to determine the resistance Φ in the upper layer of aquifers with a free level. In this case, the thickness of the stream in the upper layer m_1 and the length of the filter l are averaged, with a small approximation as follows. When placing the well filter in the upper layer of the well with a non-submersible filter, at which the hydrodynamic level reaches below the length of the filter in the upper layer l_0 ($l < l_0$), $m_1 = m_c + 0.5 \cdot S_c, b_1 = 0.5 \cdot S_c, l = m_1 - a_1$.

For wells with a submersible filter, where the hydrodynamic level is located above the filter: $m_1 = m_c + 0.5 \cdot S_c, b_1 = m_1 - l - a_1, l = l_0$.

When placing the filter in the bottom layer, $m_1 = m_c + 0.5 \cdot S_c$.

In the case of systematic vertical drainage, when averaging the sizes m_1, b_1 and l, instead of the dislevelment S_c it is recommended to use the ascent h in the upper layer.

2.3. Identification of the relations for the calculation of the resistance $\overline{\phi}$ for terrain with a homogeneous layer

$$\overline{\phi} = \frac{1}{m} \cdot \bar{f} \tag{6}$$

In the previous formula $\bar{f}$ is determined with equation (4), in which $\overline{f_{ci}}$ is evaluated according to the relationship (5).

The solid lines for the filter placement near the top and bottom boundaries of the layer, the dotted line (Figure 2): for filters of length l< 0,5·m_i, located approximately in the middle of the layer $b_i + \frac{l}{2} = (0{,}35 \dots 0{,}65) \cdot m_i$.

3. Development of the numerical model for the phreatic aquifer in the Gherăești - Bacău area

Mathematical modelling of groundwater flow involves knowledge of the entire system of groundwater flow, geological and hydrogeological knowledge (hydraulic conductivity, transmissivity, porosity etc.) [5, 6].

Based on the level measurements carried out in the field, the lithological descriptions made during the construction of the boreholes of the catchment front, the hydrogeological sections through these boreholes made available by the beneficiary, it is concluded that the aquifer system presents itself as a continuous environment within its natural limits, on the entire study area.

Figure 3 shows the boreholes and observation points where level measurements were made. Using them, the map of the initial piezometric surface was developed.

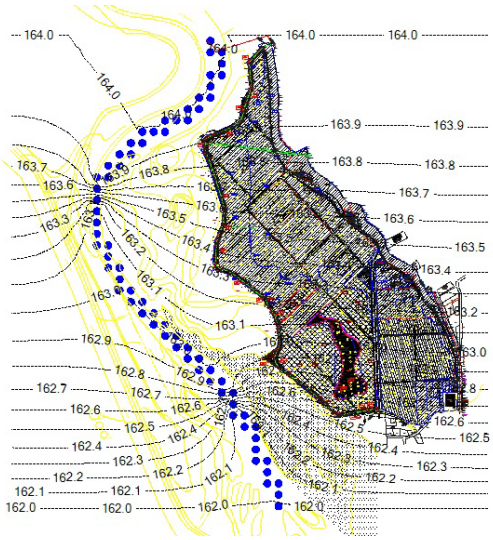

Figure 3. Map of the initial piezometric surface

Aspects related to the flow regime were taken into account: with free level or under pressure, model sizing, boundary geometry, boundary conditions for the aquifer water flow system, initial conditions of the aquifer layer, litho-stratigraphic characteristics, homogeneity, anisotropy, the transfer mechanisms within the domain. The studied hydro structure was schematized, developing a unilayer model.

Based on the presented data, the modelling area was established and the boundary conditions were defined [7]:

- Dirichlet type condition – imposed hydraulic elevation, upstream elevation being given by the 164.00 m hydroisohypses, respectively the downstream elevation corresponding to the 162.00 m hydroisohypses;
- Cauchy-type conditions (potential-dependent flow) on the Bistrița river, the imposed elevations are those representing the free surface of the water in the river;
- Limit type conditions in depth, given by the impermeable layer resulting from the drillings within the catchment front;
- Lines of constant or variable potential, respectively streamlines, correspond from a mathematical point of view to mixed-type boundary conditions (Dirichlet, von Neuman) (Figure 4).

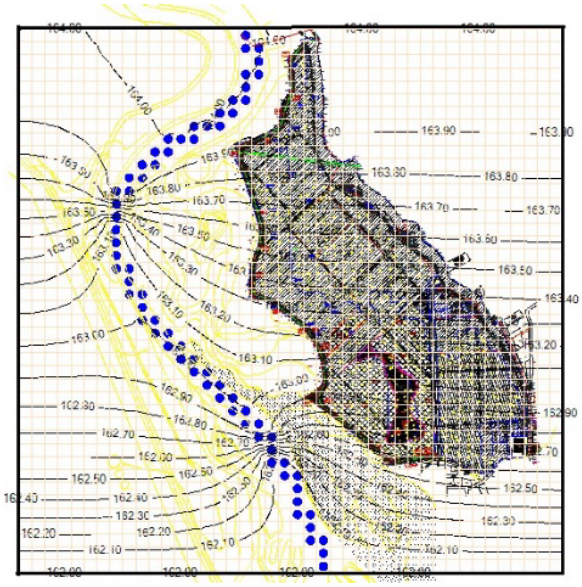

Figure 4. Defining the boundary of the modelled domain in the study area

The data can be entered interactively, with the possibility of modifying certain parameters such as, for example, permeability discretization, base elevations, layer granularity, hydraulic conductivity.
The perimeter of the hydraulically significant area was included in the active area of the numerical model, the adjacent areas being eliminated. In the horizontal plane, a discretization *dx* = 2100 m, *dy* = 2100 m was used (Figure 5).

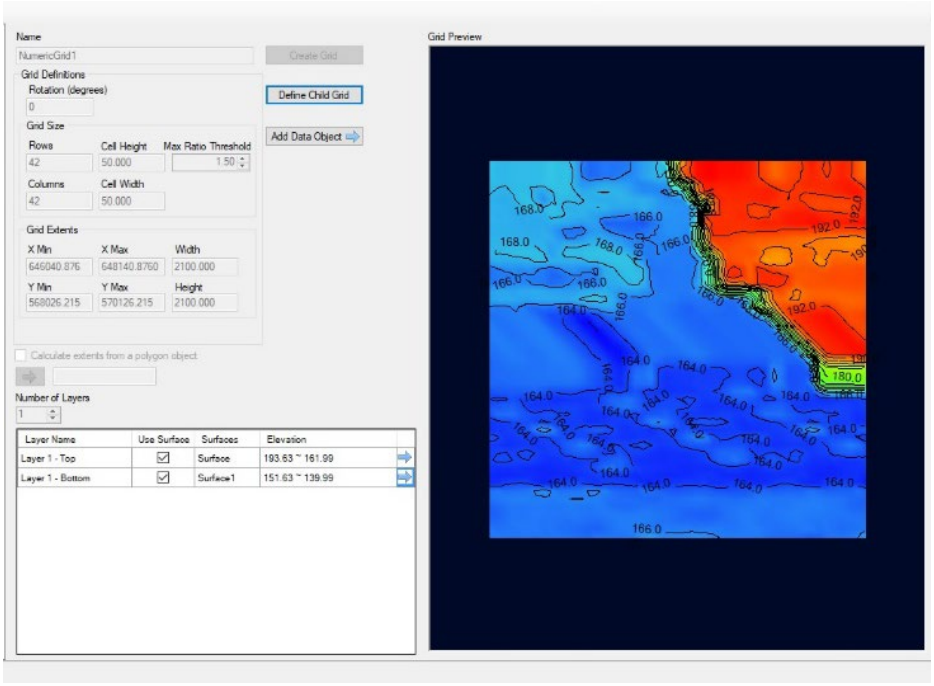

Figure 5. Discretization of the studied domain

The elements used to determine the land surface in the studied area are presented in figure 6, Figure 7 and Figure 8.

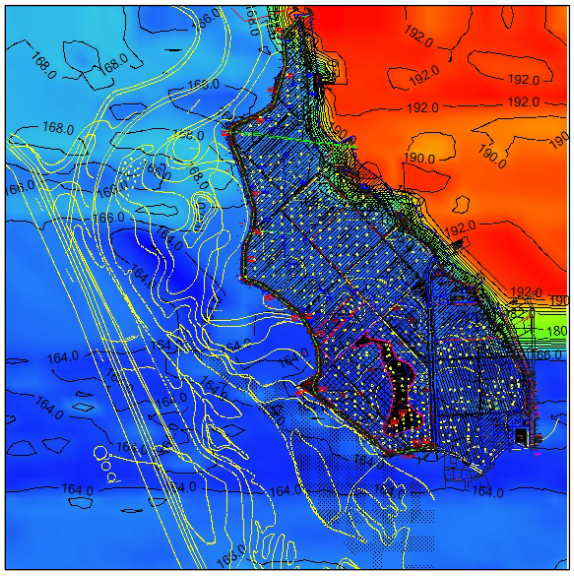

Figure 6. The modelled surface with the highlighted land elevations

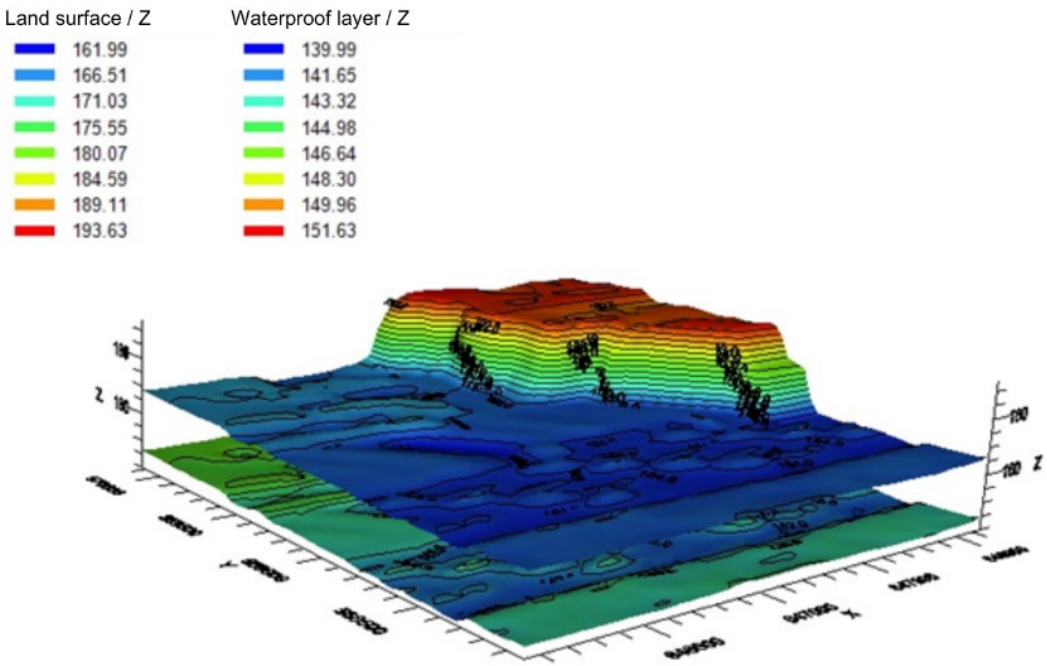

Figure 7. 3D representation of the land surface and waterproof layer

In the vertical plane, a vertical discretization was used. This discretization allows the appropriate vertical placement of the modelled objects at different elevations, the different zoning of permeability as well as different thicknesses of the aquifer (Figure 8).

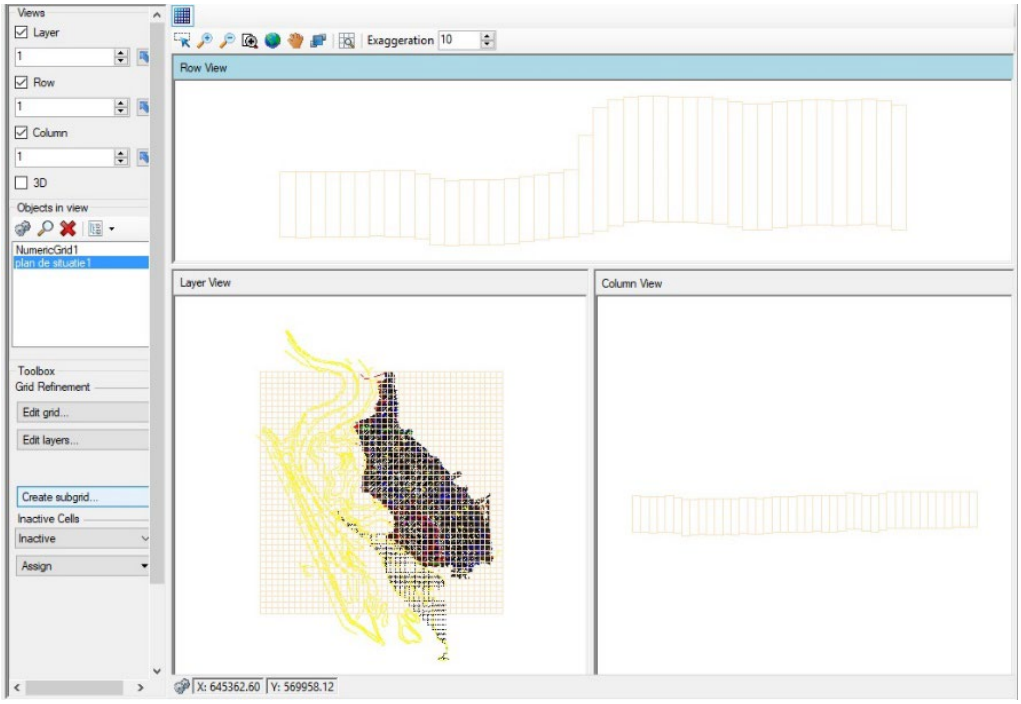

Figure 8. Discretization of the model in plan, cross-section and longitudinal section

Based on these modelling parameters, the numerical flow model and its calibration will be designed. The model is materialized through hydroisohypses, flow directions and hydraulic gradients. These parameters are overlayed on the real situation through a basic hydrogeological map.
The boundary conditions were expressed from considerations regarding the schematization of the area of interest.
In the mathematical modelling of groundwater flow processes the calibration process includes the adaptation, possibly the adjustment of the input data, of the model so that the results obtained through the numerical simulation correspond to the situation in the field [8].
The calibration of the model consists in adjusting the field data (permeabilities) and the boundary conditions in reasonable ways so that by running the model and obtaining the corresponding hydroisohypses they overlap the levels from the existing boreholes (Table 1, Figure 9).

Table 1. Coordinates and measured levels of observation wells

Bore no.	x	y	Elevation	Well bottom	Logger id	Screen_top	Screen_bottom	Observed head
F 11	647837.51	568530.86	163.6	157.9	1	163	159	162.68
F1	646742.3558	568373.2083	162.81	157.11	1	162	158	161.4
F2	646795.3066	568228.6014	164.76	158.06	1	163	159	161.34
F3	646840.8212	568125.062	165.8	158.1	1	163	159	161.68

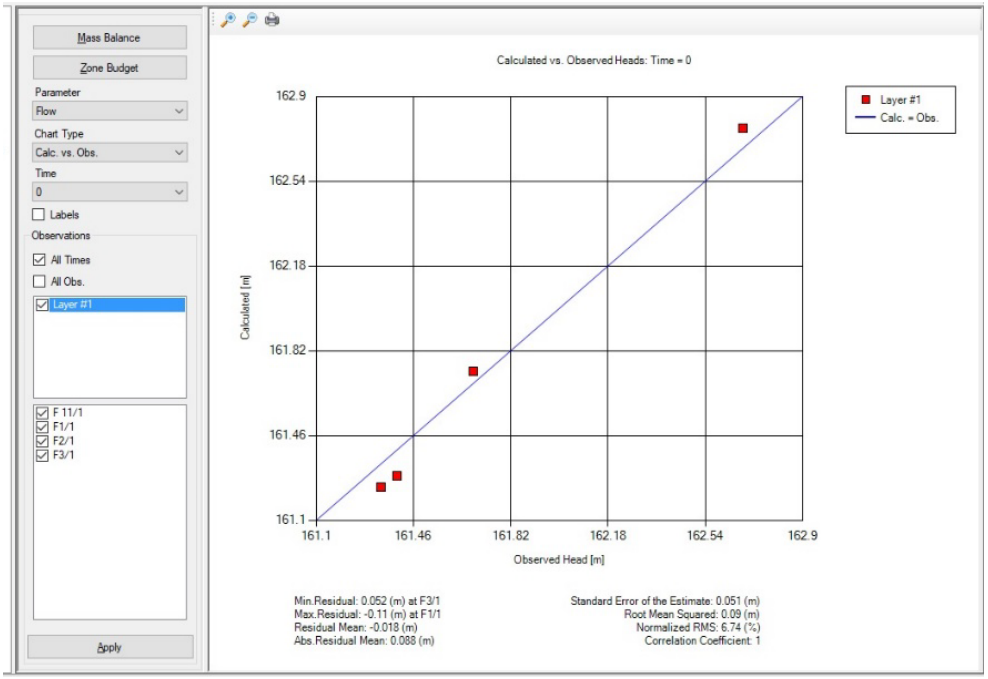

Figure 9. Calculated piezometric levels vs. measured piezometric levels

The total error obtained was 0.051 m. Since the size of the domain is not very large, the result can be considered as a very good one.
The map of piezometric surfaces resulting from the calibration process with the distribution of capture wells on the discretized domain is presented in Figure 10.

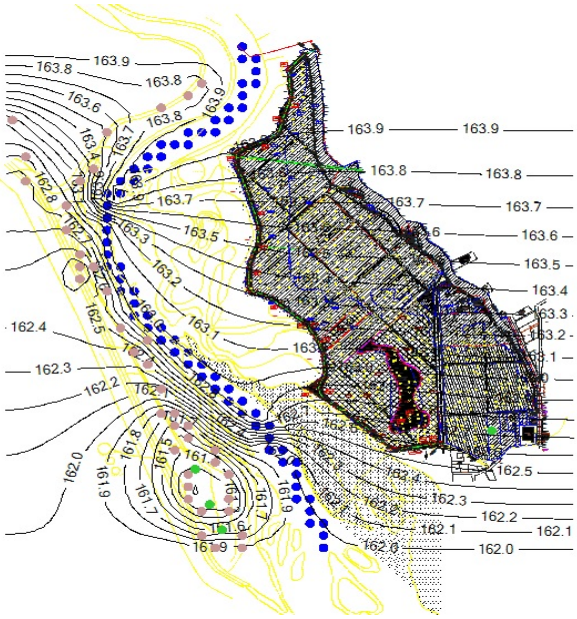

Figure 10. Map of piezometric surfaces with capture wells

The 2D and 3D representation of the evolution of the piezometric elevations in the case of drilling wells in the Gherăești area is shown in Figure 11.

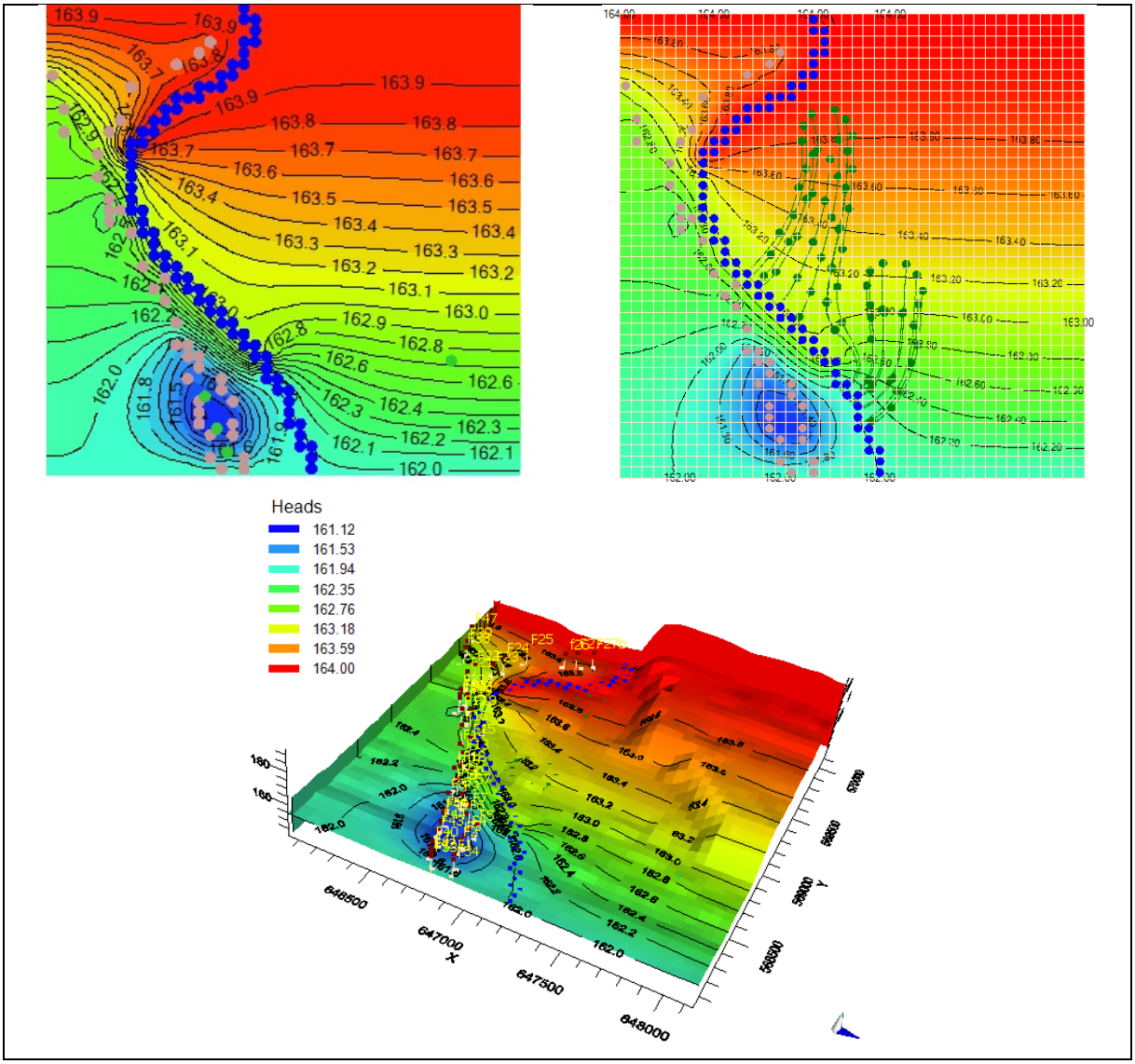

Figure 11. 2D and 3D representation of the evolution of the piezometric elevations in the case of drilling wells in the Gherăești area

According to the mathematical model, the aquifer is mainly supplied from the high area (terrace), the groundwater inflow being approximately 500 l/s, and secondary from precipitation over the entire surface with a flow rate of 125 l/s.
There is also an important connection between the aquifer and the Bistrița River, which drains the aquifer with a flow rate of 370 l/s.

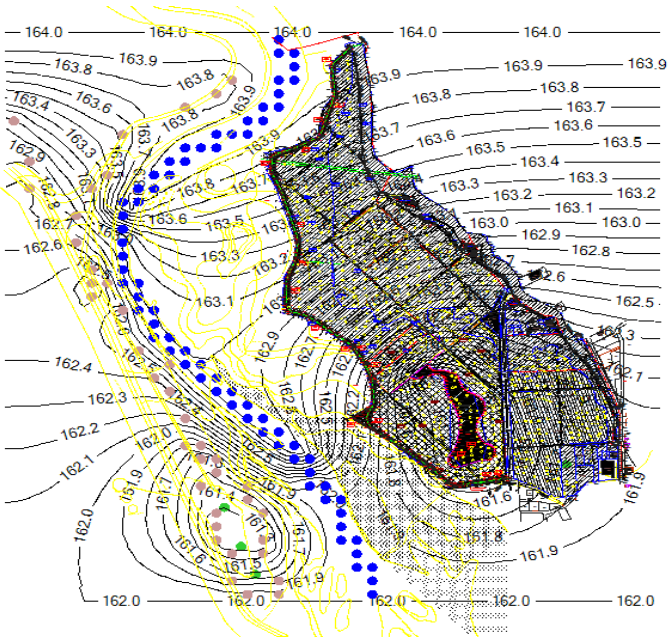

Figure 12. Map of piezometric surfaces in the case of drilling wells in the Gherăești area and the designed recreational lake

4. Conclusion

There are a multitude of models for the simulation of groundwater dynamics in the case of catchments with wells, varying from simple to complex. A realistic approach requires a good knowledge of the classic modelling structure, mainly because every groundwater modelling system must be flexible enough to be integrated into a model of the entire system.

The hydrodynamic spectra determined on the model give a complete picture of the movement of water towards the catchment fronts. Based on them, the specific flow along the catchment fronts can be determined, the main element in establishing the optimal distances between the water catchment wells and the designed recreational lake.

By running the flow model, the map of hydroisohypses and the velocity field in the study area were obtained. Furthermore, the simulation of the flow and transport model in the groundwater was carried out.

According to the mathematical model, the aquifer is mainly supplied from the high area (terrace), the inflow of underground water being considerable. There is also an important connection between the aquifer and the Bistrița River.

The flow captured by the wells in the Gherăești area represents approximately 20% of the total transited flow (at a maximum flow exploited by a borehole of Q=6.0 l/s), and the location of the designed recreational lake, according to the layout plan in the study area, does not affect the water levels in the catchment area.

5. References

[1] McDonald, M. G. and A. W. Harbugh. – *A modular three-dimensional finite-difference ground-water flow model.* U.S. Geological Survey Techniques of Water-Resources Investigations Book 6, 1988.

[2] Wen-Hsing Ciang, Kinzelbach, *Processing MODFLOW, A Simulation system for modelling grounwater flow and pollution*, 2005.

[3] x x x - *Visual Modflow Pro,* U.S. Geological Survey Modular Ground-water model (2007).

[4] Toacă, D., Bartha I., Neagu, M. R., Marcoie, N., - *Aquifers Hydrodynamic Modeling using Analogical and Numerical Model, for Underground Water's Capture.* Bul. Inst. Politehnic, Iaşi, Tomul LII (LVI), Fascicula 3-4, s. Hidrotehnică, 2007.
[5] Danchiv, A., Stematiu, D., *Metode numerice în hidrogeologie*. Ed. Didactică şi Pedagogică, R.A. Bucureşti, 1997.
[6] Zidaru, Gh., *Mişcări potenţiale şi hidrodinamica reţelelor de profile*. Ed. Didactică şi Pedagogică, Bucureşti, 1981.
[7] Reichard, E. G., *Groundwater – surface water management with stochastic surface water supplies: A simulation optimization approach*, Water Resources Research, 1995
[8] Riefler R.G., D. P. Ahifeld, *The impact of numerical precision on the solution of confined and unconfined optimal hydraulic control problems*, Hazardous Waste & Hazardous Materials, 1996.

water

MDPI

Article

Linking Nutrient Dynamics with Urbanization Degree and Flood Control Reservoirs on the Bahlui River

Nicolae Marcoie [1], Șerban Chihaia [1], Tomi Alexăndrel Hrăniciuc [1,*], Cătălin Dumitrel Balan [2], Elena Niculina Drăgoi [2] and Mircea-Teodor Nechita [2,*]

[1] Faculty of Hydrotechnics, Geodesy and Environmental Engineering, "Gheorghe Asachi" Technical University of Iasi, Bd. Prof. Dimitrie Mangeron, No. 65, 700050 Iaşi, Romania; nicolae.marcoie@academic.tuiasi.ro (N.M.); serban.chihaia@dap.rowater.ro (Ș.C.)

[2] Faculty of Chemical Engineering and Environmental Protection "Cristofor Simionescu", "Gheorghe Asachi" Technical University of Iasi, Bd. Prof. Dimitrie Mangeron, No. 73, 700050 Iaşi, Romania; catalin-dumitrel.balan@academic.tuiasi.ro (C.D.B.); elena-niculina.dragoi@academic.tuiasi.ro (E.N.D.)

* Correspondence: tomi-alexandrel.hraniciuc@academic.tuiasi.ro (T.A.H.); mircea-teodor.nechita@academic.tuiasi.ro (M.-T.N.)

Abstract: This work analyzed the nutrient dynamics (2011–2022) and discharge (2005–2022) for the Bahlui River at four distinctive locations: Parcovaci—a dam-protected area that has been untouched by agriculture or urbanization; Belcesti—a primarily agricultural area, also dam-protected; Podu Iloaiei—a region influenced by agriculture and urbanization; and Holboca—placed after a heavily urbanized area. The analysis focused on determining a series of statistical indicators using the Minitab 21.2 software. Two drought intervals and one flood interval were analyzed to highlight daily discharge evolution during the selected period, showing that the constructed reservoirs successfully control the streamflow. For the entire period, the evolution of mean and median values of the streamflow is consistent, considering the locations' positions from the source to the river's end. The total nitrogen and total phosphorus were selected as representative quality indicators. The study follows the influence of the analyzed areas' characteristics and reservoirs' presence on nutrient dynamics. The results showed that the most influential factor that impacts nutrient dynamics is the reservoirs' presence, which controls the discharge, creates wetlands and swamps, and implicitly impacts nutrient concentration.

Keywords: discharge; flood control; nitrogen; phosphorus; urbanization degree; Bahlui River

Citation: Marcoie, N.; Chihaia, Ș.; Hrăniciuc, T.A.; Balan, C.D.; Drăgoi, E.N.; Nechita, M.-T. Linking Nutrient Dynamics with Urbanization Degree and Flood Control Reservoirs on the Bahlui River. *Water* **2024**, *16*, 1322. https://doi.org/10.3390/w16101322

Academic Editor: Yuanrong Zhu

Received: 22 March 2024
Revised: 3 May 2024
Accepted: 3 May 2024
Published: 7 May 2024

1. Introduction

Rivers' eutrophication is not a new problem [1], and it is an expected natural phenomenon in climates with prolonged dry seasons [2]. It is caused by an uncontrolled increase in nutrient concentration (e.g., nitrogen and phosphorus) followed by excessive growth of various aquatic plants that leads to water poisoning, death of aquatic animals, and sometimes irreversible damage to aqueous ecosystems. In regions without natural dry seasons, "nutritional pollution" can result from climate changes and human activities like urbanization, intensive agriculture, and industrial growth, all of which are interconnected and contribute to climate change [3]. It is generally recognized that extensive urbanization affects river courses [4]; industrial expansion is the cradle for countless pollutants, while intensive agriculture is the primary source of inorganic nutrients like nitrogen and phosphorus. Climate change causes intense events that generate heavy rainfalls and floods followed by severe and prolonged droughts. The former washes the lands and transports the nutrients to rivers and water reservoirs. At the same time, the latter ensures the concentrations increase due to water evaporation and the temperatures required for the occurrence of unnatural eutrophication. Unfortunately, this global phenomenon affects the rivers and coastal regions on all continents [5–7]. There are numerous reports in the

literature regarding the spatiotemporal evolution of nutrients in various rivers across the globe—see Table S1 and Figure S1 in Supplementary Materials.

A bibliometric study performed using the Scopus platform and the VOSviewer software, version 1.6.19, yielded 1210 results for "climate change and eutrophication and nutrients or nitrogen or phosphorus" search terms in title/abstract/keywords, starting from 2000 till the present day. The four significant clusters identified by VOSviewer were eutrophication, nitrogen, water quality, and nutrients, as shown in Figure 1.

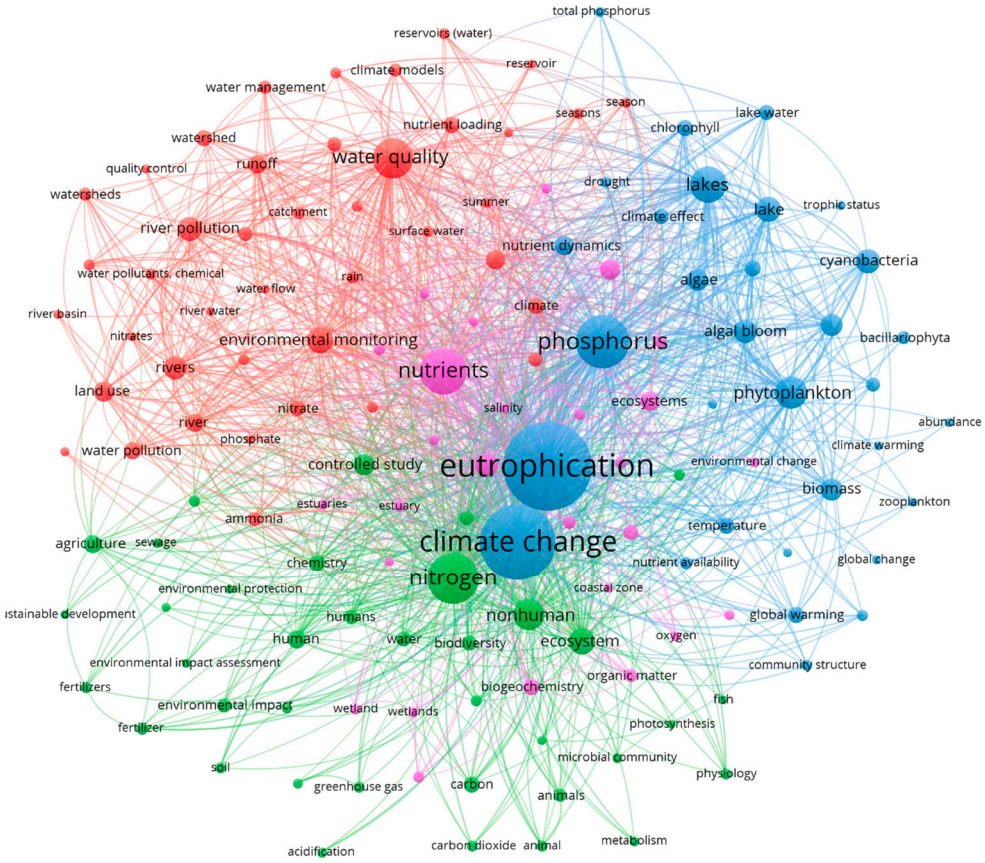

Figure 1. VOSviewer bibliometric map linking nutrient dynamics with climate change.

Based on previous experiences, predictions can be made to prevent unwanted phenomena through various actions: reducing the amount of fertilizers during the rainy season and using reservoirs and dams for sustainable river-flow management during drought periods.

Unfortunately, for various reasons, e.g., political—some countries keep the data private; economic—some countries cannot afford such studies, some regions are not yet integrated into the global perspective [8]. In some countries, there are records for hundreds of years regarding river floods, discharge variation, and drought periods [9], while in others, such types of analysis and data records are incipient. Nevertheless, the importance of such studies on a global scale is generally acknowledged nowadays, and the impact of climate change on nutrient dynamics reflected in water quality in rivers is undeniable [8].

This paper contributes to the knowledge in the particular field of river nutrient monitoring with information regarding the long-term (2011–2022) evolution of nitrogen and phosphorus in Bahlui River, Iasi County, Romania. The nutrient dynamics were linked with urbanization degree and flood control reservoirs based on the data recorded at four specific locations: (i) Parcovaci—as a pristine location—close to the river's spring, in a forest region, where the first dam on the river course was built; (ii) Belcesti—as a rural location—where the main activity is agriculture/farming, the place of the second reservoir (Tansa); (iii) Podu Iloaiei—a small town with mixed industrial/farming activities; and (iv)

Holboca—located close to the river mouth, after Iasi, the third largest city in Romania. The primary hypothesis is that a correlation between the analyzed aspects is present and can be the basis for predicting river discharge and nutrient variation in a specific context.

To the authors' knowledge, such a comprehensive report with such a manner of data interpretation on the Bahlui River has never been published. However, some reports regarding nutrients' evolution/concentrations have been presented in local or low-circulation magazines [10–13]. These reports only present daily analysis and/or short periods of nutrient/pollutant evolution and are usually focused on specific areas, such as the Iasi municipal area [14,15]. The flow discharge data span a longer period (2005–2022) than the nutrient monitoring (2011–2022), having been systematically conducted at the sites studied since 2011.

2. Materials and Methods

2.1. Research Area and Sampling Locations

The length of the hydrographical network of the Bahlui River is more than 3.100 km, of which only 119 km are included in the main river from spring to mouth [16]. The surface of the Bahlui River catchment covers 2025 km^2 and is the most important tributary of the Jijia River [17]. The river basin has a hilly terrain with large successive valleys and terraces. The valleys are deep and narrow, flanked by high hills with a slope of around 10%. The river basin has an average altitude of approximately 155 m. The mean slope of the river system varies, being 3‰ in the most upstream part, 1.6‰ in the middle part, and 0.5‰ in the downstream part. Precipitation runoff is the main water source for the river, accounting for 85–95% of the inflow [18]. The Bahlui River basin is located in an area with an annual precipitation of approximately 500 mm. Several factors contribute to the high complexity of the main river, its tributaries, and reservoirs. (i) Intense soil erosion during flood waves and moderate soil erosion in agricultural areas, leading to high levels of suspended solids. (ii) Sedimentation, gradually altering riverbeds and reservoirs, reducing water storage capacity and flood protection. High precipitation in the Bahlui River basin causes significant soil erosion [19], occasionally resulting in landslides [20].

The Bahlui River is a rain-fed river system with many ungauged and temporary tributaries for which no data were available [13,21]. The average discharge ranges between 2.8 m^3/s [10,14] and 4 m^3/s [19,22]. Only approximately 30% of the length of the network has permanent flow [22]. The length and surface area of the main tributaries of the Bahlui River are presented in Table 1 [16,22].

Table 1. The main tributaries of the Bahlui River.

No.	Bank	River	Length [km]	Surface Area [km^2]
1	Right	Bahluet	40	500
2		Voinesti	25	131
3		Nicolina	18	171
4		Magura	25	78
5	Left	Gurguiata	31	129
6		Cacaina	21	60
7		Ciric	19	56
8		Hoisesti	11	27
9		Chirita	15	39
10		Totoesti	11	25
11		Bogonos	9	36
12		Fundu Vaii	7	12
Various ungauged tributaries				838

Four sampling sites were selected from the Bahlui River catchment, as shown in Figure 2: Pârcovaci, Belcești, Podu Iloaiei, and Holboca. Each site has specific particularities: (i) Pârcovaci is placed relatively close to Bahlui's spring, in a forest area, and is actually

the first village crossed by the river—there is no significant influence of agriculture or urbanization on this site; the first important dam on the Bahlui River is placed in Pârcovaci; (ii) Belcești is a commune, in an agricultural region; in the vicinity of Belcești, the important Tansa-Belcești dam was built on the Bahlui River in order to prevent flooding; (iii) Podu Iloaiei is a small town with less than 10,000 inhabitants; a dam lake performing as a water reservoir is located on the Bahlueț River from the Bahlui River basin; and (iv) prior to reaching the commune of Holboca that is a part of the Iaşi metropolitan area, the Bahlui River crosses Iasi city, the third largest city in Romania by number of inhabitants. To summarize, the data come from four sites, representing (i) a region with no influence from agriculture or urbanization that is dam protected; (ii) a predominantly agricultural region that is dam protected; (iii) a mixed region influenced by both agriculture and urbanization; and (iv) a highly urbanized region. The GPS coordinates where the measurements were performed are 47°27′03.7″ N, 26°49′08.2″ E—Parcovaci, 47°18′04.7″ N, 27°06′02.0″ E—Belcesti, 47°12′33.4″ N, 27°17′41.5″ E—Podu Iloaiei, 47°07′46.2″ N, 27°44′12.0″ E—Holboca. The Google Earth images for the selected sites are presented in Figures S3, S5, S7, and S9, while the corresponding Corine land cover images are displayed in Figures S4, S6, S8, and S10.

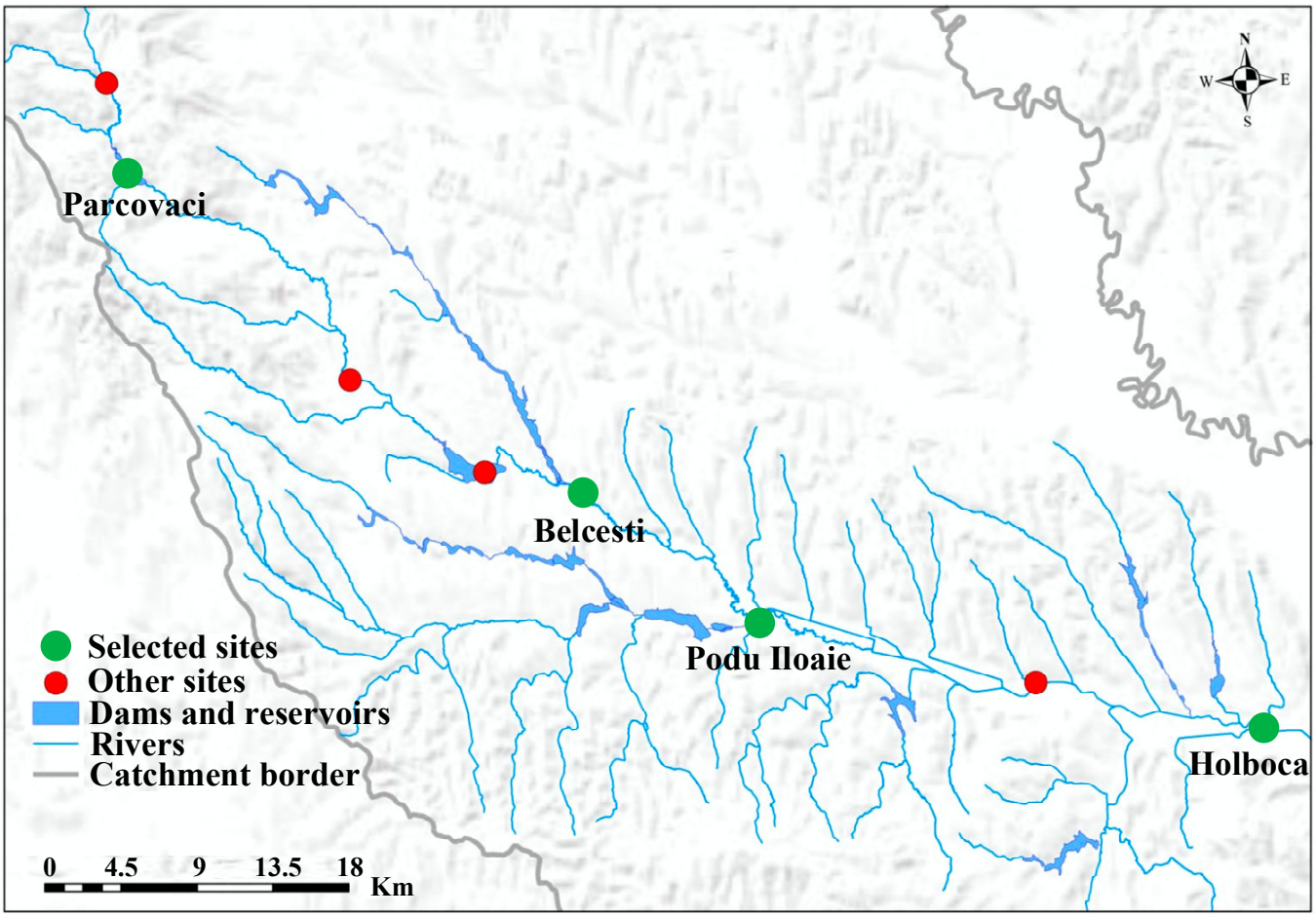

Figure 2. Sampling locations placement on Bahlui River catchment.

2.2. Historical Milestones: Flood and Drought Periods

Iasi, the historic city that served as the capital of Moldavia and later Romania, has a complex history with the Bahlui River, which cuts through the middle of the city. The evolution of the river's color and smell through the seasons was the subject of many local debates. A long series of floods were recorded during the 19th century. Between 1950 and 2006, 62 floods were reported for the Bahlui River basin [23], of which 15 were with flows between 50 and 90 m^3/s [24]. However, there are 4 floods with impressive flows (Table 2)

that left a mark in Iasi history [24], the most representative being the one registered in 1932 (Figure S2, Supplementary Materials) [25].

Table 2. The most important documented floods and drought periods on the Bahlui River.

Floods			Drought Periods		
Year	**Month**	**Flow [m^3/s]**	**Years**	**Season**	**Flow [m^3/s]**
1932	April	600	1953–1954	Winter	>0.001
1969	July	160	1962–1963		
1971	August	108	1963–1964		
1975	June	182	1954, 1958, 1959, 1962, 1992, 2000	Summer	

Since the Bahlui's discharge is rain-dependent, two distinct periods affect the flow: (i) the winter, when water is stored as snow and ice; and (ii) the drought periods. During the second half of the 19th century, minimum discharges were lower than 0.001 m^3/s (Table 3), and even water depletion was reported [26].

Table 3. The reservoirs in the Bahlui River system.

No.	Year	River	Reservoir	Average Flow [m^3/s]	Sub-Basin Area [km^2]
1	1964	Bahluet	Podu Iloaiei	1.06	500
2		Ciric	Aroneanu	0.10	50
3		Valea Locii	Ciurbesti	0.22	82
4		Valea Lunga	Chirita	0.08	40
5		Ezareni	Ezareni	0.06	27
6	1968	Voinesti	Cucuteni	0.25	131
7	1975	Bahlui	Tansa	0.84	346
8	1978	Gurguiata	Plopi	0.21	117
9	1980	Ciric	Ciric III	0.11	57
10	1982	Carlig (Cacaina)	Carlig	0.06	46
11		Nicolina	Ciurea	0.10	36
12		Ezareni	Cornet	0.03	13
13		Valea Locii	Barca	0.08	40
14	1983	Carlig (Cacaina)	Vanatori	0.03	23
15		Valea Oii	Sarca	0.20	91
16	1985	Bahlui	Parcovaci	0.42	95
17	1988	Fundu Vaii	Rediu	0.02	8.6

2.3. Hydrotechnical Infrastructure

Nowadays, approximately 70% of the Bahlui basin is hydrotechnically managed [26]. No less than 17 reservoirs with different functions, such as flood protection, irrigation, water supply, and fishery, have been built in the river's basin (Table 3) [21,22].

The critical roles of hydrotechnical structures and engineering infrastructure are to act as protection instruments, reduce hydrological vulnerability, and contribute to a sense of security [27]. In addition to that, a series of socioeconomic aspects are directly influenced by the presence of hydrotechnical structures such as the formation of characteristic ecosystems (lakes, wetlands, and swamps), diversification of land use given by the water supply, irrigation facilities, fish farming, watersports, and tourism. There are also several drawbacks related to forest loss, sediment and nutrient gathering, and landscape modification, but

the mentioned benefits compensate to some extent [28]. The impact of these storage lakes on river discharge, water quality, and nutrient dynamics is fundamental. However, while floods can be prevented and, to some extent, controlled, the prolonged drought periods are difficult to manage for a rainfall-dependent river, particularly for a region where agriculture and farming are the main economic activities.

2.4. Statistical Analysis

In order to analyze the available data supplied by the Administratia Nationala Apele Romane (National Administration Romanian Waters, https://rowater.ro (accessed on 5 February 2024)), a set of preprocessing steps was applied. First, the data were verified to ensure their validity; no digitized data were used during the preparation of this manuscript. After that, the data were centralized and analyzed using the Minitab® 21.2 (64-bit) statistical software.

3. Results and Discussion

3.1. Bahlui River Discharge Monitoring during 2005–2022 Period

There are huge oscillations between the hydro-climatic extremes (droughts and floods) typically reflected by minimum and maximum discharge values. Maximum flows generate concerns about engineering flood risks, water systems infrastructure, and flood response strategies. In contrast, minimum flows generate concerns for agriculture–irrigation engineering, ecosystems, and natural resources management [29].

The classic statistical streamflow indicators for the selected locations on the Bahlui River during the 2005–2022 period are presented in Table 4. The daily discharges from 2005 to 2022 for selected locations are presented in Figure 3. Two insets associated with drought periods (2006–2007, Figure 4; and 2011–2013, Figure 5) are marked in Figure 4 and selected for further discussion in Section 3.1.1. A period of heavy rainfalls (May–August 2010, not marked in Figure 3) is also selected to be individually discussed in Section 3.1.2.

Table 4. Statistical indicators for the river discharge (m^3/s) for the 2005–2022 period.

Location	Mean	StDev *	Minimum	Q1 *	Median *	Q3 *	Maximum
Parcovaci	0.2857	1.1329	0.0180	0.0419	0.0595	0.0700	24.5915
Belcesti	0.5480	1.2975	0.0030	0.0485	0.1123	0.3063	14.8447
Podu Iloaiei	0.8103	1.3847	0.0244	0.1605	0.3358	0.7204	15.3273
Holboca	4.0199	3.8982	0.5617	2.1222	2.9667	4.3658	62.1468

Notes: * StDev represents the standard deviation; Q1, median, and Q3 represent the data quantiles.

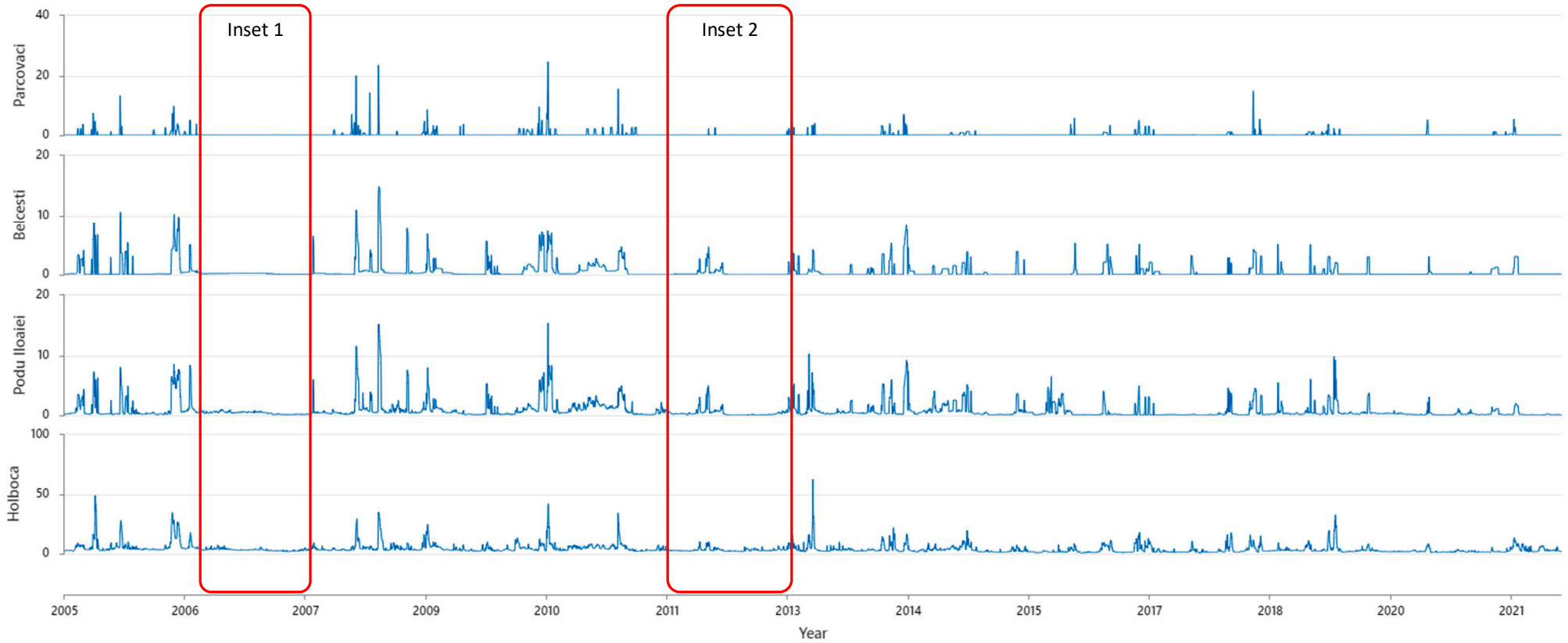

Figure 3. The Bahlui River's daily discharge variation at the selected sites (Parcovaci, Belcesti, Podu Iloaiei, and Holboca) for the 2005–2021 period *. * Insets 1 and 2 present selected drought periods, further detailed in Figures 4 and 5.

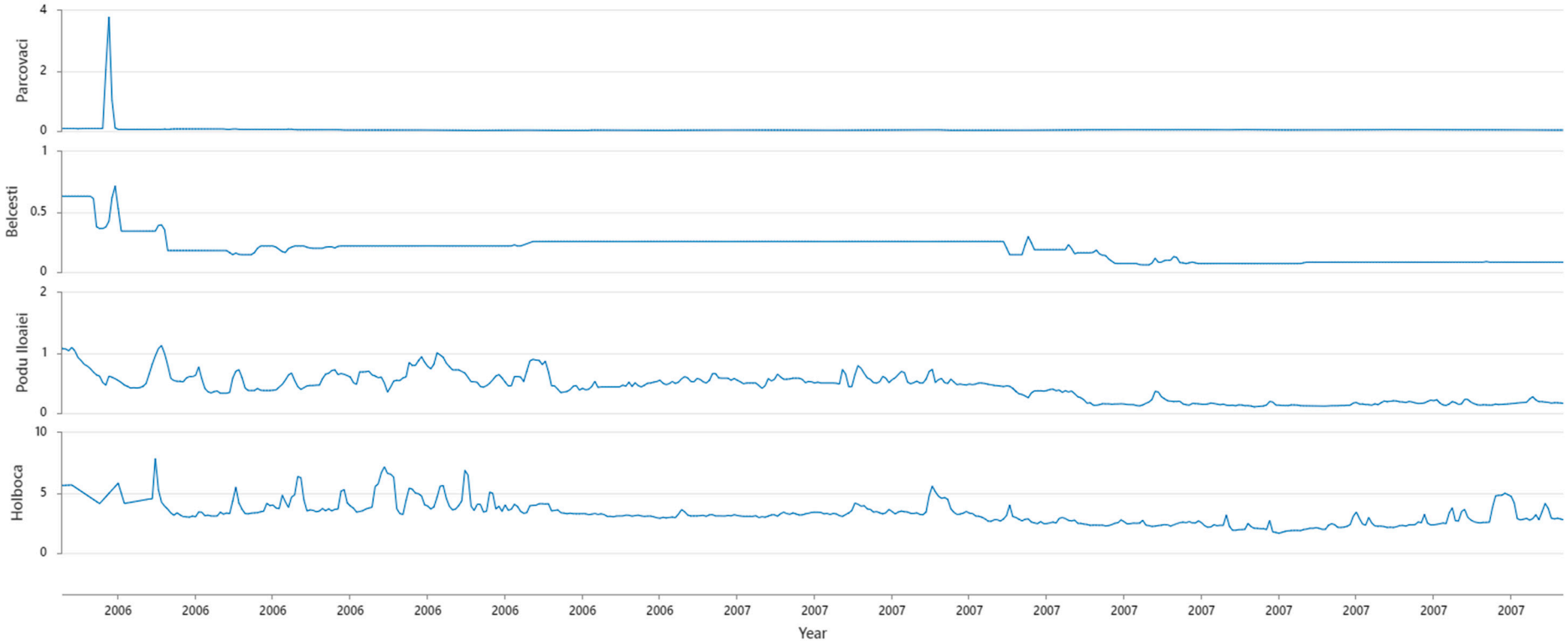

Figure 4. (Inset 1 from Figure 3). Comparative display of daily discharge (m^3/s) of Bahlui River during the 2006–2007 drought at Parcovaci, Belcesti, Podu Iloaiei, and Holboca.

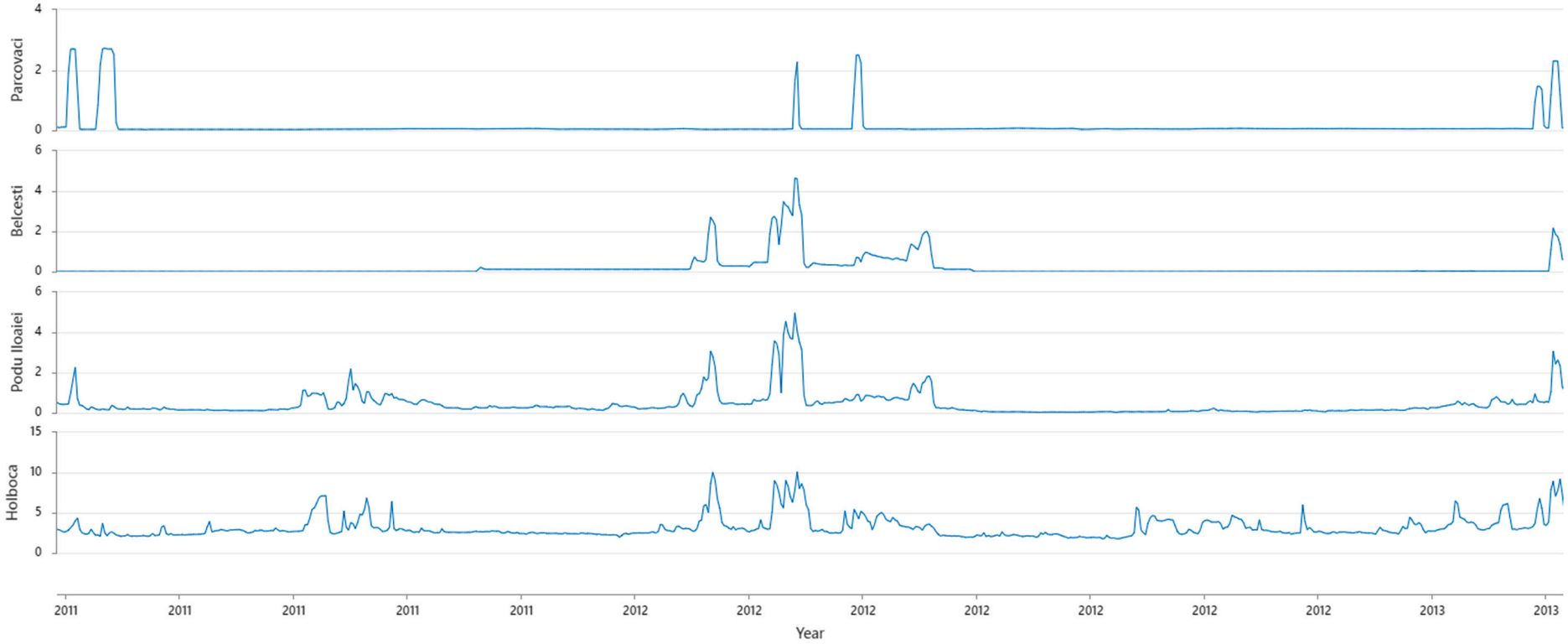

Figure 5. (Inset 2 from Figure 3). Comparative display of daily discharge (m^3/s) of Bahlui River during the 2011–2013 drought at Parcovaci, Belcesti, Podu Iloaiei, and Holboca.

Q1 is also known as the lower quartile and shows that 25% of the data fall below this threshold. The second quartile (Q2, or median) shows that 50% of the data are below it. The third quartile (Q3, or upper quartile) shows that 75% of the data are below this value. Thus, the quartiles divide the data into four equal portions. The distance between Q1 and Q3 denotes the interquartile range and reflects the variability. It shows the distribution of the middle 50% of the data.

In Table 4, the highest variability is obtained for Holboca's discharge. This can be explained by the fact that the measurements for this location are taken after the wastewater treatment plant, and it incorporates the runoff gathered from the entire area of Iasi city. Also, in case of heavy floods, this location registered high values, as shown by the peaks in Figure 2, which reach (or go over) 50 m^3/s.

The evolution of the mean and median values of the streamflow is consistent, considering the locations' positions from the source to the river's end (Figure 2). The considerably higher values computed for Holboca could be related to the tributaries feeding the river after Podu Iloaiei (Figure 2). When it comes to minimum and maximum values, some inconsistencies can be noted, such as that the minimum from Belcesti is 6-fold lower than the minimum in Parcovaci or the maximum in Parcovaci is 1.6 times higher than Belcesti and Podu Iloaiei. These inconsistencies are related to the Parcovaci and Tansa (Belcesti) dams on the main river course. The Tansa is a multi-purpose reservoir, being used as protection against floods, as a drinking water supply for the Belceşti village, the biggest commune in Iasi county, with more than 10,000 inhabitants [30], as an irrigation source, and for aquaculture [31]. Therefore, the Bahlui's level is extremely low during drought periods, sometimes close to complete depletion [32], particularly after the Belcesti reservoir. Since the mean and the median are significantly closer to the minimum than the maximum values, it can be concluded that drought periods are predominant compared to flooding intervals (see Table 2).

3.1.1. Drought Periods Examination

During the first drought interval (Figure 4), the discharge in Parcovaci and Belcesti is controlled by the Parcovaci and Tansa (Belcesti) reservoirs. The values are remarkably constant throughout the drought period, even during the few rainy days. The oscillations registered for Podu Iloaiei and Holboca are related to the increased number of permanent and temporary tributaries after Belcesti and the rare rainfalls.

The Parcovaci and Tansa dams considerably impacted the drought period 2011–2013 by maintaining a constant flow rate. Table 5 displays the streamflow statistical indicators for the chosen places on the Bahlui River during the drought years of 2006–2007 and 2011–2013. As observed, although the entire period analyzed is considered as drought, the most severe drought manifestation was in 2007, where, for all sites except Holboca, the lowest mean values and variations in Q1–Q3 are obtained. The somewhat peculiar data obtained for Holboca are related to the location of the measuring site. It is placed after Iasi and its wastewater treatment plant, that discharges into the Bahlui River, sometimes has a higher flow rate than the river itself [33].

During the first drought period, the annual evolution of mean and median values of the streamflow is consistent, considering the locations' positions from the source to the river's end (Table 5, 2006; 2007). The evolution of the median and maximum values is inconsistent with the locations' positions, highlighting the influence of the Parcovaci and Tansa (Belcesti) reservoirs. The mean and maximum values analysis during the 2011–2013 drought shows that 2012 was the driest year of the period. The second drought period (Figure 5) was also analyzed by other authors, who highlighted that 2012 was a dry year from the hydrological point of view [34].

Table 5. Statistical indicators for the river discharge during selected drought periods (m^3/s).

Location	Year	Mean	StDev	Minimum	Q1	Median	Q3	Maximum
Parcovaci	2006	0.4422	1.2262	0.0220	0.0340	0.0490	0.0690	9.6892
	2007	0.038377	0.005964	0.026400	0.033453	0.039424	0.043608	0.047896
	2011	0.3832	1.2467	0.0255	0.0349	0.0394	0.0649	15.4678
	2012	0.0827	0.2636	0.0327	0.0425	0.0469	0.0561	2.4989
	2013	0.2462	0.6966	0.0180	0.0522	0.0575	0.0670	4.2317
Belcesti	2006	0.8988	1.9029	0.0980	0.1787	0.2163	0.3899	10.1955
	2007	0.2380	0.6381	0.0600	0.0820	0.1599	0.2539	6.4773
	2011	0.6346	1.0218	0.0049	0.0049	0.0053	0.7856	4.6467
	2012	0.3182	0.6896	0.0030	0.0049	0.1123	0.2850	4.6488
	2013	0.3555	0.7908	0.0089	0.0166	0.0182	0.3951	4.1781
Podu Iloaiei	2006	1.258	1.913	0.088	0.416	0.553	0.811	8.510
	2007	0.3995	0.5660	0.1018	0.1560	0.3627	0.4998	6.0000
	2011	1.0156	1.0434	0.1033	0.2259	0.6024	1.4605	4.9478
	2012	0.4386	0.7514	0.0244	0.0667	0.1602	0.4722	4.9810
	2013	0.8127	1.1501	0.1142	0.2839	0.4223	0.7241	10.2434
Holboca	2006	6.219	5.859	2.886	3.390	4.098	5.410	34.349
	2007	3.1051	1.0214	1.6517	2.4486	3.0458	3.3346	9.3919
	2011	4.442	3.537	2.047	2.601	3.226	5.306	34.140
	2012	3.1295	1.4300	1.7623	2.3228	2.6022	3.3358	10.0813
	2013	4.560	5.117	1.608	2.539	3.307	4.390	62.147

3.1.2. Flood Episode Examination

From a hydrological point of view, the year 2010 is remembered as a year of devastating floods across Central and Eastern Europe, including Romania, Czech Republic, Slovakia, Bosnia-Herzegovina, Hungary, Croatia, southern Poland, and southern and eastern Germany [35,36]. Romanescu and Stoleriu analyzed the" exceptional" floods in the Prut basin in the summer of 2010, where river discharge reached 1600 m^3/s [37]. This event was caused by heavy rainfall, snowmelt, and saturated soil conditions.

The highest peaks for discharge values were registered on 28–29 July 2010 (Figure 6). These high discharges were preceded by heavy rainfalls on the 24th and 25th of July [36]. Unlike the previous flood intervals at the turn of the century, the urban area of the city of Iasi was protected by Bahlui's waters.

The analysis of the daily discharge statistical indicators during the May–August heavy rainfall interval from 2010 (Table 6) shows that during June 2010 the streamflow achieved the highest peaks. Only the mean values are consistent with the locations' positions on the map; the other indicators were influenced by reservoir activity.

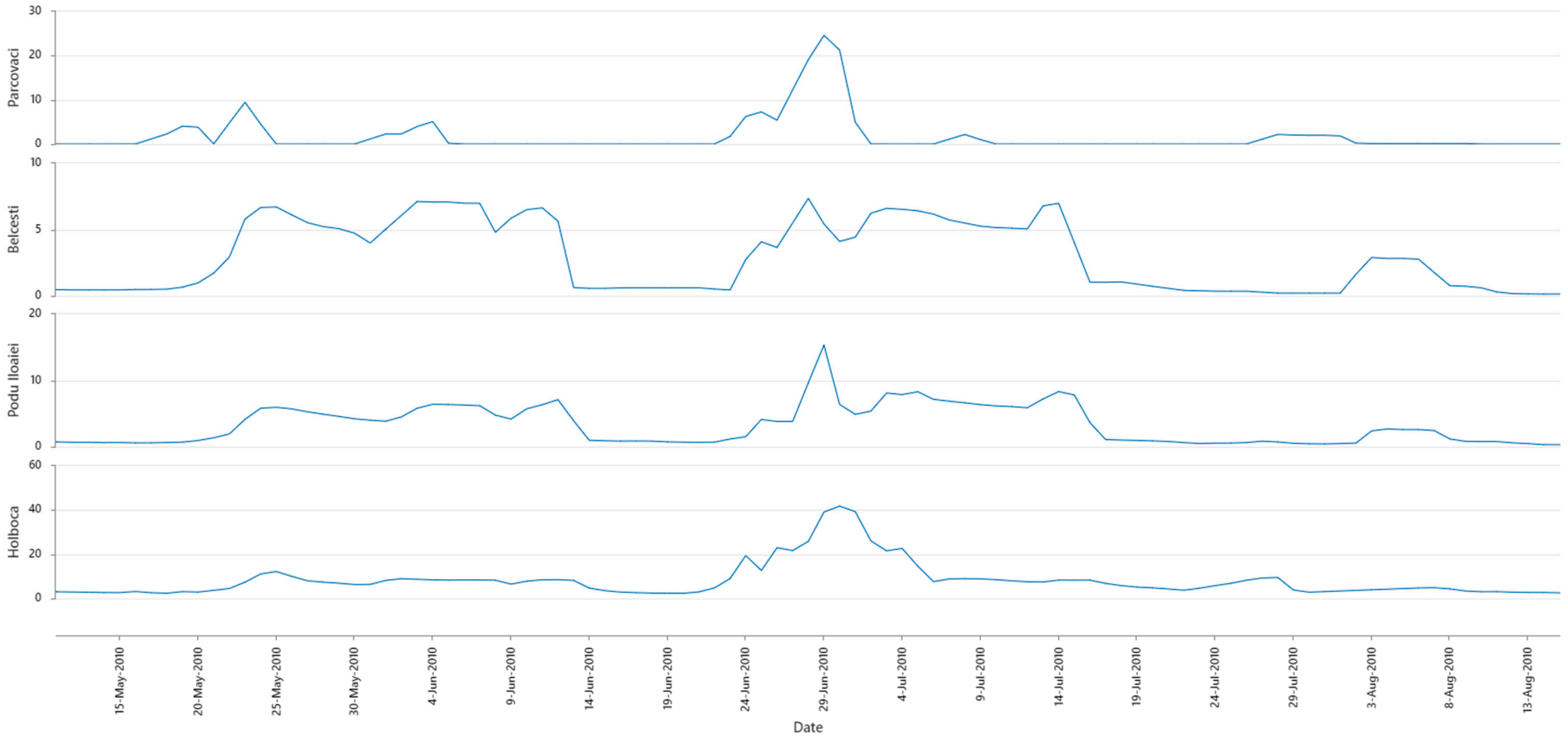

Figure 6. Comparative display of Bahlui River's daily discharge during heavy rainfalls from May to August 2010 at Parcovaci, Belcesti, Podu Iloaiei, and Holboca.

Table 6. Statistic indicators for the discharge during 2010 floods (m^3/s).

Location	Month	Mean	StDev	Minimum	Q1	Median	Q3	Maximum
Parcovaci	May	1.032	2.155	0.028	0.028	0.028	1.165	9.462
	June	3.74	6.77	0.03	0.03	0.03	5.17	24.59
	July	0.623	1.127	0.028	0.028	0.028	1.113	4.971
	August	0.1276	0.3256	0.0309	0.0371	0.0447	0.1409	1.8596
Belcesti	May	2.163	2.289	0.451	0.489	0.783	4.724	6.704
	June	3.834	2.734	0.447	0.613	4.449	6.534	7.355
	July	3.039	2.725	0.21	0.356	1.055	5.724	6.977
	August	0.651	0.943	0.14	0.14	0.14	0.732	2.894
Podu Iloaiei	May	2.054	1.94	0.577	0.691	0.94	4.131	5.947
	June	4.144	3.296	0.663	0.894	4.019	6.297	15.327
	July	3.773	3.17	0.422	0.625	3.632	6.867	8.309
	August	0.827	0.783	0.304	0.422	0.474	0.786	2.679
Holboca	May	4.61	2.74	2.376	2.898	3.047	6.382	12.204
	June	10.94	10.09	2.34	4.43	8.35	9.93	41.77
	July	9.67	7.76	2.85	5.17	7.99	8.96	39.28
	August	3.279	0.805	2.442	2.657	2.835	4.031	4.925

3.2. Nutrient Dynamics on Bahlui River during 2011–2022 Period

Individual Nutrient Analysis

The primary anthropogenic sources of N and P in rural areas are fertilizers from agriculture, animal manure from livestock production, and septic systems such as household wastewater [38]. Both N and P can be produced via natural soil processes through mineralization, weathering, and/or dissolution [39]. However, in some urban areas it was found that household activities such as lawn fertilization and pet ownership contribute more to nutrient watersheds than commercial, municipal, or industrial actions [40]. Urban runoff, including stormwater and snowmelt, drainage networks, and yard waste, is the primary carrier of pollutants in the urban environment [41].

As can be observed from Figure 7, the distribution of individual measurements indicates that the lowest values for both TN and TP are for Parcovaci. On the other hand, the largest domains are obtained for Belcesti and Holboca, where outliers are identified.

As expected, the average TN for the Parcovaci location during the analyzed period (0.6303 mg/L, Table 7) is way below the limit value of 10 mg/L [42], and the TN value is relatively constant during the entire period (Figure 8). The same behavior is observed for the TP evolution at Parcovaci (Figure 9).

Table 7. Statistical indicators for some water quality indicators analyzed in the 2011–2022 period.

Indicator	Location	Mean	StDev	Minimum	Q1	Median	Q3	Maximum
TN	Belcesti	7.367	4.528	1.230	3.895	6.220	10.250	19.890
	Holboca	8.972	3.483	1.470	6.400	8.520	10.590	25.400
	Parcovaci	0.6303	0.4488	0.1500	0.4000	0.5400	0.7000	2.9200
	Podu Iloaiei	3.971	2.297	0.250	2.360	3.460	4.670	12.300
TP	Belcesti	0.4184	0.5262	0.0600	0.1930	0.3080	0.4145	3.7300
	Holboca	1.0586	0.4969	0.2500	0.6700	0.9740	1.3125	2.4270
	Parcovaci	0.0819	0.0980	0.0025	0.0200	0.0400	0.1000	0.4670
	Podu Iloaiei	0.3729	0.2692	0.0680	0.2100	0.2980	0.4730	1.9820

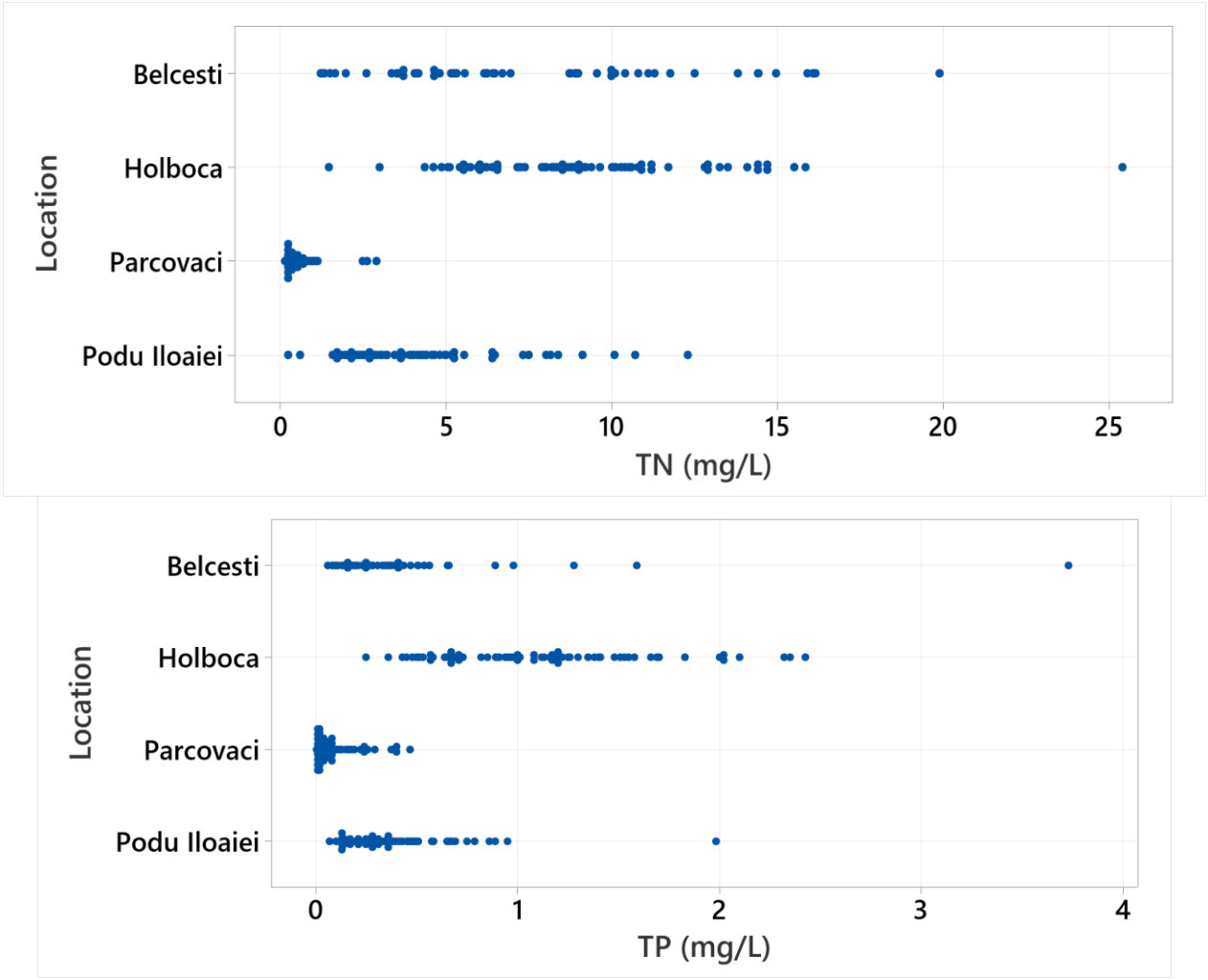

Figure 7. Variations in TN (**a**) and TP (**b**) in the selected locations for 2011–2022. Unfortunately, the TN and TP data are unavailable for all considered locations during the analyzed period. The 2011–2014 interval is missing for Belcesti.

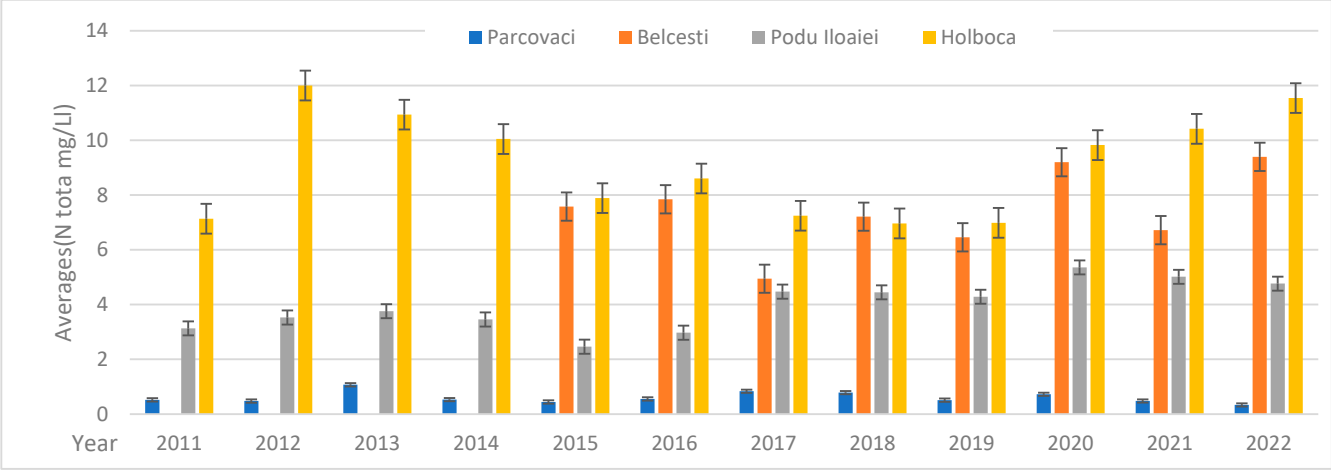

Figure 8. Average annual variation in total nitrogen.

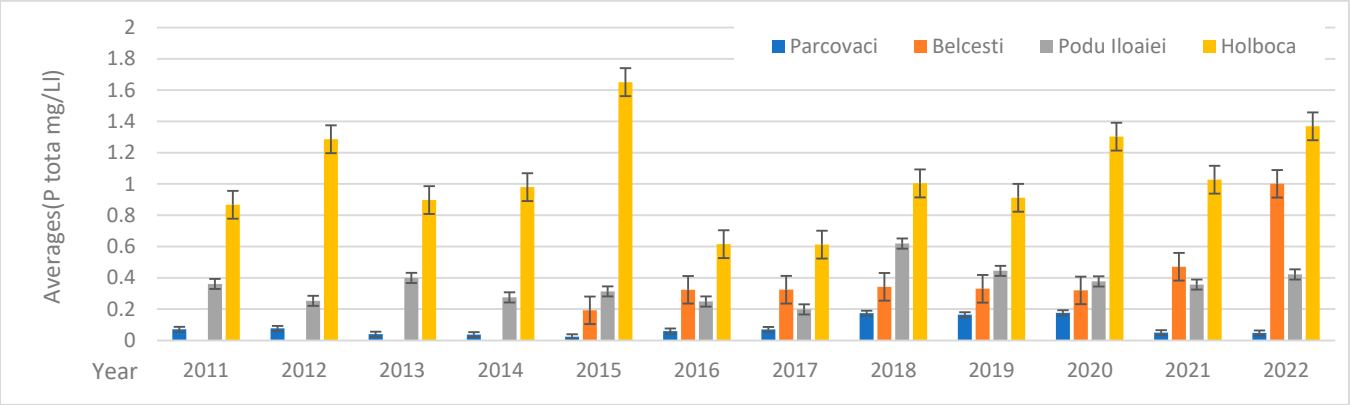

Figure 9. Average annual variation in total phosphorus.

The unexpected high level of TN in the Belcesti area (Figure 8) can be correlated with the uncontrolled use of nitrogen-based fertilizers necessary for agricultural and farming activities. Other authors also observed this aspect [19]. The highest level of TN (except 2018) was reported for the Holboca location during the entire period under study, and it is obviously correlated with the urban area of Iasi.

The highest variability is observed for TN in Belcesti, while the lowest is in Parcovaci. On the other hand, for TP, the highest variability is observed in Holboca and the lowest in Parcovaci. Excluding the 2022 reports where the TP average value is atypically high for Belcesti (Figure 9), there is a "normal" trend for this specific indicator: the pristine location exhibits the lowest values, the agricultural and mixed urban/agricultural locations show comparable values (except for in 2018, where the value is higher for the agricultural area), while after the major urban area, the value almost doubles. For the monitored period, the average values of TP (Table 7) are 0.0819 mg/L for Parcovaci and almost 13-fold higher for Holboca (1.0586 mg/L), yet below the NTPA 001/2002 [42] limit of 2 mg/L.

3.3. Discharge–Nutrient Correlation

It is generally recognized that discharge measurement is essential in nutrient load estimation. However, certain degrees of uncertainty should be considered, especially for small streams [43]. It was shown that even for the high frequency of data prelevation, paired data levels of uncertainties of up to 25% can occur in correlations between discharge and nutrients [43]. In order to correlate the nutrient dynamics with the Bahlui River's discharge, the plots presented in Figures 10–13 were drawn for the selected sites. It is relatively challenging to find rational correlations between nutrient dynamics and river discharge for the first two locations (Figures 10 and 11). The presence of the two dams (Parcovaci and Tansa) on the main river course can disturb the correspondence. The dams usually trap the nutrients and sediments transported by runoff from heavy rains. The dilution phenomenon that should typically occur with the increase in the water flow is rarely present, and at some points the TN level seems unaffected by the discharge values (e.g., January 2013 vs. August 2013, Figure 10, Parcovaci; September 2018 vs. April 2019, Figure 11, Podu Iloaiei).

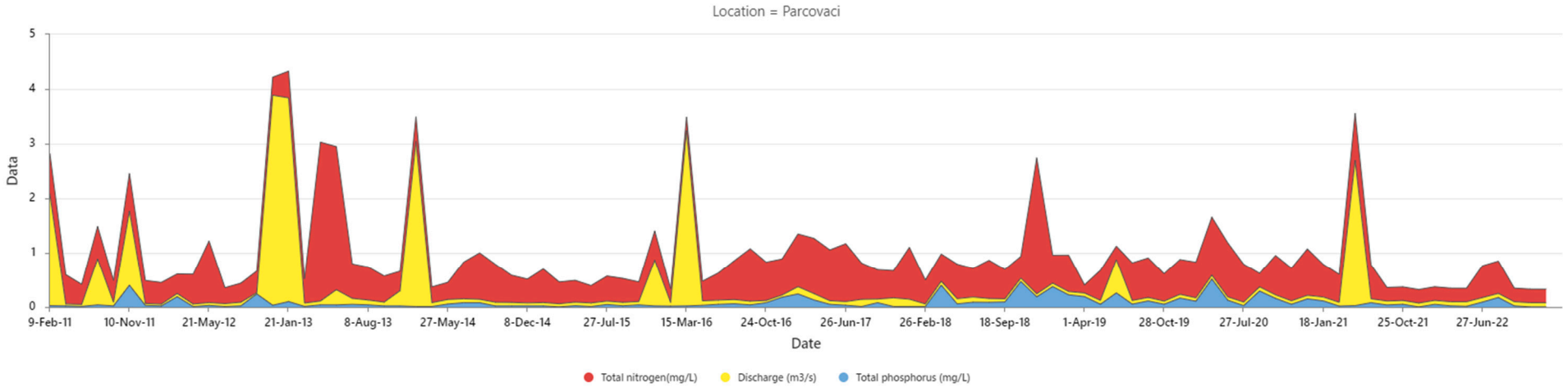

Figure 10. The variations in discharge, total nitrogen, and total phosphorus at Parcovaci for 2011–2022.

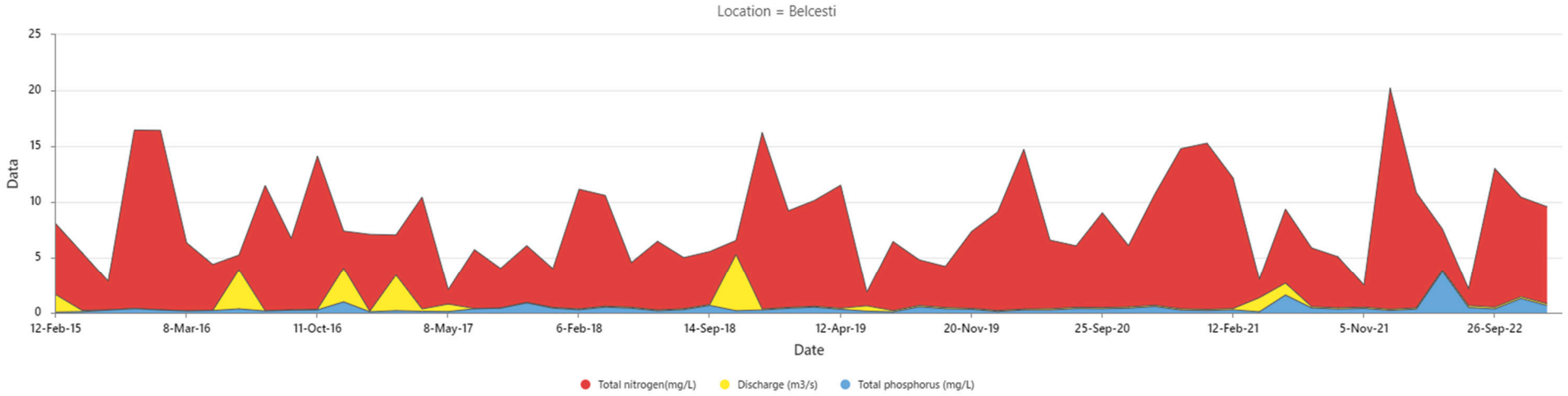

Figure 11. The variations in discharge, total nitrogen, and total phosphorus at Belcesti for 2011–2022.

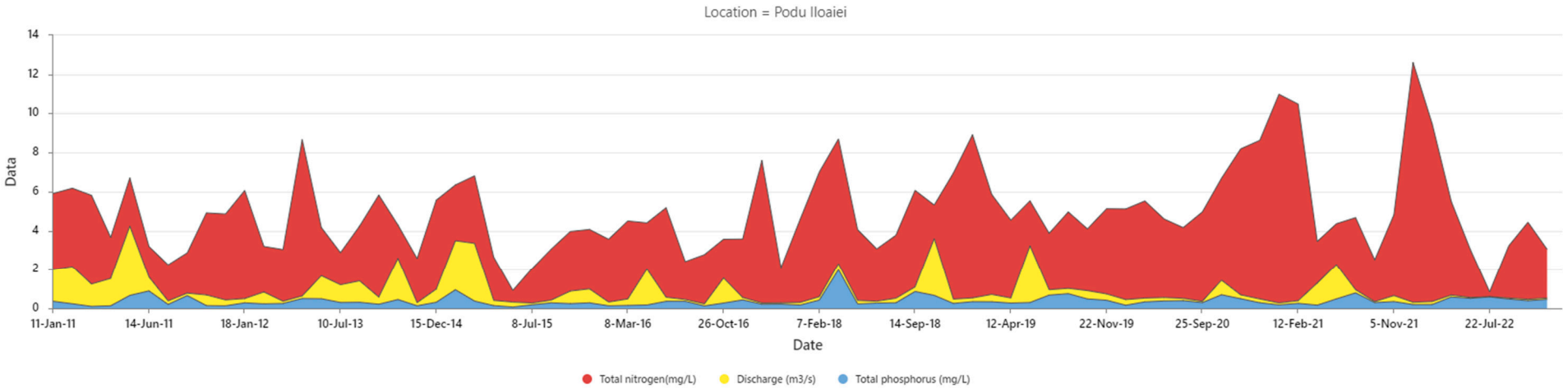

Figure 12. The variations in discharge, total nitrogen, and total phosphorus at Podu Iloaiei for 2011–2022.

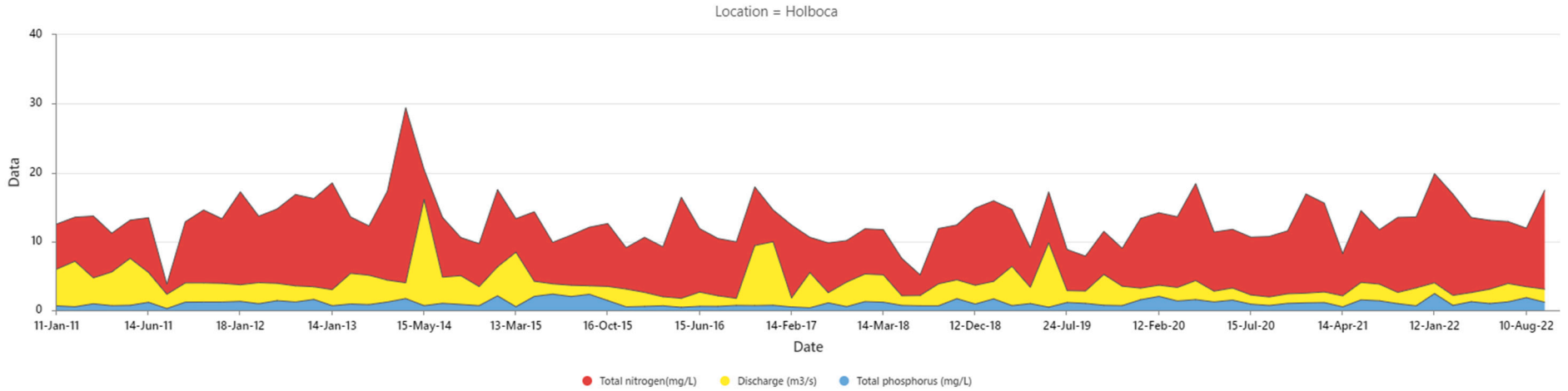

Figure 13. The variations in discharge, total nitrogen, and total phosphorus at Holboca for 2011–2022.

A correlation between the river flow rate, TN, and TP can be observed for Parcovaci between the two discharge peaks in March 2016 and June 2021 (Figure 10). As for the Belcesti site, neither TN nor TP seems to evolve in a visible connection with the river flow oscillations. The nitrogen level is relatively high in this location and exhibits peaks even at low and constant discharge, e.g., April 2019–February 2021, revealing a predisposition to eutrophication that was also reported by other authors [44]. A relatively "normal" correspondence can be seen for Podu Iloaiei in Figure 12, where the TN and TP levels typically increase with the discharge growth, with three exceptions: (i) the period June 2011–July 2013, that overlaps with the drought period (analyzed in Section 3.1.1); (ii) the period September 2018–September 2020, when another prolonged drought period was reported [45], when the TN values are high despite the low river level; and (iii) February 2018, when the TP level is atypically high. The best (visual) correlation can be observed for the last location, Holboca (Figure 13), which is close to the river's end. There, the discharge levels are higher than in all other locations, being relatively unaltered by the dam's presence and influenced by the wastewater treatment plant discharge.

A Pearson analysis was performed on the data to determine whether any statistically significant correlations could be obtained. After the data were placed in a scatter plot (Figure S11), the outliers were removed (maximum 5%). Next, the correlation indicators were determined (Table S1). As can be observed, for most cases $p > 0.05$, indicating that no significant data can support the affirmation that a correlation between parameters exists. The exceptions are for (i) Parcovaci, in the case of TP vs. TN, where a correlation of 0.35 (which is considered moderate positive) was obtained; (ii) for Belcesti, in the case of TN vs. discharge, where a correlation of −0.29 (which is considered low negative) was obtained; and (iii) for Holboca in the cases of TN vs. discharge and TP vs. TN, where correlations of −0.342 (moderate negative) and 0.417 (moderate positive), respectively, were obtained.

In order to determine if a seasonal variation can be observed for each location, analyzed parameter, and season, the means of the values were computed and are shown in Figure 14. The seasons were identified as follows: winter—December, January, and February; spring—March, April, and May; summer—June, July, and August; autumn—September, October, and November. As observed, TN's highest concentrations are obtained during the coldest season of the year for all analyzed locations, while the lowest are in the summer. Most probably due to the dam's presence, no significant seasonal correlations were observed for the other analyzed parameters.

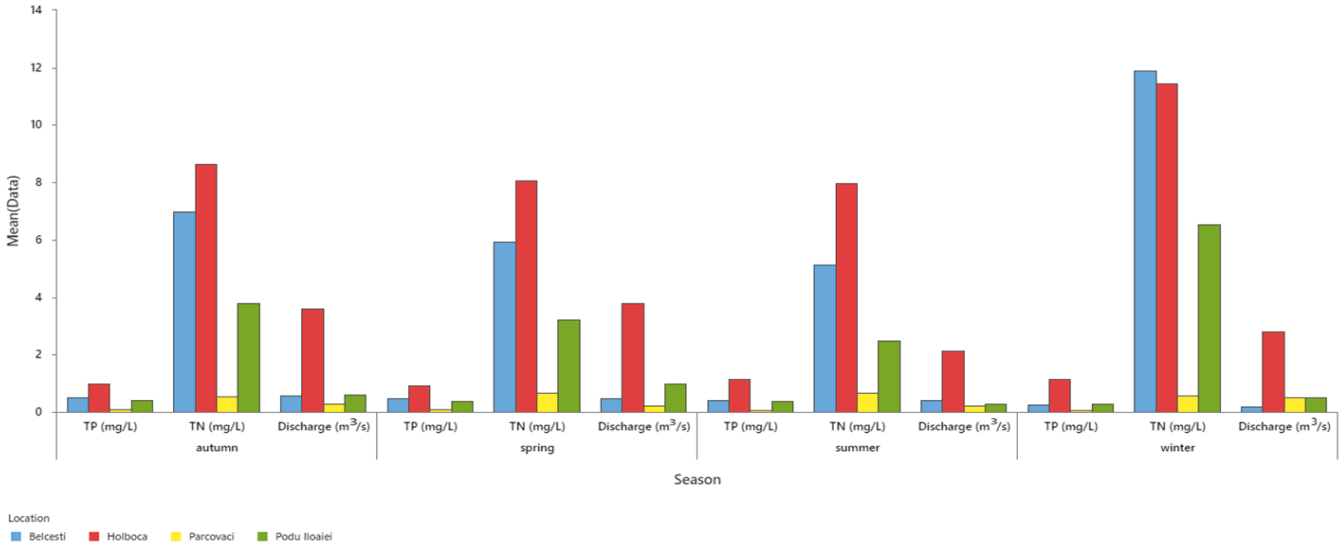

Figure 14. Average seasonal variations: discharge, total nitrogen, total phosphorus.

3.4. Nutrient Dynamics: Influence of Urbanization Degree and Flood Control Reservoirs on the Course of Bahlui River

It is evident that the nutrient dynamics are affected by a combination of natural and anthropogenic factors, each having relative influences that change with temporal and spatial scale. Like many other rivers, the Bahlui provides water for the inhabitants of its basin for irrigation, industrial, and drinking purposes. It also assimilates and/or carries industrial and municipal wastewater and manure discharges and runoff from agricultural fields, roadways, and streets [46]. From its spring to its mouth, the Bahlui River crosses lands with different degrees of development, including forests, small towns, villages, agricultural regions, and one major urban area. Two major flood-controlling reservoirs were built on the main river course, Parcovaci and Tansa (Belcesti), and another 15 with different functions, such as flood protection, water storage, and fishery, on the tributaries in its hydrographic basin. The existence of these reservoirs attenuates the impact of significant climate change effects such as extreme floods and prolonged drought periods but also affects many physical and ecological aspects and processes, including sediment transport and nutrient exchange [47]. The hydrological alterations produced by river-placed reservoirs are changes in flood frequency and magnitude, reduction in overall flow, increased or decreased summer baseflows, and altered timing of releases [48]. In addition, the grassy vegetation, especially common reed (*Phragmites australis*) and bulrush (*Typha latifolia*), plays an essential role in the retention of nutrients in the wetlands and swamps that usually form at the base of reservoirs or nearby, with small, temporary river tributaries [49,50].

3.4.1. Urbanization Degree

Halecki and coworkers discussed the lower nutrient retention capacity in urban areas compared to rural and suburban areas [51]. The high surface runoff, that is correlated with lower retention capacity, could explain the growth in both TN and TP in urban areas [46,51–53].

Holboca, the fourth location from spring to mouth considered for this study, is placed after Iasi, the third city in Romania, close to the Bahlui confluence with the Jijia River. Many authors have studied the effect of anthropogenic activities on the water quality in this part of the river [10,14,15,33,54]. As pointed out by the current report, in Holboca the nutrient levels reach the highest values of all the selected locations. Moreover, compared with the nutrient level in the first location, Parcovaci, which is a forest area with minimal human activities, there are considerable differences in magnitude. The mean value for Holboca during 2011–2022 is nearly 14-fold higher for TN and 13-fold higher for TP (Table 7). As for the rural and mixed regions, represented by the Belcesti and Podu Iloaiei locations, respectively, the nutrient level is influenced by the presence of the Tansa reservoir that controls the flow regime and by the increased number of permanent and temporary tributaries after Belcesti, which contributes to the flow development between the two locations. For most of the monitored period, except 2017, when the values were comparable, the TN values were higher in Belcesti than in Podu Iloaiei (Figure 8). As for the TP, except for the peak in 2022 in Belcesti, the values were reasonably low [42], following a similar trend (Figure 9).

3.4.2. Flood Control Reservoirs

During the past century, the Bahlui basin was highly vulnerable to floods [24] and droughts [32,55]; the inundation frequencies and the color and odor of the Bahlui waters during eutrophication periods were notorious. Nowadays, owing to massive investments in hydrotechnical structures, the vulnerability of the studied area, particularly of the selected locations, is highly diminished. Between 1960 and 1990, as many as 17 reservoirs were constructed in the Bahlui basin, as shown in Table 3. As for the selected locations, it is evident that the Parcovaci and Tansa reservoirs control the daily discharge even during drought periods, preventing river depletion (Figure 4). Hydrotechnical developments placed on the main course and/or in a river basin fundamentally impact the environment [56], producing geographical, ecological, and social changes [28], and the Bahlui River is no exception [21].

The reservoir and/or dam-induced hydrological control of the flow regime may affect the nutrient dynamics similarly (yet less aggressively) to the succession of flood and drought periods [48]. The formation of wetlands and swamps as tails of the reservoirs is also essential for nutrient dynamics. The balance in nutrient retention and release from swamps and wetlands from the river's hydrographic basin is directly related to the water level, which can be controlled naturally (flood–drought cycles) or artificially (dam discharge). The succession of seasons also plays a vital role in supplying rivers and reservoirs with organic matter that can be further (gradually) decomposed in nutrients (e.g., leaves fallen from the forest canopy in early autumn; leaves on the ground and agricultural waste brought by spring floods) [57].

The TN and TP levels are within natural limits in the Parcovaci location, presenting small fluctuations (seasonal) through the studied interval. On the contrary, the values of nutrients, particularly TN, are relatively high for the Belcesti location, which is protected by the Tansa reservoir (Figure 8). Dughilă et al. [31] analyzed the most significant water quality indicators for the Tansa Lake, including TN and TP, in 2010. It was found that the lake level of TN was much lower than that of the Bahlui River (mainly due to the nitrate component of TN). This resulted from using nitrogen fertilizers in agriculture and wastewater discharge from commercial companies and wastewater treatment plants. The TP values in the reservoir were lower than in the river, though of a different order of magnitude compared to TN (similar to the current study; Figures 8 and 9). The orthophosphate components (that are produced in sewage effluents) were considered responsible for the elevated TP values in the Bahlui River in the Belcesti location [31]. The water quality for the main reservoirs (lakes) in the Bahlui drainage basin was studied by Minea, where it was found that it is worsening, most probably due to the contribution of the tributaries that bring pollutants from uncontrolled discharges from industrial sources and malfunctioning water treatment plants [26].

4. Conclusions

The current analysis focused on a long period and aimed to cover the gaps in the reported discharge data on the Bahlui River. The results revealed that the reservoirs constructed to regulate the streamflow successfully managed the water discharge. The mean and median streamflow values followed a similar trend for the entire period, consistent with the locations from the river's source to its endpoint. This indicates that the reservoirs effectively controlled the streamflow and mitigated the effects of drought and flood periods.

The analysis of nutrients considered the impact of reservoir presence and the features of the investigated locations on their dynamics. The results indicate that reservoirs have a significant impact because they control water discharge during floods and droughts. Also, reservoirs favor the occurrence of wetlands and swamps, important aquatic habitats, which, in turn, affect the nutrient concentration. Moreover, areas with high levels of urbanization and agricultural activities showed higher nutrient concentrations, which can be explained by the accidental release of pollutants into the water bodies.

A statistical evaluation of discharge and nutrient links in different locations revealed weak correlations only for some particular cases: TN–TP in Parcovaci, TN–discharge in Belcesti, and TN–discharge and TP–TN in Holboca. Therefore, the analyzed data cannot support the initial hypothesis that the analyzed characteristics are correlated. This suggests a highly complex interaction between many factors, and a more in-depth study with a higher frequency of data acquisition, more locations, and a higher number of parameters such as chemical and biochemical oxygen demand, water and air temperature, and precipitation level is required.

Supplementary Materials: The following supporting information can be downloaded at: https://www.mdpi.com/article/10.3390/w16101322/s1, Table S1. Literature reports on the spatiotemporal evolution of nutrients in various rivers across the globe; Table S2. Pairwise Spearman correlations; Figure S1. Scopus bibliometric analysis on eutrophication, climate change, and nutrients; Figure S2. Iasi, the flood in 1932: (a) The railway station; (b) the central area. Figures S3, S5, S7, S9. Google Earth images for the selected sites: Parcovaci, Belcesti, Podu Iloaie, Holboca. Figures S4, S6, S8, S10. Corresponding Corine land cover images for the designated locations. Figure S11. Scatter plot of all available data in all locations for (A) discharge (m^3/s) versus TN (mg/L); (B) discharge (m^3/s) versus TP (mg/L); (C) TP (mg/L) versus TN (mg/L). References [58–79] are cited in the supplementary materials.

Author Contributions: Conceptualization, N.M. and M.-T.N.; methodology, N.M.; software, E.N.D.; validation, T.A.H., Ș.C. and C.D.B.; formal analysis, Ș.C.; investigation, Ș.C.; resources, C.D.B.; data curation, T.A.H.; writing—original draft preparation, N.M.; writing—review and editing, M.-T.N., END; visualization, E.N.D.; supervision, N.M.; project administration, C.D.B.; funding acquisition N.M. All authors have read and agreed to the published version of the manuscript.

Funding: This research received no external funding.

Data Availability Statement: Data are available upon reasonable request.

Conflicts of Interest: The authors declare no conflicts of interest.

References

1. O'Hare, M.T.; Baattrup-Pedersen, A.; Baumgarte, I.; Freeman, A.; Gunn, I.D.M.; Lázár, A.N.; Sinclair, R.; Wade, A.J.; Bowes, M.J. Responses of Aquatic Plants to Eutrophication in Rivers: A Revised Conceptual Model. *Front. Plant Sci.* **2018**, *9*, 451. [CrossRef]
2. Boyd, C.E. Eutrophication. In *Water Quality: An Introduction*; Springer International Publishing: Cham, Switzerland, 2020; pp. 311–322.
3. Jeppesen, E.; Moss, B.; Bennion, H.; Carvalho, L.; DeMeester, L.; Feuchtmayr, H.; Friberg, N.; Gessner, M.O.; Hefting, M.; Lauridsen, T.L.; et al. Interaction of Climate Change and Eutrophication. In *Climate Change Impacts on Freshwater Ecosystems*; John Wiley & Sons: Hoboken, NJ, USA, 2010; pp. 119–151.
4. Moldovan, A.C.; Micle, V.; Hrăniciuc, T.A.; Marcoie, N. Research on the Sustainable Development of the Bistrita Ardeleana River through the Resizing of Weirs. *Water* **2022**, *14*, 3333. [CrossRef]
5. McDowell, R.W.; Noble, A.; Pletnyakov, P.; Mosley, L.M. Global database of diffuse riverine nitrogen and phosphorus loads and yields. *Geosci. Data J.* **2021**, *8*, 132–143. [CrossRef]
6. Newcomer Johnson, T.A.; Kaushal, S.S.; Mayer, P.M.; Smith, R.M.; Sivirichi, G.M. Nutrient Retention in Restored Streams and Rivers: A Global Review and Synthesis. *Water* **2016**, *8*, 116. [CrossRef]
7. Payen, S.; Cosme, N.; Elliott, A.H. Freshwater eutrophication: Spatially explicit fate factors for nitrogen and phosphorus emissions at the global scale. *Int. J. Life Cycle Assess.* **2021**, *26*, 388–401. [CrossRef]
8. Graham, D.J.; Bierkens, M.F.P.; van Vliet, M.T.H. Impacts of droughts and heatwaves on river water quality worldwide. *J. Hydrol.* **2024**, *629*, 130590. [CrossRef]
9. Garnier, J.; Brion, N.; Callens, J.; Passy, P.; Deligne, C.; Billen, G.; Servais, P.; Billen, C. Modeling historical changes in nutrient delivery and water quality of the Zenne River (1790s–2010): The role of land use, waterscape and urban wastewater management. *J. Mar. Syst.* **2013**, *128*, 62–76. [CrossRef]
10. Neamtu, M.; Ciumasu, I.M.; Costica, N.; Costica, M.; Bobu, M.; Nicoara, M.N.; Catrinescu, C.; van Slooten, K.B.; De Alencastro, L.F. Chemical, biological, and ecotoxicological assessment of pesticides and persistent organic pollutants in the Bahlui River, Romania. *Environ. Sci. Pollut. Res.* **2009**, *16*, 76–85. [CrossRef]
11. Oiște, A.M.; Gabriela, I. Nitrate trends during the seasons on Bahlui river and its tributaries in build-up area of Iasi city. *Bull. Univ. Agric. Sci. Vet. Med. Cluj-Napoca Agric.* **2011**, *68*, 116–123. [CrossRef]
12. Benchea, R.E.; Cretescu, I.; Macoveanu, M. Monitoring of water quality indicators for improving water resources management of Bahlui River. *Environ. Eng. Manag. J.* **2011**, *10*, 327–332. [CrossRef]
13. Barjoveanu, G.; Teodosiu, C.; Cojocariu, C.; Augustijn, D.; Craciun, I. Instruments for integrated water resources management: Water quality modeling for sustainable wastewater management. *Environ. Eng. Manag. J. (EEMJ)* **2013**, *12*, 1679–1690.
14. Zaharia, C. Evaluation of water pollution status in Bahlui River (Iasi town area) due to domestic and urban wastewater treatment activities. *J. Eng. Stud. Res.* **2015**, *21*, 79–88. [CrossRef]
15. Zaharia, C.; Teslaru, M.I. Control and analysis of some water quality indicators of Bahlui River in Iasi county area (spring season). *Bull. Polytech. Inst. Iasi Ser. Chem. Chem. Eng. Sect.* **2012**, *58*, 69–79.
16. Mihu-Pintilie, A.; Romanescu, G. Determining the potential hydrological risk associated to maximum flow in small hydrological subbasins with torrential character of the river Bahlui. *Present Environ. Sustain. Dev.* **2011**, *5*, 255–266.

17. Tutunaru, I.D.; Blindaru, T.; Pricop, I.C. The assessment of the cultural heritage's vulnerability to flash floods in Bahlui river basin, Iasi County. *Eur. J. Sci. Theol.* **2013**, *9*, 233–242.
18. Crenganiş, L.M.; Telişcă, M. GIS application in water resources management and environmental engineering. *Glob. J. Adv. Pure Appl. Sci. [Online]* **2013**, *1*, 657–664.
19. Boers, P.; Lammens, E.; Perjoiu, M.; Clipa, H.; Coman, I. *Nutrients and Silt in the Bahlui River System*; National Administration "Apele Romane": Bucharest, Romania, 2006.
20. Rotaru, A.; Raileanu, P. Alunecarea de teren de la Pârcovaci, Judetul Iasi [Pârcovaci landslide, Iasi County]. In Proceedings of the International PIARC Seminar on "Managing Operational Risk on Roads", Iaşi, Romania, 5–7 November 2009.
21. Giurma, I.; Craciun, I.; Giurma, C.-R. The analysis of the impact of storage lake on environment using the chemical characterization of the water resources. Case study Bahlui Basin River. *"Ovidius" Univ. Ann. Constantza. Ser. Civ. Eng.* **2007**, *1*, 119.
22. Ludikhuize, D.; Savin, A.; Schropp, M. *A Sobek Model for the Bahlui River*; National Administration "Apele Romane": Iasi, Romania, 2004.
23. Nicu, I.C. Hydrography. In *Hydrogeomorphic Risk Analysis Affecting Chalcolithic Archaeological Sites from Valea Oii (Bahlui) Watershed, Northeastern Romania: An Interdisciplinary Approach*; Springer International Publishing: Cham, Switzerland, 2016; pp. 19–29.
24. Schropp, M.; Savin, A. *Reducing the Flood Frequency for the City of Iaşi*; National Administration "Apele Romane": Arnhem, The Netherlands; Iaşi, Romania, 2003.
25. Bălinișteanu, O. *Iașiul anului 1932, un oraș calamitat*; Ziarul Lumina: Bucharest, Romania, 2019.
26. Minea, I. The evaluation of the water chemistry and quality for the lakes from the south of the Hilly Plain of Jijia (Bahlui drainage basin). *Lakes Reserv. Ponds* **2010**, *4*, 131–144.
27. Albulescu, A.-C.; Minea, I.; Boicu, D.; Larion, D. Comparative Multi-Criteria Assessment of Hydrological Vulnerability—Case Study: Drainage Basins in the Northeast Region of Romania. *Water* **2022**, *14*, 1302. [CrossRef]
28. Połomski, M.; Wiatkowski, M. Impounding Reservoirs, Benefits and Risks: A Review of Environmental and Technical Aspects of Construction and Operation. *Sustainability* **2023**, *15*, 16020. [CrossRef]
29. Langat, P.K.; Kumar, L.; Koech, R. Identification of the Most Suitable Probability Distribution Models for Maximum, Minimum, and Mean Streamflow. *Water* **2019**, *11*, 734. [CrossRef]
30. Prezentare Generala. Available online: https://comunabelcesti.ro/despre-comuna/prezentare-generala/ (accessed on 3 April 2024).
31. Dughilă, A.; Iancu, O.G.; Râșcanu, I.D. Geochemical evaluation of quality indicators for the water of the Tansa Lake from the Jijia catchment, Romania. *Carpathian J. Earth Environ. Sci.* **2012**, *7*, 79–88.
32. Minea, I. Minimum discharge in Bahlui basin and associated hydrologic risks. *Aerul Si Apa. Compon. Ale Mediu.* **2010**, 508. Available online: https://www.proquest.com/scholarly-journals/minimum-discharge-bahlui-basin-associated/docview/1335068855/se-2 (accessed on 3 April 2024).
33. Breabăn, I.G.; Stan, O.C. The Influence of the Anthropogenic Activities on the Bahlui Water Quality, Holboca Section (Iassy county). *Seminarul Geografic "D. Cantemir"* **2006**, *26*, 169–179.
34. Tutunaru, D.-I.; Pricop, C.-I.; Crăciun, I.; Blidaru, T.-V.; Crăciun, E.; Timofte, M.-C. Assessment of the impact and type of drought recorded in 2012 in the lower basin of the river Jijia. *Lucr. Semin. Geogr. "Dimitrie Cantemir"* **2013**, *35*, 5–16.
35. Bissolli, P.; Friedrich, K.; Rapp, J.; Ziese, M. *Flooding in eastern central Europe in May* 2010—Reasons, evolution and climatological assessment. *Weather* **2011**, *66*, 147–153. [CrossRef]
36. Ionita, M.; Nagavciuc, V. Extreme Floods in the Eastern Part of Europe: Large-Scale Drivers and Associated Impacts. *Water* **2021**, *13*, 1122. [CrossRef]
37. Romanescu, G.; Stoleriu, C.C. Exceptional floods in the Prut basin, Romania, in the context of heavy rains in the summer of 2010. *Nat. Hazards Earth Syst. Sci.* **2017**, *17*, 381–396. [CrossRef]
38. Blaas, H.; Kroeze, C. *Excessive nitrogen and phosphorus in European rivers:* 2000–2050. *Ecol. Indic.* **2016**, *67*, 328–337. [CrossRef]
39. Guignard, M.S.; Leitch, A.R.; Acquisti, C.; Eizaguirre, C.; Elser, J.J.; Hessen, D.O.; Jeyasingh, P.D.; Neiman, M.; Richardson, A.E.; Soltis, P.S.; et al. Impacts of Nitrogen and Phosphorus: From Genomes to Natural Ecosystems and Agriculture. *Front. Ecol. Evol.* **2017**, *5*, 70. [CrossRef]
40. Hobbie, S.E.; Finlay, J.C.; Janke, B.D.; Nidzgorski, D.A.; Millet, D.B.; Baker, L.A. Contrasting nitrogen and phosphorus budgets in urban watersheds and implications for managing urban water pollution. *Proc. Natl. Acad. Sci. USA* **2017**, *114*, 4177–4182. [CrossRef] [PubMed]
41. Müller, A.; Österlund, H.; Marsalek, J.; Viklander, M. The pollution conveyed by urban runoff: A review of sources. *Sci. Total Environ.* **2020**, *709*, 136125. [CrossRef]
42. *Normative of February 28, 2002 Regarding the Establishment of Limits of Pollutant Loading of Industrial and Urban Wastewater at Discharge into Natural Receptors*; NTPA-001/2002 Published in the Official Gazette, Part I nr. 187 of 20 March 2002; Romanian Government Decision: Bucharest, Romania, 2002.
43. Lloyd, C.E.M.; Freer, J.E.; Johnes, P.J.; Coxon, G.; Collins, A.L. Discharge and nutrient uncertainty: Implications for nutrient flux estimation in small streams. *Hydrol. Process.* **2016**, *30*, 135–152. [CrossRef]
44. Stoleriu, A.F.; Breaban, I.G.; Stoleriu, A.P. Assessing Water Quality from Tansa Barrier Lake (Romania) Using Sentinel-2 Data. *Int. Multidiscip. Sci. GeoConf. SGEM* **2021**, *21*, 247–254.

45. Rakovec, O.; Samaniego, L.; Hari, V.; Markonis, Y.; Moravec, V.; Thober, S.; Hanel, M.; Kumar, R. *The* 2018–2020 Multi-Year Drought Sets a New Benchmark in Europe. *Earth's Future* **2022**, *10*, e2021EF002394. [CrossRef]
46. Mouri, G.; Takizawa, S.; Oki, T. Spatial and temporal variation in nutrient parameters in stream water in a rural-urban catchment, Shikoku, Japan: Effects of land cover and human impact. *J. Environ. Manag.* **2011**, *92*, 1837–1848. [CrossRef]
47. Yang, F.; Yu, Z.; Bouwman, A.F.; Chen, H.; Jian, H.; Beusen, A.H.W.; Liu, X.; Yao, Q. Human-driven long-term disconnect of nutrient inputs to the Yellow River basin and river export to the Bohai Sea. *J. Hydrol.* **2023**, *618*, 129279. [CrossRef]
48. Batalla, R.J.; Gómez, C.M.; Kondolf, G.M. Reservoir-induced hydrological changes in the Ebro River basin (NE Spain). *J. Hydrol.* **2004**, *290*, 117–136. [CrossRef]
49. Fisher, J.; Acreman, M.C. Wetland nutrient removal: A review of the evidence. *Hydrol. Earth Syst. Sci.* **2004**, *8*, 673–685. [CrossRef]
50. Jiang, B.; Mitsch, W.J. Influence of hydrologic conditions on nutrient retention, and soil and plant development in a former central Ohio swamp: A wetlaculture mesocosm experiment. *Ecol. Eng.* **2020**, *157*, 105969. [CrossRef]
51. Halecki, W.; Stachura, T.; Fudała, W. Capacity of River Valleys to Retain Nutrients from Surface Runoff in Urban and Rural Areas (Southern Poland). *Water* **2022**, *14*, 3259. [CrossRef]
52. Mallin, M.A.; Johnson, V.L.; Ensign, S.H. Comparative impacts of stormwater runoff on water quality of an urban, a suburban, and a rural stream. *Environ. Monit. Assess.* **2009**, *159*, 475–491. [CrossRef]
53. Khatri, N.; Tyagi, S. Influences of natural and anthropogenic factors on surface and groundwater quality in rural and urban areas. *Front. Life Sci.* **2015**, *8*, 23–39. [CrossRef]
54. Oişte, A.M.; Breabăn, I.G. Organic and Inorganic contaminants in the Bahlui River in the built-up area of Iasi city. In Proceedings of the Water Resources and Wetlands, Tulcea, Romania, 14–16 September 2012.
55. Minea, I.; Sfîcă, L. Assessment of hydrological drought in the north-eastern part of Romania. *Aerul Si Apa. Compon. Ale Mediu.* **2017**, 93–100. Available online: https://scholar.google.com/scholar?hl=en&as_sdt=0,5&q=Assessment+of+hydrological+drought+in+the+north-eastern+part+of+Romania&btnG= (accessed on 3 April 2024).
56. Moldovan, A.C.; Hrăniciuc, T.A.; Micle, V.; Marcoie, N. Research on the Sustainable Development of the Bistrita Ardeleana River in Order to Stop the Erosion of the Riverbanks and the Thalweg. *Sustainability* **2023**, *15*, 7431. [CrossRef]
57. Udeigwe, T.K.; Wang, J.J. Biochemical Oxygen Demand Relationships in Typical Agricultural Effluents. *Water Air Soil Pollut.* **2010**, *213*, 237–249. [CrossRef]
58. Soro, M.-P.; N'Goran, K.M.; Ouattara, A.A.; Yao, K.M.; Kouassi, N.G.L.B.; Diaco, T. Nitrogen and phosphorus spatio-temporal distribution and fluxes intensifying eutrophication in three tropical rivers of Côte d'Ivoire (West Africa). *Mar. Pollut. Bull.* **2023**, *186*, 114391. [CrossRef] [PubMed]
59. Mbaye, M.L.; Gaye, A.T.; Spitzy, A.; Dähnke, K.; Afouda, A.; Gaye, B. Seasonal and spatial variation in suspended matter, organic carbon, nitrogen, and nutrient concentrations of the Senegal River in West Africa. *Limnologica* **2016**, *57*, 1–13. [CrossRef]
60. Mararakanye, N.; Le Roux, J.J.; Franke, A.C. Long-term water quality assessments under changing land use in a large semi-arid catchment in South Africa. *Sci. Total Environ.* **2022**, *818*, 151670. [CrossRef] [PubMed]
61. Dalu, T.; Wasserman, R.J.; Magoro, M.L.; Froneman, P.W.; Weyl, O.L.F. River nutrient water and sediment measurements inform on nutrient retention, with implications for eutrophication. *Sci. Total Environ.* **2019**, *684*, 296–302. [CrossRef]
62. Green, W.J.; Stage, B.R.; Preston, A.; Wagers, S.; Shacat, J.; Newell, S. Geochemical processes in the Onyx River, Wright Valley, Antarctica: Major ions, nutrients, trace metals. *Geochim. Cosmochim. Acta* **2005**, *69*, 839–850. [CrossRef]
63. Kim, D.; Lim, J.-H.; Chun, Y.; Nayna, O.K.; Begum, M.S.; Park, J.-H. Phytoplankton nutrient use and CO2 dynamics responding to long-term changes in riverine N and P availability. *Water Res.* **2021**, *203*, 117510. [CrossRef] [PubMed]
64. Nguyen, T.T.N.; Némery, J.; Gratiot, N.; Strady, E.; Tran, V.Q.; Nguyen, A.T.; Aimé, J.; Peyne, A. Nutrient dynamics and eutrophication assessment in the tropical river system of Saigon – Dongnai (southern Vietnam). *Sci. Total Environ.* **2019**, *653*, 370–383. [CrossRef] [PubMed]
65. Yang, H.F.; Zhu, Q.Y.; Liu, J.A.; Zhang, Z.L.; Yang, S.L.; Shi, B.W.; Zhang, W.X.; Wang, Y.P. Historic changes in nutrient fluxes from the Yangtze River to the sea: Recent response to catchment regulation and potential linkage to maritime red tides. *J. Hydrol.* **2023**, *617*, 129024. [CrossRef]
66. Ravi, N.K.; Srivastava, A.; Ram, K.; Jha, P.K. Nutrient chemistry and eutrophication risk assessment of the Ghaghara river, India. *Water Supply* **2021**, *21*, 3486–3502. [CrossRef]
67. Salim Aoubid, H.; Opp, C. Nitrogen and Phosphorus Discharge Loads Assessment Using the SWAT Model: A Case Study of the Shatt Al-Arab River Basin. *Appl. Sci.* **2023**, *13*, 8376. [CrossRef]
68. Mosley, L.M.; Priestley, S.; Brookes, J.; Dittmann, S.; Farkaš, J.; Farrell, M.; Ferguson, A.J.; Gibbs, M.; Hipsey, M.; Huang, J.; et al. Extreme eutrophication and salinisation in the Coorong estuarine-lagoon ecosystem of Australia's largest river basin (Murray-Darling). *Mar. Pollut. Bull.* **2023**, *188*, 114648. [CrossRef] [PubMed]
69. Johnston, S.G.; Maher, D.T. Drought, megafires and flood - climate extreme impacts on catchment-scale river water quality on Australia's east coast. *Water Res.* **2022**, *218*, 118510. [CrossRef] [PubMed]
70. Tenebe, I.T.; Julian, J.P.; Emenike, P.C.; Dede-Bamfo, N.; Maxwell, O.; Sanni, S.E.; Babatunde, E.O.; Alves, D.D. Multi-Dimensional Surface Water Quality Analyses in the Manawatu River Catchment, New Zealand. *Water* **2023**, *15*, 2939. [CrossRef]
71. Jarosiewicz, A.; Obolewski, K.; Ożgo, M. Long-term trends in nutrient concentrations in Polish coastal rivers. *Ocean Coast. Manag.* **2015**, *118*, 37–46. [CrossRef]

72. Garnier, J.; Némery, J.; Billen, G.; Théry, S. Nutrient dynamics and control of eutrophication in the Marne River system: Modelling the role of exchangeable phosphorus. *J. Hydrol.* **2005**, *304*, 397–412. [CrossRef]
73. Soana, E.; Gervasio, M.P.; Granata, T.; Colombo, D.; Castaldelli, G. Climate change impacts on eutrophication in the Po River (Italy): Temperature-mediated reduction in nitrogen export but no effect on phosphorus. *J. Environ. Sci.* **2024**, *143*, 148–163. [CrossRef]
74. Yin, S.; Gao, G.; Li, Y.; Xu, Y.J.; Turner, R.E.; Ran, L.; Wang, X.; Fu, B. Long-term trends of streamflow, sediment load and nutrient fluxes from the Mississippi River Basin: Impacts of climate change and human activities. *J. Hydrol.* **2023**, *616*, 128822. [CrossRef]
75. Rattan, K.J.; Corriveau, J.C.; Brua, R.B.; Culp, J.M.; Yates, A.G.; Chambers, P.A. Quantifying seasonal variation in total phosphorus and nitrogen from prairie streams in the Red River Basin, Manitoba Canada. *Sci. Total Environ.* **2017**, *575*, 649–659. [CrossRef] [PubMed]
76. Castillo, M.M.; Carrillo, L.; Jarquín-Sánchez, A.; Alcérreca-Huerta, J.C.; Álvarez-Merino, A.; Lázaro-Vázquez, A. Transport of nutrients into the southern Gulf of Mexico by the Grijalva–Usumacinta rivers. *Hydrol. Process.* **2023**, *37*, e14838. [CrossRef]
77. Pacheco, F.S.; Ometto, J.P.H.B.; Gomes, L.; Tôsto, K.; Miranda, M.; Loverde-Oliveira, S.; Pessi, D.D.; Cox, C. Nutrient Balance and Use Efficiency in Agricultural Lands in the Vermelho River Watershed, Upper Pantanal, Brazil. *J. Geophys. Res. Biogeosci.* **2021**, *126*, e2020JG005673. [CrossRef]
78. Perillo, V.L.; Bohn, V.Y.; Menéndez, M.C.; Ronda, A.C.; Vitale, A.J.; Perillo, G.M.E.; Piccolo, M.C.; Cuadrado, D.G. Spatial and seasonal dynamics of phosphorous and physicochemical variables in the Negro River Estuary (Argentina): A preliminary approach. *Environ. Sci. Pollut. Res.* **2022**, *29*, 15490–15500. [CrossRef]
79. Pizarro, J.; Vergara, P.M.; Rodríguez, J.A.; Sanhueza, P.A.; Castro, S.A. Nutrients dynamics in the main river basins of the centre-southern region of Chile. *J. Hazard. Mater.* **2010**, *175*, 608–613. [CrossRef] [PubMed]

sustainability

MDPI

Article

Research on the Sustainable Development of the Bistrita Ardeleana River in Order to Stop the Erosion of the Riverbanks and the Thalweg

Aurelian Cosmin Moldovan [1,*], Tomi Alexandrel Hrăniciuc [2], Valer Micle [1,*] and Nicolae Marcoie [2]

[1] Faculty of Materials and Environmental Engineering, Department of Environment Engineering and Entrepreneurship of Sustainable Development, Technical University of Cluj-Napoca, 103-105 Muncii Blvd., 400641 Cluj-Napoca, Romania
[2] Faculty of Hydrotechnics, Geodesy and Environmental Engineering, "Gheorghe Asachi" Technical University of Iasi, Dimitrie Mangeron Blvd. nr. 65, 70050 Iasi, Romania; tomi-alexandrel.hraniciuc@academic.tuiasi.ro (T.A.H.); nicolae.marcoie@academic.tuiasi.ro (N.M.)
* Correspondence: cosminaurelianmoldovan@yahoo.com (A.C.M.); valer.micle@imadd.utcluj.ro (V.M.)

Abstract: The impact of dams and reservoirs on the aquatic ecosystem of rivers is a very important topic for water resource management. These hydrotechnical facilities change the natural hydro-morphological regime of the rivers. This paper analyzed the hydrodynamic characteristics of an undeveloped riverbed section downstream of the Colibița reservoir, from the Bistrita Ardeleana River hydrographic basin. After processing the data obtained on the field, two hydraulic models were made using the MIKE 11 program, which aimed to identify the hydraulic parameters such as the wet section, the depth, and the water velocity. The first modeling was used for the flow rate of Q = 54.5 m^3/s: the water depth was between 1.952 m and 2.559 m; and the water velocity varied between 1.148 m/s and 1.849 m/s. The second modeling was used for a flow rate of Q = 178 m^3/s and showed that the water depth had values between 3.701 m and 4.427 m; and the water velocity varied between 1.316 m/s and 2.223 m/s. Following the granulometric analysis, the average diameter of the particle in the thalweg was D50 = 25.18 mm. The conclusion reached as a result of hydraulic modeling and granulometric analyses indicated that hydromorphological processes take place along the length of the analyzed sector, which have negative effects on water quality as well as on the instability of the riverbed. To make the riverbed safe along the entire studied length, we managed to identify some alternative solutions that have the role of stabilizing the banks, respectively, to stop the deepening of the thalweg. The alternative hydrotechnical constructions will increase the roughness of the riverbed, essentially reducing the water speed and increasing the favorable conditions for the retention of alluvium.

Keywords: rivers; dams; sustainable development; the morphology of rivers; green methods; hydraulic modeling

Citation: Moldovan, A.C.; Hrăniciuc, T.A.; Micle, V.; Marcoie, N. Research on the Sustainable Development of the Bistrita Ardeleana River in Order to Stop the Erosion of the Riverbanks and the Thalweg. *Sustainability* **2023**, *15*, 7431. https://doi.org/10.3390/su15097431

Academic Editors: Carina da Conceição Mendes de Almeida and Venkata Krishna Kumar Upadhyayula

Received: 21 March 2023
Revised: 21 April 2023
Accepted: 28 April 2023
Published: 30 April 2023

1. Introduction

Water made life possible on Earth; it represents a critical resource for humans and animals whenever human settlements develop. Climate change influences the water cycle in nature. Extreme weather events, such as droughts and heavy rainfall that increase in proportion to the extent of climate change, exert a negative impact on water resources. Water scarcity limits economic development in many regions of the world [1]. 71% of the Earth's surface is covered with water. The oceans (Atlantic, Arctic, Antarctic, Pacific, and Indian) represent 96.5% of Earth's water, 2.5% represents the total amount of fresh water, while the totality of the water in the hydrographic basins of the rivers represents 1% [1,2].

Rivers play a key role in providing drinking water to the population. They act as filters and provide a variety of habitats for a wide range of plants and animals. Globally,

only 37% of rivers longer than 1000 km remain free-flowing throughout their length, and 23% flow uninterruptedly to the ocean [3–5].

The quality of water in rivers depends on the integrity of water bodies and the quality of life in rivers. Human interventions that reduce the longitudinal connectivity of rivers and streams, which have increased in number, significantly affect the biodiversity of rivers and, implicitly, the quality of water [3].

When watercourses are degraded or ecologically damaged, many of the ecosystem services important to human society are lost. The high fragility of rivers crossing urban areas to anthropogenic disturbances leads to the restricted use of natural resources [6,7].

A degraded stream is defined as a river that does not function to its biological hydrological potential [8].

The alteration of the hydrological and morphological processes of the watercourses causes the deterioration of the habitats for the biota and disturbs the functionality of the ecosystem [4].

Human activities such as the construction of diversions, weirs, and dams represent a persistent threat to freshwater biodiversity [9] and exert a negative impact on rivers, implicitly on the functionality of aquatic ecosystems [10,11]. The impact of dams and reservoirs on the aquatic environment of rivers is an important topic in global water resources management. These hydrotechnical constructions change the natural hydromorphological regime of rivers, negatively affecting their functionality and are associated with several environmental impacts, such as habitat fragmentation, poor water quality, nutrient depletion, loss or modification of biodiversity, remodeling of trophic networks, ichthyofauna, reduction of riparian biodiversity the river [5,9–18]. Worldwide, the decline of river biodiversity has recently been linked to the reduced functionality of the riverbed substrate. The riverbed substrate (hyporheic zone) plays an important role in the life cycle of many aquatic species, therefore for aquatic biodiversity [19].

The impact of large dams is not only limited to direct effects on the hydromorphology of the aquatic or riverine ecosystem but also on downstream localities, which extend to ecological environments [16].

In most rivers around the world, varying degrees of sediment reduction have been observed due to transverse hydrotechnical constructions [15]. Transversal hydrotechnical constructions negatively affect natural aggregate transport, creating imbalances between hydromorphological processes and the storage process in the coastal area [3,20]. Structural degradation of rivers can lead to limited availability of alluvial material [19].

Hydromorphological changes to the river due to dams are substantially better understood in the downstream sections of the river than in the sections of the river upstream of accumulations, especially on mountain watercourses [5].

Rivers are under huge threat all over the world and huge amounts of money are being invested in restoring them [21]. The watercourse restoration, also called river recovery, represents a set of measures to bring back, as close as possible, the original state of the ecosystems along the entire length of a heavily anthropized water course [7]. In general, river restoration aims at hydromorphological and ecological changes that improve the natural state of aquatic and riparian ecosystems through a variety of restoration methods [18,21–23].

It is essential to distinguish between restoration projects designed to reconnect rivers and projects designed to reconfigure rivers. It is important to distinguish the differences between ecological restoration of the river that helps restore ecological integrity and restoration intended for other outcomes such as aesthetic or recreational enhancements that do not necessarily improve ecological functions [23].

The definition of watercourse restoration is not limited to structural engineering (stabilizing of riverbanks) but also opens ways to include other aspects of river restoration as part of river management [24].

In the last two decades, the revitalization of anthropogenic rivers has been established in Europe as a measure to achieve the good ecological status of water bodies, as required

by the EU Water Framework Directive (European Commission, 2000), while protecting the objectives downstream of floods. The implementation of the Water Framework Directive in ensuring sustainable water management has been implemented taking into account river basins [1,25,26]. These legislative efforts and necessary actions conclusively aim at increasing the heterogeneity of ecosystems. Worldwide, the number of restoration projects and the use of public financial resources to finance these projects has increased significantly and is expected to further increase [25].

Most countries currently promote projects that include alternative solutions with natural components and that have the role of incorporating the recreational activities etc. of human society [27]. Ecologically focused watercourse restoration projects may involve the use of alternative technical solutions that use local materials such as trees, boulders, shrubs, and timber for landscape development, flood mitigation, reducing hydromorphological processes, and increasing the chemical and biological quality of water and the variety of the biotope [7,28].

Alternative hydrotechnical constructions that have clear or gray-green elements are promoted and designed to: cope with high flows recorded during extreme floods or flash floods; create longitudinal and transversal connectivity of ecosystems in the riverbeds that cross human settlements [29–31].

Working with natural hydro-technical systems, which are powered by a diversity of life within them, provides a range of benefits to society, ranging from carbon storage, clean water and air, to the reduction of climate change impacts and protection against floods and other environmental hazards [32].

The concern within the European Union as well as at the global level regarding the sustainability of watercourses and the environment has encouraged the improvement and acceleration of the practices used in the recovery of water courses, but even so, specialists in the field of water management encounter problems in terms of promoting environmentally friendly or green infrastructure methods [11].

In order to restore or remake aquatic ecosystems, it would also be important to control the amount of water released from the reservoirs and to calculate the environmental flow, corresponding to most fish species. It is known that flow forecasting is one of the most difficult tasks for the owners in the management of water supply or energy production. Research on the flow required to conserve aquatic habitat began in the 1970s and has been commonly used for river management, including dam operation, water regulation, and hydrographic basin management [33,34].

In the present paper, we analyzed the hydrodynamic characteristics of a river bed sector located in the municipality of Bistrița are analyzed. Two flow rates recorded on the Bistrita Ardeleana water course at the Bistrita hydrometric station were used for the hydraulic modeling. The first flow rate used had a value of Q = 54.5 m^3/s and was recorded following heavy rainfall and water discharges from the Colibița reservoir. The second flow was Q = 178 m^3/s, being the highest flow in the last 15 years.

After performing the two simulations, it was possible to identify the values of the local hydraulic parameters for the analyzed sector. In order to be able to determine the instability of the riverbed due to hydromorphological processes, it was necessary to determine the size of the particles in the thalweg, this being done with the help of granulometric analysis.

The results obtained from hydraulic modeling and granulometric analyses indicate that hydromorphological processes take place along the length of the studied section, processes that have negative effects on water quality as well as on the objectives located in the immediate vicinity due to the instability of the riverbed.

In order to strengthen the riverbed along the entire studied length as well as to improve the water quality, we managed to identify some alternative solutions. These are used to withstand erosion speeds and have the role of stabilizing the riverbanks, respectively to reduce the water speeds, and to stop the deepening of the thalweg. The alternative hydrotechnical constructions will increase the roughness of the bed, implicitly reducing the water speed, and increasing the favorable conditions for the retention of alluvium.

2. Materials and Methods

2.1. Study Area

The hydrographic basin of the Bistrita Ardeleana River is located in the north-east of Transylvania, more precisely on the administrative territory of Bistrita–Nasaud county, geographically located in the central-northern area of Romania, between coordinates 46°45′–47°37′ north latitude and 23°27′–25°36′ east longitude.

The Bistrita Ardeleana River springs from the central group of the Eastern Carpathians (the Calimani Mountains) crosses the Livezi–Bargau Depression and before pouring into the Sieu River, it crosses the hills of Bistrita, a subunit of the Transylvanian Subcarpathian (Figure 1). The hills and the depression are made up of clayey, marly, tuff formations, trapped in a crease system. The catchment area of the river and its tributaries is 650 km^2, and its elevation varies between 350 m and 1990 m [11,35–38].

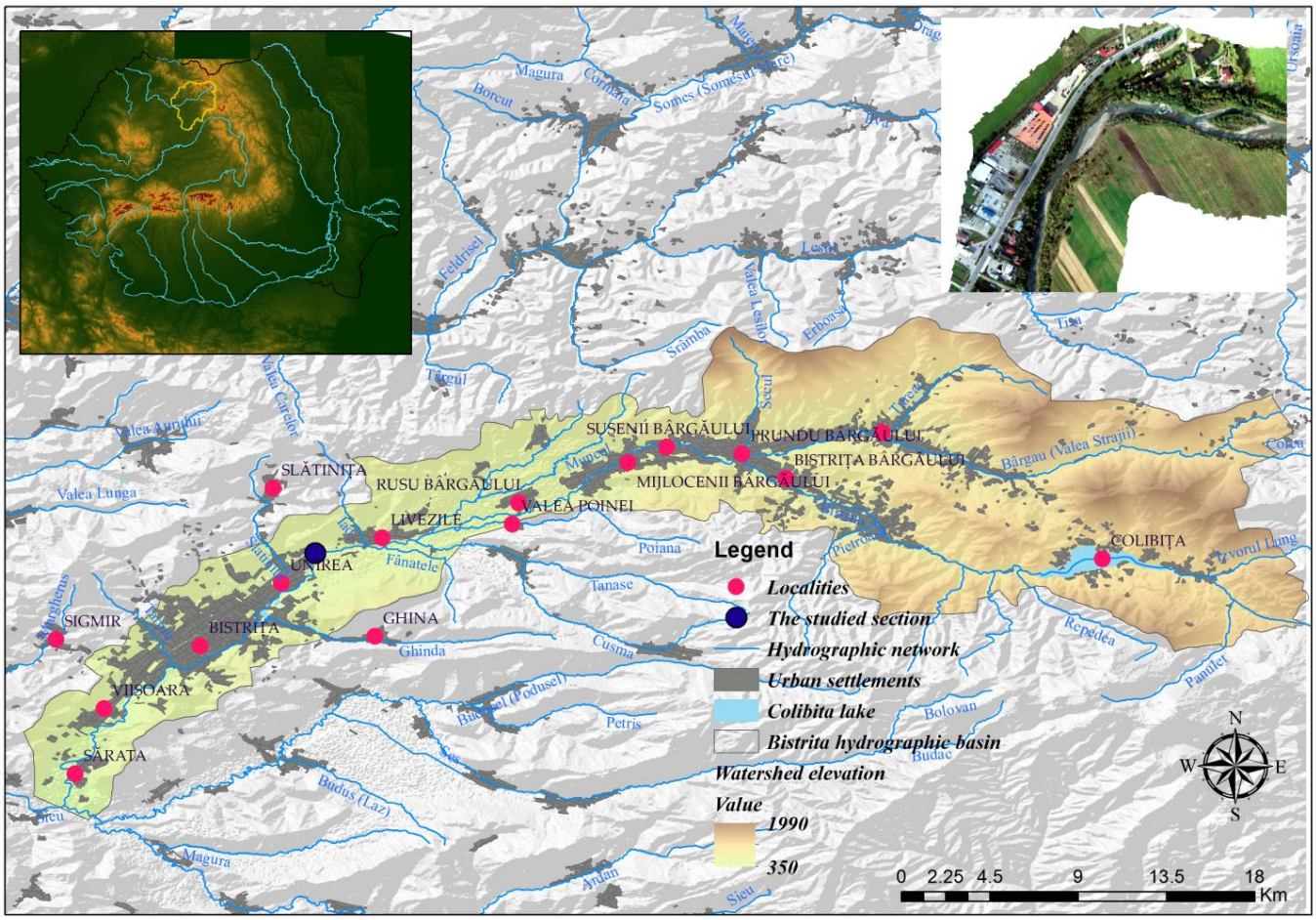

Figure 1. The location of the studied area in relation to the national territory and the hydrographic basin of the Bistrita Ardeleana River.

During winter, this area experiences a climate regime influenced by air currents of polar origin from the west. The transitional seasons (spring, autumn) are shorter compared to those in southern Romania, and the summers are warm and quite humid. The average annual air temperature is between 0 and 2 °C on the mountain peaks and 9.1 °C in the municipality of Bistrița. Atmospheric precipitation is particularly high, in the mountain area the average annual amounts are between 850 and 1400 mm [39].

2.2. Methods Used

In the present paper, RTK measurements were made for the area under study with the help of the Leica GS14 GNSS GPS and the Leica CS10 controller, being of high accuracy, and

thanks to the differential precision corrections transmitted by the permanent stations in the ROMPOS network. The topographical measurements were made upstream to downstream. After carrying out the measurements on the riverbed of the Bistrita River, along the length of the analyzed sector, the procedure of data processing followed, this being carried out in the AutoCAD 2023 software. The profiles formed by the points from the measurements were imported, after which the drawing of the characteristic lines was followed. Phantom 4 Pro drone flights were conducted to obtain an updated orthophotoplan and a more realistic image of the section of the watercourse studied in this paper (Figure 2). A sample of alluvial material was taken from the thalweg of the riverbed for granulometric analysis. Sampling of natural aggregates was carried out from the area considered representative of the entire analyzed sector. The surface considered representative is located between transversal profile 5 and transversal profile 6. The sample of alluvial material was taken to demonstrate that on the analyzed river bank section, thalweg erosions occur at certain flow rates. The processing of the alluvial material was carried out with the electromagnetic sieving machine model A 059-3.

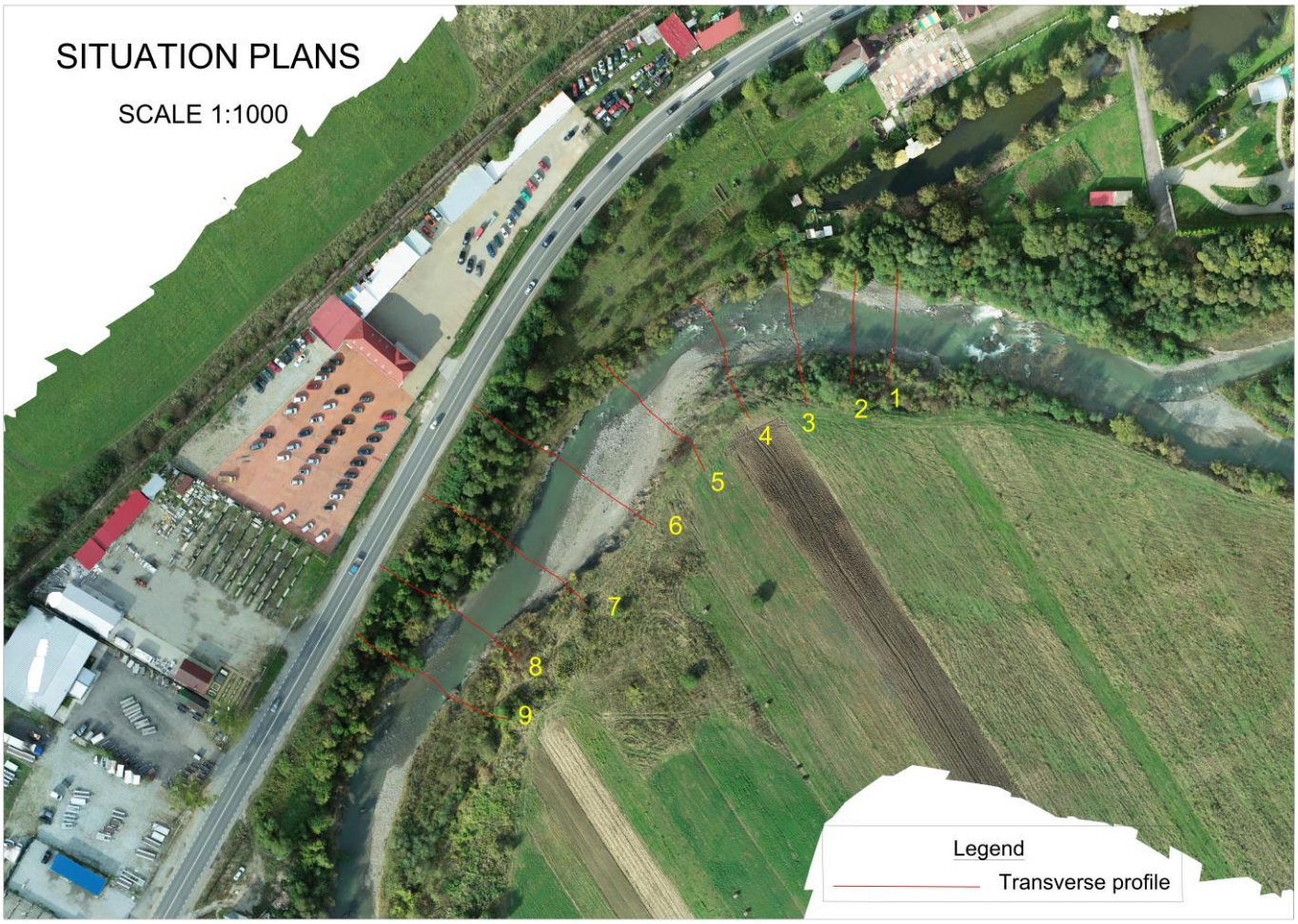

Figure 2. The hydraulic network and the position of the cross sections are plotted in the orthophotoplan.

The processing of the images captured with the professional drone was carried out with the Agisoft Metashape program. In order to achieve correct georeferencing, GCPs (Ground Control Points) were used [40]. For the georeferencing of the images, three GCPs (Ground Control Points) were used, being raised in the field with the Rover GNSS South Galaxy G1 equipment. Thanks to the images captured by the drone, a cloud of topographical points was obtained, after which the studied sector was represented in 3D format (Figure 3).

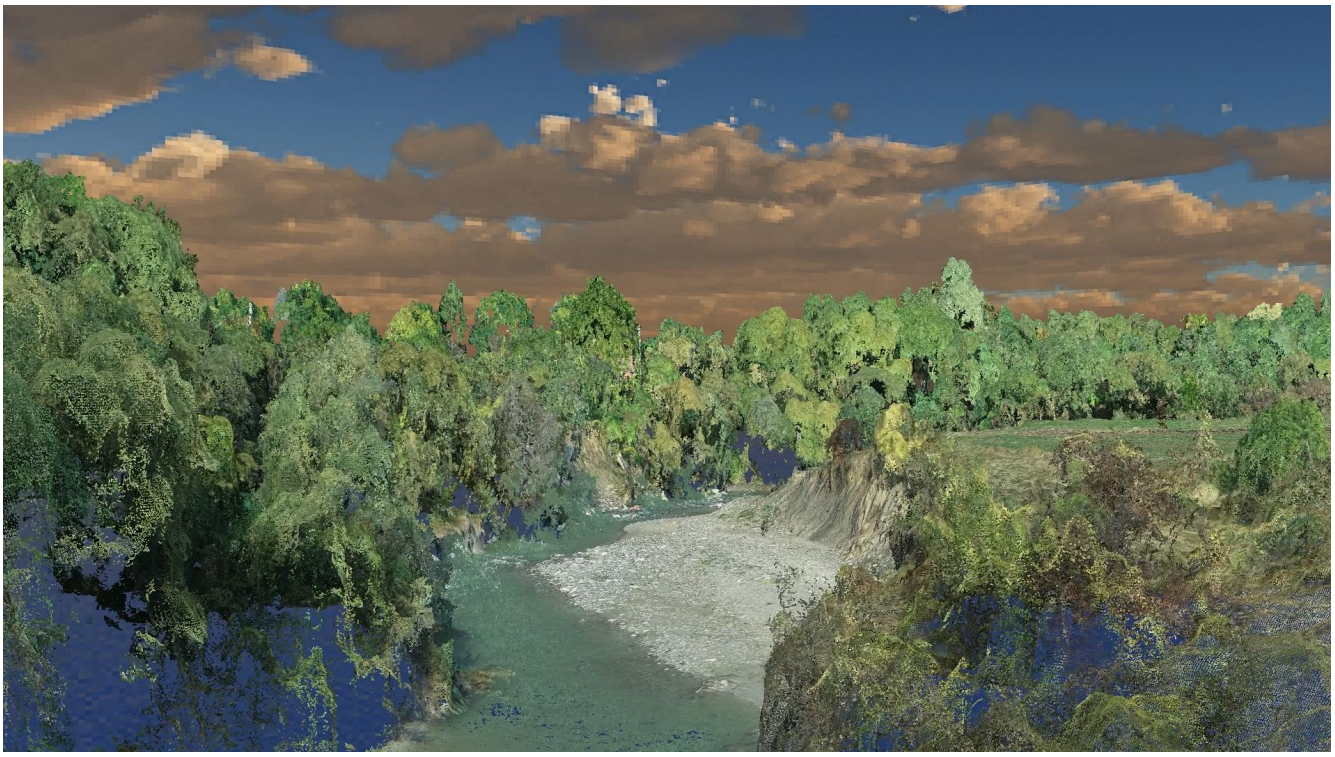

Figure 3. The 3D image of the studied sector, made with the help of point clouds obtained from professional drone measurements.

Based on the data obtained from the field, hydraulic modeling was carried out for a constant flow, which has a permanent and non-uniform movement. The purpose of this modeling was to identify the hydraulic parameters such as the wet section and the depth and the velocity of the water, which vary spatially, more precisely along the stream.

In order to be sure of the need to promote hydraulic constructions with environmentally friendly materials, two hydraulic models were made. The length of the sector analyzed in hydraulic modeling is 198 m.

MIKE 11 software was used for hydraulic modeling; this is an engineering software capable of simulating water speed, water level, flow, sediment transport, etc. [41]. Saint-Venant mathematical equations were used to perform hydraulic simulations in the one-dimensional system.

In the one-dimensional system, they are as follows:

The continuity Equation (1) is

$$\frac{\partial Q}{\partial x} + b_S \frac{\partial h}{\partial t} = q \tag{1}$$

The momentum Equation (2) is

$$\frac{\partial Q}{\partial t} + \frac{\partial \left(\alpha \frac{Q^2}{A}\right)}{\partial x} + gA\frac{\partial h}{\partial x} = 0 \tag{2}$$

where x is the longitudinal distance along the channel (m), h is the flow depth, t is the time (s), A is the cross-sectional area of flow (m^2), B is the width of the channel (m), Q is the integrated discharge (m^3/s), α the vertical velocity distribution coefficient, g is the acceleration of the gravity (m/s^2), and q leads to the basic equations used in MIKE 11 into these equations [41]:

$$\frac{\partial Q}{\partial x} + \frac{\partial A}{\partial t} = q \tag{3}$$

Two hydraulic models were made for two flows recorded in the hydrographic basin of the Bistrița Ardeleana River:

Q = 54.5 m^3/s represents the flow recorded following the heavy rainfall recorded in the hydrographic basin of the Bistrița Ardelena River in September 2022, this flow also being influenced by the controlled water discharges from the Colibița reservoir;

- Q = 178 m^3/s represents a flow recorded at the Bistrita hydrometric station in 2019, this being the highest flow recorded in the last 15 years [42].

The simulations being in the one-dimensional system, the obtained results were represented graphically in the MIKE View program.

Following the interpretation of the results, we managed to identify alternative solutions or methods (environmentally friendly) that will contribute to the restoration of the water course.

ArcGIS 10.6 software was used to cartographically represent the critical sector, and the graphic representation of the identified green alternative methods was made using AutoCAD Map 3D 2023 software.

What would the alternative methods of restoration or restoring the watercourse of the studied section consist of?

The bioengineering methods used in hydrotechnical constructions with the role of defense or protection of the riverbanks and stopping the degradation of the thalweg are as follows:

- live fascines or branches;
- boulder revetment;
- vegetated rock gabions;
- crib wall;
- live stakes;
- vegetated rock rolls;
- coir rolls;
- shrubs;
- root wad;
- mats reinforced with grass.

All the methods listed above will reduce the negative effects of variations in flows and levels due to natural floods or resulting from the production of electricity on the riverbanks as well as on the thalweg in the studied sector (Figure 4).

Hydrotechnical constructions are needed to stop erosions and reduce the degradation of the thalweg on both banks of the river. The green hydro-technical constructions with the role of protecting the banks and stopping the degradation of the thalweg have the following lengths:

- right bank—217.5 m;
- left bank—149.5 m.

The hydrotechnical constructions proposed for the studied sector start on the right bank. The proposed solution for the right bank of the Bistrita Ardeleana River has the role of stopping the erosion of the bank and reducing the degradation of the thalweg.

The works will start upstream to downstream and will start with the vegetated rock gabions on a length of 46 m, being placed on a bed of live fascines or branches. Downstream of the vegetated rock gabions for a length of 88 m, work will be done to divert the watercourse with the help of 18 root wad of the following species: wicker (Salix fragilis), willow (Salix cinerea), or white willow (Salix alba).

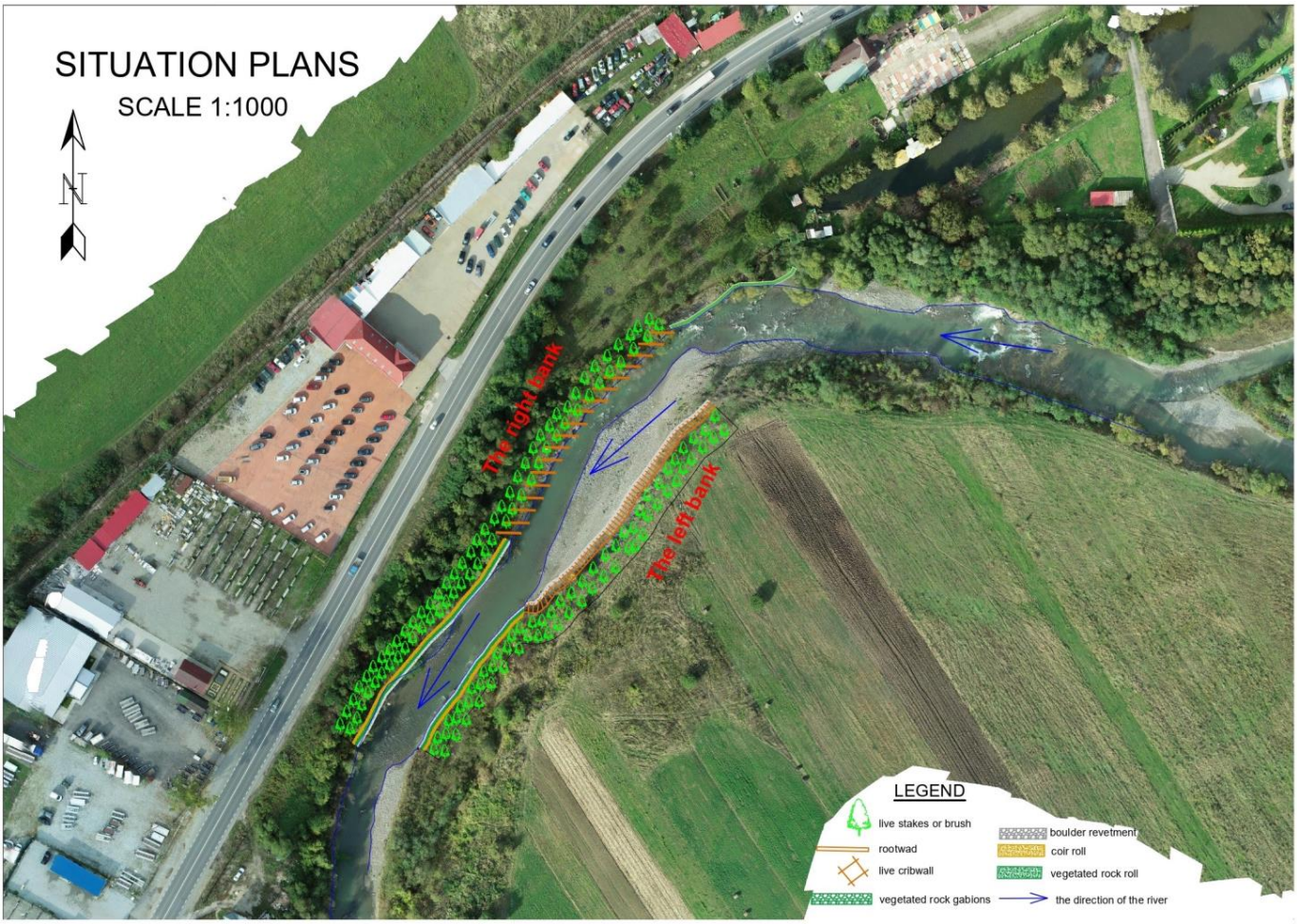

Figure 4. Graphical representation of the identified alternative methods.

The distance between trees should be 3 times the diameter of the roots. Trunks can be between 2 m and 3 m long with a diameter between 30 cm and 60 cm. They need to be placed or positioned in such a way that they will interpolate the direction of the river flow [32,43]. After the root wads are installed in the trenches, they will be covered with boulders, gravel, and soil to anchor them [32]. In order to control erosion due to meteoric water, mats reinforced with grass will be installed (Figure 5).

A third component of the hydrotechnical construction on the right bank for a length of 55.5 m consists of the following: reprofiling the bank and the installation of two rollers. One is a vegetated rock roll and the second one will be a coir roll, both anchored with the help of stakes, so that at the end they are covered with earth mixed with gravel.

Along the entire length of the hydrotechnical construction proposed for the right bank, live stakes or shrubs can be planted, so that they can increase the effectiveness of the construction in the long term.

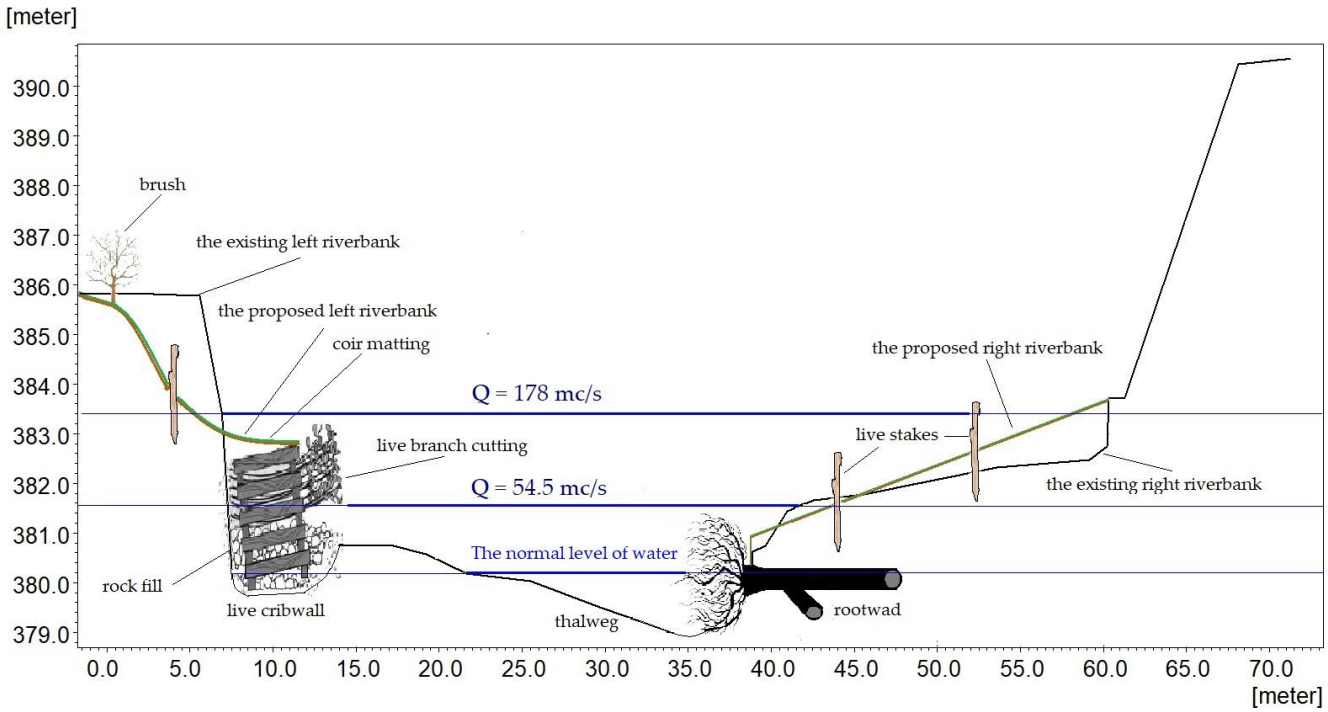

Figure 5. Graphical representation of green methods for both banks of the river in cross-section P6.

As for the methods or solutions proposed for the left bank, they will start like the works on the right bank, from upstream to downstream.

Given the height of the eroded bank (between 3.38 m and 4.97 m) which has an almost vertical slope, one solution is to defend the bank with crib walls with living material plus reprofiling the riverbank to have greater stability.

In fact, the hydrotechnical construction on this bank will include several environmentally friendly methods such as live fascines or branches, boulder revetment, crib wall, vegetated rock rolls, coir rolls, mats reinforced with grass, and planting live stakes or shrubs.

The crib walls with living material will be installed over a length of 94 m. These are box-shaped constructions made of soft wood, logs with a diameter between 20 cm and 40 cm, or square timber filled with local material [44–46].

When the works begin, a trench of 2 m width and 0.5–1 m depth will be made. The ditch must be made outwards because the crib walls are located in steps facing the water course. To provide stability to the crib walls, they will be secured at the corners by pillars driven into the ground. On the side facing the watercourse of the trench, bundles of live fascines will be placed from place to place. Later, a boulder revetment will be arranged along the entire length of the trench. Additionally, along the ditch, logs or square timber will be placed parallel at a distance of 1.5 m. On top of them along the entire length of the trench, logs or square timber with a length of 2 m each will be placed transversely, these being fixed at a distance of 1.5 m between them. This process will be repeated two or three times, the formed cell will be filled with soil mixed with stone with a diameter of 10 cm. The next step is to form a layer of fascines cut to a length of 2 m, placed with the cut towards the bank, these being covered with a layer of a mixture consisting of stone and soil. The process will be repeated with the laying of the logs longitudinally and transversely and that of forming the fascine bed. Both processes will continue until a height of 2 m is reached (Figure 5) [43,44].

After the completion of the crib walls downstream of them, the installation of vegetated rock rolls will continue for a length of 55.5 m, respectively coir rolls. At the end, mats reinforced with grass will be mounted and live stakes or shrubs will be planted along the entire length of the hydrotechnical construction proposed for the left bank.

The last necessary step after the completion of the hydrotechnical constructions would be the installation of a fence to restrict the access of animals and citizens to the water.

3. Results

The results will be presented first for the flow rate Q = 54.5 m^3/s and then for the flow rate Q = 178 m^3/s. In both variants, an initial water depth of 0.3 m was taken into account for the modeled river sector.

Table 1 shows the mileage of the cross-sections used in the hydraulic simulations to obtain the values of the local parameters. The graphic representation of the transverse profile 6 is used to represent the maximum water level for the two analyzed situations.

Table 1. The mileage of the transversal sections made in the studied sector.

Section	Kilometre (m)
P1	0.0
P2	13.41
P3	33.28
P4	56.53
P5	89.70
P6	119.62
P7	150.79
P8	176.19
P9	198

Considering the above, the hydraulic simulations were carried out for two situations in which the flow rates had the values of Q = 54.5 m^3/s recorded following heavy rainfall, this being also influenced by the controlled water discharges from the Colibița reservoir and Q = 178 m^3/s representing a flow recorded at the Bistrita hydrometric station in 2019, this being the highest flow recorded in the last 15 years [42].

In the graphs presented below for both analyzed hydraulic models, the lines have the following meanings:

- the continuous black line positioned in the upper part of the graph represents the upper elevation of the right bank of the river from P 1 upstream to P 9 downstream;
- the dotted black line represents the upper level of the left bank of the river from P 1 upstream to P 9 downstream;
- the blue contour represents the water level in the longitudinal profile;
- the dotted line inside the blue contour represents the minimum water level for the hydraulic models, the minimum depth of 0.3 m from which the modeling started;
- the lower continuous black line that supports the water level represents the river valley;
- the continuous blue line indicates the maximum water level in the cross-section;
- the broken green line indicates the minimum level in the model, more precisely the minimum depth of 0.3 m taken into account along the entire length of the river sector;
- the continuous and thick red line represents the water speed in the longitudinal profile;
- the dotted red line indicates the initial speed of the water at the very beginning of the modeling until the water fills the bed up to the maximum level corresponding to the studied flow rate.

3.1. Hydraulic Modeling on the River Bistrita Ardeleana, Where the Flow Has a Value of Q = 54.5 m^3/s

In Figure 6 we can see the water level in the longitudinal profile of the river sector taken into account for the flow rate Q = 54.5 m^3/s.

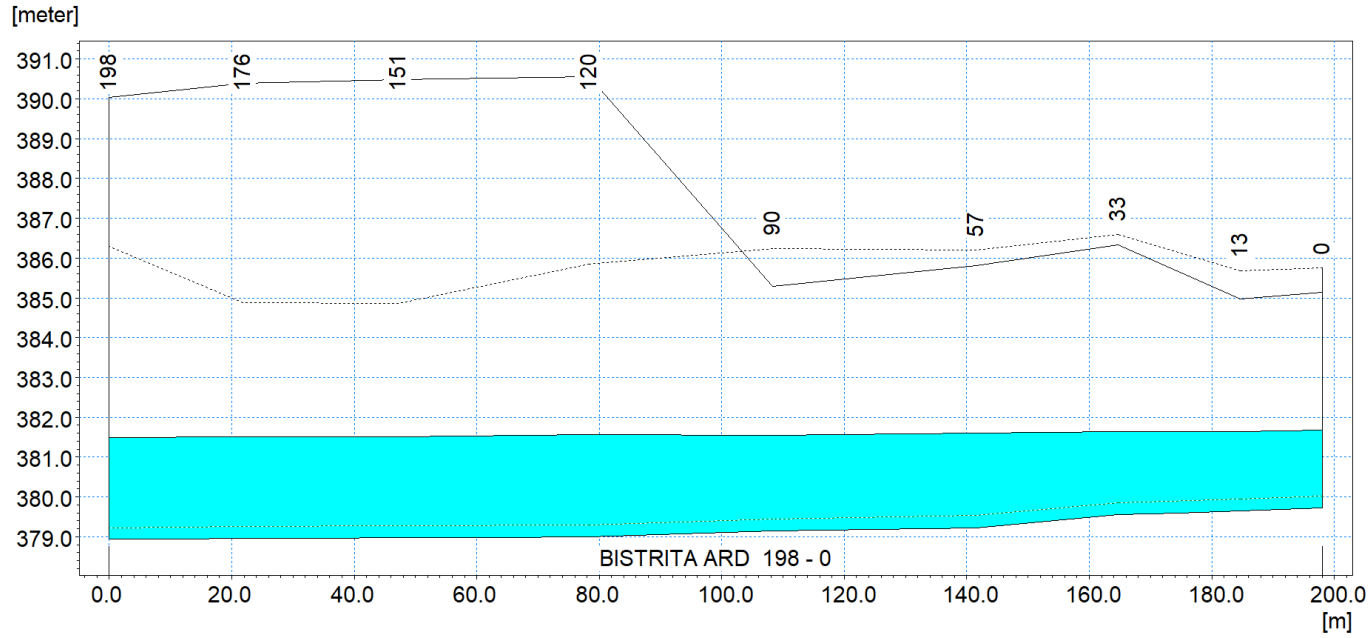

Figure 6. The water level in the longitudinal profile for Q = 54.5 m^3/s.

In Figure 7 we can see the maximum water level in one of the cross sections for the flow rate Q = 54.5 m^3/s.

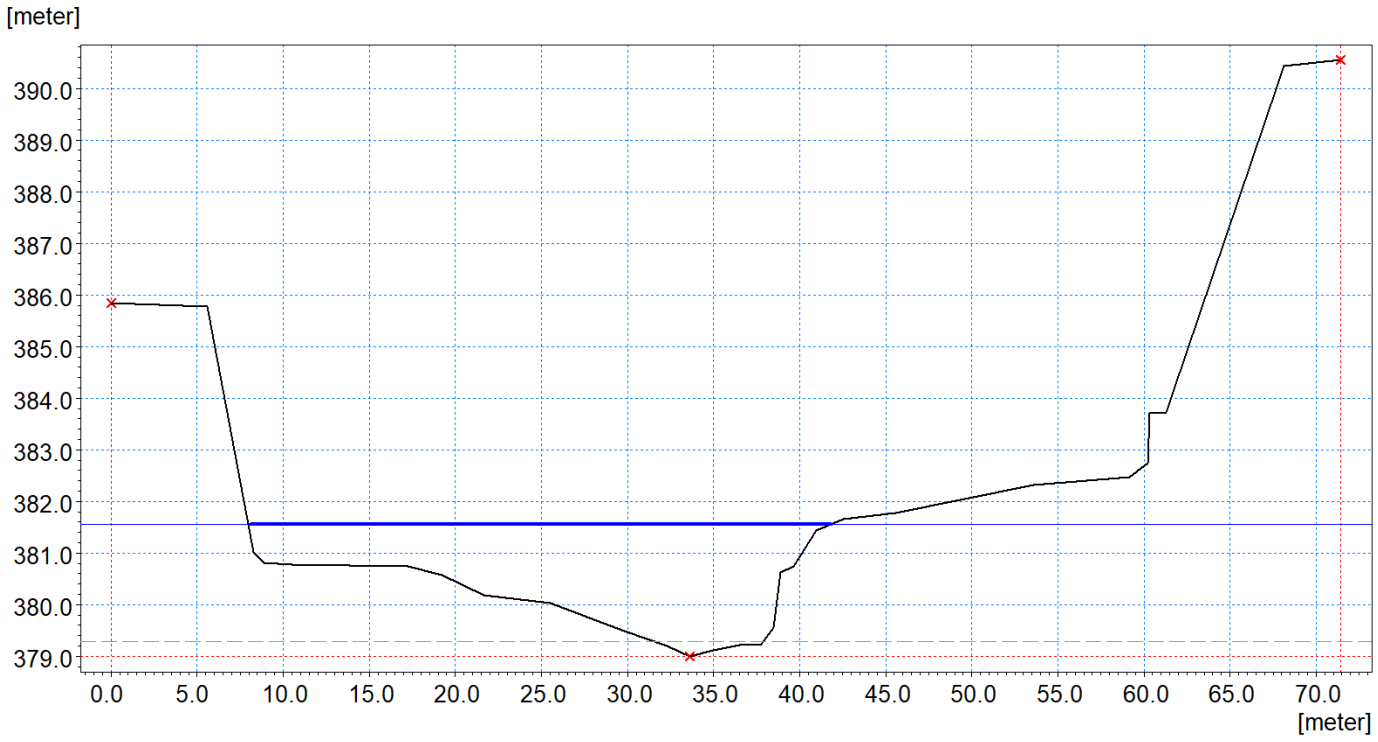

Figure 7. The maximum water level in the transverse profile P6 for the flow rate Q = 54.5 m^3/s.

In Figure 8, the water depth in each cross-section is represented graphically, respectively, for the maximum value of the depth for the flow rate Q = 54.5 m^3/s.

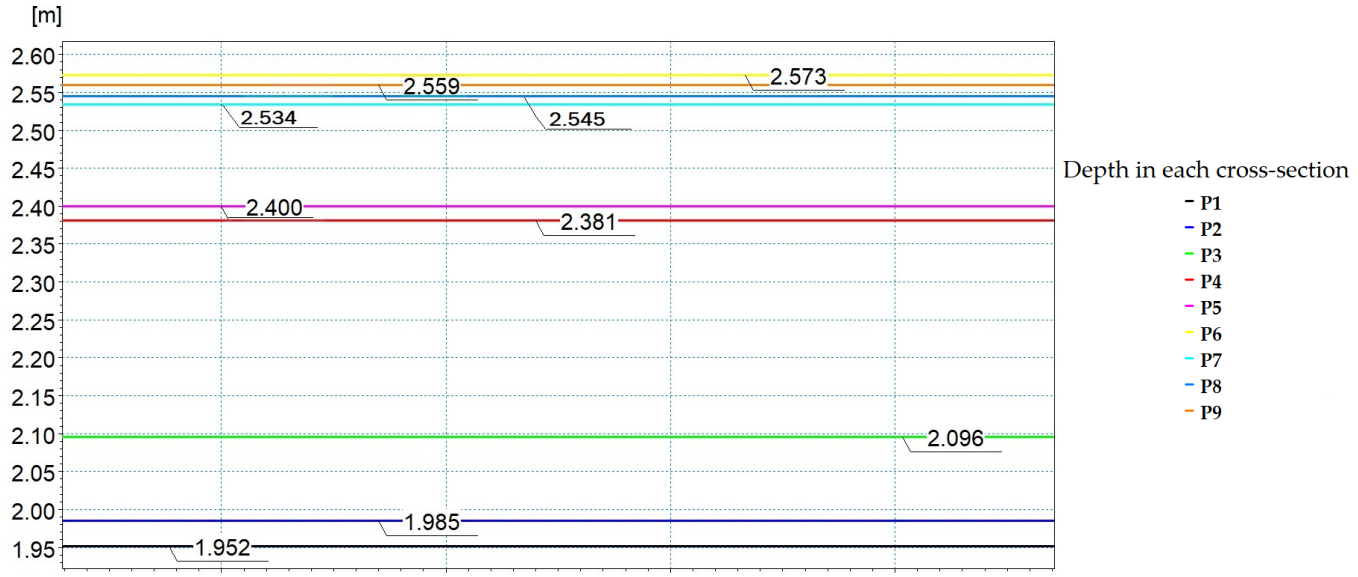

Figure 8. Water depth in each cross-section in graphical form for flow rate Q = 54.5 m^3/s.

In Figure 9, we can see the water speed, in the longitudinal profile along the sector studied in the modeling.

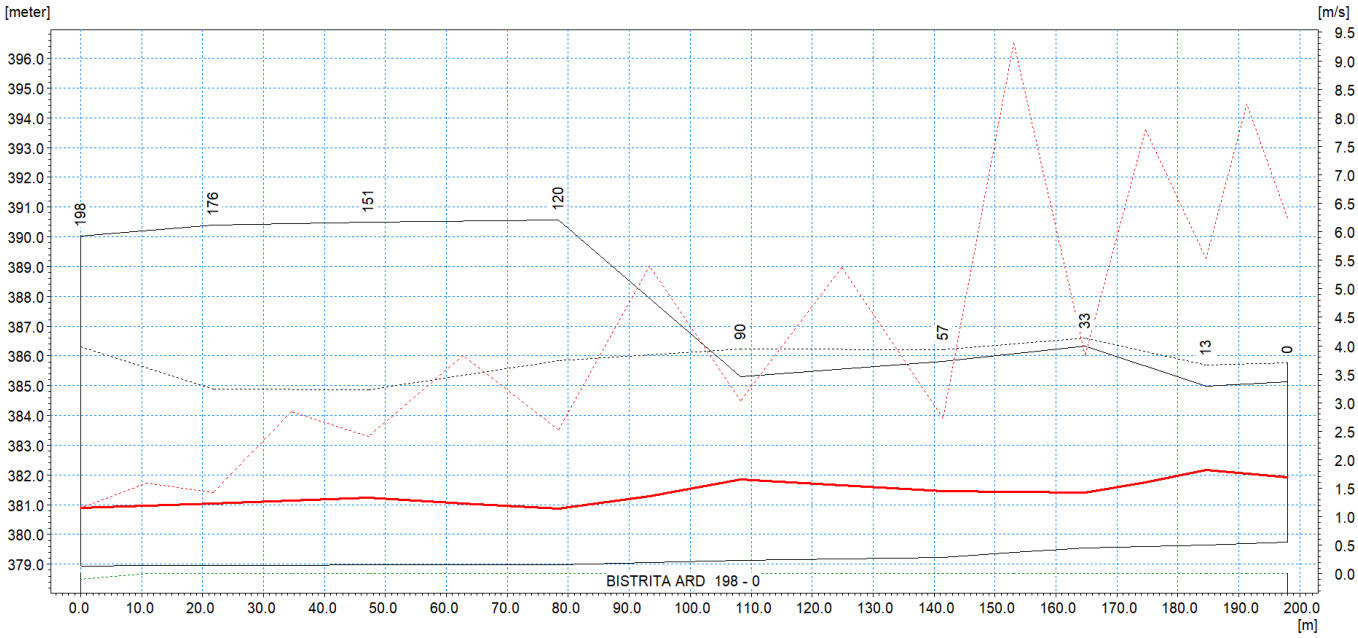

Figure 9. Water velocity in the longitudinal profile for Q = 54.5 m^3/s.

In the table below (Table 2) the values recorded in all 9 cross-sections for the following parameters are transcribed: water depth, water level, and water velocity for the flow rate Q = 54.5 m^3/s.

Table 2. Water level, depth, and velocity in each cross-section for flow rate Q = 54.5 m^3/s.

Section/Q		Q = 54.5 m^3/s		
Section	**Kilometer (m)**	**Water Level (m)**	**Water Depth (m)**	**Water Velocity (m/s)**
P1	0.00	381.682	1.952	1.698
P2	13.41	381.635	1.985	1.819
P3	33.28	381.646	2.096	1.426
P4	56.53	381.611	2.381	1.455
P5	89.70	381.540	2.400	1.661
P6	119.62	381.563	2.573	1.148
P7	150.79	381.514	2.534	1.338
P8	176.19	381.505	2.545	1.235
P9	198	381.499	2.559	1.158

3.2. Hydraulic Modeling on the Ardelean Bistrita River, Where the Flow Has a Value of Q = 178 m^3/s

In Figure 10 you can see the water level in the longitudinal profile of the analyzed river sector for the flow rate Q = 178 m^3/s.

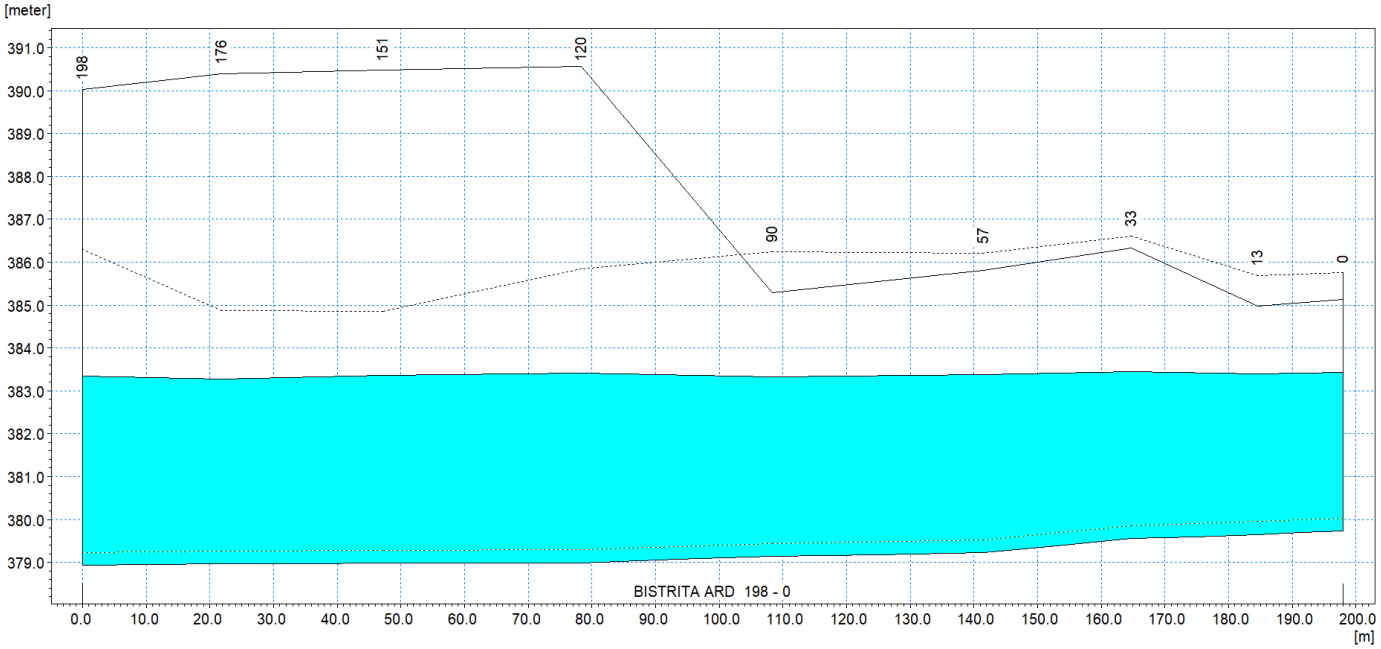

Figure 10. Water level in the longitudinal profile of the section analyzed for Q = 178 m^3/s.

In Figure 11 we can see the maximum water level in one of the cross sections for the flow rate Q = 178 m^3/s.

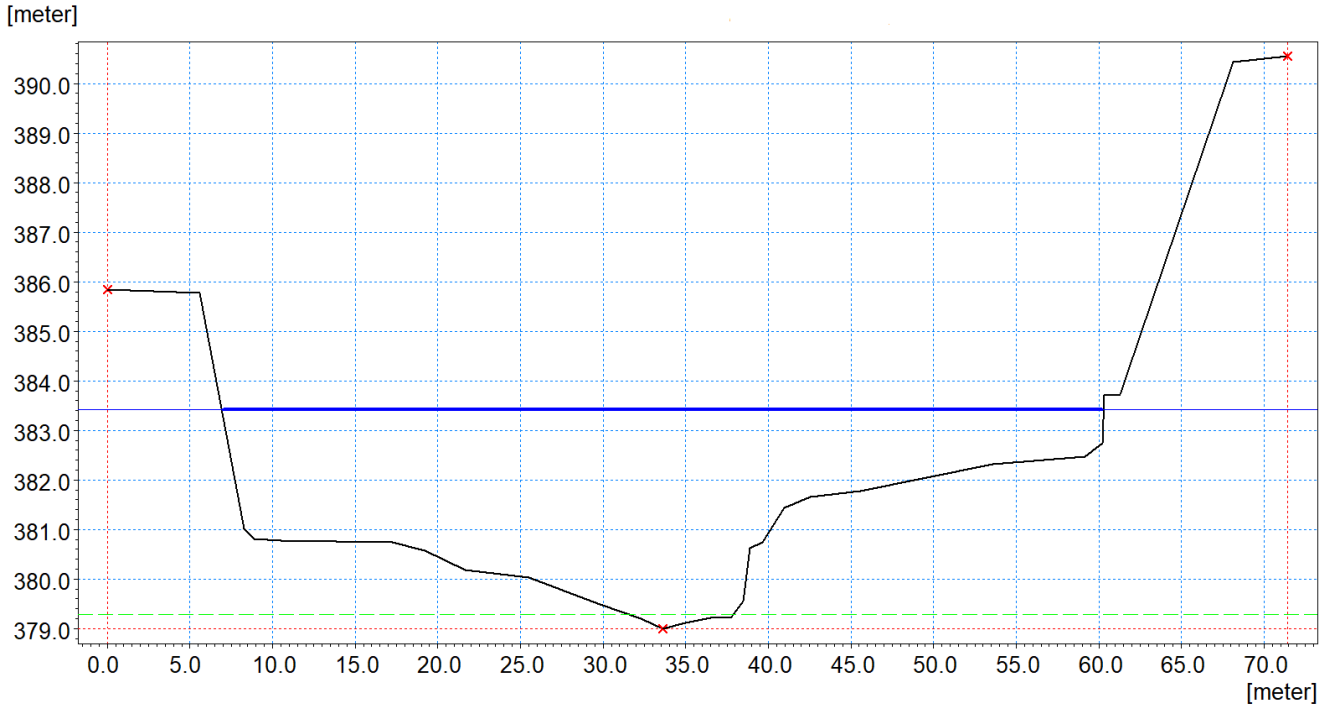

Figure 11. Graphical representation of maximum water level in cross profile 6 for flow Q = 178 m^3/s.

In Figure 12, the water depth in each cross-section is represented graphically, respectively, for the maximum value of the depth for the flow rate Q = 178 m^3/s.

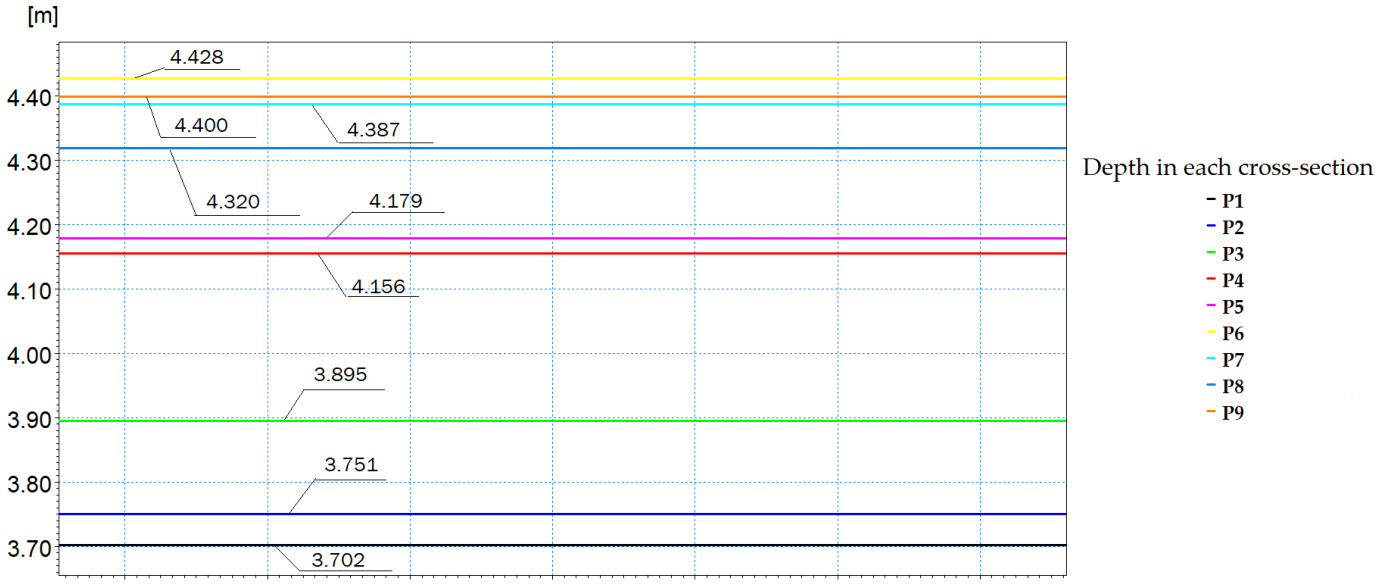

Figure 12. Water depth in each cross-section in graphical form for flow rate Q = 178 m^3/s.

In Figure 13, the water speed can be seen in the longitudinal profile along the sector studied in the modeling.

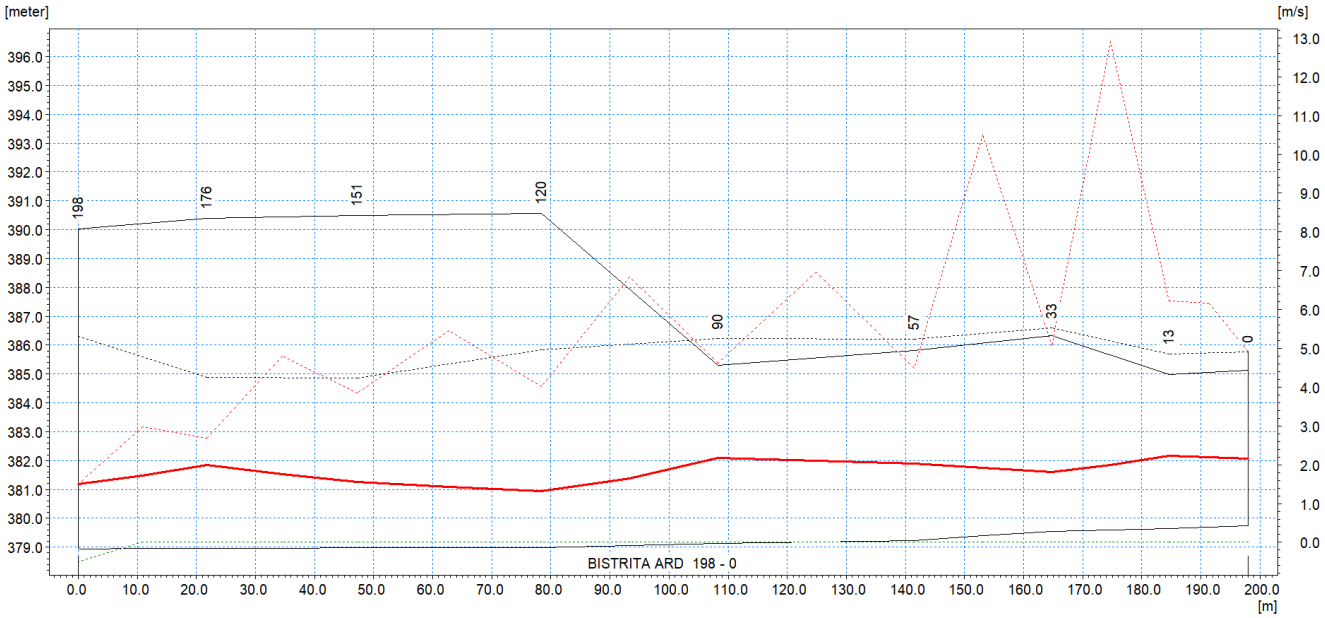

Figure 13. Graphical representation of water velocity in the longitudinal profile for Q = 178 m^3/s.

In the table below (Table 3), the values recorded in all nine cross-sections for the following parameters are transcribed: water depth, water level, and water velocity for the flow Q = 178 m^3/s.

Table 3. Water level, depth, and velocity in each cross-section for flow rate Q = 178 m^3/s.

Section/Q		Q = 178 m^3/s		
Section	**Kilometer (m)**	**Water Level (m)**	**Water Depth (m)**	**Water Velocity (m/s)**
P1	0.00	383.431	3.701	2.163
P2	13.41	383.401	3.751	2.223
P3	33.28	383.445	3.895	1.819
P4	56.53	383.385	4.155	2.031
P5	89.70	383.318	4.178	2.182
P6	119.62	383.417	4.427	1.316
P7	150.79	383.366	4.386	1.559
P8	176.19	383.279	4.319	1.995
P9	198	383.339	4.399	1.509

4. Discussion

Hydraulic modeling for the two flows Q = 54.5 m^3/s and Q = 178 m^3/s was carried out for a constant flow, having a permanent and non-uniform movement. Local parameters such as wetted section, depth, and velocity vary spatially, specifically along the stream. With the help of simulation, the average water speed and water depth were determined in all nine transverse profiles measured in the analyzed sector.

In each section, based on the study of the sector in the field, the rugosity was chosen both in the minor and in the major riverbed, consulting the specialized literature. The main factors that influence the flow and modify the roughness coefficient are the microrelief of the riverbed, the covering or protection of the riverbed with vegetation, and the irregularity in the plan and the section of the riverbed [47,48].

According to the simulation for the flow rate Q = 54.5 m^3/s, the water depth in the studied sector is between 1.952 m (transverse profile 1) and 2.559 m (transverse profile 9).

The water velocity in this sector at the flow rate Q = 54.5 m^3/s varies lengthwise, depending on the shape of the riverbed or sections of the riverbed, with values between 1.148 m/s (transverse profile 6) and 1.849 m/s (transverse profile 2).

The modeling carried out for the flow rate Q = 178 m^3/s shows us that the water depth for the analyzed water body had values between 3.701 m (transverse profile 1) and 4.427 m (transverse profile 6). The recorded water velocity for the flow rate Q = 178 m^3/s had values between 1.316 m/s (transverse profile 6) and 2.223 m/s (transverse profile 2).

In order to be able to determine the existence of hydromorphological processes, it was necessary to take a sample of alluvial material from the section considered representative of the analyzed sector. Following the granulometric analysis, the average diameter of the particle in the thalweg is determined. According to the analysis, the sample of natural aggregates from the fluvial sector, the sieve through which 50% of the sample passed has a diameter of 25.18 mm (D50) (Figure 14).

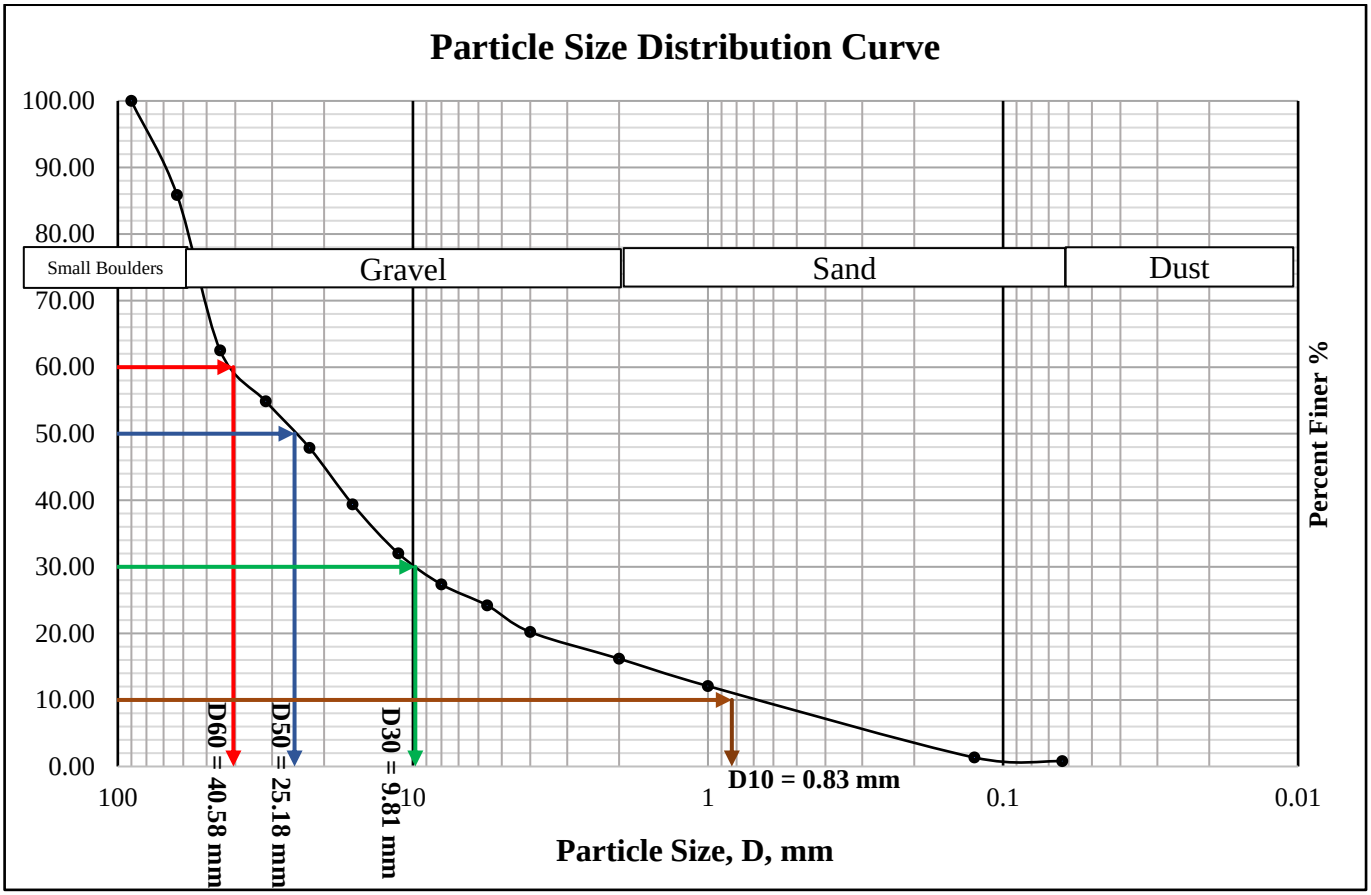

Figure 14. Granulometric curve of the alluvial material taken from the Bistrita river bed.

According to Table 4, which shows the average particle entrainment speed according to PD 95-2002- Normative regarding the hydraulic design of bridges and footbridges, the sample taken from the bottom of the riverbed had a D50 = 25.18 m, representing medium river gravel for which, at a water depth of 2 m, the average particle entrainment speed was 2 m/s. Thus, according to the modeling for the flow rate Q = 54.5 m^3/s, the water velocity in certain sections (transverse profiles 1, 2, and 3) can move particles with a diameter close to D50. The rest of the particles with a diameter smaller than D50 for depths greater than 2 m (transverse profiles 4–9) will all be set in motion and thus the hydromorphological process of bank erosion and valley deepening occurs. In the case of the simulation for the flow rate Q = 178 m^3/s, the water velocity can set in motion the particles with a diameter close to D50 only in cross-section 2. In the rest of the cross-sections, the water velocity sets in motion all the particles smaller than D50.

Table 4. Table with the average particle entrainment speed Va (m/s) [49].

The Name of the Constitutive Lands of the Thalweg	D50 (mm)	Average Water Depth ($h_{average}$, in m)									
		2	**3**	**4**	**5**	**6**	**8**	**10**	**12**	**14**	**16**
Fine sand	0.15	0.6	0.7	0.7	0.8	0.9	1.0	1.1	1.2	1.3	1.3
Small sand	0.5	0.7	0.9	1.0	1.0	1.1	1.3	1.4	1.5	1.6	1.7
Pearly sand and small sand with gravel	1.0	0.9	1.0	1.2	1.3	1.4	1.5	1.7	1.8	1.9	2.0
Lage sand and pearly sand with gravel	2.5	1.1	1.3	1.4	1.6	1.7	1.9	2.0	2.2	2.3	2.5
Gravel with large sand	6.0	1.4	1.6	1.7	1.9	2.0	2.2	2.4	2.6	2.7	-
Fine river gravel	15.0	1.7	1.9	2.1	2.3	2.4	2.6	2.8	3.0	3.2	-
Medium river gravel	25.0	2.0	2.3	2.6	2.7	2.9	3.1	3.4	3.6	-	-
Large river gravel	60.0	2.5	2.8	3.0	3.2	3.3	3.6	3.9	4.1	-	-
Very small boulder	140.0	3.0	3.4	3.6	3.8	4.0	4.4	4.6	-	-	-
Medium boulder	250.0	3.6	4.0	5.2	4.5	4.7	5.0	5.3	-	-	-
Large boulder	450.0	4.2	4.6	4.9	5.1	5.3	5.7	-	-	-	-
Very large boulder	750.0	4.9	5.3	5.6	5.9	6.1	6.4	-	-	-	-
Clays and sandy loams with poor composition γ = 1.0 t/m^3		1.0	1.0	1.0	1.2	1.3	1.5	1.6	1.8	1.9	2.0
Clays and sandy loams with poor composition γ = 1.4 t/m^3		1.2	1.3	1.4	1.5	1.6	1.8	1.8	1.8	2.2	-
Clays and sandy loams with poor composition γ = 1.8 t/m^3		1.5	1.7	1.8	1.9	2.0	2.2	2.4	2.4	2.5	-

It is very clear that at these depths and water velocities, a lot of thalweg particles with a diameter of less than 25 mm, which represent approximately half of the sample according to the study, are set in motion and significant erosion occurs on the thalweg and both river banks. Of course, once they are set in motion, even larger particles will be set in motion, by rolling or dragging, because they lose their stability through the mechanical connection they have with the other particles already set in motion.

It can also be observed that the entire studied sector is set in an area of pronounced curvature and not in alignment. Thus, in this section, in addition to the speed of the water, it acts very strongly through a process of force and accentuated erosion and the centrifugal force. Centrifugal force, as it is known, it is one of the main factors that influence the formation and evolution of minor riverbeds. It can be seen from the orthophotoplan that the right bank of the meander is a concave bank, being heavily eroded, the erosion evolving after each flood. On the left bank which is convex, we can see alluvium deposits, which are deposited after each flood when the depth and the speed of the water decreases in this section.

According to Table 5, a water velocity of 0.98 m/s is required to move the isolated particles for non-cohesive soils with a diameter of 25 mm. In the simulation performed for the flow rate of Q = 54.5 m^3/s, the lowest value of the speed was 1.148 m/s and for the flow rate Q = 178m^3/s the lowest recorded water speed was 1.316 m/s.

Table 5. Values of the unit speed of moving isolated particles for non-cohesive soils [50].

Particle Diameter (mm)	V_{li} (m/s)	Particle Diameter (mm)	V_{li} (m/s)	Particle Diameter (mm)	V_{li} (m/s)
10	0.83	42	1.38	65	1.69
15	0.86	44	1.41	70	1.73
20	0.90	46	1.44	75	1.76
25	0.98	48	1.47	80	1.80
30	1.04	50	1.50	85	1.84
32	1.11	52	1.54	90	1.88
34	1.17	54	1.56	95	1.91
36	1.24	56	1.59	100	1.95
38	1.29	58	1.62	150	2.40
40	1.35	60	1.65	200	2.60

According to the table below (Table 6), the mass entrainment speed of alluvium for non-cohesive soils with a diameter of 25 mm to 40 mm is between 1.4 m/s and 1.8 m/s.

Table 6. Unit mass entrainment speeds of alluvium for non-cohesive soils [50].

The Name of Alluvium	Particle Diameter (mm)	V_{lm} m/s
Dust and mud	0.005–0.05	0.15–0.21
Fine sand	0.05–0.25	0.21–0.32
Medium sand	0.25–1.0	0.32–0.57
Large sand	1.0–2.5	0.57–0.65
Small pebbles	2.5–5.0	0.65–0.80
Medium pebbles	5.0–10	0.80–1.00
Coarse pebbles	10–15	1.00–1.20
Small gravel	15–25	1.20–1.40
Medium gravel	25–40	1.40–1.80
Large gravel	40–75	1.80–2.40
Small boulders	75–100	2.40–2.80
Medium boulders	100–150	2.80–3.40
Big boulders	150–200	3.40–3.90
Small blocks	200–300	3.90–4.40
Medium blocks	400–300	4.40–4.80

After analyzing the results obtained from the hydraulic modeling for the two flow rates recorded on the Bistrita Ardeleana watercourse, it was observed that for the flow rate of 54.5 m^3/s, the unit mass entrainment speeds of the alluvium were below 1.4 m/s and only at a few sections (cross profiles 6–9). For the flow rate of 178 m^3/s, unit mass entrainment velocities of alluvium below 1.4 m/s were recorded only in transverse profile 6, the rest having high velocity values.

Previous studies such as the research paper by Florek, J. and Wyrębek, M. used 1D modeling carried out in the HEC-RAS program for mountain rivers in southern Poland. Following the interpretation of the results obtained by them, five sections were found where the riverbed is unstable; three of them are in the transverse profiles 16, 18, and

20 where the average diameter of the particles is 68 mm and 46 mm respectively. These dimensions are characteristic of the alluvial material consisting of large gravel. The flow rates considered were 4.69 m^3/s, 42.38 m^3/s, and 3.5 m^3/s [51]. According to Table 6, the mass entrainment speed of alluvium with a diameter of 46–48 mm is between 1.8 m/s and 2.40 m/s.

As in the case of the sector analyzed in our work, in some cross-sectional profiles, the particles with a diameter smaller than the average diameter of the particles may be set in motion by rolling or crawling when the recorded flow rates are lower than those analyzed.

Even if different programs were used to create the hydraulic model, as well as the values of the monitored parameters differing, the purpose of the modeling was to identify or confirm the existence of erosions along the length of the analyzed sectors and to emphasize the importance of promoting green hydrotechnical constructions to return to the state of the river as natural as possible.

It is obvious that floods with increased flows over time can accelerate hydromorphological processes compared to low recorded flows [52]. The length of the unstable river bed is consistent with the controlled discharges from the reservoir, topography, and geological structure [53].

The application of the solutions identified for the defense of the banks to withstand erosion speeds and to stabilize the banks, respectively, and the application of the green solution to reduce the water speeds and stop the deepening of the thalweg are necessary for this analyzed sector. The hydrotechnical constructions identified for the safety of the two banks will increase the roughness of the riverbed, thus reducing the water speed, creating favorable conditions for the retention of alluvium. The vegetation in the minor river bed has a very important role in protecting the surface of the bed from instability through the root system [54].

The green methods proposed for the analyzed sector will be part of future research activity, in which their hydrodynamic behavior will be analyzed as well as the hydrodynamic characteristics of the studied body of water, having as examples similar research carried out by Lama, G. F. C. et al. and Pasquino V. et al. [55,56].

5. Conclusions

According to the modeling for the flow rate Q = 54.5 m^3/s, the water velocity in certain sections can move particles with a diameter close to D50. The rest of the particles with a diameter smaller than D50 for depths greater than 2 m will all be set in motion. In the case of the simulation for the flow rate Q = 178 m^3/s, the water velocity can set in motion the particles with a diameter close to D50 only in cross-section 2. In the rest of the cross-sections, the water velocity sets in motion all the particles smaller than D50.

In regard to the movement of isolated particles for non-cohesive soils with a diameter of 25 mm, it is necessary to have the velocity of the water at a value of 0.98 m/s. In the simulation performed for the flow rate of Q = 54.5 m^3/s, the lowest speed is 1.148 m/s and for the flow rate Q = 178m^3/s the lowest recorded water speed is 1.316 m/s.

In conclusion, in the analyzed sector, strong erosions occur both on the thalweg and on the banks at high flows due to abundant precipitation and controlled water discharges from the Colibița reservoir, at high flows recorded during extreme floods, the erosions are large-scale. Thus, it is recommended that hydrotechnical constructions with the role of protection against erosion should be carried out in this sector.

The hydrotechnical constructions aim to limit the morphological modeling or to consolidate the river bed artificially. These conventional constructions have a negative impact on the longitudinal and vertical connectivity of rivers.

Critical or unstable sectors on watercourses can become safe with the help of bioengineering, more precisely with green methods. This is possible given that these alternative constructions use natural elements that have positive effects on the ecosystem.

Morphological phenomena occur in the studied section that modify the river bed even at normal flows. At high flows also influenced by water discharges from the Colibita

reservoir or at high flows recorded during extreme floods, the erosions or degradations are large-scale.

Thus, it is recommended to promote hydrotechnical constructions with the role of stopping the morphological modifications of the minor riverbed. This should be done taking into consideration that these erosions or degradations endanger the stability of the sector, since on the right bank in the immediate vicinity is the national or European road as well as a residential area, which over time could be affected due to the instability of the sector.

The bioengineering methods identified can be used to stop river banks or thalweg erosion of the Bistrita Ardeleana River. Green methods can significantly increase the diversity of the aquatic ecosystem. It helps to the accumulation of alluvium and the removal of excess moisture accumulated in the soil on the two banks of the river.

The profitability of these alternative constructions is very high due to the materials used, they are found in the immediate vicinity of the studied water course and the low labor force. Their resistance during natural floods as well as during the period of increased flows resulting from the production of energy (with daily frequency) gives them increased effectiveness.

These hydrotechnical constructions have a flexibility that allows them to withstand a slight instability of the foundation without damage unlike conventional methods (monolithic concrete).

Hydrotechnical constructions with natural elements could be used to replace hydrotechnical constructions destroyed or damaged by floods or the passage of time.

Author Contributions: Conceptualization: A.C.M. and T.A.H.; data curation: A.C.M., T.A.H., V.M. and N.M.; formal analysis: A.C.M., T.A.H., V.M. and N.M.; investigation: A.C.M. and V.M.; methodology: A.C.M., T.A.H., V.M. and N.M.; resources: A.C.M.; software: A.C.M., T.A.H. and N.M.; supervision: V.M. and N.M.; validation: A.C.M., T.A.H., V.M. and N.M.; visualization: A.C.M., T.A.H. and V.M.; writing—original draft: A.C.M.; writing—review and editing: A.C.M., T.A.H., V.M. and N.M. All authors have read and agreed to the published version of the manuscript.

Funding: This research received no external funding.

Institutional Review Board Statement: Not applicable.

Informed Consent Statement: Not applicable.

Data Availability Statement: Not applicable.

Conflicts of Interest: The authors declare no conflict of interest.

References

1. Klimaszyk, P.; Gołdyn, R. Water Quality of Freshwater Ecosystems in a Temperate Climate. *Water* **2020**, *12*, 2643. [CrossRef]
2. Mnyango, S.S.; Thwala, M.; Oberholster, P.J.; Truter, C.J. Using Multiple Indices for the Water Resource Management of a Monomictic Man-Made Dam in Southern Africa. *Water* **2022**, *14*, 3366. [CrossRef]
3. Stanciu, E.; Runceanu, G. (Eds.) *Refacerea Conectivității Longitudinale a Râurilor și Pâraielor din România. Ghid Pentru Obținerea Aprobărilor Necesare Pentru Implementarea Proiectelor de Refacere*; Fundația pentru Arii Protejate: Brasov, Romania, 2019; pp. 5, 10. Available online: https://www.carpathia.org/wp-content/uploads/2019/01/Manual-Conectivitate_Rauri-LIFE.pdf (accessed on 15 July 2020).
4. Staentzel, C.; Kondolf, G.M.; Schmitt, L.; Combroux, I.; Barillier, A.; Beisel, J.-N. Restoring fluvial forms and processes by gravel augmentation or bank erosion below dams: A systematic review of ecological responses. *Sci. Total Environ.* **2020**, *706*, 135743. [CrossRef] [PubMed]
5. Liro, M.; Nones, M.; Mikuś, P.; Plesiński, K. Modelling the Effects of Dam Reservoir Backwater Fluctuations on the Hydrodynamics of a Small Mountain Stream. *Water* **2022**, *14*, 3166. [CrossRef]
6. Palmer, M.; Allan, J.D.; Meyer, J.; Bernhardt, E. River Restoration in the Twenty-First Century: Data and Experiential Future Efforts. *Restor. Ecol.* **2007**, *15*, 472–481. [CrossRef]
7. Kim, J.-J.; Atique, U.; An, K.-G. Long-Term Ecological Health Assessment of a Restored Urban Stream Based on Chemical Water Quality, Physical Habitat Conditions and Biological Integrity. *Water* **2019**, *11*, 114. [CrossRef]
8. Cristescu, C. Morfologia Albiilor şi Conceptul de Restaurare a Râurilor (Thesis Chapter). Ph.D. Thesis, Transilvania University of Braşov, Braşov, Romania, 2006. [CrossRef]

9. Liu, X.; Olden, J.D.; Wu, R.; Ouyang, S.; Wu, X. Dam Construction Impacts Fish Biodiversity in a Subtropical River Network, China. *Diversity* **2022**, *14*, 476. [CrossRef]
10. Ma, X.; Yang, H.; Zhong, X.; Zeng, P.; Zhou, X.; Zeng, S.; Dong, X.; Min, W.; Huang, F. eDNA Metabarcoding Analysis of the Composition and Spatial Patterns of Fish Communities in the Sanbanxi Reservoir, China. *Sustainability* **2022**, *14*, 12966. [CrossRef]
11. Moldovan, A.C.; Micle, V.; Hrăniciuc, T.A.; Marcoie, N. Research on the Sustainable Development of the Bistrita Ardeleana River through the Resizing of Weirs. *Water* **2022**, *14*, 3333. [CrossRef]
12. Paredes-Beltran, B.; Sordo-Ward, A.; de-Lama, B.; Garrote, L. A Continental Assessment of Reservoir Storage and Water Availability in South America. *Water* **2021**, *13*, 1992. [CrossRef]
13. Amasi, A.; Wynants, M.; Blake, W.; Mtei, K. Drivers, Impacts and Mitigation of Increased Sedimentation in the Hydropower Reservoirs of East Africa. *Land* **2021**, *10*, 638. [CrossRef]
14. Yan, F.; Li, N.; Yang, Z.; Qian, B. Ecological Risk Evaluation of Baihetan Dam Based on Fuzzy Hazard Quotient Model. *Water* **2022**, *14*, 2694. [CrossRef]
15. Charoenlerkthawin, W.; Namsai, M.; Bidorn, K.; Rukvichai, C.; Panneerselvam, B.; Bidorn, B. Effects of Dam Construction in the Wang River on Sediment Regimes in the Chao Phraya River Basin. *Water* **2021**, *13*, 2146. [CrossRef]
16. Zhang, X.; Fang, C.; Wang, Y.; Lou, X.; Su, Y.; Huang, D. Review of Effects of Dam Construction on the Ecosystems of River Estuary and Nearby Marine Areas. *Sustainability* **2022**, *14*, 5974. [CrossRef]
17. Leite, T.; Borgwardt, F.; Branco, P. Understanding the Impacts of River Network Fragmentation on Freshwater Fish Species. *Biol. Life Sci. Forum* **2022**, *13*, 73. [CrossRef]
18. Nam, S.; Gutierrez, M.; Diplas, P.; Petrie, J. Effects of Hydropower Dam Operation on Riverbank Stability. *Infrastructures* **2021**, *6*, 127. [CrossRef]
19. Pander, J.; Mueller, M.; Geist, J. A Comparison of Four Stream Substratum Restoration Techniques Concerning Interstitial Conditions and Downstream Effects. *River Res. Appl.* **2015**, *31*, 239–255. [CrossRef]
20. Mury, A.; Jeanson, M.; Collin, A.; James, D.; Etienne, S. High Resolution Shoreline and Shelly Ridge Monitoring over Stormy Winter Events: A Case Study in the Megatidal Bay of Mont-Saint-Michel (France). *J. Mar. Sci. Eng.* **2019**, *7*, 97. [CrossRef]
21. Dai, D.; Brouwer, R.; Lei, K. Measuring the economic value of urban river restoration. *Ecol. Econ.* **2021**, *190*, 107186. [CrossRef]
22. Paterson-Shallard, H.; Fisher, K.; Parsons, M.; Makey, L. Holistic approaches to river restoration in Aotearoa New Zealand. *Environ. Sci. Policy* **2020**, *106*, 250–259. [CrossRef]
23. Wohl, E.; Lane, S.N.; Wilcox, A.C. The science and practice of river restoration. *Water Resour. Res.* **2015**, *51*, 5974–5997. [CrossRef]
24. Basak, S.M.; Hossain Md, S.; Tusznio, J.; Jurczak, M.G. Social benefits of river restoration from ecosystem services perspective: A systematic review. *Environ. Sci. Policy* **2021**, *124*, 90–100. [CrossRef]
25. Schirmer, M.; Luster, J.; Linde, N.; Perona, P.; Mitchell, E.; Barry, D.; Cirpka, O.; Schneider, P.; Vogt, T.; Durisch-Kaiser, E. River restoration: Morphological, hydrological, biogeochemical and ecological changes and challenges. *Hydrol. Earth Syst. Sci. Discuss.* **2013**, *10*, 10913–10941. [CrossRef]
26. Perkins, D.M.; Hull, T.; Bubb, N.; Cunningham, A.; Glackin, R.; Glen, T.; Smith, S.; Davies, B. Putting the 'Beaver' Back in Beverley Brook: Rapid Shifts in Community Composition following the Restoration of a Degraded Urban River. *Water* **2021**, *13*, 3530. [CrossRef]
27. Asnake, K.; Worku, H.; Argaw, M. Integrating River restoration goals with urban planning practices: The case of Kebena river, Addis Ababa. *Heliyon* **2021**, *7*, E07446. [CrossRef]
28. Lavelle, A.M.; Chadwick, M.A.; Chadwick, D.D.A.; Pritchard, E.G.; Bury, N.R. Effects of Habitat Restoration on Fish Communities in Urban Streams. *Water* **2021**, *13*, 2170. [CrossRef]
29. Shakya, R.; Ahiablame, L. A Synthesis of Social and Economic Benefits Linked to Green Infrastructure. *Water* **2021**, *13*, 3651. [CrossRef]
30. Tzioutzios, C.; Kastridis, A. Multi-Criteria Evaluation (MCE) Method for the Management of Woodland Plantations in Floodplain Areas. *ISPRS Int. J. Geo-Inf.* **2020**, *9*, 725. [CrossRef]
31. Markus-Michalczyk, H.; Michalczyk, M. Floodplain Forest Restoration as a Nature-Based Solution to Create Climate-Resilient Communities in European Lowland Estuaries. *Water* **2023**, *15*, 440. [CrossRef]
32. Roca, M.; Escarameia, M.; Gimeno, O.; de Vilder, L.; Simm, J.D.; Horton, B.; Thorne, C. *Green Approaches in River Engineering—Supporting Implementation of Green Infrastructure*; HR Wallingford: Wallingford, UK, 2017; ISBN 978-1-898485-16-2. Available online: https://eprints.hrwallingford.com/1250/1/Green_approaches_in_river_engineering.pdf (accessed on 16 October 2020).
33. Ibañez, S.C.; Dajac, C.V.G.; Liponhay, M.P.; Legara, E.F.T.; Esteban, J.M.H.; Monterola, C.P. Forecasting Reservoir Water Levels Using Deep Neural Networks: A Case Study of Angat Dam in the Philippines. *Water* **2022**, *14*, 34. [CrossRef]
34. Kim, S.; Jung, K.; Kang, H. Response of Fish Community to Building Block Methodology Mimicking Natural Flow Regime Patterns in Nakdong River in South Korea. *Sustainability* **2022**, *14*, 3587. [CrossRef]
35. Gogaltan, F.; Marinescu, G.G. *Aur pentru Zei. O Descoperire Aparţinând Epocii Bronzului de la Bistriţa-Dealul Târgului (Nord-Estul Transilvaniei). Gold for the Gods: A Bronze Age Discovery from Bistriţa-Dealul Târgului (North-East Transylvania)*; MEGA: Cluj Napoca, Romania, 2018.
36. Moldovan, C.; Silaghi, R. The Morphological Impact of the Colibița Hydrotehnical System on the Bistrita Ardeleana Riverbed. In Proceedings of the 2021" Air and Water—Components of the Environment" Conference Proceedings, Cluj-Napoca, Romania, 20 March 2021; pp. 89–94. [CrossRef]

37. Ieleicz, M.; Pătraru, I. *Geografia Fizică a României*; Universitară: Bucuresti, Romania, 2005; pp. 208–209, 236. Available online: https://pdfcoffee.com/geografie-fizica-romania-i-ielenicz-pdf-free.html (accessed on 29 May 2017).
38. Tivadar, A. *Contribuții la Istoria Alimentării cu Apă a Orașului Bistrița*; Tipomur: Târgu Mureș, Romania, 1995.
39. Sofronie, C. *Amenajări Hidrotehnice în Bazinul Hidrografic Someș-Tisa*; Gloria: Cluj-Napoca, Romania, 2000; p. 123.
40. Șmuleac, A.; Șmuleac, L.; Man, T.E.; Popescu, C.A.; Imbrea, F.; Radulov, I.; Adamov, T.; Pașcalău, R. Use of Modern Technologies for the Conservation of Historical Heritage in Water Management. *Water* **2020**, *12*, 2895. [CrossRef]
41. MIKE 11, A Modelling System for Rivers and Channels, Reference Manual, Danish Hydraulic Institute. 2017, p. 425. Available online: https://manuals.mikepoweredbydhi.help/2017/Water_Resources/Mike_11_ref.pdf (accessed on 4 July 2022).
42. *Rapoart hidrometric al debitelor de apă pe râul Bistrița la stația hidrometrică Bistrița*; Sistemul de Gospodărire al Apelor: Bistrița, Romania, 2019.
43. Tourbier, J.T.; Westmacott, R.N. Manual of Urban Rivers Rehabilitation Techniques. *Westmacott*. 2005. Available online: https://www.csu.edu/cerc/researchreports/documents/ManualOfUrbanRiverRehabilitationTechniques2005_000.pdf (accessed on 14 December 2020).
44. Cretan, A. Construcții Hidrotehnice și Rețele Tehnico-Edilitare, Suport de curs. Available online: https://www.ct.upt.ro/studenti/cursuri/cretan/index.htm (accessed on 1 September 2022).
45. Blăgoi, O.; Mitroi, A. *Soluții Moderne și Clasice pentru Lucrări de Protecție pe Cursurile de Apă*; Performatica: Iasi, Romania, 2013; p. 6.
46. Silvica, O. Amenajări și Construcții Hidrotehnice, Suport de curs. Available online: https://pdfcoffee.com/qdownload/amenajari-si-constructii-hidrotehnice-pdf-free.html (accessed on 20 December 2020).
47. Cioc, D. *Hidraulica*; Editura Didactică și Pedagogică: București, România, 1975; p. 297.
48. Nistoran, D.E.; Moatăr, F.; Manoliu, M.; Ionescu, C.S. *Hidraulică Tehnică*; Editura Printech: București, România, 2007; p. 56.
49. Normativ Privind Proiectarea Hidraulică a Podurilor și Podețelor—PD 95-2002. Available online: https://www.mdlpa.ro/userfiles/reglementari/Domeniul_XXVI/26_82_PD_95_2002.pdf (accessed on 28 February 2023).
50. Dan, E. *Regularizări de Râuri și Căi de Comunicație*; Editura Didactică și Pedagogică: București, România, 1964; p. 113.
51. Florek, J.; Wyrębek, M. Procedure of Numerical Modelling and Estimation of Sieve Curve Changes as a Tool to Define Riverbed's Erodibility. *Sustainability* **2023**, *15*, 1468. [CrossRef]
52. Lacko, M.; Potočki, K.; Škreb, K.A.; Bezak, N. Joint Modelling of Flood Hydrograph Peak, Volume and Duration Using Copulas—Case Study of Sava and Drava River in Croatia, Europe. *Water* **2022**, *14*, 2481. [CrossRef]
53. Obodovskyi, O.; Habel, M.; Szatten, D.; Rozlach, Z.; Babiński, Z.; Maerker, M. Assessment of the Dnieper Alluvial Riverbed Stability Affected by Intervention Discharge Downstream of Kaniv Dam. *Water* **2020**, *12*, 1104. [CrossRef]
54. Xu, Y.; Valyrakis, M.; Gilja, G.; Michalis, P.; Yagci, O.; Przyborowski, Ł. Assessing Riverbed Surface Destabilization Risk Downstream Isolated Vegetation Elements. *Water* **2022**, *14*, 2880. [CrossRef]
55. Lama, G.F.C.; Crimaldi, M.; Pasquino, V.; Padulano, R.; Chirico, G.B. Bulk Drag Predictions of Riparian Arundo donax Stands through UAV-Acquired Multispectral Images. *Water* **2021**, *13*, 1333. [CrossRef]
56. Pasquino, V.; Saulino, L.; Pelosi, A.; Allevato, E.; Rita, A.; Todaro, L.; Saracino, A.; Chirico, G.B. Hydrodynamic behaviour of European black poplar (*Populus nigra* L.) under coppice management along Mediterranean river ecosystems. *River Res. Appl.* **2018**, *34*, 586–594. [CrossRef]

PAPER • **OPEN ACCESS**

Hydroinformatics tools used to quantify the impact of urban expansion on water bodies, in the context of the intensification of extreme phenomena (Bacău urbanization case study)

To cite this article: Nicolae Marcoie *et al* 2023 *IOP Conf. Ser.: Earth Environ. Sci.* **1136** 012015

Hydroinformatics tools used to quantify the impact of urban expansion on water bodies, in the context of the intensification of extreme phenomena (Bacău urbanization case study)

Nicolae Marcoie[1], Daniel Toma[1], Valentin Boboc[1], Tomi Alexăndrel Hrăniciuc[1] and Cătălin Dumitrel Balan[2,3]

[1] Faculty of Hydrotechnical Engineering, Geodesy and Environmental Engineering; "Gheorghe Asachi" Technical University of Iasi, 700050, Iasi, Romania
[2] Faculty of Chemical Engineering and Environmental Protection; "Gheorghe Asachi" Technical University of Iasi, 700050 Iasi, Romania
[3] Author to whom any correspondence should be addressed

cbalan@ch.tuiasi.ro

Abstract. The present study presents the results of the use of hydraulic and hydrological modeling in order to maintain the quantitative and qualitative parameters of the groundwater Capture Front Gherăești, Bacau County. With the help of specialized hydro-computer programs such as: Visual MODFLOW for groundwater dynamics, and Mike 11 for hydraulic modeling, the impact of urban development projects on surface and groundwater bodies can be simulated and anticipated. The results obtained are used in the Project to assess the impact of the project on water bodies (SEICA). SEICA contributes significantly to maintaining the quality of water bodies by making reasoned decisions that ensure the sustainability of urban development projects.

1. Introduction and study objectives

Population growth and its concentration around large cities lead to a horizontal and vertical expansion of the urban area with a significant impact on groundwater and surface water bodies. Whether we are talking about new industrial parks, residential neighborhoods, leisure areas or shopping malls, these are a challenge for integrated water resources management. By integrated management in this context, we understand both the provision of water and the maintenance of its quality parameters.

This paper uses a recent method of impact assessment SEICA (2019) which through the impact quantification algorithm significantly reduces the subjectivity of the team of evaluators.

The objective of the study is to maintain the quality of water bodies (Gherăești Capture Front) and to protect the urban development project (Recreation Area Project) against floods and landslides due to extreme weather phenomena (Tudose et al 2011). The global warming felt in recent years by the intensification of extreme weather phenomena such as strong winds, large amounts of precipitation in short periods of time, and floods have also been reported in the Bacau study area.

Solving these challenges (maintaining water quality and protection against extreme weather events) must be done from the design phase of projects taking into account impact assessment studies (Neamtu et al 2021, SEICA 2019). The analyzed project is located in the northeast of Bacau on the left bank of the river Bistrita, as can be seen in Figure 1.

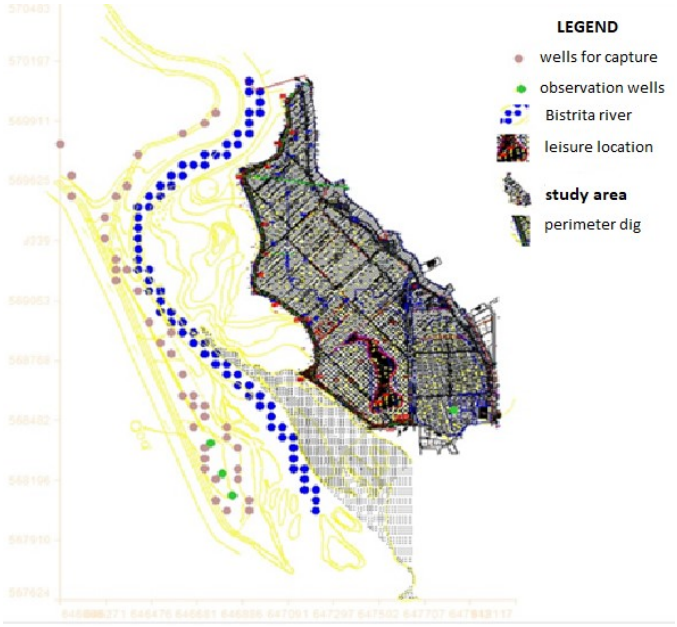

Figure 1. Study area Project Bacau Leisure Center.

The investment made by the beneficiary contributes to solving a very current problem, namely the expansion of the urban area (M.D.R.A.P., 2017) ensuring a high degree of safety (against floods) and comfort (through the created recreational area), in a city full development such as Bacău. The protection dam and the recreational lake lead to an increase in land use. The realization of the project aims in the first phase (fencing with protection dam and lake) the establishment of an area protected from floods, thus creating the possibility of using the land for the recreational base.

By making the investment, the following benefits will be created in the studied area:

- protection, development of the land;
- beautification of the current location;
- road arrangement.
- in the lateral part towards the left bank of the Bistrița river, the protection dam will be built (protection against floods and any other dangerous hydro-meteorological phenomena), L = 2257.38m, H variable.

Simultaneously with the works for the proposed protection dam, works will be carried out for the establishment of the recreational lake with an area S = 3.18 ha (SEICA 2019).

Currently, the perimeter under study is a former orchard of fruit trees, currently partially deforested, located in the city of Bacău, Șerbănești neighborhood. The reason for the deforestation was the fact that the normal operating life of the orchard had expired, as it was aged and unproductive.

The purpose of the impact assessment is to identify and quantify the pressures and impacts of the protection dam, the lake and the operation of the recreational base on the groundwater and surface water body in accordance with EU Directive 2014/52 of the European Parliament and of the Council of 16.04.2014, amending the EU Directive 2011/92 on the elaboration of the effects of certain public and private projects on the environment (Marcoie et al 2019, Comanita et al 2018, SEICA 2019). In order to remove the land from the effect of the floods in order to place some objectives of socio-economic interest, the following were used:

- Detailed topographic studies to determine the flood curves and the location of future investment objectives;
- Hydrological studies prepared by ABA Siret Bacău through which it was possible to determine the elevations of the flood curve and the elevations of the protective dam.

2. Methodology

The SEICA (Impact Assessment Study on the Water Body) project (SEICA 2019) was used as working tools. which, in addition to the classical procedure imposed, used in the study the results obtained by the adequate assessment study software Mike 11 hydraulic modeling program for surface water (Hraniciuc 2016), the Visual MODFLOW program developed by U.S. Geological Survey Ground-Water software for the underground body and The adequate assessment study.

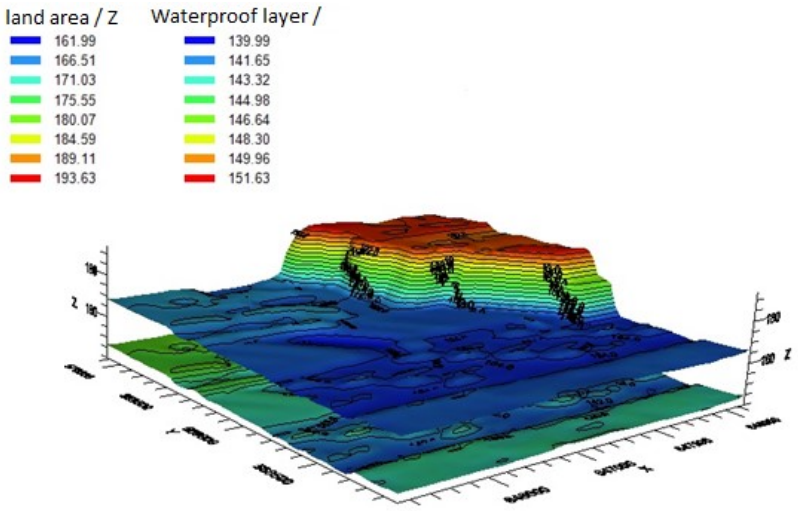

Figure 2. 3D representation of the studied surface in the Visual MODFLOW program software.

An image of the results obtained after running the software Mike 11 hydraulic modeling program for surface waters can be seen in Figures 2 and 3. Figure 2 is an example of a graphical representation of the terrain under study using the Visual MODFLOW software program.

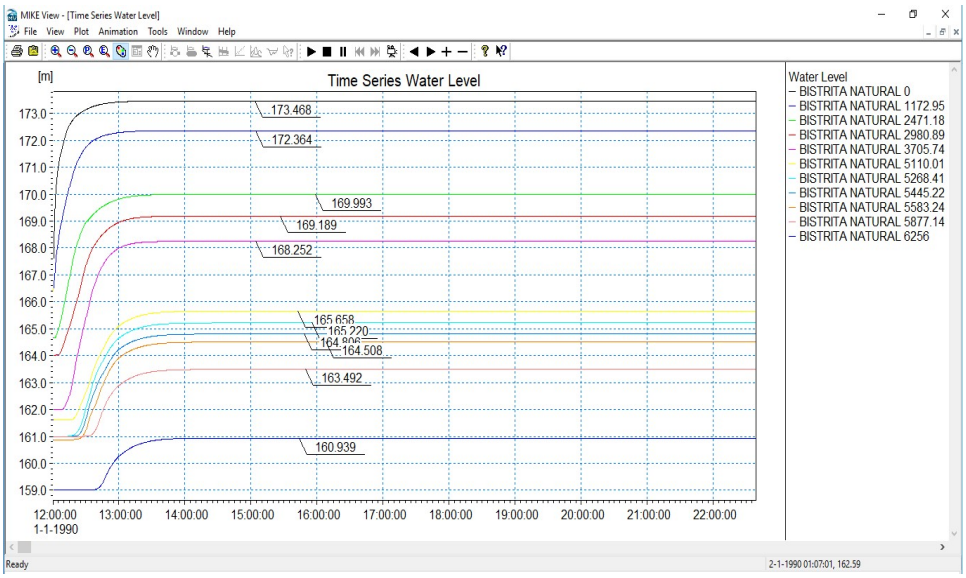

Figure 3. The values of the maximum water levels in the sections studied from P8 to P17 at a flow rate of Q = 1900 m^3/s.

The software used simulates the parameters of the surface and groundwater body in different stress situations (in the presence of the project, at maximum and minimum flows etc).

3. Case study impact assessment Bacau Recreation Area Project

The Ministry of Waters and Forests issues on July 4, 2019 the SEICA Framework Content - Water Impact Assessment Study, which is a recent procedure for assessing the impact on surface or groundwater bodies. With publication in the Official Gazette no. 615bis of July 25, 2019 becomes indispensable in assessing the impact of projects on water bodies (Marcoie et al 2019, Robu et al 2008).

The assessment of the impact of the project on the groundwater body uses a series of multidisciplinary information that ultimately leads to the quantification and determination of the level of impact, including the cumulative impact, its duration and whether it leads to the deterioration of the water body (Zechariah 2003).

The elaboration of the impact study took into account the following:

- Potential impact on the groundwater body – Impact on the hydrostatic level in the boreholes on the right bank of the Bistrița River (Gherăești catchment front), Influences on the groundwater flow by creating the recreational lake, which takes over some of the groundwater.
- Potential impact on the body of surface water – Narrowing of the drainage section of the Bistrița riverbed, through the construction of the protection dam, The potential impact induced by the reduction of the drainage section of the Bistrița river was analyzed, namely the possibility of flooding the areas of interest (Hraniciuc et al 2016).
- Potential impact on biodiversity – By conducting the Adequate Evaluation Study on the Bacau Recreation Base project.

In this study it was followed if the structural and functional relations that maintain the integrity of the site ROSPA0063 Buhuși-Bacău-Bereşti accumulation lakes are affected (Gache 2005, Feneru 2000).

4. Results and conclusions

The main potential ways of affecting the quality of the groundwater from which the water supply of the Gheraiesti Capture Front is made, caused by the construction of the recreational lake and the perimeter dam on the left bank of Bistrita, were analyzed. The results of the evaluation are summarized in Table 1.

Table 1. Evaluation of potential ways to affect groundwater quality.

No.	Potential pressure exerted	Potential impact and quantification	Preventive measures	Residual impact	Reduction measures
1	On the groundwater flow by making the agreement lake (Gheraes Capture Front)	Above the hydrostatic level in the wells drilled on the right bank. Minor negative	Application of the operating and maintenance regulations	Not	Not necessary
2	By narrowing the drainage section of the Bistrița riverbed, by building the protection dam	Exceeding the right dike canopy at a probability of exceeding 0.5% Moderately negative	Raising the right dike with minimum guard heights	Not	Not necessary
3	Impaired site ROSPA0063 Buhuși-Bacău-Bereşti accumulation	The project in the analyzed perimeter will not affect the structural and functional relations that maintain the integrity	The execution of construction works for the creation of a lake and the perimeter dam,	Not	Not necessary

lakes	of the site ROSPA0063 accumulation lakes Buhuși-Bacău-Bereşti Moderately negative	should not take place during the nesting and rearing periods of the chicks, i.e. between May 15 and August 15

1. Even if the impact is manifested, it is in all cases minor, local, temporary and reversible, so that no significant depreciation is foreseen on the quantity and quality of the groundwater from which the water system is supplied.

2. In conclusion, the elevation level of the proposed dam on the left bank is not exceeded by the maximum water level for the considered flow (Q = 1900 m^3/s). Regarding the elevation of the existing dam on the right bank, for the flow taken into account, in some sections, it is exceeded by the maximum water level, and in the others it is at the limit in danger, very close to the canopy. Practically with or without the construction of the project, the right bank presents the same dangers regarding the overcoming of the canopy at a probability of 0.5% (Hraniciuc et al 2019, Marcoie et al 2019).

3. As a result of the presented aspects, we consider that the project from the perimeter subject to analysis will not affect the structural and functional relations that maintain the integrity of the site ROSPA0063 Buhuși-Bacău-Bereşti accumulation lakes. In order to avoid any impact on bird species, we recommend that the construction of recreational lake and perimeter dam construction works not take place during the nesting and rearing periods of the chicks of the two species that could become vulnerable due to possible presence on the site, i.e. in May 15 - August 15 (Donița et al 2015, Neamtu et al 2021, Comanita et al 2017).

Based on the data obtained by simulating the existence of the project in the proposed area with the help of Visual MODFLOW and Mike 11 software for hydraulic modeling, respecting the steps required by the SEICA procedure (SEICA 2019) impact assessment we have reached the following results:

- The project does not present the risk of effects, respectively the risk of deterioration of the water body condition, at the level of quality and quantity element.
- The assessment of the cumulative impact of the project with the projects on water or in connection with the authorized / under authorization / approved / under approval / planned waters on which the project will belocated on the Gherăești Capture Front is insignificant.
- The project adds value, safety and aesthetics to the site through the landscaping works and facilities created, contributing to the sustainable modernization of the Bacau leisure area.

References

[1] Brîndușa Robu, Laura Bulgariu, M Macoveanu 2008 The impact in environment by presence in soil of chrome ions, *University of Agricultural Sciences and Veterinary Medicine of Iaşi, Agronomie Journal of Scientific Papers - Agronomy Series*, **51**, 185-190

[2] Carmen Gache 2005 The monitoring of the human impact on the avifauna's evolution in the important birds' areas from the Prut River basin, *Scientific Annals of the University „Al. I. Cuza "Iaşi, s. Animal Biology*, 195-203

[3] Comanita E.-D., Simion I.M., Cozma P., Hlihor R.M., Campean T., Gavrilescu M. 2017 Application of cost-benefit analysis for an eco-product manufactured from production waste, *Proceedings of Int. Chemical, Biological and Environmental Engineering*, **101**, 91-98

[4] Comanita E.-D., Cozma P., Simion I.M., Rosca M., Gavrilescu M. 2018 Evaluation of eco-efficiency by multicriteria decision analysis. Case study of eco-innovated and eco-designed products from recyclable waste, *Environmental Engineering and Management Journal*, **17**, 1791-1804

[5] Donița, N., Popescu, A., Pauca-Comanescu, M., Mihailescu, S., Biris, I.A. 2005 Habitats of

Romania, *Silvica Technical Publishing House. Bucharest*
[6] Feneru Fl., 2000 - Population's dynamics of some aquatic bird species in the lake Lilieci natural reserve - 1996-2000, Scientific Studies and Research vol.5, pp. 245-248, *Alma Mater Publishing House, University of Bacău*
[7] Hraniciuc T.A., Nicolae Marcoie, Cătălin Dumitrel Balan 2019 Determination of the flood defence embankment elevation crown, using advanced hydrodynamic modelling, *Int. Conf. On Environmental Engineering and Management, ICEEM10,* Iasi, Romania
[8] Hraniciuc Tomi Alexandrel, Petru Cercel 2016 Coupled Hydrological and Hydraulic Modeling of Dangerous Meteorological Phenomena, *16th International Multidisciplinary Scientific Geoconference SGEM*, Albena, Bulgary, **I**, 211-218
[9] Marcoie N., Toaca D., Hraniciuc T.A., Balan C.D., Andriescu P., Boboc V., Toma D., Pavel V.L. 2019 The impact of the embakment and the recreational lake on capturing front with drilling wells, *Int. Conf. on Environmental Engineering and Management, ICEEM10,* Iasi, Romania
[10] Ministry of Waters and Forests – Framework Content of July 4, 2019 of SEICA Water Impact Assessment Study, Official Gazette no. 615bis of July 25
[11] Ministry of Regional Development and Public Administration, National Housing Strategy, 2017
[12] Water Law, Law no. 107 of September 25, 1996, Official Gazette no. 244 of October 8, 1996
[13] Neamtu R, B Sluser, O Plavan, C Teodosiu 2021 Environmental monitoring and impact assessment of Prut River cross-border pollution, *Environmental Monitoring and Assessment* **193**(6), 1-16
[14] Robu B., Bulgariu L., Bulgariu D., Macoveanu M. 2008 Quantification of impact and risk induced in surface water by heavy metals: case study Bahlui river Iasi, *Environmental Engineering and Management Journal*, **7**, 263-267
[15] ROSPA0063 Buhusi-Bacau-Beresti accumulation lakes, Management Plan of the Special Avifauna Protection Area
[16] Zaharia, C. 2003 Legislation for environmental protection, Alexandru Ioan Cuza University Publishing House, Iaşi
[17] Tudose O.G., Cazacu M.M., Timofte A., Balin I. 2011 ESYRO Lidar system developments for troposphere monitoring of aerosols and clouds properties, *Conf. of Remote Sensing of Clouds and the Atmosphere*, vol. **XVI**, 8177
[18] Directive 2011/92 / EU of the European Parliament and of the Council of 13 December 2011 on the assessment of the effects of certain public and private projects on the environment
[19] Visual MODFLOW Pro, U.S. Geological Survey Modular Ground-water model 2007
[20] Danish Hydraulic Institute 2014 MIKE 21 Flow Model FM_Hydrodynamic Module_User Guide
[21] Danish Hydraulic Institute 2014 MIKE 21 & Mike 3 Flow Model FM_Hydrodynamic and Transport Module_Scientific Documentation.

Environmental Engineering and Management Journal

March 2021, Vol.20, No. 3, 467-478
http://www.eemj.icpm.tuiasi.ro/; http://www.eemj.eu

"Gheorghe Asachi" Technical University of Iasi, Romania

DETERMINATION OF THE FLOOD DEFENSE EMBANKMENT ELEVATION CROWN, USING ADVANCED HYDRODYNAMIC MODELING

Tomi Alexandrel Hrăniciuc[1*], Nicolae Marcoie[1], Cătălin Dumitrel Bălan[2]

[1] *"Gheorghe Asachi" Technical University of Iasi, Faculty of Hydrotechnical Engineering, Geodesy and Environmental Engineering, Romania*
[2] *"Gheorghe Asachi" Technical University of Iasi, Faculty of Chemical Engineering and Environmental Protection, Romania*

Abstract

The accelerated economic and social development of some urban areas has as result the construction of different social and economic objectives in areas with a potential flood risk too, although the good practices prohibit this thing. Thus, the application of different structural and non-structural measures with the defense role against flooding those areas, is necessary. The national management strategy of the flood risk provides the application of some policies, procedures and practices in order to reduce this risk, so that all the citizen to develop in a sustainable social environment. This paper has as purpose the determination of the height of this type of hydrotechnical works (embankments) with defense role against floods of social as well economic objectives. Considering that these embankments have as purpose not only the defense against floods of an inhabited area, but also the protection of some natural water resources, the work can be included in the field of environmental problems. Very important and an additional argument to the environmental problem is the fact that Lilieci Reservoir that represents also study area, was declared wildlife reserve and is part of the special avifauna protection area Lilieci with a total surface of over 2.6 km². More than 100 species of birds, live in the over 10 hectares of reeds and rushes on the territory of the reservation and on the water surface.
Many areas of our country declared natural reserves are in danger or even destroyed year by year due to devastating floods. Thus, it is necessary to take protection measures for these areas so particularly important for the biodiversity conservation. This document presents step by step the determination of the elevation crown of these works with the defense role against floods on the natural habitat, using the advanced hydraulic modelling.

Keywords: biodiversity conservation, climatic changes, environmental protection, flood risk, quasi-2D hydraulic modelling

Received: June, 2020; Revised final: December, 2020; Accepted: January, 2021; Published in final edited form: March, 2021

1. Introduction

Recently, more and more specialists from various specialized sectors, are discussing the problem of the climatic changes and their effect on different fields. Indeed, the economic and industrial development from the last hundred years, which was based on the excessive consumption of hydrocarbons, determined considerable CO_2 emissions in the atmosphere, having the effect of global warming, resulting in climatic changes throughout the Earth (Qi et al., 2019; Stentoft et al., 2021; Toaca et al., 2012).

The climate changes have had a considerably effect also on the hydrological regime from our country. Thus, the rains have acquired a torrential character, their intensity being accentuated very much, resulting in the so-called rapid floods that have catastrophic effects on the areas where they overflow (Bartha et al., 2014; Boariu, 2016; Boariu and Bofu, 2016).

*Author to whom all correspondence should be addressed: e-mail: hraniciuc_tomi@yahoo.com; Phone: 0744140682

Some of these areas represent future residential fields or even are part from the protected areas, being declared natural reserves and have as purpose the biodiversity protection and conservation. It is discussed the problem of the protection and of defending these areas against catastrophic floods that may occur during periods of the year with heavy rainfall or during the sudden melting of snow. The protection of these objectives can be made both by taking structural measures as well as non-structural measures for flood defense. It is recommended to apply both of the measures for a higher degree of protection. The non-structural measures prevent generally the catastrophes by various means, such as restricting the building permits in the areas with high flood risk, by well-developed hydrologic forecasts, by the land management, by anti-erosion measures applied at the level of the hydrographic basin and last but not least, by insuring the goods in the area exposed to risk. The structural measures are those, which include all the hydrotechnical works and constructions, with the purpose of protection against floods (Boboc et al., 2018; Cercel et al., 2015).

In this case, there will be applied structural measures for the flood defense of the area under study and namely, flood defense embankments. It is discussed how to determine more accurately and in a short time as possible, the elevation crown of these embankments so that they withstand the fierce flash floods. The answer to our problem would be the advanced hydraulic modelling, using the latest generation software. Building a hydraulic model, one can investigate in a very short time, the results obtained for different flows as well as the degree of the protection insurance, offered by the present embankments as well as the proposed ones.

2. Material and methods

The soft used to determine the elevation crown of the defense embankments is Mike 11, which is a professional engineering software for simulating flow, sediment transport and water quality in rivers, canals and other water bodies. The MIKE 11 hydrodynamic module (HD) uses an implicit, finite difference scheme for the computation of unsteady flows in rivers and estuaries (Bartha et al., 2012; Danish Hydraulic Institute, 2017a, 2017b; Waldman et al., 2017). The mathematical equations underlying modeling, are the Saint-Venant equations in one-dimensional system Eqs. (1-2) (Bartha et al., 2012).

- One-dimensional system:

Continuity equation:

$$\frac{\partial \zeta}{\partial t} + \frac{\partial (u h)}{\partial x} = 0 \quad (1)$$

Momentum equation:

$$\frac{\partial u}{\partial t} + u\frac{\partial u}{\partial x} + g\frac{\partial \zeta}{\partial x} + c_f \frac{u|u|}{h} = 0 \quad (2)$$

where: y - the water local depth; A - the cross section area; B - the width of the water surface; Z - water level (compared to baseline), defined as: $\zeta = h+z_b(m)$; h - the local water depth (m); z_b – thalweg local level (m); u - flow velocity (m/s) and c_f - the coefficient of friction (dimensionless).

MIKE 11 software is designed as an interface that includes several editors (Danish Hydraulic Institute, 2017a, 2017b).

MIKE 11 allows for two different types of bed resistance descriptions: Chezy and Manning, respectively.

The description is set in the Hydrodynamic Editor under the Bed Resistance tab. For the Chezy description, the bed resistance term in the momentum equation is described as given by (Eq. 3). For the Manning description, the term is given by (Eq. 4).

$$\frac{qQ\|Q\|}{C^2 AR} \quad (3)$$

where: Q is discharge; A is flow area; R is the resistance or hydraulic radius.

$$\frac{qQ\|Q\|}{M^2 AR^{4/3}} \quad (4)$$

The Manning number, M, is equivalent to the Strickler coefficient. Its inverse is the more conventional Manning's n. The value of n is typically in the range 0.01 (smooth channel) to 0.10 (thickly vegetated channel). The corresponding values for M are from 100 to 10. The Chezy coefficient is related to Manning's n by means of Eq. (5): (Danish Hydraulic Institute, 2017a, 2017b).

$$C = \frac{R^{1/6}}{n} = MR^{1/6} \quad (5)$$

The hydraulic model will be made using the cross sections measured through the riverbed. We will first create the one-dimensional hydrodynamic model based on which we will analyze the results, in our case, the water level. The input data will be considered the calculation and verification flow rates according to the hydrological studies for the studied area. Table 1 shows the main editors of the MIKE 11 software.

If the water level will exceed the crown of the defense works, then we must determine also the water depth resulted from the flooded meadow. In this case, a single one-dimensional hydraulic model is not enough. We will build a quasi-2D hydraulic model that can simulate also the flood plains, in case that the crown of the embankments is exceeded by the water level. It will be possible to determine the depth of the water as well as its level behind the embankments, including the assessment of the flood risk on the environment.

Table 1. Editors includes in Mike 11

Simulation editor	Hydrodynamic editor
Rivers Network editor	Advection - dispersion editor
Cross section editor	WQ, ECO - Lab editor
Boundary editor	Sediment Transport editor
Rainfall - runoff editor	Flood Forecasting editor

Very important are also other resulted hydraulic parameters such as the water speed, which is necessary for the assessment of the flood risk or the transport capacity. Based on the hydraulic model, can be performed simulations and forecasts using simultaneously also other modules such as investigations related to the quality of the water, pollutant dispersion, sediment transport, all being included in the specific problems of the environmental protection.

3. Case study

The case study is located in the northeastern part of Bacau City, Romania, along Bistrita riverbed, downstream of Lilieci accumulation, as shown in Fig. 1. This is a protected area of national interest that corresponds to the class IV (natural reserve of avifauna type). The present work has as purpose the determination of the elevation crown of the defense embankments against floods based on the levels in Bistrita River downstream of Lilieci accumulation, for flows with certain calculation probabilities.

The levels in the riverbed have been determined, according to the flow with the probability of 1% having the value of 1900 cbm/s, the flow with the probability of 0.5% having the value of 2215 cbm/s, the flow corresponding to the value of the maximum capacity of discharge from Lilieci lake having the value of 1960 cbm/s as well as the flow with the probability of 0.1% having the value of 3585.3 cbm/s.

For the study area, topographic measurements were made for the determination of the cross sections, necessary for building the hydraulic model. On the right bank of Bistrita River, there is already a defense embankment against floods. In the future, it is proposed to build a new defense embankment against floods on the left bank of Bistrita River, downstream of Lilieci accumulation, which will protect against floods a future area of community interest, as shown in Fig. 2.

The problem is to determine the elevation crown of the new proposed embankment on the left bank of Bistrita River, so that this to not be exceeded by the extreme floods. It will be also determined the protection degree of the present embankment on the right bank, namely at which flows resists without exceeding the crown.

The modelling will be made in permanent motion, namely constant flows, introduced in the model at the upstream end. The cross sections will be divided in the minor riverbed, respectively the major left riverbed and major right riverbed. The roughness coefficient „n" in the minor riverbed, after Manning, was considered n = 0.05, in the idea of taking a safety margin, regarding the existence in the riverbed of some big river boulders, trees, rich vegetation that increases the roughness coefficient. Regarding the roughness coefficient from the major riverbed, this was considered according to the use of the land on the two banks, consulting the orthophoto plans corresponding to the studied sector

Fig. 1. Case study location

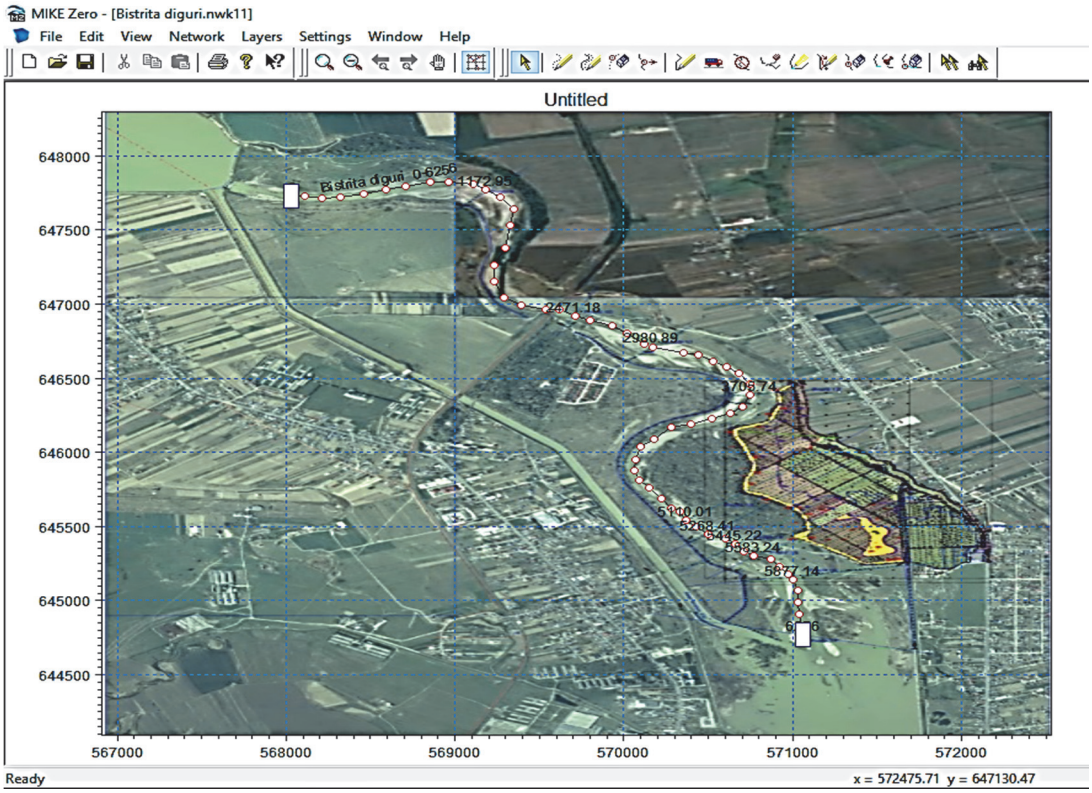

Fig. 2. Area of study

Thus, for the forest was considered the roughness coefficient n= 0.15, for orchards, n=0.10, for unproductive land n=0.07, for grasslands n=0.05 and for arable land n=0.05 (Hraniciuc et al., 2016, 2017a, 2017b). It will be create first a unique one-dimensional 1D hydraulic model, based on the cross sections measured through the riverbed. If the crown of the proposed embankment is not exceeded by the water level correspondingly to the probabilities taken in account, then the study is considered completed. But if for one of the flows, the water level exceeds the elevation crown of the proposed embankment, the building of quasi-2D model is needed in order to be able to analyze the effects of the flood wave on the protected area.

Once we have chosen the type of the model (hydrodynamic in our case), we practically go the basic stages to start a simulation. (Hraniciuc et al., 2016, 2017a, 2017b). The first stage involves editing the river networks. The river networks editor has two main functions:

- introduction and editing of the network;
- overview of all model information from the current simulation.

The network editing includes:

- digitization of the river networks and their connection;
- defining the hydraulic structures on each river;
- defining the entry points within a river basin.

The digitization of the network was made based on the *georeferenced orthophoto* plans from the respective area, as shown in Fig. 3. The built hydrographic network is indicated by the dotted line and the black numbers present on it represent the chainage where the cross sections are located.

The second stage represents the editing of the cross sections. The editor of the cross sections manages all the cross sections stored, but allows also to be viewed (Hraniciuc et al., 2016, 2017a, 2017b). Each cross section is unique and is identified by the following three keys:

- the name of the river;
- topographic identification;
- chainage;

There are two types of data on the cross sections:

- gross and unprocessed measured data;
- processed derived data.

Fig. 4 represents the positioning in the plan of the cross sections and in Fig. 5 is presented the visualization of a section and the characteristic gross data. Fig. 5 shows both the raw data of a cross section, such as the coordinates of each point, the roughness coefficient in both the minor and major riverbed, chainage, present on the left side of the figure and the allure of the cross section on the right side drawn with black line. The red vertical lines divide the section into minor riverbed and major riverbed using some markers and the blue lines indicate the variation of the roughness coefficient over the entire section.

The next stage is the editing the boundary conditions. This editor is used to specify the boundary conditions for a certain model from MIKE 11. It is used not only to specify the usual boundary conditions like the water level, the inlet flow rates or the inlet

hydrographs but also to specify the lateral flows, outflows along a river, concentration of solutions in a hydrograph, different meteorological data and certainly, boundary conditions used in the connection with the structures applied to the model.

The introduction of boundary conditions is very important. We cannot practically run the modelling without having introduced these conditions. In Fig. 6 can be seen the file of the boundary conditions for the case study.

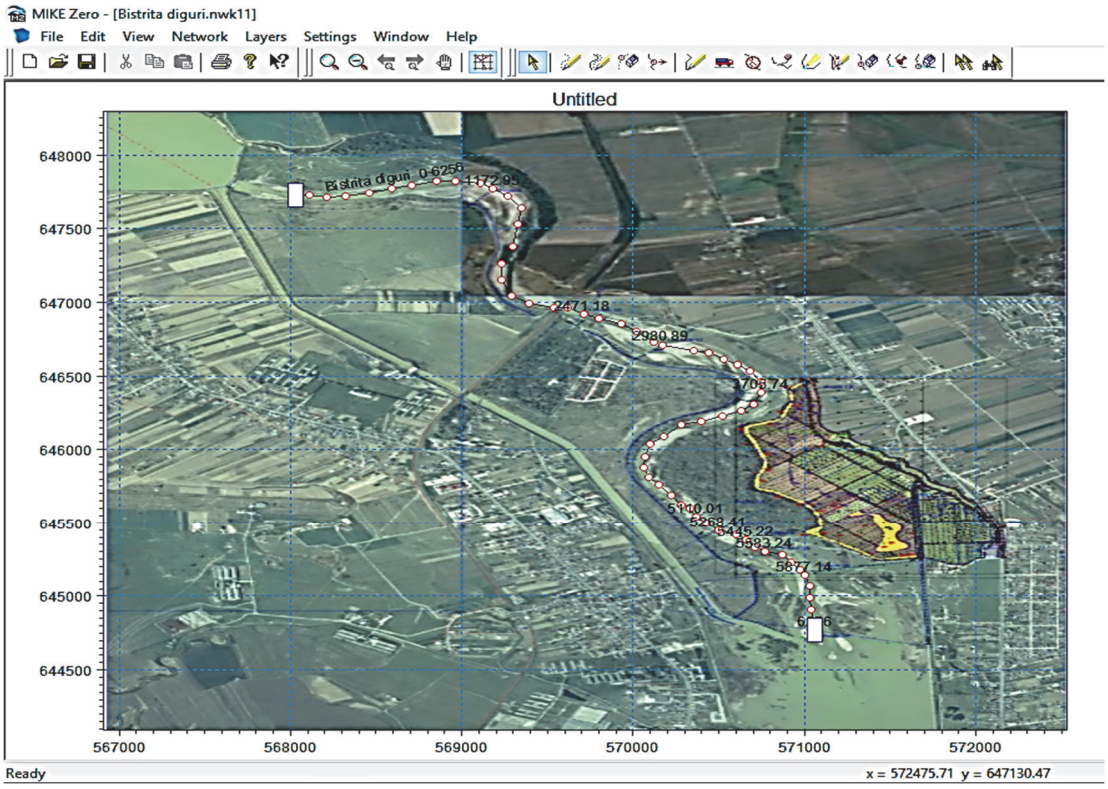

Fig. 3. The hydrographic network (downstream sector of Lilieci accumulation)

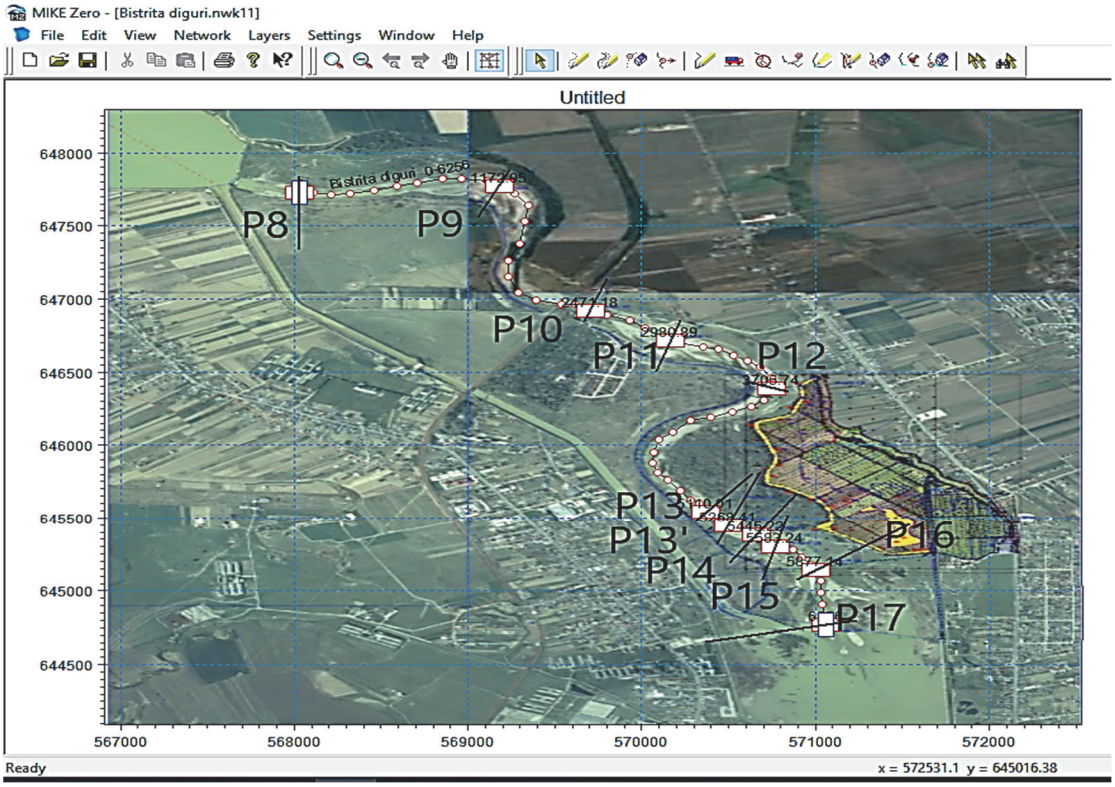

Fig. 4. Positioning of the cross sections (P8-P17)

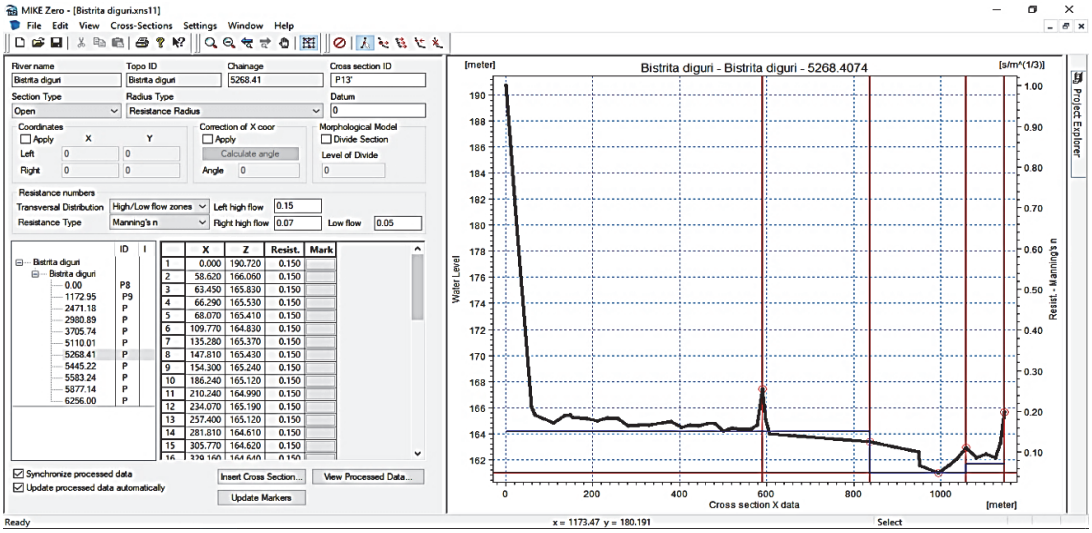

Fig. 5. View on the gross data of a cross section

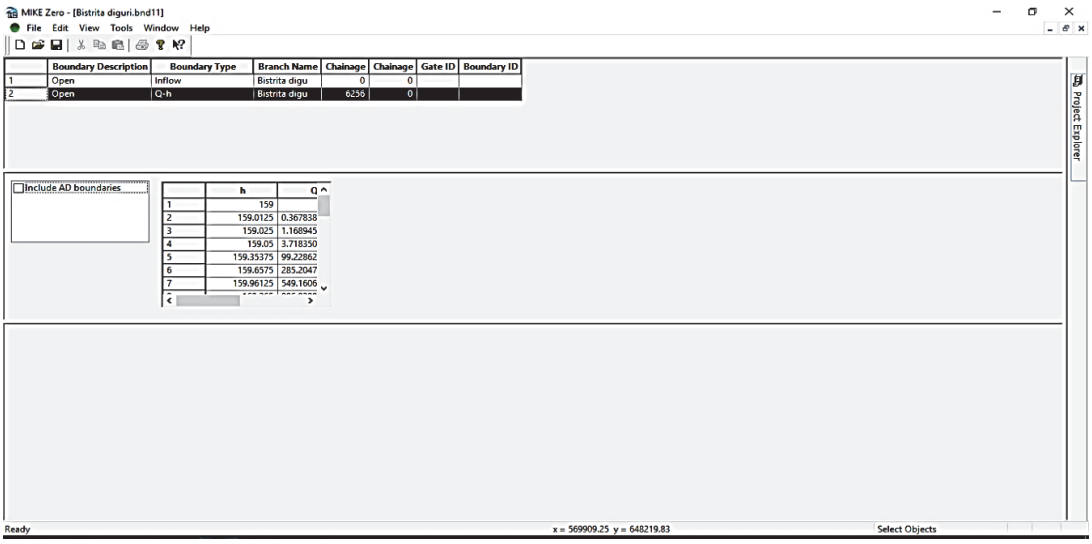

Fig. 6. Boundary condition in the relation flow-level

The last stage involves editing the hydrodynamic model. This editor is used for setting the additional data used in simulation. Most of the parameters in this editor have unspecified values and, in most cases, it is enough to get satisfactory simulation results. Among the additional parameters, we can list: initial conditions such as the level, the flow, the depth, conditions regarding the influence of the wind, of the waves, resistances in calculations, different coefficients, maps, etc. In Fig. 7 can be observed the window for editing the initial conditions, which in the present case are null. Was not introduced any initial flow rate through the riverbed, and no initial water depth (Hraniciuc et al., 2016, 2017a, 2017b).

After introducing these last conditions, practically one can start the simulation, if we don't have any errors introduced in the other editors.

4. Results and discussion

The simulation was made in permanent motion, namely, constant flows were introduced as boundary conditions, for the probabilities reminded in the paragraphs. First, we interpret the results for the one-dimensional 1D hydraulic model, considering the proposed embankment for the left bank of the river (Hraniciuc et al., 2016, 2017a, 2017b). Have been introduced in the model 11 cross sections designated P8, P9, P10, P11, P12, P13, P13', P14, P15, P16 and P17. Thus, will be analyzed the water level resulted for each flow, in longitudinal profile an in each cross section. Will compare these levels with the elevation crown of the proposed embankment on the left bank, but also with that on the right bank, following if they are exceeded by the resulted levels. Thus, for the flow with the flow rate with the probability of 1%, Q=1900 cbm/s, in longitudinal profile, the water level is shown in Fig. 8.

Above the blue contour that represents the water level, the line of the right bank can be observed (immediately above the water level, figured with continuous line, and the line of the left bank much higher with discontinued line). One can observe that none of the banks is exceeded by the water level.

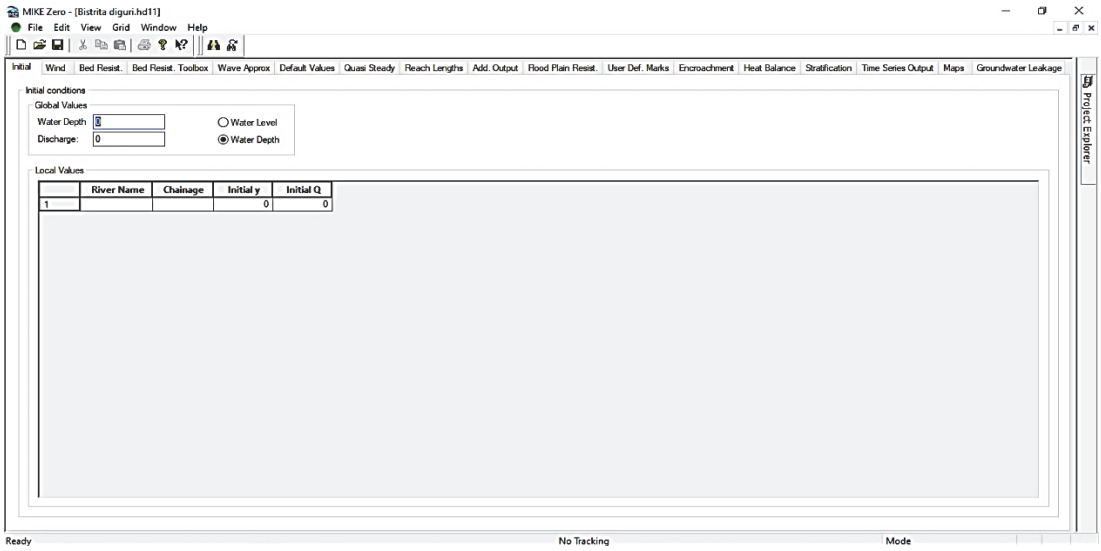

Fig. 7. Initial conditions

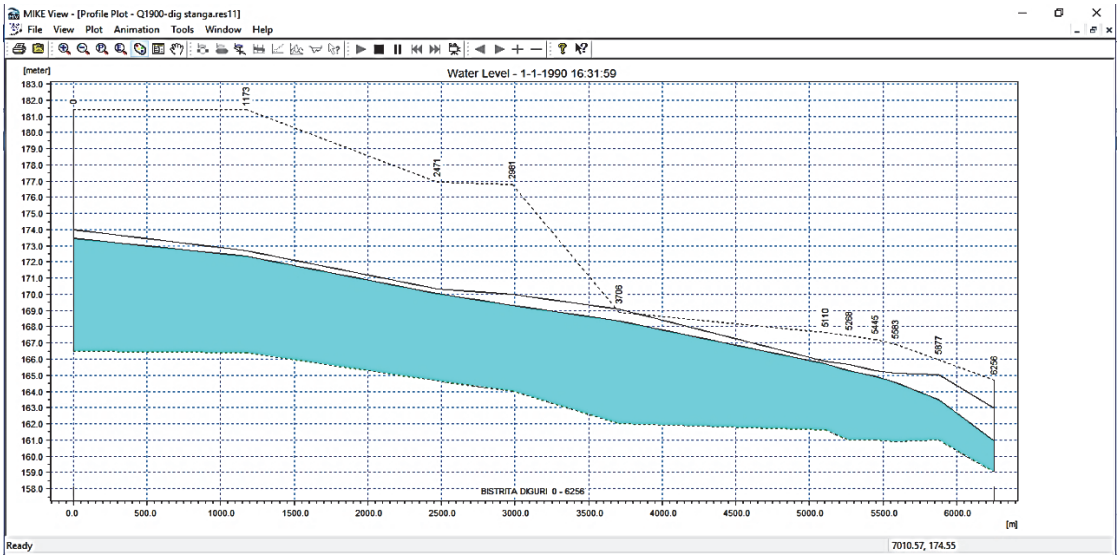

Fig. 8. The free water level in longitudinal profile (Q=1900 cbm/s)

In Fig. 9, we will show as example, the water level from the section P14, where the two embankments on the left bank, respectively the right bank can be observed. In Fig. 10 can be observed the maximum water levels in all the sections of the model.

The legend shows the water level in each cross section indicated by the chainage of the section, from 0 for section P8 to kilometer 6256 for section P17, in chronological order. You can also see the color associated with each cross section corresponding to the lines with the water level resulting from the graph. As it can be seen in the situation with the proposed embankment on the left bank, for the flow with the probability of 1% with Q=1900 cbm/s, the free water level doesn't exceed the crown of the existent embankment on the right bank and doesn't exceed the crown of the proposed embankment on the left bank of the river. The proposed embankment on the left bank of the river is included in the model in the cross sections from P12 up to P15 inclusive.

For the flow rate Q=1960 cbm/s resulted from the modelling that neither the crown of the embankment existent on the right bank, nor the crown of the proposed embankment on the left bank, are exceeded by the water level.

For the flow with the probability of 0.5%, with Q = 2215 cbm /s, Fig. 11 shows the water level resulted in the longitudinal profile.

For the flow with the probability of 0.5% having Q = 2215 cbm/s, from the analysis of the results, it was observed that the maximum water level doesn't exceed in any section the crown of the proposed embankment on the left bank of the river. Thus, the water level is very close to the elevation crown of the proposed embankment in section P12, as it can be seen in Fig. 12, so there is no danger level. (Hraniciuc et al., 2016, 2017a, 2017b).

Regarding the crown of the existent embankment on the right bank, this is exceeded by the maximum water level in the sections P9, P10, P13.

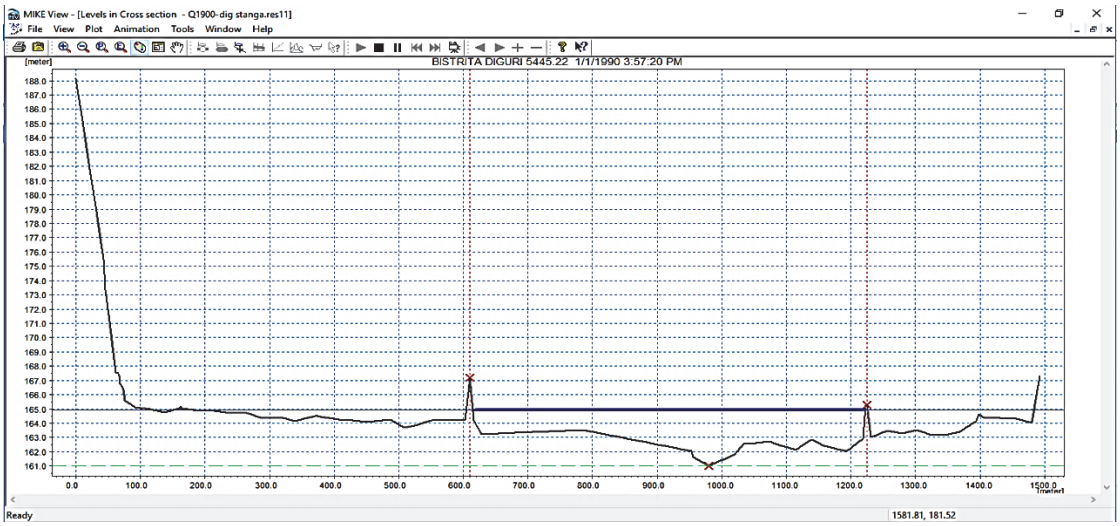

Fig. 9. The free water level in the section P14 (Q=1900 cbm, /s) - doesn't exceed the crown of the embankments

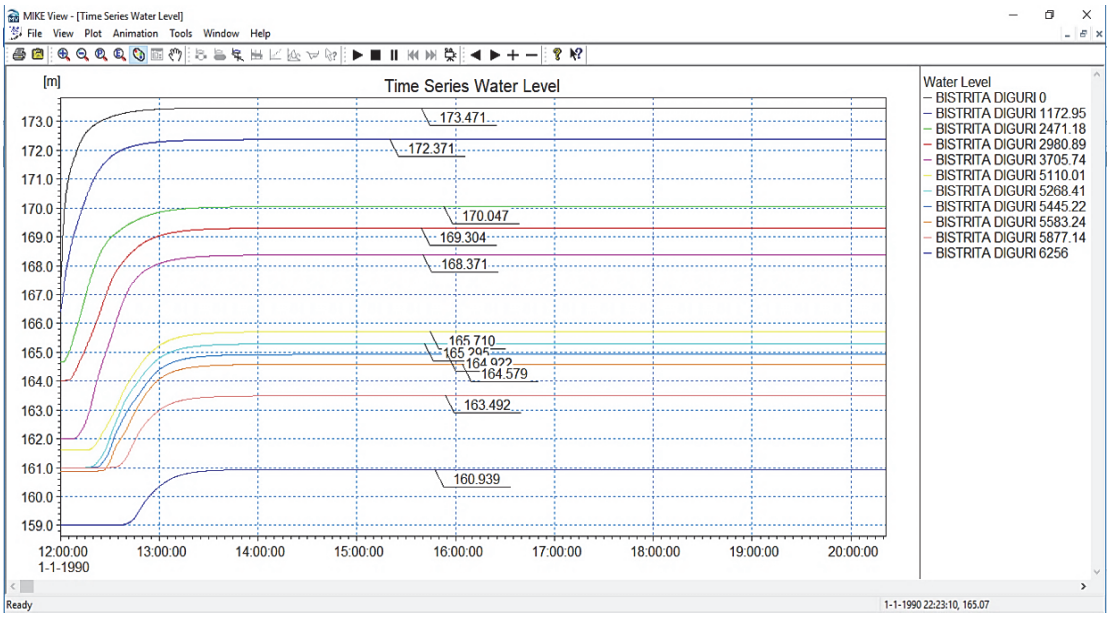

Fig. 10. The maximum water levels in all sections from P8 up to P17 (Q=1900 cbm/s) - regime arranged with the proposed embankment on the left bank

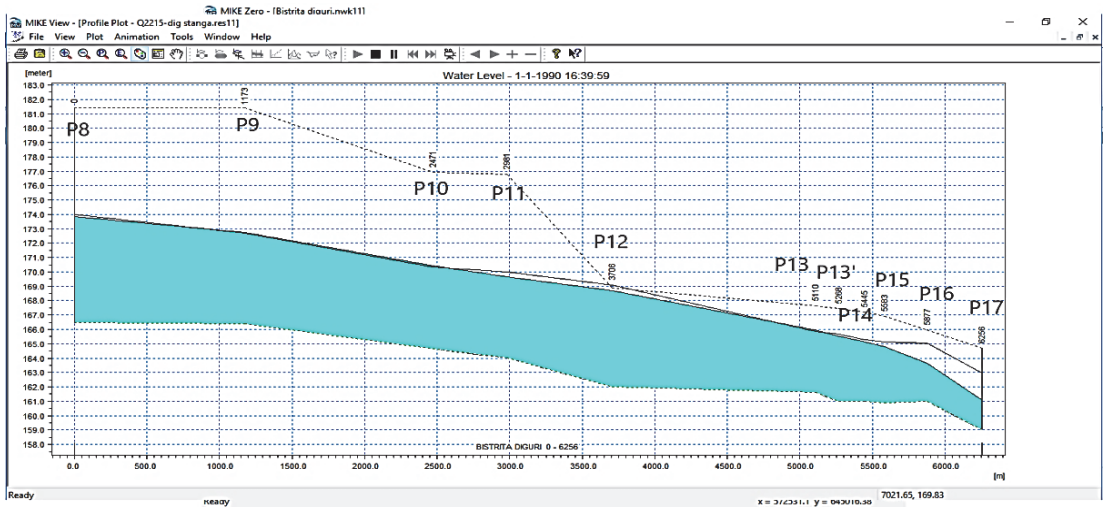

Fig. 11. The free water level in longitudinal profile (Q=2215 cbm/s)

Next, we will analyze the results, in case of building a new quasi-2D model too. This model is necessary to be built in case that we have floodplains, like the land behind a flood defense embankment, as in Fig. 13. The 1D image shows how to represent a simple one-dimensional hydraulic model, based only on simple cross sections. This model cannot simulate the flow in floodplains. The quasi-2D image shows how the quasi-2D hydraulic model is represented, and is a model that can simulate flow in a floodplain as represented in the middle image. The 2D image shows how to represent a two-dimensional hydraulic model, which is based on a numerical terrain model for simulation and not on cross sections as in 1D and Quasi-2D. The 1D-2D image shows a combined hydraulic model 1D with 2D, applied on a sector where both the data from the cross sections and the data from the numerical terrain model are used. The combined models are used if in a region we do not have exact data from the minor riverbed and then we use the cross sections, and in the major riverbed we use the data from the numerical model of the terrain.

In case of the quasi-2D model, two separate connections will be built. One will represent the main river, the other will represent the floodplain behind the proposed embankment. They will be connected at the level of the crown of the embankment of a channel that will allow the water to pass over the embankment only in case that the crown will be exceeded by the water level. The resulted network can be observed in Fig. 14. Practically a second connection was built containing the floodplain behind the embankment on the left bank.

Thus, the section behind the embankment will be filled with water only in the case that the embankment is exceeded by the water level from the main river. One simple 1D model cannot model this passage over the crown of the embankment and to show how deep the water would be in each section, so the construction of the quasi-2D model was necessary.

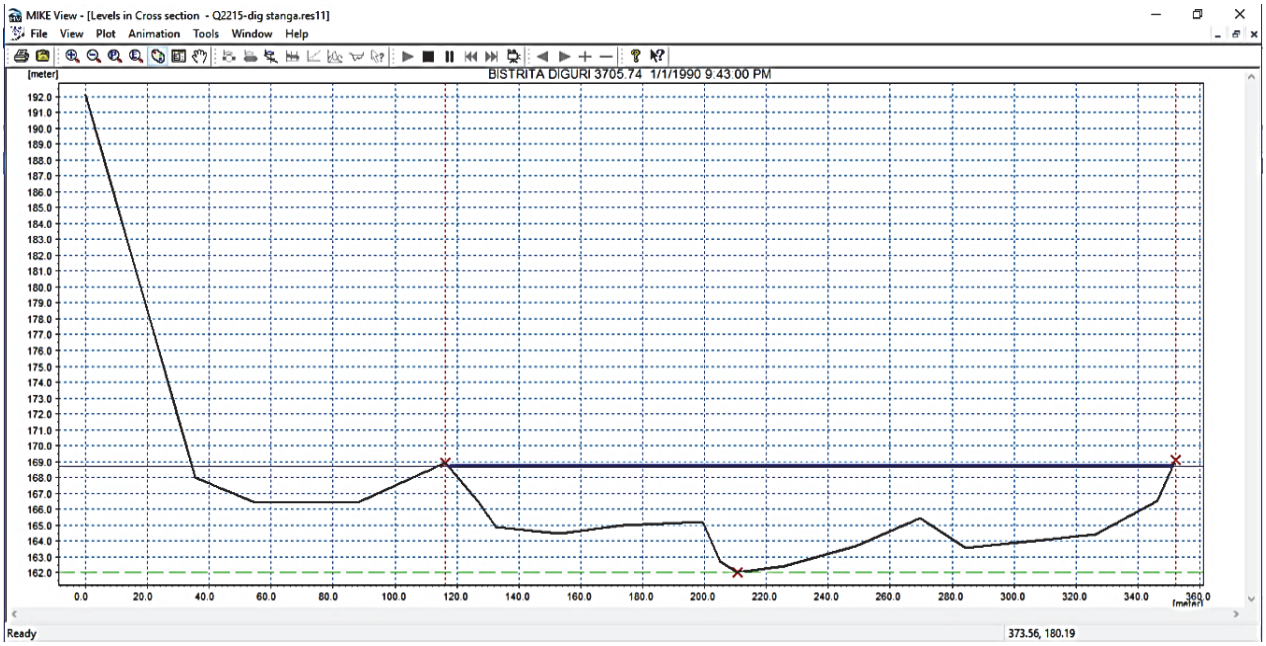

Fig. 12. The free water level in the section P12 (Q=2215 cbm/s)

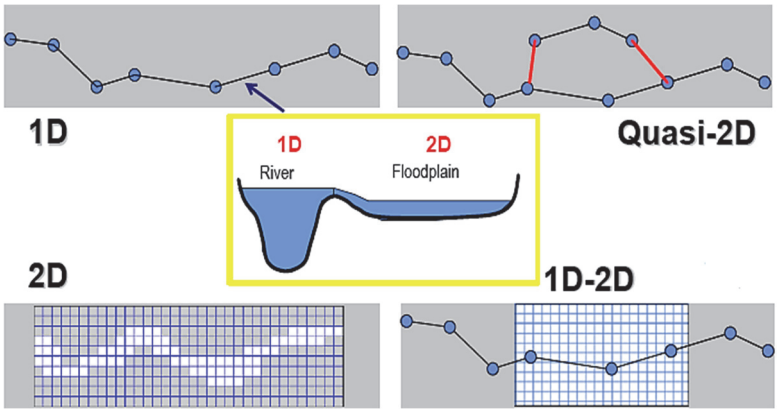

Fig. 13. Types of numeric models used for flood modelling

Following the simulation for the quasi-2D network, it was noted that for the flow with the probability of 1% as well for the flow with the probability of 0.5%, the crown of the embankment on the left bank is not exceeded. For the flow with the probability of 0.1% having the value Q (0.1%)=3585.3 cbm/s, the results of the modelling were centralized in the Table 2. For the flow with the probability of 0.1% it can be seen that the only one section where the crown of the embankment is exceeded, is in section P12. The result is a difference of 77 cm between the maximum water level resulted in Bistrita River and the crown of the embankment, the water overflowing the embankment.

This thickness of the overflowing blade of 77 cm, could cause a big breach in the body of the embankment on a significant length, considering that between the section P12 and P13 which is quite large distance, we don't have any information about the level of the crown of the embankment (no other section). In the other sections, the crown of the embankment is not exceeded by the water level, the minimum difference being 90 cm. In Table 3 are shown the maximum water levels, the lowest elevations of the land and the depths resulted in the corresponding sections behind the embankment (flooded plain).

It can be seen that a water depth between 3 m and 4.5 m results, which means a very high risk of floods for the land behind the embankment. The results can be also seen in longitudinal profile as in Figs 15 and 16.

Fig. 14. Quasi - 2D network

Table 2. The results in Bistrita River for Q (0.1%)=3585,3 cbm/s

Cross section	*Chainage*	*Heights of the embankment crown*	*Water level in Bistrita River*
P12	3705.74	168.90	169.671
P13	5110.01	167.62	166.708
P13'	5268.41	167.44	166.274
P14	5445.22	167.21	165.913
P15	5583.24	166.94	165.484

Table 3. The results with the water level behind the embankment for Q (0.1%) = 3585.3 cbm/s

Cross section	*Chainage*	*The lowest level of the land (m)*	*Maximum water level (m)*	*Maximum water depth (m)*
P12	12	166.42	169.779	3.359
P13	1296.95	164.72	167.767	3.047
P13'	1440	164.20	167.760	3.560
P14	1640	163.68	167.755	4.075
P15	1750	163.25	167.754	4.504

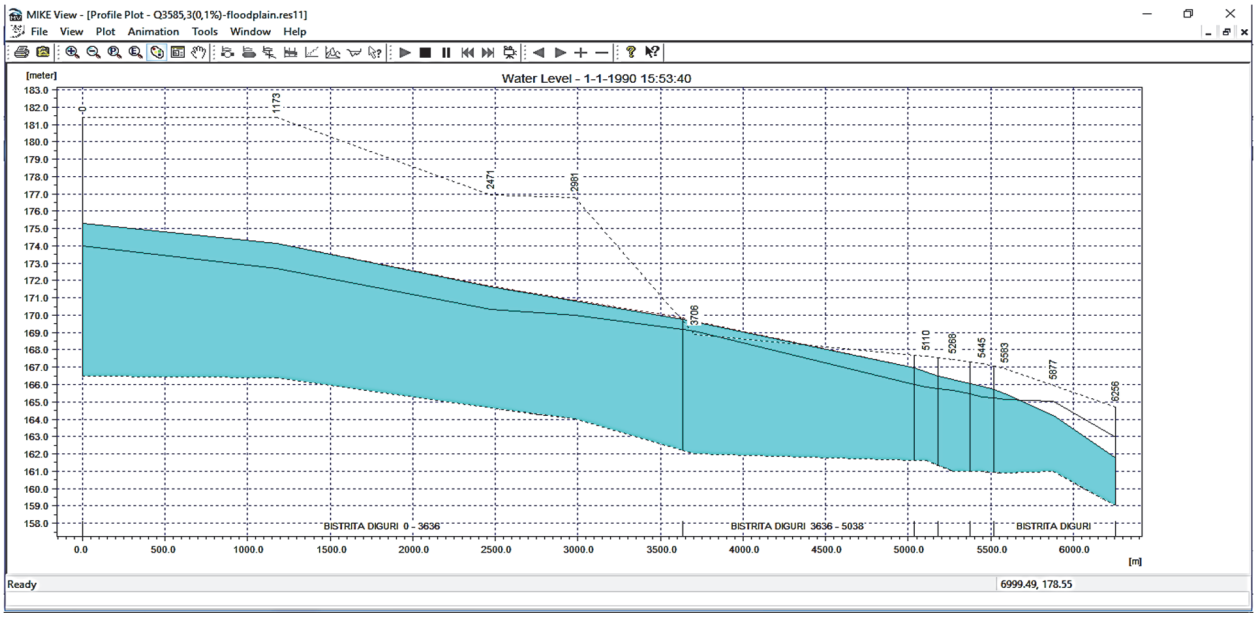

Fig. 15. The maximum water level in Bistrita River for Q 0.1% in longitudinal profile

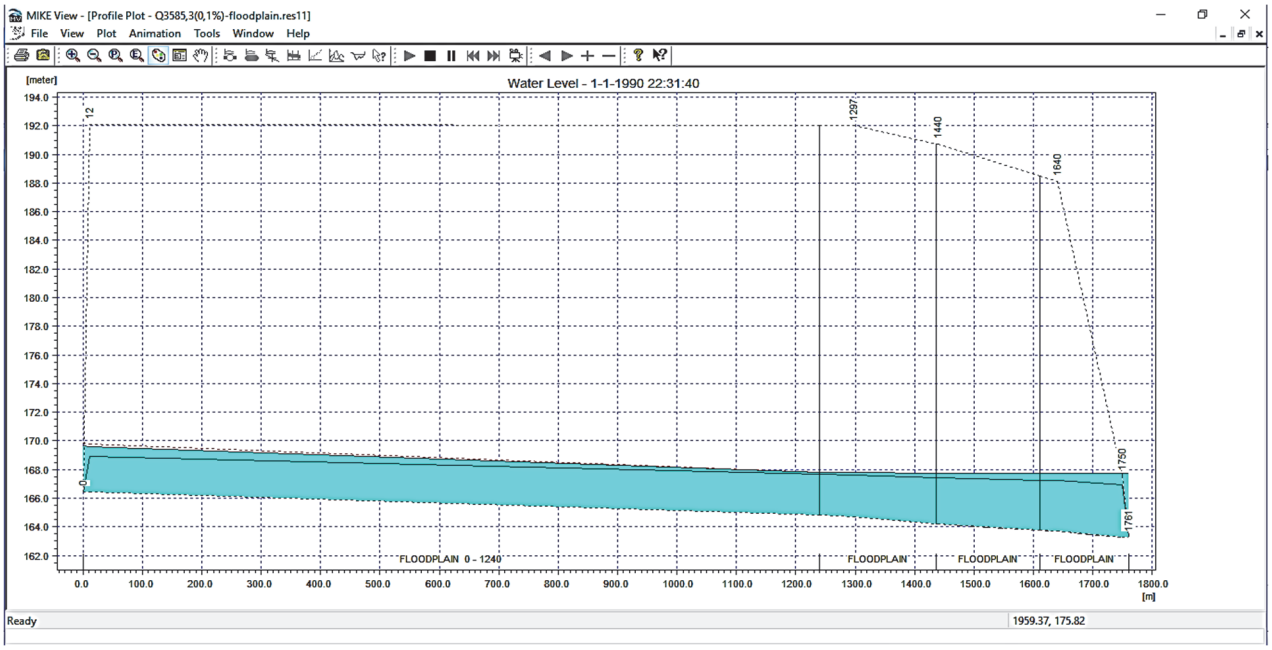

Fig. 16. The maximum water level behind the embankment (the floodplain between the sections P12-P15) for Q 0.1% in longitudinal profile

5. Conclusions

Due to the intensive increase of the volume of waste, of air and water pollution, the environmental problems should be treated with more interest in the future by specialists in all fields. The climatic changes cause also more and more imbalances at the level of the planet. One of the effects is the change of the hydrologic regime. Thus, in some regions, the rains became more aggressive in terms of intensity, resulting in massive hydrologic runoff. These runoffs lead inevitably to floods that can cause major flooding of the areas with high risk for this type of hazard. We can avoid in such way a social, economic and environmental risk.

This document has as purpose the determination of elevation crown for the defense works against floods in a region that was declared wildlife reserve. Thus, on the sector of Bistrita River, downstream of Lilieci accumulation, from Bacau County, on the left bank of the river was proposed the building of a flood defense embankment in order to protect a land surface from the risk of floods. This defense work should resist and must not be exceeded by the water levels for flows with probabilities up to 0.1%, namely the flow that can occur once every thousand years.

In order to determine the level corresponding to this flow and more than this, the volume and the depth of the water resulted behind the embankment in

case that this could be exceeded, the hydraulic model was used. The hydraulic model became in the last time an indispensable tool for all specialists in this field, because the manual classical calculations have no satisfactory results in certain situations, respectively, the results based on the model are more accurate and explicit. The working time is also much shorter than the classical calculations used in the past, and so, in crisis situations, the modelling becomes even more a priority.

It can be seen from the results of the modelling, that it was possible to determine with accuracy in all sections, the water level for all the flows taken in account, as well as the protection degree of the proposed embankment. Very important, it can be seen that the water depth behind the embankment could be determined, in case that its crown was exceeded by the water level corresponding to the flow with the probability of 0.1%. The classical calculations would find these values with greater difficulty. For this, a quasi-2D model was necessary, the simple 1D models not being able to predict the water passage over the crown of the embankment.

It was found after running the program that the crown of the embankment is not exceeded by the water level corresponding to the flows with probability of 1% and 0.5%. Instead, for the probability of 0.1% occurs an exceeding of the crown of the embankment near section P12 close to section P13. Thus, in order to ensure the maximum protection degree, the crown of the embankment between the sections P12 and P13 should be raised with at least 0.5 m above the maximum water level, corresponding to the flow with the probability of 0.1% of Bistrita River.

In conclusion, the use of the modern software for hydraulic modelling, for solving such environmental problems is recommended, due to the strong tools it has, the speed of finding the results and last but not the least its explicit visualization.

References

Bartha I., Vlad L.M., Toma D., Toaca D., Cotiusca-Zauca D., (2014), Rehabilitation and extension of wetlands within floodplains of embanked rivers, *Environmental Engineering and Management Journal,* **13**, 3143-3152.

Bartha I., Marcoie N., Toma D., Toaca D., Gabor V., Molnar A.G., Lupusoru A., (2012), *The Free Level Post-Darcy Filtration Through Homogenous Media*, Conf. on Modelling Fluid Flow (CMFF'12), The 15th Int. Conf. on Fluid Flow Technologies, Budapest, Hungary, September 4-7, Conf. Proc., vol. II, 622-627.

Boariu C., (2016), Safety assurance on existing dams. Case study - Sarca Dam, *Bulletin of the Polytechnic Institute of Iasi, Hydrotechnics Section*, **62**, 59-66.

Boariu C., Bofu C., (2016), Works with a minimum environmental impact in riverbeds, *Environmental Engineering and Management Journal*, **15**, 1205-1211.

Boboc V., Sarbu G.C., Marcoie N., Toma D., (2018), *Aspects Regarding Modeling of the Flood Caused by Earth Dams Failure*, Proc. 18th Int. Multid. Sci. Geoconference SGEM 2018, vol. 18, 79-86.

Cercel P., Boariu C., Vorovei C., (2015), The rehabilitation and assurance the abandoned hydro accumulations, Case study, *Bulletin of the Polytechnic Institute of Iasi, Hydrotechnics Section*, **LXI**, 1-2.

Danish Hydraulic Institute, (2017a), MIKE 11, A Modelling System for Rivers and Channels, Reference Manual, On line at: https://manuals.mikepoweredbydhi.help/2017/Water_Resources/Mike_11_ref.pdf.

Danish Hydraulic Institute, (2017b), MIKE 11, A Modelling System for Rivers and Channels, User Guide, On line at: https://manuals.mikepoweredbydhi.help/2017/Water_Resources/MIKE11_UserManual

Hraniciuc T.A., Boariu C., Bofu C., (2016), *Calibration of Minor Bed Rivers Hydraulic Parameters Using Modern Software,* Proc. 16th Int. Multid. Sci. GeoConference SGEM 2016, Albena, vol. 1, 105-112.

Hraniciuc T.A., Cercel P., Boariu C., Bofu C., (2017a), *Creating Flood Hazard Maps Using 2D Hydraulic Models,* Proc. 17th Int. Multid. Sci. Geoconference SGEM 2017, Albena, vol. 17, 173-182.

Hraniciuc T.A., Cercel, P., Trofin F., Boariu C., Bofu C., (2017b), *Considerations on Water Storage Lakes Safety in Case of Extreme Meteorological Phenomena. Case Study - Mileanca Water Storage Lake,* Proc. 17th Int. Multid. Sci. Geoconference SGEM 2017, Albena, vol. 17, 165-172.

Qi W., Liu J., Leung F., (2019), A framework to quantify impacts of elevated CO_2 concentration, global warming and leaf area changes on seasonal variations of water resources on a river basin scale, *Journal of Hydrology,* **570**, 508-522.

Stentoft P.A., T. Munk-Nielsen T., Møller J.K., Madsen H., Valverde-Pérez B., Mikkelsen P.S., Vezzaro L., (2021), Prioritize effluent quality, operational costs or global warming? – using predictive control of wastewater aeration for flexible management of objectives in WRRFs, *Water Research*, 116960, https://doi.org/10.1016/j.watres.2021.116960

Toaca D., Bartha I., Marcoie N., Gabor V., Toma D., Lupusoru A., (2012), Effect of groundwater abstraction from wells on aquifers, *Journal of Environmental Protection and Ecology*, **13**, 764-774.

Waldman S., Bastón S., Nemalidinne R., Chatzirodou A., Venugopal V., Side J., (2017), Implementation of tidal turbines in MIKE 3 and Delft3D models of Pentland Firth & Orkney Waters, *Ocean & Coastal Management,* **147**, 21-36.

Environmental Engineering and Management Journal

December 2011, Vol.10, No. 12, 1959-1966
http://omicron.ch.tuiasi.ro/EEMJ/

"Gheorghe Asachi" Technical University of Iasi, Romania

THE FREE LEVEL UNIFORM POST-DARCY FILTRATION THROUGH A SPHERE-MADE HOMOGENOUS MEDIUM

Iosif Bartha*, Nicolae Marcoie, Daniel Toma, Daniel Toacă, Victor Gabor, Aron Gabor Molnar

"Gheorghe Asachi" Tehnical University of Iasi, Faculty of Hydrotehnical Engineering, Geodesy and Environmental Engineering, Department of Hydroamelioration and Environmental Protection, 65 Prof.dr.docent Dimitrie Mangeron Street, 700050, Iasi, Romania

Abstract

This paper refers to the post-Darcy free level uniform filtration. The capillary tube fascicle model is applied to this filtration. The theoretical Chézy coefficient is computed and also experimentally verified for a homogenous and isotropic material, made of glass spheres. The typical features for the free-level post-Darcy filtration (depending on slope) are the lover, critical and higher stages flows.

Key words: post-Darcy filtration, free level flows, hydraulic parameters, the capillary tube model

Received: August, 2011; Revised final: December, 2011; Accepted: December, 2011

1. Introduction

Engineering practice is frequently using filtering structures and materials including voids in which the motion of free level liquids overruns the Darcy law's volubility domain which is acceptable for laminar flows and weak inertia (up to a $Re_{d_p} < 4$).

Such flows correspond to the Forchheimer zone of high inertia ($\mathrm{Re}_{d_p} = 4...180$), to the transition zone ($\mathrm{Re}_{d_p} = 180...900$) and to the turbulent zone ($\mathrm{Re}_{d_p} > 900$) (Comiti et al., 2000). Such flows occur through filtering dams, filtering bridges (Bogomolov and Konstantinov, 1962), flows in the mobile river beds (Klark, 2005) in debries gullies, permeable marine dams etc.

The post-Darcy free level uniform filtration takes place for hydraulic gradients $i < 1$ and implies the taking into account of the inertial losses, not only of the viscous ones (Montillet et al., 2006).

For the description of motion we use the filtration model that uses the parallel capillary tubes fascicles (Comiti and Renaud, 1989).

For post Darcy motions, implying viscous and inertial frictions, the λ coefficient has the next form:

$$\lambda = \frac{a}{\mathrm{Re}_{d_p}} + b \tag{1}$$

where a and b are coefficients, and Re_{d_p} is the Reynolds number computed for the pores' fictive diameter d_p.

The theoretical deductions, experimentally calibrated (Bartha et al., 2010a; Montillet, 2004; Wahyudi et al., 2002) are leading to the next equation:

$$\lambda = \frac{64}{\mathrm{Re}_{d_p}} + 0.7743 \tag{2}$$

* Author to whom all correspondence should be addressed: e-mail: i_bartha@yahoo.com

In the zone of rough turbulence, $\lambda \approx 0.7743$, and the effect of viscous energy losses being negligible (Bartha et al., 2010; ID_2298, 2010).

2. The free level post-Darcy uniform filtration in homogenous and isotropic media

This type of filtration implies that the axis of bed's bottom, the piezometrical line and the energy line must be parallel (Fig. 1).

$$i_t = i_p = i_e = \frac{\Delta H}{L} = tg\theta \sim \sin\theta \tag{3}$$

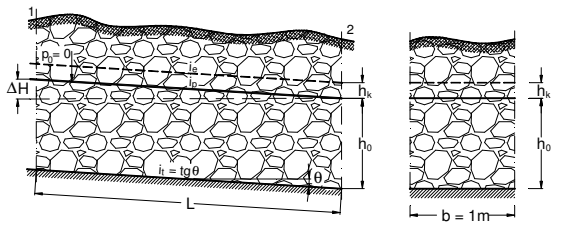

Fig. 1. The post-Darcy uniform filtration

The parameters of uniform filtration are: the normal depth h_0, the apparent normal velocity V_0, for the condition of equation 3, the underground channel bed being uniformly tilted to an angle θ and conveying the specific flow:

$$q = \frac{Q}{b} \tag{4}$$

From the Weisbach relation for head losses:

$$i = \frac{\Delta H}{L'} = \lambda \frac{1}{d_p} \frac{V_0^2}{2g} \tag{5}$$

The post-Darcy filtration apparent velocity results as:

$$V_0 = \sqrt{\frac{2 \cdot g \cdot d_p}{\lambda}} \sqrt{i} = k_{pD} \sqrt{i} \tag{6}$$

where k_{pD} is the post-Darcy filtration coefficient.

The real path of filtration is actually longer (through the model's tortuous tubes), being even amplified by the tortuosity:

$$L' = \tau L \tag{7}$$

where τ is the tortuosity $(\tau > 1)$. Just in case, the theoretical tortuosity can be accepted, as it is given by Schlichter (Forchheimer, 1914)

$$\tau = \frac{1 + \cos\delta}{\sin\delta \sqrt{1 + 2\cos\delta}} \tag{8}$$

or the values resulted from experiments conducted with the pressurized infiltrometer (Bartha et al., 2010a; Bartha et al., 2010b;). The setting angle for the uniform spheres has been marked with δ (for rhomboidal setting $\delta = 60°$).

Due to fact that the filtration real path is superior to the geometrical path, the calculation slope is inferior to the geometrical one, $i = i_p / \tau$.

For the post-Darcy filtration the equation of the apparent velocity is acceptable under the form given by Chézy and proposed by Izbas (Bogomolov and Konstantinov, 1962).

$$V_0 = c_f \mathrm{n} \sqrt{d_s i} \tag{9}$$

where: n is the porosity, d_s – the diameter of solid particles of the permeable medium and c_f – the Chézy coefficient. Izbas C.V. has considered the filtration model on a filtering material made of identical spheres having a diameter d_s.

The Chézy coefficient can be approximately computed as it follows:

- for rounded solid particles, with $0.7 \text{ cm} \le d_s \le 5.75 \text{ cm}$, $n = 0.4$ and $0.1 < i < 1$

$$c_f = 20 - \frac{14}{d_s} \tag{10}$$

- for rugged solid particles with $d_s < 5$ cm

$$c_f = 20 - \frac{5}{d_s} \tag{11}$$

In Eqs. (9), (10) and (11) d_s is expressed in *cm*, the velocity results in *cm/s,* and the Chézy coefficient in $cm^{0,5} / s$ (Bogomolov and Konstantinov, 1962).

By admitting the filtration model in a fascicle of tortuous equivalent capillary tubes (Bartha et al., 2010; Comiti and Renaud, 1989), for the filtration apparent velocity, the next equation is proposed:

$$V_0 = C_{pD} \cdot n \cdot \sqrt{d_p \cdot i} \tag{12}$$

in which the tortuous tubes diameter is d_p, the calculation slope is i (it depends on tortuosity) and C_{pD} is the Chézy coefficient for the post-Darcy filtration.

From Eqs. (6) and (12) the post-Darcy filtration coefficient is now resulting:

$$k_{pD} = c_{pD} \cdot n \sqrt{d_p} = \sqrt{\frac{2gd_p}{\lambda}} \tag{13}$$

The real velocity within tortuous cylindrical fictive pores is:

$$V = \frac{V_0}{n} \tag{14}$$

The diameter of the cylindrical fictive pores can be computed from:

$$d = \frac{4n}{(1-n)A_d} \tag{15}$$

where A_d is the specific dynamic fictive area defined by:

$$A_d = \frac{\text{The area of the particle exposed to flow}}{\text{The volume of the solid particle}} \tag{16}$$

The specific static area is:

$$A_s = \frac{\text{The average area of the solid particle}}{\text{The average volume of the solid particle}} \tag{17}$$

(Comiti and Renaud, 1989).

Generally $\frac{A_d}{A_s} < 1$, and the value $\frac{A_d}{A_s} = 1$ appears only for permeable medium made of individual particles with punctual mutual contact.

For spherical particles:

$$A_d = A_s = \frac{6}{d_s} \tag{18}$$

respectively:

$$d_p = \frac{2}{3}\frac{n}{1-n}d_s \tag{19}$$

From Eqs. (2) and (13) it results:

$$k_{pD} = \sqrt{\frac{2gd_p}{\frac{64}{\mathrm{Re}_{d_p}} + 0.7743}} \tag{20}$$

respectively:

$$C_{pD} = \frac{1}{n}\sqrt{\frac{2g}{\frac{64}{\mathrm{Re}_{d_p}} + 0.7743}} \tag{21}$$

in which:

$$\mathrm{Re}_{d_p} = \frac{\rho V_0 d_p}{\mu} = \frac{2}{3}\frac{\rho V_0}{\mu}\frac{n}{1-n}d_s \tag{22}$$

The Eqs. (20) and (21) are valid for filtration that takes place in the Forchheimer and in the transition domains. By making it particular for the developed turbulence domain $(\mathrm{Re}_d \geq 900)$ we obtain:

$$k_{pDt} = \sqrt{\frac{2gd_p}{0.7743}} = 5.0338\sqrt{d} \tag{23}$$

and

$$C_{pDt} = \frac{5.0338}{n} \tag{24}$$

Eqs. (12)-(24) are using the International System measurement units.

3. The experimental verification of the Chézy coefficient on the free level uniform filtration

By laboratory measurements conducted on an experimental installation the free level post-Darcy uniform filtration has been verified. The installation includes the C4MKII channel and the F1-10 ARMFIELD supply unit (Figs. 2-4).

The main features of the basic installation are: channel length 5.41 m, width b = 78 mm, height h = 0.25 m and a slope adjustable on the range $i = \pm 4\%$. The maximum supply flow is $Q = 2.0$ l/s. The depth of water in channel is adjustable with the various height overflows, with the plane gate and by adjusting the flow with three taps of various sizes. The uniform permeable material – made of glass spheres with diameters of 2, 1, 0.5 and 0.25 cm – is located in the channel's middle section. The control of depths in the measurement sections is provided with scaled piezometrical tubes and readings with a Ni 07, Karl Zeiss-Jena surveyor's level. The channel's slope is measured with this same surveyor's level.

Depths are measured also with a hook gauge. Accuracy of depth measurements is 0.2 mm.

The length of the permeable material section is L = 1.20 m, and the length between measurement sections is L_{meas}=0.82 m.

Tests have been conducted for the variants from Table 1, that is a total of 81 measurements for diameters of solid material, different slopes and normal depths, allowed by the limits of the installation.

Table 1. Number of variants studied on characteristics

No.	***d_s*** *(cm)*	***No. slopes*** *(i)*	***No. depths*** *(h_0)*
1	2	5	22
2	1	5	21
3	0.5	5	21
4	0.25	5	17

Each test refers to three measurements of the next parameters: the volume, the time for flow, the depths in the upstream and downstream measurement sections, the channel slope, the channel width, the porosity and the water temperature. It has been accepted an uniform motion, for the situation when the depth gap in the measurement section is not

exceeding a value of $\varepsilon h_0 \leq 0.5$ mm. This uniform motion has been provided by a rough adjustment of the level with the downstream overflow and a fine adjustment of level with the downstream gate, and by adjusting flows with three taps of different sizes.

From direct measurements carried on volumes, times, depths, channel widths, diameters of used spheres, porosities and temperatures, there have been computed several values: the flows $\left(Q = \frac{W}{t}\right)$, the apparent velocities $\left(V_0 = \frac{Q}{b \cdot h_0}\right)$, and then the diameter of fictive pores with Eq. (19), the Reynolds number (Eq. 22) and finally the experimental Chézy coefficient:

$$C_{\exp} = \frac{V_0}{\sqrt{d_p \cdot i \cdot \tau}} \tag{25}$$

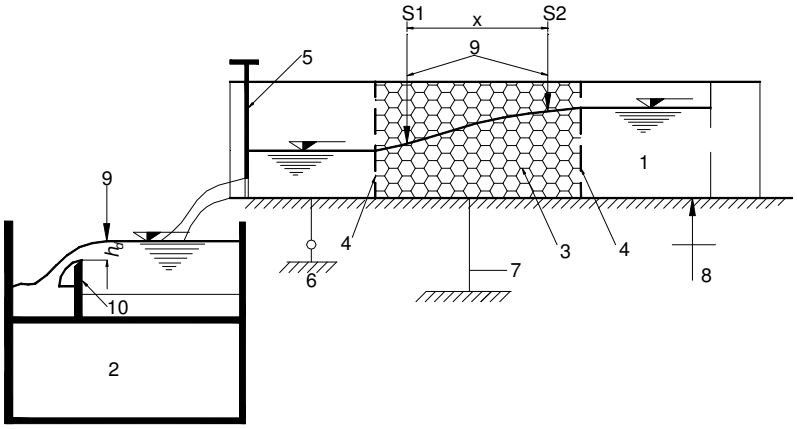

Fig. 2. Experimental installation. 1. C4MKII channel; 2. F1-10 base stand; 3. permeable porous wall (glass spheres); 4. support sieve wall; 5. adjusting weir; 6. free bearing; 7. joint support; 8. channel slope adjustment; 9. hook gauge; 10. overflow

Fig. 3. Basic experimental installation

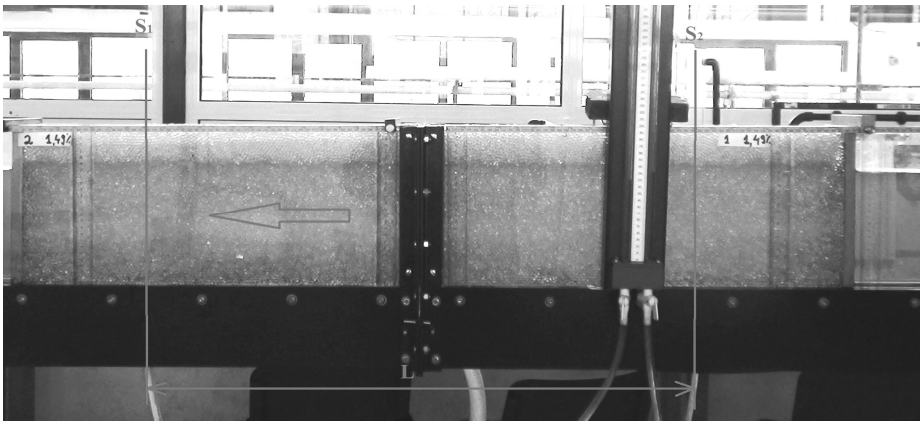

Fig. 4. Work section with measurement areas

Table 2. Experimental and theoretical results for the uniform filtration via spheres of $d_s = 2$ cm

d_s (cm)	d_p (cm)	n (-)	i (-)	Q (cm^3/s)	h_0 (cm)	v_0 (cm/s)	Re_{dp} (-)	C_{exp} ($cm^{0.5}/s$)	C_{calc} ($cm^{0.5}/s$)	$\delta C = \frac{C_{exp} - C_{calc}}{C_{calc}}$
2	1.039	0.438	0.0308	262.664	17.80	1.887	194.169	9.533	9.625	-0.0096
				200.650	13.97	1.838	189.037	9.281	9.586	-0.0318
				133.973	9.10	1.883	193.720	9.511	9.622	-0.0115
			0.0253	281.303	20.25	1.777	182.788	9.902	9.537	0.0383
				257.550	17.90	1.840	189.325	10.256	9.589	0.0696
				166.100	12.20	1.741	179.146	9.705	9.507	0.0208
				138.500	10.00	1.772	182.242	9.872	9.532	0.0356
				109.550	7.60	1.844	189.669	10.275	9.591	0.0712
			0.0225	266.281	20.83	1.635	168.182	9.661	9.411	0.0266
				228.208	18.60	1.569	161.442	9.274	9.346	-0.0078
				144.967	12.00	1.545	158.960	9.131	9.322	-0.0205
				143.905	11.23	1.639	168.564	9.683	9.414	0.0286
				106.155	8.60	1.579	162.421	9.330	9.356	-0.0028
			0.0135	193.300	21.70	1.139	117.212	8.692	8.801	-0.0124
				181.270	19.20	1.208	124.229	9.213	8.906	0.0345
				149.490	17.60	1.086	111.763	8.288	8.714	-0.0488
				146.725	15.70	1.195	122.971	9.119	8.888	0.0261
				104.955	12.40	1.083	111.372	8.259	8.707	-0.0514
			0.0075	135.570	23.00	0.754	77.559	7.717	7.996	-0.0350
				116.474	19.00	0.784	80.663	8.026	8.077	-0.0064
				96.633	16.40	0.754	77.532	7.714	7.996	-0.0352
				67.716	10.80	0.802	82.503	8.209	8.123	0.0106

Table 3. Experimental and theoretical results for uniform filtration via spheres of $d_s = 1$ cm

d_s (cm)	d_p (cm)	n (-)	i (-)	Q (cm^3/s)	h_0 (cm)	v_0 (cm/s)	Re_{dp} (-)	C_{exp} ($cm^{0.5}/s$)	C_{calc} ($cm^{0.5}/s$)	$\delta C = \frac{C_{exp} - C_{calc}}{C_{calc}}$
1	0.467	0.412	0.0265	111.890	17.30	0.827	38.210	6.723	6.875	-0.0221
				96.520	14.80	0.834	38.529	6.779	6.894	-0.0168
				98.500	14.65	0.860	39.722	6.989	6.966	0.0032
				62.410	10.50	0.760	35.116	6.178	6.676	-0.0746
				56.120	8.50	0.844	39.006	6.863	6.923	-0.0087
			0.0230	112.4500	18.87	0.7624	35.213	6.650	6.683	-0.0049
				82.0100	15.20	0.6901	31.876	6.020	6.450	-0.0668
				79.2700	12.57	0.8069	37.267	7.038	6.816	0.0325
				47.8200	8.97	0.6822	31.507	5.950	6.423	-0.0737
			0.0180	84.8500	19.00	0.5712	26.384	5.632	6.014	-0.0635
				85.4100	15.90	0.6871	31.736	6.775	6.440	0.0519
				58.5100	12.47	0.6003	27.728	5.919	6.128	-0.0341
				54.4100	9.90	0.703	32.470	6.931	6.493	0.0674
			0.0140	84.4100	19.17	0.5633	26.018	6.298	5.983	0.0527
				56.2200	15.95	0.4509	20.824	5.041	5.485	-0.0810
				51.1100	13.05	0.501	23.138	5.601	5.718	-0.0205
				36.6000	10.45	0.448	20.692	5.009	5.471	-0.0845
			0.0091	50.8300	19.50	0.3334	15.400	4.624	4.845	-0.0458
				43.7300	16.57	0.3376	15.595	4.682	4.871	-0.0388
				35.6200	14.10	0.3231	14.925	4.481	4.782	-0.0629
				27.9400	11.65	0.3068	14.169	4.254	4.677	-0.0905

Table 4. Experimental and theoretical results for uniform filtration via spheres of $d_s = 0.5$ cm

d_s (cm)	d_p (cm)	n (-)	i (-)	Q (cm^3/s)	h_0 (cm)	v_0 (cm/s)	Re_{dp} (-)	C_{exp} ($cm^{0.5}/s$)	C_{calc} ($cm^{0.5}/s$)	$\delta C = \frac{C_{exp} - C_{calc}}{C_{calc}}$
0.5	0.234	0.412	0.0400	64.8486	19.00	0.4366	10.097	4.081	4.031	0.0122
				57.5636	16.25	0.4531	10.480	4.235	4.098	0.0333
				46.8947	12.10	0.4957	11.466	4.633	4.264	0.0865
			0.0350	59.5298	19.30	0.3945	9.125	3.942	3.852	0.0233
				51.5332	16.60	0.3971	9.184	3.968	3.864	0.0269
				41.7202	13.90	0.3839	8.879	3.836	3.805	0.0081
				32.3697	10.95	0.3781	8.745	3.778	3.779	-0.0003
				29.3456	8.55	0.439	10.154	4.387	4.041	0.0855
			0.0250	48.7746	20.00	0.3119	7.215	3.688	3.462	0.0653
				45.8211	17.50	0.3349	7.746	3.960	3.576	0.1071
				38.8932	14.80	0.3361	7.774	3.974	3.582	0.1093
				24.0361	9.50	0.3236	7.485	3.826	3.521	0.0867
			0.0200	37.5377	20.85	0.2303	5.326	3.044	3.006	0.0126
				33.2037	18.10	0.2346	5.427	3.102	3.033	0.0227
				30.9066	15.35	0.2575	5.957	3.404	3.168	0.0747
				25.3092	12.70	0.2549	5.896	3.369	3.153	0.0688
			0.0140	23.4786	22.65	0.1326	3.067	2.095	2.311	-0.0935
				20.6355	16.45	0.1605	3.711	2.535	2.533	0.0009
				16.6332	13.80	0.1542	3.566	2.436	2.485	-0.0197
				13.4616	11.20	0.1537	3.556	2.429	2.481	-0.0211
				10.4013	8.55	0.1556	3.599	2.458	2.496	-0.0149

Table 5. Experimental and theoretical results for uniform filtration via spheres of $d_s = 0.25$ cm

d_s (cm)	d_p (cm)	n (-)	i (-)	Q (cm^3/s)	h_0 (cm)	v_0 (cm/s)	Re_{dp} (-)	*Obs.*
0.25	0.118	0.415	0.0290	24.25447	18.95	0.164	1.913	$Re_{dp} < 5$ the Darcy law is applied to filtration
				14.44113	16.40	0.113	1.316	
				12.63916	13.70	0.118	1.379	
				10.86903	10.20	0.136	1.592	
			0.0250	20.86864	19.64	0.136	1.588	
				18.03749	17.07	0.135	1.580	
				13.75536	12.64	0.139	1.626	
				11.02449	10.47	0.135	1.574	
			0.0201	13.34993	16.67	0.1025	1.197	
				9.803628	14.04	0.0893	1.043	
				8.03341	10.47	0.0982	1.147	
			0.0149	8.344914	20.68	0.0516	0.603	
				5.736908	17.56	0.0418	0.488	
				4.478249	12.81	0.0447	0.523	
			0.0098	7.266024	15.70	0.0592	0.692	
				5.626374	14.80	0.0486	0.568	
				4.183784	11.33	0.0473	0.552	

The experimental results that have been obtained in reference to the Chézy coefficient, $C_{exp,}$ have been compared to the theoretical values of the same coefficient C_{calc}, computed with Eq. (21), determining also the relative errors (δC) .

The results for the four studied diameters are summarized in Tables 2 - 5.

In case when the used permeable material is made of glass spheres having $d_s = 0.25$ cm , for the studied slopes the results will be the motions that occur in the laminar and the weak inertia domains $\left(\mathrm{Re}_{d_p} < 5\right)$. In such cases the Darcy law is to be applied when computing the free level filtration.

The relative deviations of the Chézy coefficient, as a function of $C_{\exp}$ are corresponding to Fig. 5, and as a Re_{d_p} function, to Fig. 6.

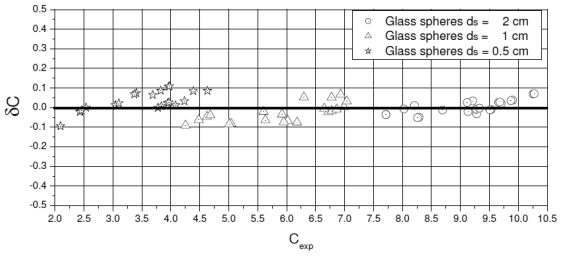

Fig. 5. The Chézy coefficients deviations δC compared to $C_{\exp}$

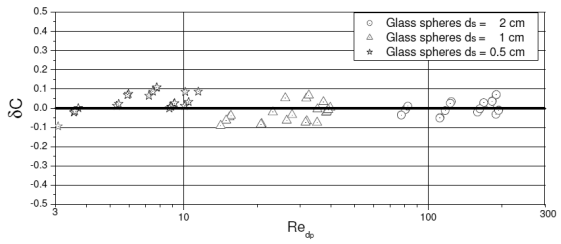

Fig. 6. The deviations of Chézy coefficient δC compared to Re_{d_p}

Taking into account the difficulties for reaching a uniform filtration the results are acceptable and allow us to put in practice the theoretical results.

4. The energy analysis of the free level filtration in the post-Darcy domain

As the free-level liquid currents that appear in channels, for the free level post-Darcy filtration the cross section's specific energy is as it follows (Fig. 7):

$$e = h + \frac{\alpha v^2}{2g} = h + \frac{\alpha Q^2}{2gn^2A^2} \tag{26}$$

where A is the apparent cross section, and v – the velocity within pores.

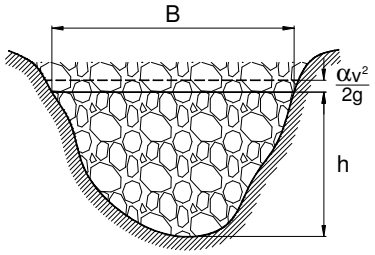

Fig. 7. Defining cross section specific energy

The horizontal reference plane is passing through the section's lowest point.

The kinetic term has to be considered, starting with the Forchheimer domain and, hence, Eq. (26) admits a minimal real value for the critical depth that is to be calculated from the next condition:

$$\frac{\alpha Q^2}{g} = \frac{n^2 A_{cr}^3}{B_{cr}} \tag{27}$$

It can be stated that in the post-Darcy filtration the flows are featuring three stages: upper, critical and lower stages. The graph $e = f(h)$ looks as in Fig. 8.

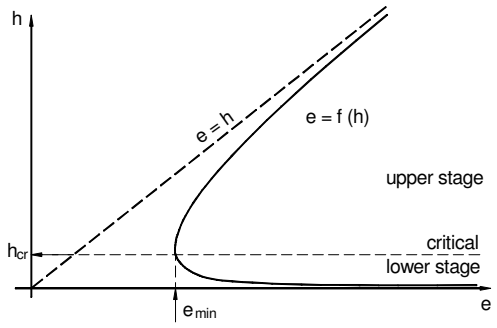

Fig. 8. Graph of cross section specific energy $e = f(h)$

The uniform velocity critical status $h_{cr} = h_0$ defines the critical slope that is obtained by replacing the motion in pores within the mass conservation equation $(Q = A \cdot V)$, thus:

$$i_{cr} = \frac{Q^2}{A_{cr}^2 C_{pDcr}^2 n^2 d} \tag{28}$$

The velocity distribution for filtration currents is almost uniform on the cross section and due to this the Coriolis coefficient (for correction of the kinetic term) can be considered $\alpha = 1$.

5. Conclusions

The post-Darcy free-level uniform filtration can be calculated with a capillary, tortuous tube filtration model. The Chézy type equation for the apparent velocity defines the Chézy coefficient in the post-Darcy domain. This theoretically computed coefficient has been experimentally verified and can be used in engineering calculations.

The post-Darcy free level filtration, due to the effects brought by the kinetic term and the kinetic head losses, allows the implementation of an energy analysis formally identical as the one for liquid currents within channels, having, for $\mathrm{Re}_{d_p} > 5$, flows in upper, critical and lower stages.

For those hydraulic calculations for free level filtration we have to state from the start the flow condition, that can be of Darcy type ($\mathrm{Re}_{d_p} < 5$) or post-Darcy type ($\mathrm{Re}_{d_p} > 5$). Depending on this the proper calculation method is then applied.

Acknowledgments

The paper on results of grant PN II, ID_2298, financed by UEFISCDI, contract 589/2009 CNCSIS-UTI and project PERFORM-ERA "Postdoctoral Performance for integration in the European Research Area (ID-57649), financed by the European Social Fund and the Romania Government are based.

References

Bartha I., Marcoie N., Toacă D., Toma D., Gabor V., Molnar A. G., Lupuşoru A., (2010a), Post-Darcy filtration through rigid permeable media, *Environmental Engineering and Management Journal*, **9**, 1727-1734.

Bartha I., Marcoie N., Toma D., Gabor V., Toacă D., (2010b), Research of filtration through uniform geometry permeable material-glass spheres, *Anals of the University "Ovidius" Constanţa, Construction Series,* **XIII**, 165-172.

Bogomolov A.I., Konstantinov N.M., (1962), *Hydraulic computation,* (in Russian), Moskow, Scientific and Technical Publishing House.

Comiti J., Sabiri N.E, Montillet A., (2000), Experimental characterization of flow regimes in various porous media III: limit of Darcy's or creeping flow regime for Newtonian and purely viscons non-Newtonian fluids, *Chemical Engineering Science*, **55**, 3057-3061.

Comiti J., Renand M., (1989), A new model for determining mean structure parameters of fixed beds from pressure drop measurements: application to beds packed with parallelepipedal particles, *Chemical Engineering Science*, **44**, 1539-1545.

Forchheimer P., (1914), *Hydraulics*, (in German), Leipzig and Berlin, Druck and Verlang von B.G. Teubner.

ID-2298, (2010), *Turbulent frow through rigid permeable porous media*, (in Romanian), project ID-2298, National Council for Scientific Research in Universities, Bucharest, Romania, On line at: www.hidromed.ro.

Klark M., (2005), *Design of an endoscopic 3-D, Particle Tracking Velocimetry System and its Application in Flow Measurement within Grave Layer*, PhD Theses, Ruperto Carola University, Heidelberg, Germany.

Montillet A., (2004), Flow through a Finite Packed Bed of Spheres: A Note on the limit of Applicability of the Forchheimer Type Equation, *ASME, Journal of Fluids Engineering*, **126**, 1-5.

Montillet A., Akkari E., Comiti J., (2006), About a correlating equation for predicting pressure drops through packed beds of spheres in a large range of Reynolds numbers, *Chemical Engineering and Processing*, CEP-5147, On line at: www.elsevier.com?locate/cep.

Wahyudi I., Montillet A, Kalifa A.O.A., (2002), Darcy and post-Darcy flows within different sands, *Journal of the Hydraulic Research*, **40**, 519-525.

Environmental Engineering and Management Journal

December 2010, Vol.9, No. 12, 1727-1735
http://omicron.ch.tuiasi.ro/EEMJ/

"Gheorghe Asachi" Technical University of Iasi, Romania

POST-DARCY FILTRATION THROUGH RIGID PERMEABLE MEDIA

Iosif Bartha*, Nicolae Marcoie, Daniel Toacă, Daniel Toma, Victor Gabor, Aron Gabor Molnar, Adina Lupuşoru

"Gheorghe Asachi" Tehnical University of Iasi, Faculty of Hydrotehnical Engineering, Geodesy and Environmental Engineering, Department of Hydroamelioration and Environmental Protection, 65 Prof.dr.docent Dimitrie Mangeron Street, 700050, Iasi, Romania

Abstract

This paper presents the Post-Darcy filtration in different permeable media. The capillary tube model of filtration is used. The study is focused on the fluid's movement through uniform geometry glass spheres, river gravel and crushed rock. For all the filtration domain the unification of friction factor is achieved.

Key words: capillary tubes model, flow parameters, Post-Darcy filtration

Received: November, 2009; Revised: November, 2010; Accepted: November, 2010

1. Introduction

In 1856, Henry Darcy has discovered that, during the flowing at low velocities of a monophasic liquid within porous media, the superficial velocity v_0 is directly proportional to the pressure gradient ∇p and inversely proportional with the dynamic viscosity coefficient μ, the proportionality factor being the permeability coefficient k_p (Eq. 1)(Darcy, 1856):

$$\nabla p = \frac{dp}{dl} = \frac{k_p}{\mu} \cdot v_0 \qquad (1)$$

After Reynolds' relevant experiments, focused on the flow type in 1883 and the velocity's non-linear effect developed upon it, it has been shown also that the major parameter within filtration process is not the superficial velocity, but the Reynolds number, which is a function of this velocity. The Reynolds number is a relative measure of viscous and inertial forces.

In 1901 it has been ascertained that the filtration superficial velocity may deviate from the Darcy law for a range of higher Reynolds numbers in water filters (that is, for the same pressure head, lower superficial velocities have been obtained), fact that lead to a re-defining of the superficial filtration velocity, as a power form (Eq. 2):

$$\nabla p = -c_1 \cdot v_0^{c_2} \qquad (2)$$

or approximated as 2nd or 3rd order polynomials (Forchheimer, 1914) (Eqs. 3, 4):

$$\nabla p = a v_0^2 + b v_0 \qquad (3)$$

$$\nabla p = c v_0^3 + a v_0^2 + b v_0 \qquad (4)$$

A filtration process at velocities higher as the Darcy domain is of great theoretical and practical importance in the hydrocarbons extraction process (liquid or gaseous) (Friedel and Voigt, 2006), in the hydraulics of permeable bed rivers (Klark, 2005), and for flows over permeable walls (high-density built areas, dense vegetation areas).

Although other approaches exist (Blunt, 2001, Carlig and Macoveanu, 2009; Holzbecher, 1998) the studies of these movements are useful for dispersing polluting substances within built areas, for the defining of oxygen and carbon dioxide exchanges in forests and crop fields, and also in the case of forest fires propagation (Breugem, 2005; Klov, 2000).

* Author to whom all correspondence should be addressed: i_bartha@yahoo.com

Moreover, the post-Darcy filtration occurs also in the drains and wells filters, in rockfeel bridges, dams, groins, dykes, filtering cofferdams, that is, all the situations where the movement deviates from the Darcy flow.

The present paper is a study devoted to theoretically and experimentally determination of the post-Darcy filtration parameters within a rigid permeable media.

2. Flow models through permeable media

The dissipation of fluid current hydraulic energy within porous media has important technical meanings in numerous engineering domains. During more than 150 years of studies focused on the filtering processes, there have been developed several flow models. These models can be divided in five classes as it follows: *phenomenological models, geometrical models* (based on the flow within pipelines and channels), *statistical models*, *models based on the Navier-Stokes equations* and *models based on the flowing around solid objects* (Comiti and Renoud, 1989).

All these models include unknown parameters which are to be determined experimentally. Most of the experiments are defining the macroscopic pressure loss within a permeable media of known thickness, as a function of flow's superficial velocity (Montillet, 2004; Wahyudi et al., 2002). For a relatively large range of Reynolds numbers (including those for the low inertia, the Forchheimer, the transition and the turbulent domains) the equation (2) is frequently used, converted in the form of Eq. (5) (Comiti and Renoud, 1989):

$$\frac{\Delta p}{L v_0} = M v_0 + N \qquad (5)$$

where $\Delta p/L$ is the pressure gradient; v_0 – the filtration superficial velocity; L – thickness of the filtration path (experimentally measured); M and N – the linear regression coefficient, statistically computed.

The pressure loss depends, besides these factors, on the fluid physical properties: the density ρ; the kinematic viscosity coefficient μ (which, at their turn, are a function of temperature); the geometrical features of the permeable media; the particles' diameter d_p and the porosity n**.** For solid spherical particles the d_p factor is precisely their diameter.

The pressure loss, besides all the stated factors, depends also on the solid-liquid contact area, defined by means of the static specific area A_S and the dynamic specific area A_d defined by the ratios (5a, 5b):

$$A_S = \frac{mean\ surface\ of\ particle}{mean\ volume\ of\ particle} \qquad (5a)$$

$$A_d = \frac{solid\ particles\ surface\ exposed\ to\ the\ flow}{total\ volume\ of\ the\ solid} \qquad (5b)$$

The flow regime through pores is characterized by the microscopic Reynolds number, which can be expressed by Eq. (6):

$$Re_{d_p} = \frac{\rho v_o d_p}{\mu} \qquad (6)$$

The geometrical model of flow into thin tubes

It is assumed that the pores of the permeable material are similar to a bundle of m tortuous tubes having a diameter - d and a length – L' with a total area – A. The filtering column has a total apparent volume – W, a diameter – D and a total length – L (Comiti and Renoud, 1989; Seguin et al., 1998). The trajectories of path lines are longer than the filtering column's length and are describing curved paths between the particles (Fig. 1).

The tortuosity is defined by Eq. (7):

$$\tau = \frac{L'}{L} \qquad (7)$$

The fictive diameter of model tubes, d, results by making equal the real volume of pores with the tubes bundle volume (Eq. 8):

$$d = \frac{4W}{A} = \frac{4n}{A_d(1-n)} \qquad (8)$$

The velocity within the fictive tubes becomes (Eq. 9):

$$v = \frac{v_0 L'}{nL} = \frac{v_0 \tau}{n} \qquad (9)$$

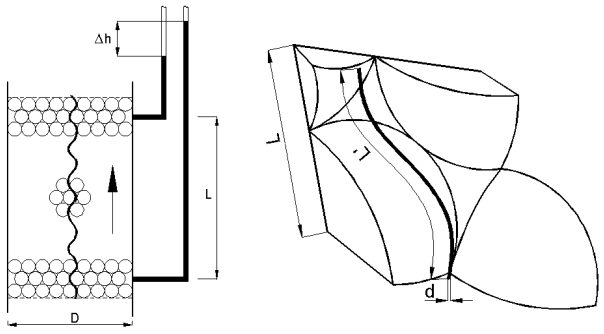

Fig.1. The capillary tubes model for filtration

The head loss for low Reynolds numbers, that include the weak inertia domain and the Forchheimer domain, can be assimilated to the sum of two terms (Eq. 10):
- the first term, proportional to the velocity within pores, due to the viscous resistance on the contact area;
- the second term, proportional to the square of the velocity, due to inertial resistances, kinetic energy losses at the stream's direction changes

$$h_r = \frac{\Delta p}{\gamma} = \left(\frac{64}{Re_p} + \lambda_t \right) \cdot \frac{L'}{d} \cdot \frac{v^2}{2g} \qquad (10)$$

where γ is the fluid's specific weight; Re_p - the Reynolds number of the motion within fictive tubes for a length L' and a diameter d; λ_t - the Darcy-Weisbach coefficient for turbulent flows.

The general accepted form for the filtration coefficient λ is (Eq. 11):

$$\lambda = \frac{\alpha}{Re} + \beta \qquad (11)$$

where α = 64 and β = 0,7743. Frequently, the technical litterature uses the friction factor f instead of λ, where $f = \lambda/4$.

The term of viscous resistance results from the Poiseuille equation (12):

$$\frac{(\Delta p)'}{L'} = \frac{2\mu}{d^2} \cdot v \qquad (12)$$

equation which, for the macroscopic length of filtration's path L', porosity n, tortuosity τ, and the dynamic specific area A_d, against the filtration superficial velocity, becomes (Eq.13):

$$\frac{(\Delta p)'}{L} = \frac{2\mu \cdot \tau^2 (1-n)^2 A_d^2}{n^3} v_0 \qquad (13)$$

The term that corresponds to the loss of kinetic energy is to be calculated as in the case of very rough pipes, due to the very frequent changes of trajectory directions and flow sections (Eq. 13a):

$$\left(\frac{\Delta p}{\gamma} \right)'' = \lambda_t \frac{L'}{d} \frac{v^2}{2g} \qquad (13a)$$

The equivalent roughness of the filtration's fictive tortuous tubes is accepted as the tubes' diameters, $k_e = d$ (Comiti and Renoud, 1989), the λ coefficient can be computed with the Prandtl-Nikuradze equation, the results being λ_t = 0.7743 or $f = \lambda/4$ = 0.1935. After replacements the next equation is obtained:

$$\frac{(\Delta p)''}{L} = \frac{\lambda_t \rho \tau^3 (1-n) A_d}{8n^3} v_0^2 \qquad (14)$$

After replacing equations (10), (13) and (14) the equation (15) results.

$$\frac{(\Delta p)}{L v_0} = \frac{2\mu\tau^2 (1-n)^2 A_d^2}{n^3} + \frac{\lambda_t \rho \tau^3 (1-n) A_d}{8n^3} v_0 \qquad (15)$$

which has the form of equation (5) with:

$$M = \lambda_t \frac{\rho \tau^3 (1-n) A_d}{8n^3} \qquad (16)$$

and

$$N = \frac{2\mu\tau^2 (1-n)^2 A_d^2}{n^3} \qquad (17)$$

If the temperature of the experimental fluid is known, it is then possible to obtain the density ρ and the dynamic viscosity coefficient μ, respectively the porosity of the permeable material, n. Via experimental measurements performed for the macroscopic head loss and the superficial velocity, by means of statistical processing, the factors M and N are then obtained (with a determination coefficient R). Thus, with equations (16) and (17) two parameters can be defined: the tortuosity τ and the dynamic specific area A_d.

A generalization can result from the possibility to compute the λ coefficient as a function of the fictive Reynolds number in tubes, Re_p (Eqs. 18, 19).

$$\lambda = 4f = \frac{(\Delta p)}{L} \frac{n^3}{2\rho\tau^3 (1-n) A_d v_0^2} \qquad (18)$$

$$Re_p = \frac{\rho \tau v_0}{\mu (1-n) A_d} \qquad (19)$$

The pressure gradient becomes (Eq. 20):

$$\frac{\Delta p}{L} = \frac{1}{2} \frac{\tau \mu^2 (1-n)^3 A_d^3}{\rho n^3} Re_p \left[1 + \frac{\lambda Re_p}{64} \right] \qquad (20)$$

or the hydraulic slope (Eq. 21):

$$i = \frac{1}{2}\frac{\tau v^2 (1-n)^3 A_d^3 Re_p}{gn^3}\left(1+\frac{\lambda Re_p}{64}\right) \quad (21)$$

In this study, these elements are computed for three different permeable materials.

3. The experimental installation

The experimental installation includes a cylindrical infiltrometer, a water supplying unit, a connection between these and an outlet, with the possibility of flow measuring (volumetric measurement) - (Fig. 2a, b, c) (ID-2298, 2009).

The infiltrometer (Bartha and Marcoie, 2010; Bartha et al., 2010) has a nominal diameter D = 100 mm and a total length of 2.60 m, the distance between the extreme pressure plugs being L = 2 m.

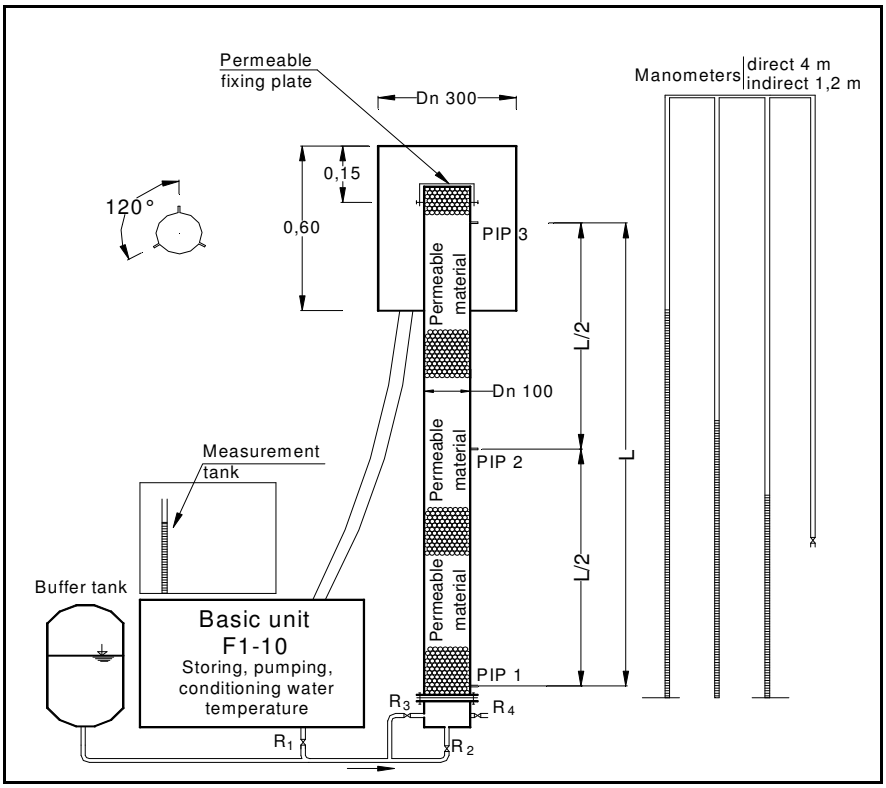

a)

b)

c)

Fig 2. The experimental installation (a - general view; b - general lay-out of the installation, equipped with direct pressure gauges; c - general lay-out of the installation, equipped with indirect pressure gauges)

The upstream and downstream end of the measurement section is limited by a permeable wall that is fixing the granular material. The loading of granular material is performed by vibration technique, process that together with the permeable limiting walls provides the perfect immobility of the solid phase, during the experiments.

The water supply source is a storage and pumping installation, F1-10 ARMFIELD type, that provides the maximal hydraulic parameters: H_{pump}= 18 mWC and Q = 1.5 L/s. The supply source and the infiltrometer are connected via flexible hoses, with a buffer tank mounted in derivation (pressure pulse dampener).

All hydraulical parameters within this installation are controlled via three spherical valves *R1, R2, R3*, the last having a lesser diameter, in order to ensure a fine control of flows. Valve *R4* is used to measure the permeable material's porosity.

The infiltrometer is equipped with three presure intake plugs mounted at an equal distance ΔL = 1 m. Each port has three holes with d_{PIP} = 0.8 mm at 120^0.

Flow measurement is volumetric and measurements' maximal relative errors are $\delta Q \leq$ 0.001. The head loss is measured with inclined tube differential micro-pressure gauges, for $\Delta h \leq 0.1$ mWC, with direct differential pressure gauges for $0.1 \leq \Delta h \leq 4$ mWC and with mercury indirect differential pressure gauges for $4 \leq \Delta h \leq 15$ mWC. On the pressure transmission hoses capillary sections are mounted, having the role to compensate the pressure pulses. For measuring the fluid's temperature a thermometer with 0.1^0C accuracy is to be used, and time is measured with a 0.01 s accuracy chronometer.

4. Experimental results

For experiments carried for the post-Darcy filtration there have been used three types of permeable materials, granular, rigid, with four different diameters for each, these materials being: glass spheres, with $d_p = d_p \pm$ 0.01 mm, river gravel and crushed rock (Fig. 3).

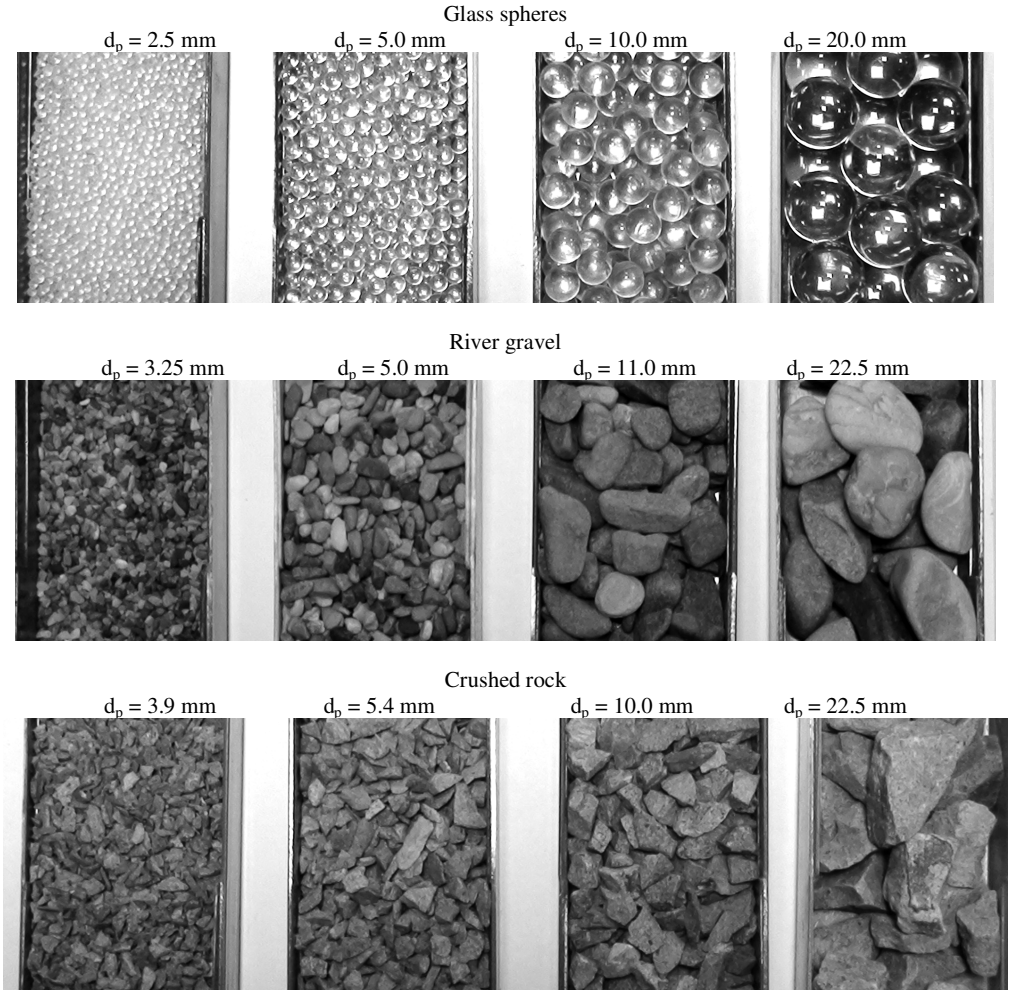

Fig 3. Experimental permeable material

The head loss has been measured for various flows; also the material porosity and the water temperature have been determined. The flow volumetric measurements have been performed by three repetitions, and for the head losses by two repetitions (at the last value there is an extra verification of the measurements correctness through $\Delta h_{1-3} = \Delta h_{1-2} + \Delta h_{2-3}$ from the three pressure ports). The hydraulic slope and the superficial velocity $(i,v_0)_i$ have been computed, the pairs of values being statistically processed, thus obtaining the M and N parameters of Eq. (5). The values for the diameters of the experimental porous material particles d_p, the porosity n, M, N and the determination coefficient R, respectively the number of measurements NEM are listed in Table 1. By means of Eqs. (16) and (17) the specific dynamical area A_d and the tortuosity τ have been computed, and, afterwards, with equation (8), there have been computed the fictive diameter of the tortuous tubes in which water flows. All these values are listed in Table 1. The pairs of values $(i,v_0)_i$ can be retrieved in the corresponding graphs, that is Figs. 4, 6, 8, for each filtering material used in experiments, and the same has been done also for $(i/v_0,v_0)_i$ this generating the graphs from Figs. 5, 7, 9. In fact these last graphs are defining straight-lines compliant to Eq. (5).

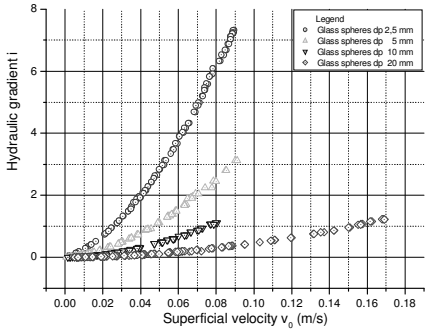

Fig. 4. The hydraulic slope as a function of the superficial velocity in the case of filtration through permeable material made of glass spheres

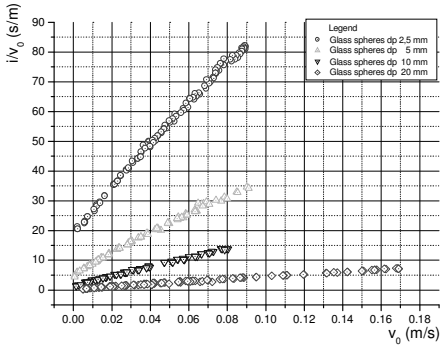

Fig. 5. Straight-lines of Eq. (5) for a permeable material made of glass spheres

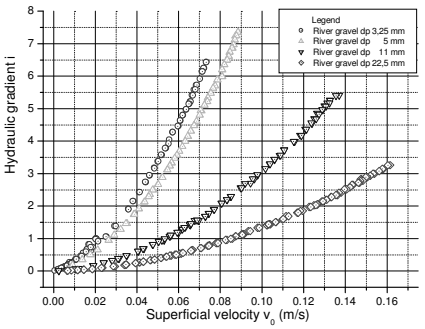

Fig. 6. The hydraulic slope as a function of the superficial velocity in the case of filtration through river gravel

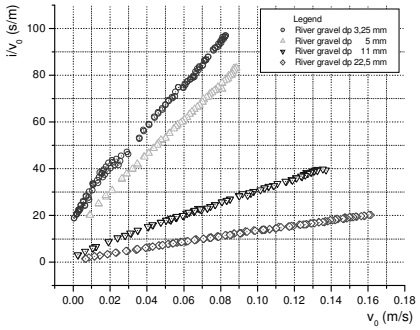

Fig. 7. Straight-lines of Eq. (5) for river gravel

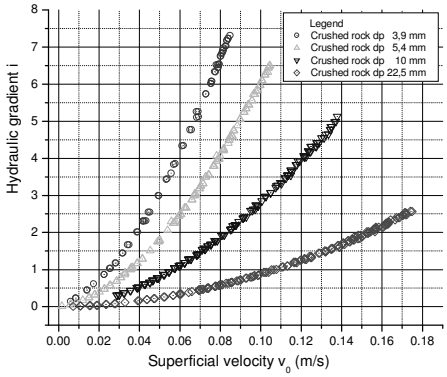

Fig. 8. The hydraulic slope as a function of the superficial velocity for crushed rock

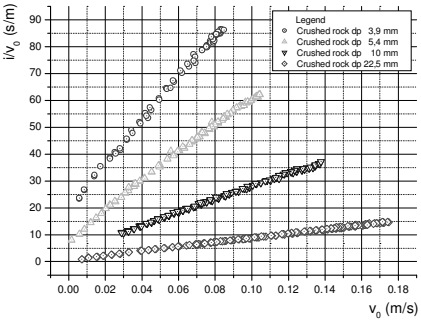

Fig. 9. Straight-lines of Eq. (5) for crushed rock

Table 1. Hydraulic parameters for the experimental material

Material	*dp (mm)*	*n*	*M* ($s^2 m^{-2}$)	*N* ($s^1 m^{-1}$)	*R*	*NEM*	*τ*	A_d (m^{-1})	$10^3 d$ *(mm)*
Glass spheres	2.5	0.3163	694.2278	20.9321	0.998	115	1.119	2322	0.797
	5.0	0.3550	324.1792	5.0470	0.998	92	1.197	1330	1.655
	10.0	0.3543	155.8957	1.2377	0.998	86	1.178	665	3.229
	20.0	0.4079	43.1188	0.1820	0.997	131	1.113	363	7.580
River gravel	3.25	0.3251	911.3753	21.1756	0.998	118	1.315	2066	0.933
	5.0	0.3241	765.0261	14.9615	0.999	96	1.312	1731	1.008
	11.0	0.3306	272.532	3.5200	0.999	100	1.131	1031	1.916
	22.5	0.3728	118.0391	1.5214	0.999	123	1.006	971	2.45
Crushed rock	3.9	0.3965	789.5090	20.7250	0.999	90	1.410	2946	0.89
	5.4	0.3841	520.1989	9.1933	0.997	123	1.359	1932	1.29
	10.0	0.3915	238.8276	4.1526	0.999	174	1.154	1554	1.66
	22.5	0.4219	80.2307	0.7679	0.999	187	1.061	884.6	3.30

It can be seen that the straight-lines of Eq. (5) are approximately acceptable on the domain of the velocity measurements. After the calculation of parameters λ (Eq. 18) and Re_p (Eq. 19), Fig. 10 graphically shows the values $(Re_p, f)_i$ for all experimental materials and diameters ($4f = \lambda$), thus certifying the valability of a type (11) equation for the post-Darcy filtration, respectively:

$$f = \frac{16}{Re_p} + 0.1936 \qquad (22)$$

The proportion in which viscous and inertial losses contribute to the total pressure losses can be determined from equations (10), (13) or (14), in function of the Reynolds number computed for the fictive tube diameter d and for the velocity of fluid within them, v. The term $64/Re$ within Eq. (10) is the viscosity's contribution, and λ_t is the inertial contribution to the total head losses.

The percentage of viscous and inertial losses applied to the global losses, in function of Re_p number, are corresponding to the values entered in Table 2, and Fig. 11, respectively.

The filtration can be considered a Darcy type filtration for $Re_p \leq 0.89$, when inertial losses are reaching about 1% of total losses. The domain of weak inertia corresponds to Reynolds numbers $0.89 \leq Re_p \leq 4.3$, at upper limit the inertial losses reaching up to 5% of total losses.

Calculations, in this domain too, can be performed with the Darcy equation.

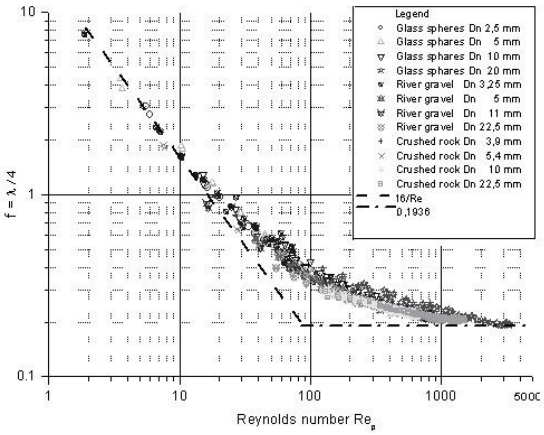

Fig. 10. Graph of function $f - Re_p$ general for all experimental filtering materials

The domain of high inertia (the Forchheimer domain) occurs for $4.3 < Re_p \leq 180$, when inertial energy losses are reaching (5-69) % of total losses. These three domains, together, belong to a laminary flow regime. The domain for the transition regime extends for $180 < Re_p < 900$, the proportion of inertial losses reaching (69-92) %. Starting at a Re_p=350-450 local turbulences within pores already start to occur. A turbulent filtration regime is defined for $Re_p > 900$.

Table 2. Contribution of viscous and inertial losses to the total losses

Re_p		0.01	0.89	1	4.3	10	100	180	900	1000	10000
Head loss (%)	Δp_μ	99.998	98.93	98.80	95.05	89.21	45.25	31.47	8.41	7.63	0.82
	Δp_i	0.012	1.07	1.20	4.95	10.79	54.75	68.53	91.59	92.37	99.18

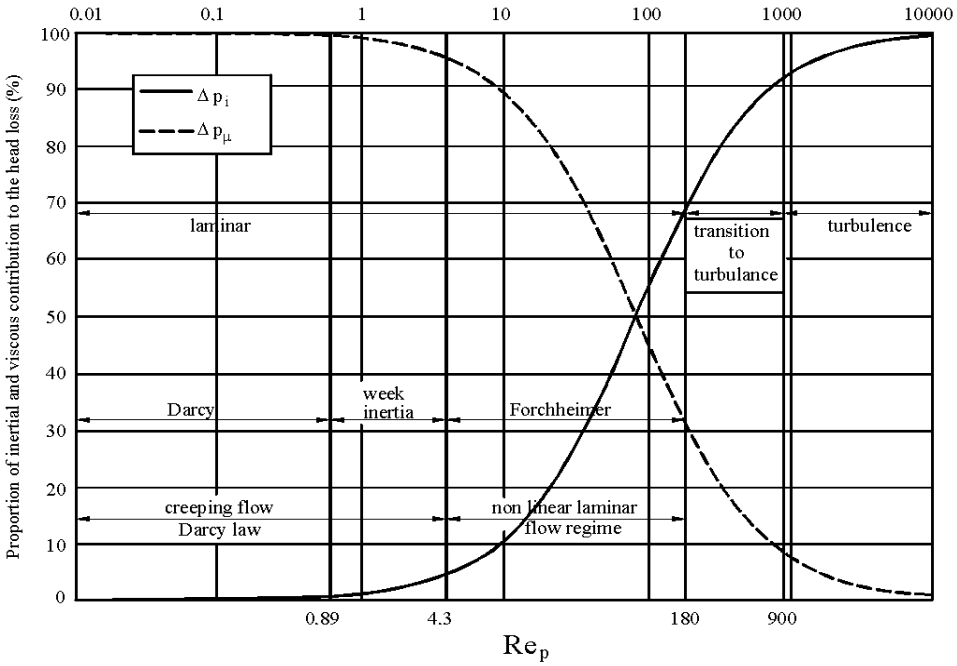

Fig. 11. Filtration regimes of a Newtonian fluid

5. Conclusions

In certain situations it has been seen that flowing of liquids through porous media occurs within the post-Darcy domain. The real filtration phenomena are approximately satisfied by the thin tubes geometrical model and are able to solve engineering problems. In the case of post-Darcy flows, besides head losses due to viscosity, certain inertial losses also occur, losses that must be taken into equation for hydraulic calculations.

Acknowledgments

The paper on results of grant PN2, ID_2298, financed by CNCSIS, contract 589/2009 CNCSIS-UTI and project PERFORM-ERA "Postdoctoral Performance for Integration in the European Research Area" (ID-57649), financed by the European Social Fund and the Romanian Government are based.

References

Bartha I., Marcoie N., (2010), Post-filtration through rigid, permeable media and real situations in engineering practice, *Anals of the University "Ovidius" Constanţa, Construction Series*, **XII**, 155-164.

Bartha I., Marcoie N., Toma D., Gabor V., Toacă D., (2010), Research of filtration through uniform geometry permeable material-glass spheres, *Anals of the University "Ovidius" Constanţa, Construction Series*, **XIII**, 165-172.

Blunt M.J., (2001), Flow in porous media — pore-network models and multiphase flow, *Current Opinion in Colloid & Interface Science,* **6**, 197-207.

Breugem W.P., (2005), *The Influence of Wall Permeability on Laminar and Turbulent Flows*, PhD Thesis, Technical University Delft, The Netherlands.

Carlig E.-D., Macoveanu M., (2009), Hydrodynamic modelling of pollution with LNAPL generated by waste dump from metal working industry, *Environmental Engineering and Management Journal*, **8**, 43-48.

Comiti J., Renoud M., (1989), A new model for determining mean structure parameters of fix beds from pressure drop measurements: application to beds packed with parallelipipedal particles, *Chemical Engineering Science*, **44**, 1539-1545.

Comiti J., Sabiri N.E., Monteillet A., (2000), Experimental characterization of flow regime in various porous media - III: limit of Darcy's creeping flow regime for Newtonian and purely viscous non-Newtonian fluids, *Chemical Engineering Science*, **55**, 3057-3061.

Darcy H.Ph.G., (1856), *The Public Fountains of the City of Dijon*, (in French), Librairie des Corps Impèriaux des Ponts et Chaussèes et des Mines, Paris.

Forchheimer Ph., (1914), *Hydraulics*, (in German), Leipzig and Berlin, Druck and Verlag von B.G. Teubner.

Friedel T., Voigt H.D., (2006), Investigation of non-Darcy flow in tight-gas reservoirs with fractured wells, *Journal of Petroleum Science and Engineering*, **54**, 112-128.

Holzbecher E.O., (1998), Modeling density-driven flow in porous media: principles, numerics, software, Vol. 1, Springer.

ID-2298, (2009), *Turbulent flow through rigid permeable porous media*, (in Romanian), Project ID-2298, NationaL Council for Scientific Research in

Univeristies, Bucharest, Romania, On line at: www.hidromed.ro.

Klark M., (2005), *Design of an endoscopic 3-D*, *Particle Tracking Velocimetry System and its Application in Flow Measurements within Gravel Layer*, PhD Thesis, Ruperto Carola University, Heidelberg, Germany.

Klov T., (2000), *High Velocity Flow in Fractures*, PhD Thesis, University Trondheim, Norway.

Montillet A., (2004), Flow through a finite packed bed of spheres: a note on the limit of applicability of Forchheimer - type equation, *Journal of Fluids Engineering*, **126**, 1-5.

Seguin D., Montillet A., Comiti J., (1998), *E*xperimental characterization of flow regimes in various porous media - I: limit of laminar flow regime, *Chemical Engineering Science*, **53**, 3751-3761.

Seguin D., Montillet A., Comiti J., Huet F., (1998), Experimental characterization of flow regimes in various porous media - II: Transition to turbulent regime, *Chemical Engineering Science,* **53**, 3897-3909.

Wahyudi I., Montillet A., Khalifa A.O.A., (2002), Darcy and post-Darcy flows within different sands, *Journal of Hydraulic Research*, **40**, 519-525.